FACTORS AFFECTING ADHESION OF POLYMERS DURING COINJECTION

by

WUTTIPONG RUNGSEESANTIVANON

BSc., MSc. (Polymer Science)

A thesis submitted in partial fulfilment of the requirements for the degree of Doctor of Philosophy in Engineering

University of Warwick, School of Engineering

December 2000

DEDICATION

To Sirada my Wife

ACKNOWLEDGEMENTS

The author is grateful to Dr. Gordon F. Smith for his guidance, helpful suggestions and many instructive discussions that we have had throughout the duration of this project. Completion of this thesis would not have been possible without his support and assistance.

I would like to express my thanks to Mr. Robert J. Coates and Mr. Amrick Singh for the close-support that they offered throughout the three years of this project.

Acknowledgements are due to the National Metal and Materials Technology Centre (MTEC), the Ministry of Science, Technology and Environment of Thailand for their support and sponsorship of my studies in the United Kingdom.

Last, but by no means the least, I would like to thank my wife, Sirada, for her support over many years whilst I have been studying in UK.

DECLARATION

I declare that all the work described in this thesis was undertaken by myself unless otherwise acknowledged in the text and that none of the work has previously been submitted for any academic degree. All sources of quoted information have been acknowledged by means of references.

Wuttipong Rungseesantivanon

SUMMARY

The co-injection moulding process was studied. The experimental work from several tools, such a square plaque plate moulding has led to an understanding of the mechanism of dual injection mould filling. Emphasis has been focussed the relationships between the rheological property of the polymers and the relevant moulding parameters. The skin-core formations, which correlate to these relationships, were also studied. Many factors were introduced for understanding the effect on the skin-core adhesion where the two polymers are incompatible. In this case a compatibiliser was found to be one of the most important factors. In the presence of compatibiliser, the chemical reaction between active functional groups of skin and compatibiliser in the core occurred. Suitable conditions were necessary to produce good bonding between skin and core. The greater thickness of skin layer and greater simultaneous injection times led to more probability for the skin and core active functional groups to react with each other before the skin became no-flow layer. Methods available to achieve these thicknesses and simultaneous injection times were possible by controlling the moulding parameters, such as melt temperature, tool temperature, injection speeds, and lengths of simultaneous phase; these parameters could affect the skin-core thickness formations and their adhesion to different degrees.

CONTENTS

LIST OF FIGURES

Page

Chapter II

Chapter III

Chapter IV

Chapter VI

Chapter VII

Appendix III

Appendix IV

Appendix V

Appendix VI

Appendix VIII

LIST OF TABLES

Page

Chapter II

Chapter III

Chapter VI

Chapter VII

Appendix I

Appendix III

Appendix VI

Appendix VII

Appendix VIII

ABBREVIATIONS

PP	Polypropylene
PA6	Polyamide 6
PA66	Polyamide 6,6
PBT	Polybutylene terephthalate
PS	Polystyrene
St	Styrene
PE	Polyethylene
NBDCA	Norbornene-2, 3-dicarboxylic anhydride
EVOH	Ethylene vinyl alcohol
EP	Ethylene-propylene rubber
GMA	Glycidyl methacrylate
MA	Maleic anhydride
(E, VA, GMA)	Ethylene-vinyl acetate-glycidyl methacrylate copolymer
-*g*-	Graft copolymer
-*b*-	Block copolymer
-co-	Alternating copolymer

Chapter I

Introduction

This work is related to the development of granular injection paint technology (GIPT) [1], which aims to coat thermoplastic components in the mould by paint. This technique was designed to meet industrial painting requirements with the co-injection moulding process (alternative name is sandwich injection moulding process) [2-6]. The technique uses one material in a layered combination with another to achieve an appropriate mix of properties, thus, the selection of raw materials for use as skin or core of the sandwich moulding depends on the properties required of the final part. Care has to be taken that the selected materials adhere to each other [7-9]. There are many cases in which the polymer combinations meet the engineering requirements of two-layer moulding but present poor or no adhesion between the different materials; they are incompatible thermoplastics [10-15]. For instance a nylon skin will not bond to a polypropylene core material. This work provides a realistic process technology for skin-core formation of incompatible thermoplastic polymer melts during thin-walled co-injection moulding. The problem to overcome when moulding incompatible material is interfacial adhesion, hence, compatibilisers are used to promote this bond. There were several studies on the combination of incompatible polymers incorporating compatibilisers, such as those utilising maleic anhydride grafted polypropylene (PP-g-MA) to interface polyamide (PA) with polypropylene (PP). Unfortunately, the compatibilisers are only one of the important factors, which can be employed to achieve good interfaces between polymers; the processing conditions, such as machine setting data, amount of skin and core, and rheological properties of moulding materials, are also major parameters.

This project aims to investigate the parameters affecting adhesion during the co-injection moulding process. In particular, it is the intention to focus on combinations of incompatible polymers such as polyamide on polypropylene. It is hoped to use the mechanism of this process to enable other polymers to be considered.

Chapter II

The Co-injection Moulding Process

2.1 Definition

The co-injection moulding process was also known as sandwich injection moulding process. This means injection of two or more different but compatible polymer melts sequentially or simultaneously into a mould. A layered structure is then produced by the melt which is injected first to form the skin and the subsequent melt forms the core as seen in Figure 2.1.

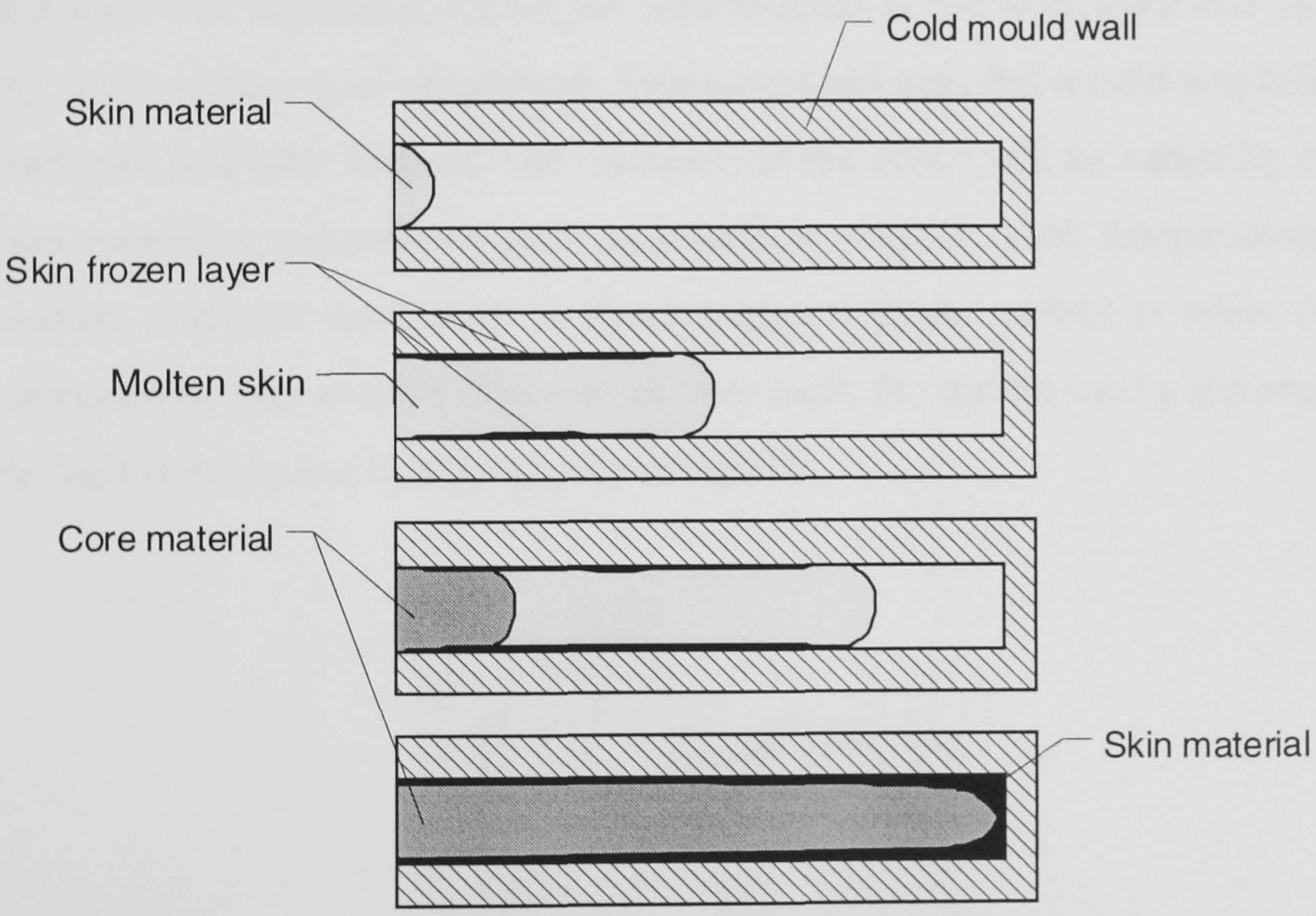

Figure 2.1 Process sequence of sandwich injection moulding [6]

2.2 Techniques for Co-injection Moulding Process

In this section, the different techniques for sandwich injection moulding process are classified using the number of melt channels in the nozzle. These are presented as follows.

2.2.1 One-channel nozzle

2.2.1.1 Single channel technique

The single channel method was patented by ICI in 1970 [2] and is schematically shown in Figure 2.2. An injection moulding machine with two cylinders was used. The polymer melts were injected sequentially into a cold mould through an adjustable valve. The melt injected first forms the skin and surrounds the core, which was injected afterwards. The formation of a skin-core structure could be explained from the mould filling process. The polymer injected first would cool and solidify at the surface as it came into contact with the cold mould wall, while a flowing region of molten polymer still existed at the centre of the flow channel. When the second polymer melt was injected it forced the first forward as the flow front and this would solidify at the surface as it progressed. This continued until the mould was filled and a sandwich part had been formed. The thickness of the skin could be varied by changing injection moulding parameters, such as injection velocity, melt temperature, mould temperature, and melt viscosities. A disadvantage with the method is when switching from injection of skin melt to injection of core melt, the mould cavity pressure drops, and the melt front comes to a temporary standstill.

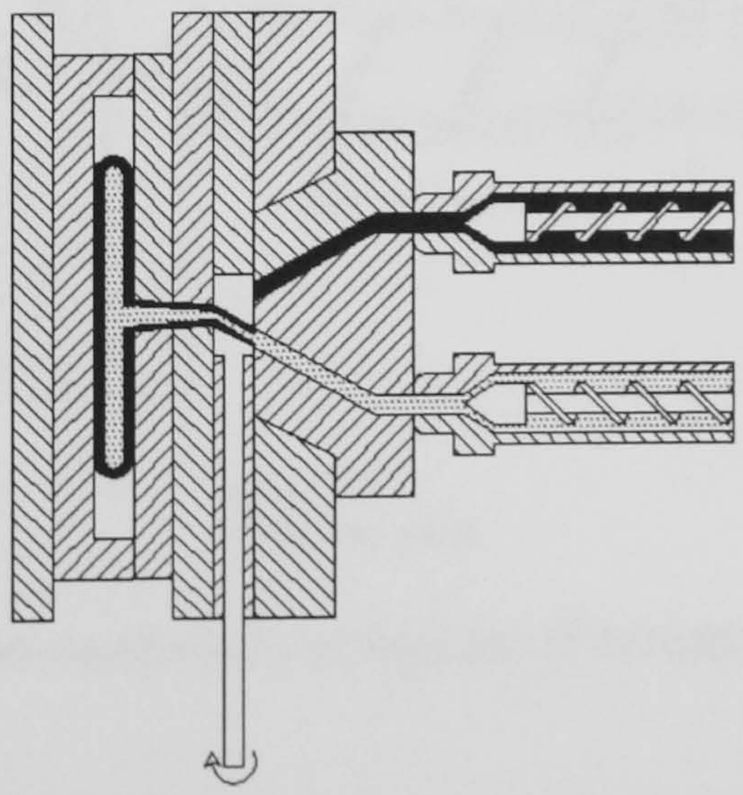

Figure 2.2 Single channel technique (ICI)

2.2.1.2 Mono-sandwich technique

The mono-sandwich technique, developed by Ferromatik Milakron [9,16], used sequential injection and was therefore similar to the single channel technique. Here

two polymer melts were layered in one injection cylinder, as shown schematically in Figure 2.3. This was achieved by melting the skin material in a separate side extruder and leading it through a special hot runner to the front of the screw in the main cylinder. The melt pressure pushed the screw backwards. When a sufficient amount of melted material had accumulated in front of the screw, the screw starts rotating and feeds the core material. The injection was then done in the same way as for normal injection moulding by pushing the screw forward. The maximum amount of core material that could be obtained depended on the mould geometry. A standard moulding machine could be rebuilt to a sandwich machine simply by connecting a side extruder to the main injection unit. Also, very thin-walled parts could be produced by this method.

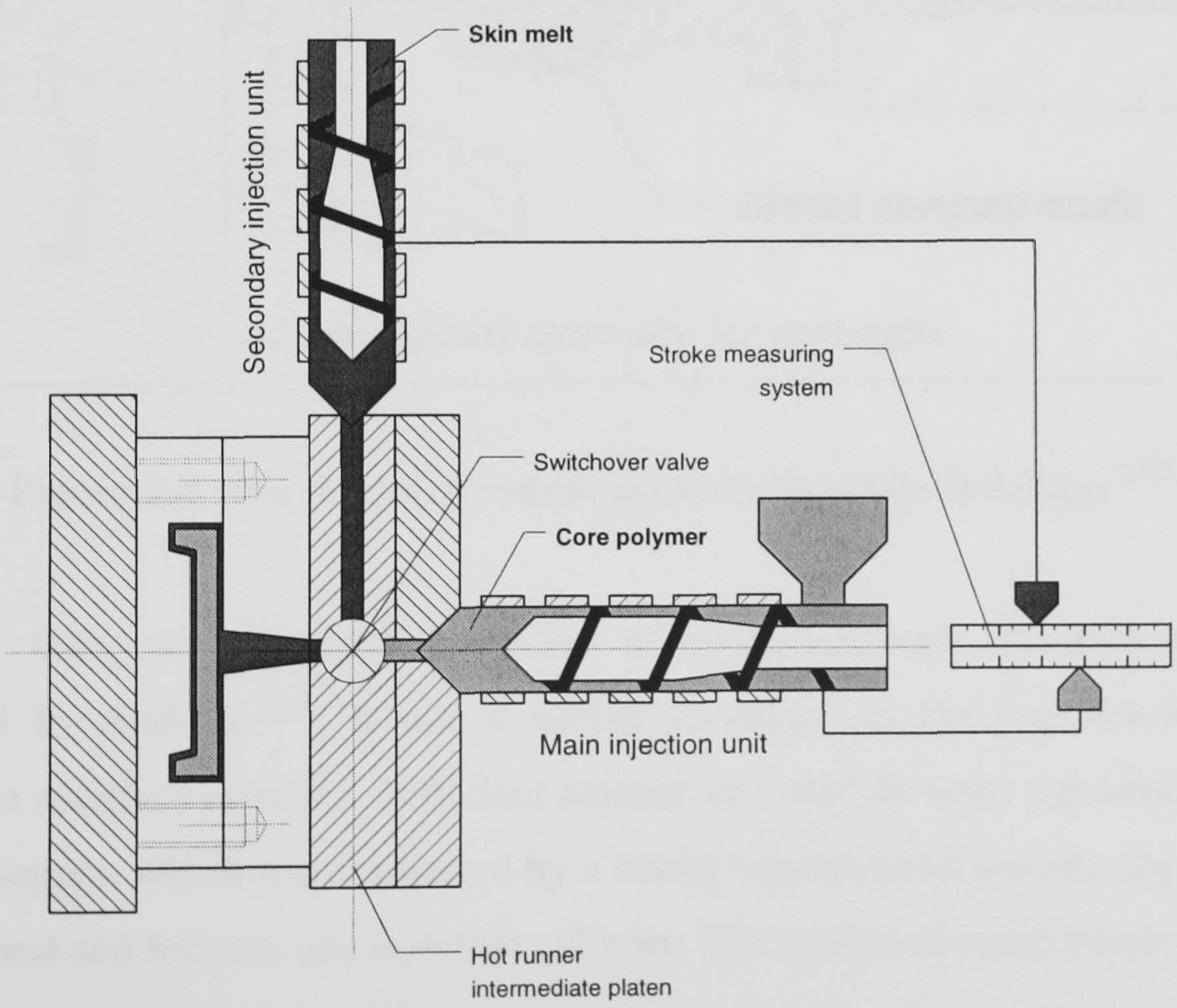

Figure 2.3 Mono-sandwich technique (Ferromatik Milakron) [9]

A further advantage was said to be the simplified exchange of materials in the cylinders due to the relatively simple construction. The process control was simple since injection was made in the same way as for normal injection moulding. One major disadvantage was the lack of detailed control of the injection process. This made moulding of parts having complicated shapes more difficult.

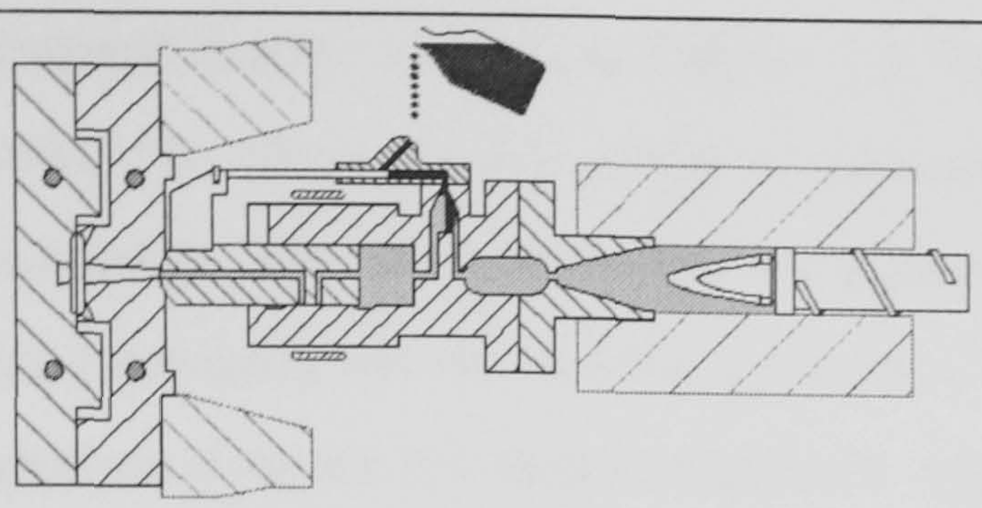

(a) feed an additive material into the special designed nozzle

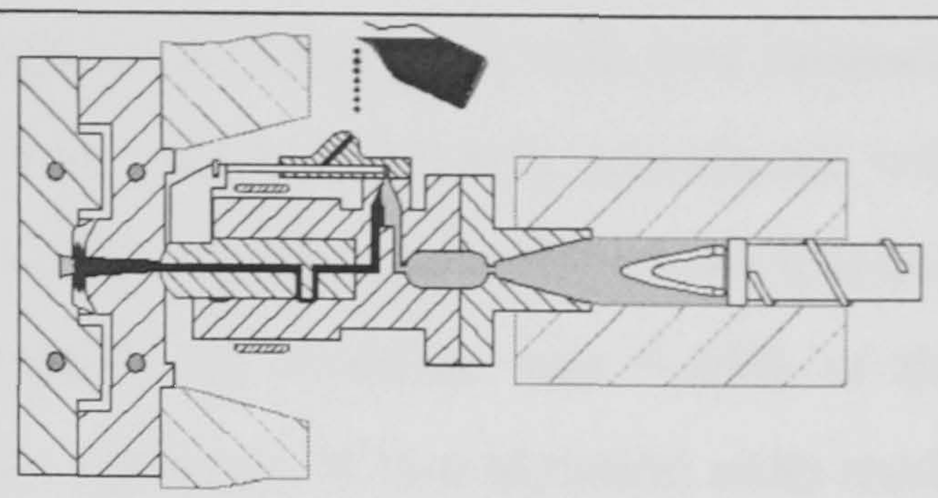

(b) sequentially inject the melts into the cavities

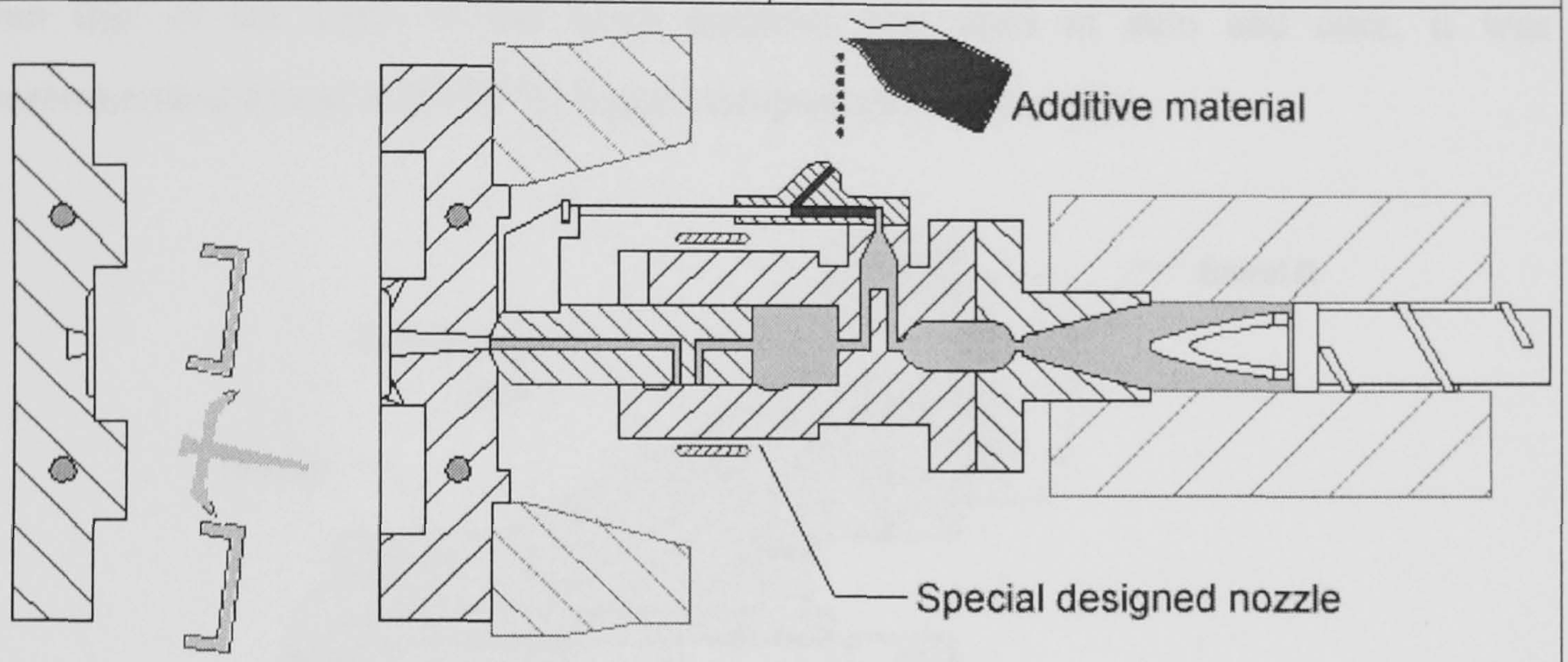

(c) open mould and ready for next cycle

Figure 2.4 The Addmix® mono-sandwich injection technique [17]

However, there was a modified version of mono-sandwich injection technique, originated by Addmix [17]. It was a similar technique to the Ferromatik one but without an ancillary extruder. Sufficient amount of materials were regulated from the separate hopper, which was controlled by a stroke measurement system; the polymers were layered and fed into one injection cylinder. The sandwich components were then moulded as mentioned previously.

2.2.2 Two-channel nozzle

2.2.2.1 Dual channel technique

The dual channel method, developed by Battenfeld [7-9] in the mid 1970s, included a phase of simultaneous injection. Two injection units were united through a specially

designed nozzle as seen in Figure 2.5. The nozzle was equipped with two separate, concentric channels that could be independently operated, opened, and closed with hydraulics. The duration of the simultaneous injection phase depended on the material and especially on the mould geometry. Typically the duration was 5-25% of the injection time for the skin component. Separate operation of two injection units made it easier to control skin thickness in various parts of a moulding. An optimum distribution of core material was obtained if the skin viscosity was kept slightly lower than that of the core. If the same material was used in skin and core, it was recommended to use a 20-30 °C higher temperature for the skin.

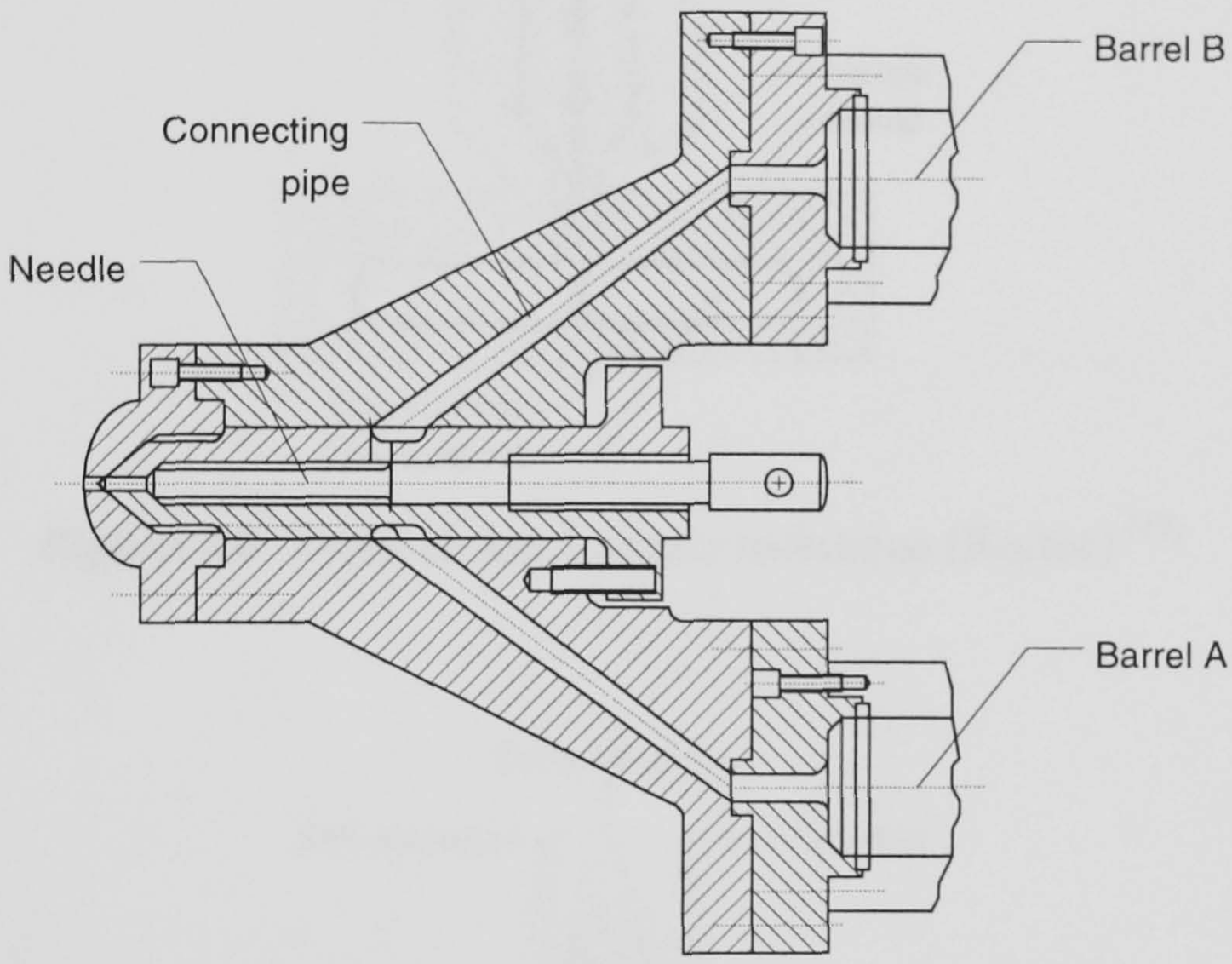

Figure 2.5 Two-channel nozzle technique (Battenfeld) [9, 18]

An advantage with the two-channel technique was the increased flexibility, such as the possibility to separately control the velocity profile of both skin and core during mould filling. Therefore the skin thickness could be adjusted in various parts of a moulding. Further amounts of skin material could be injected during holding time to seal the gate area with extra skin material and prepare for the next cycle.

2.2.3 Three-channel nozzle

A main disadvantage of those techniques described above was that, firstly, the skin thickness close to the gate area might become very thin, because frictional heat from

the flowing melts could make the skin re-melt and be flushed away in this region. Secondly, as expected, in the case of incompatible skin and core materials, the adhesion between both interfacial layers were poor. Thus, compatibilisers were needed.

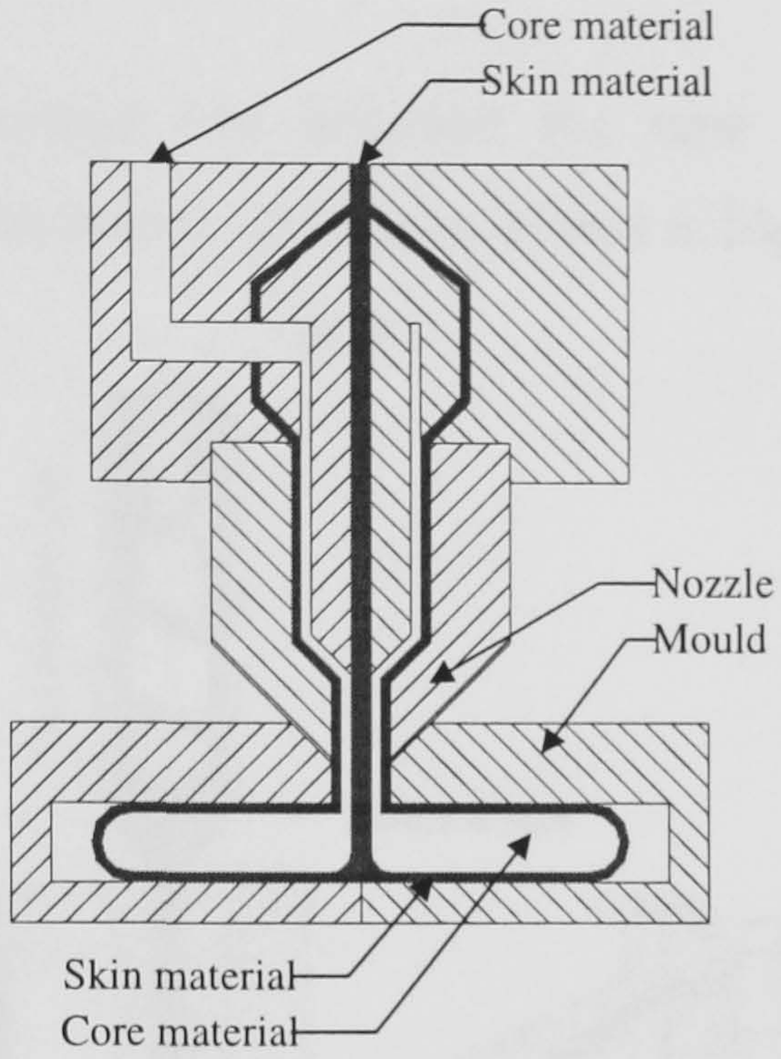

Figure 2.6 Three-channel nozzle technique (Kortec) [19]

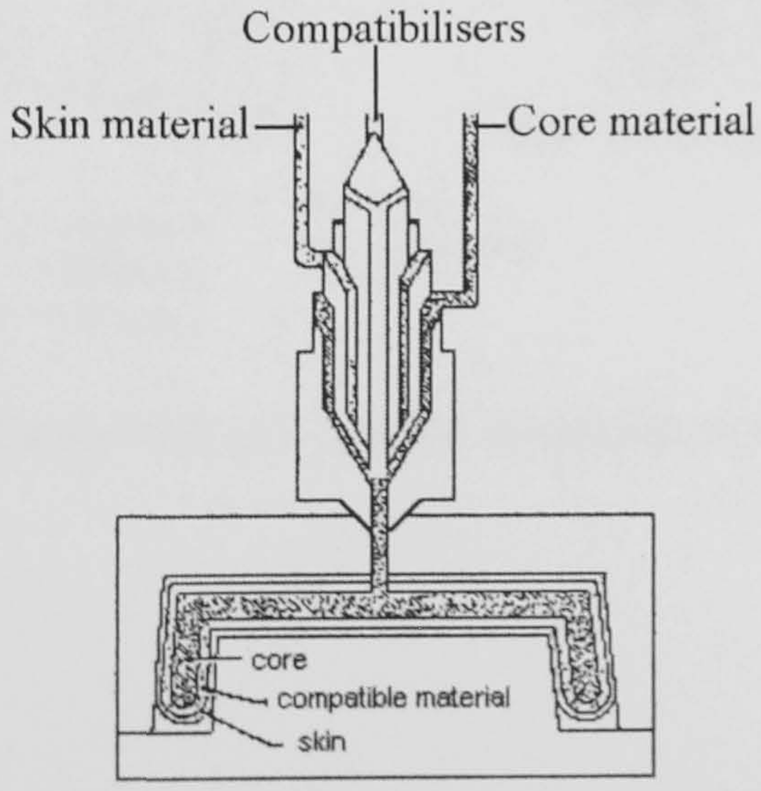

Figure 2.7 Three-channel nozzle technique (Billion) [20]

Therefore the three-channel technique was developed, as depicted in Figure 2.6 and 2.7. As seen in Figure 2.6, it was based on a three-channel nozzle with an auxiliary channel for the skin in the centre of the gate, which could reach the opposite side of the moulding. The injection of skin material to the two surfaces could be regulated separately, which gave an additional possibility to control thickness. Another

possibility was the solution to polymer incompatibility for sandwich injection moulding by using the third intermediate layer polymer as a binder adhesive; this process was proposed by the Billion Corporation of France [20]. There were obvious machine-cost disadvantages because the runner system was complex and there must be a third injection unit.

In the mean time, Battenfeld had invented the new three-channel co-injection moulding machine using the nozzle scheme as shown in Figure 2.8.

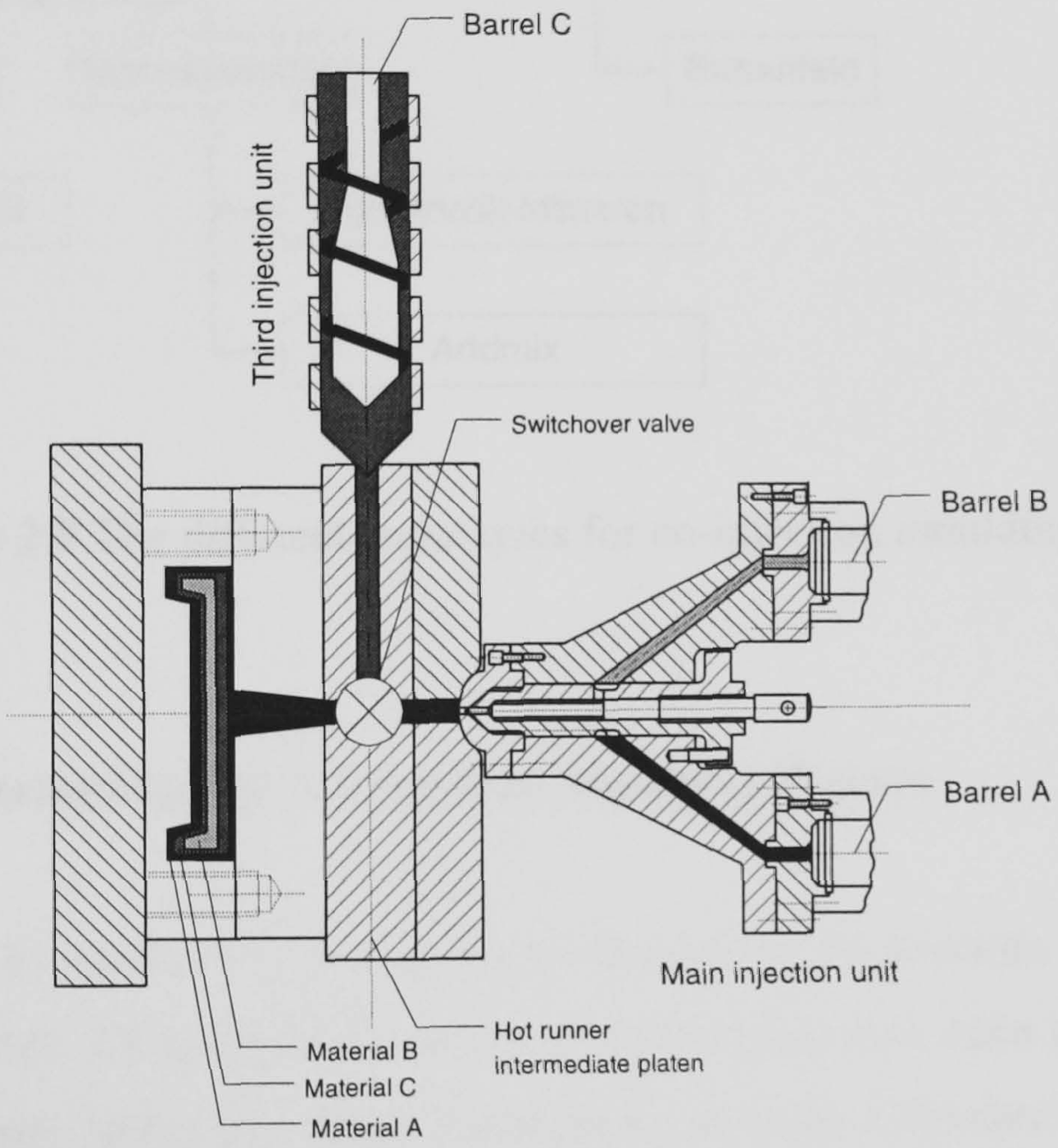

Figure 2.8 Three-channel nozzle technique (Battenfeld) [21]

The summary of co-injection moulding techniques was illustrated in Figure 2.9.

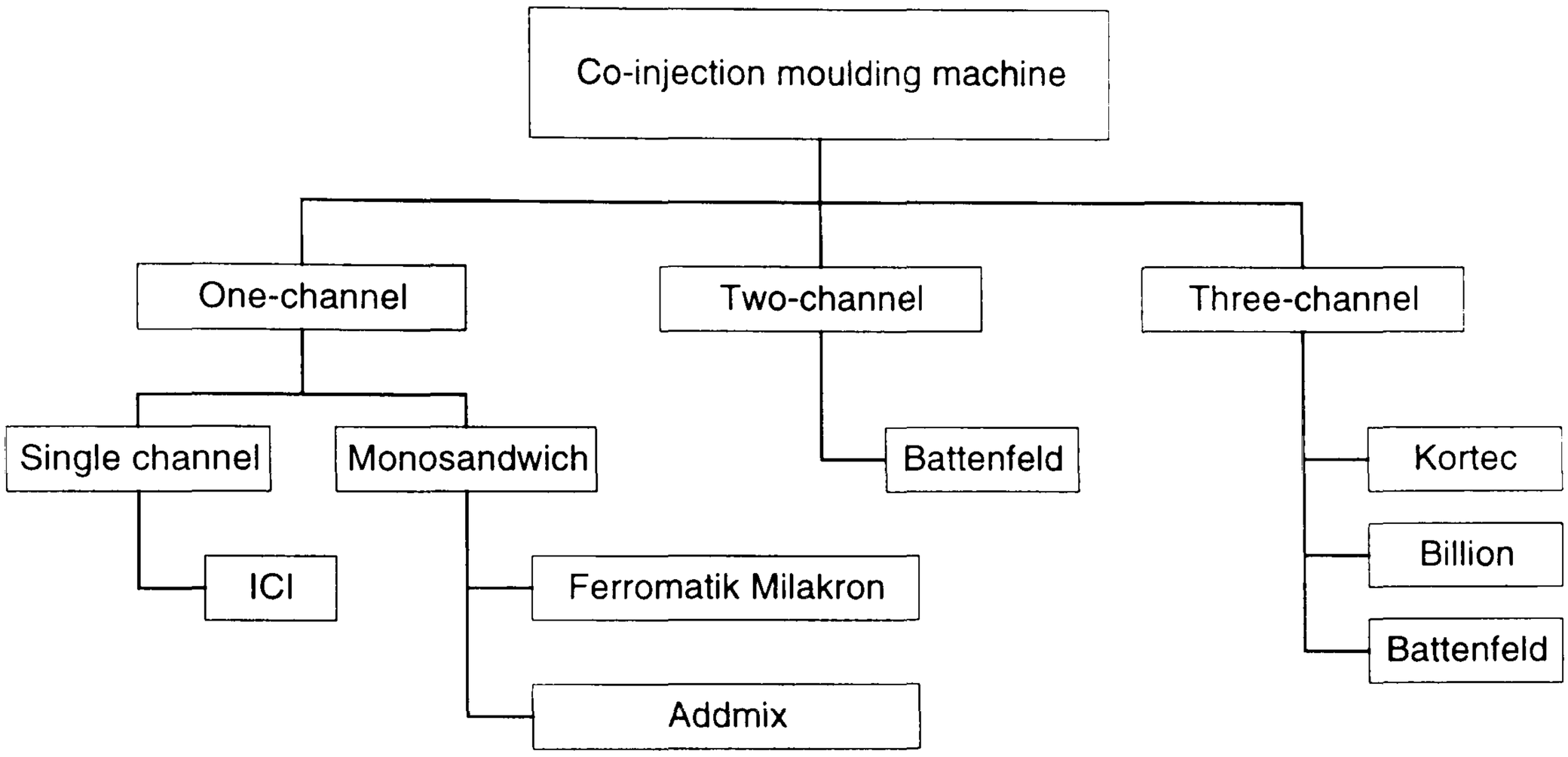

Figure 2.9 The different techniques for co-injection moulding process.

2.3 Process Technology for Co-injection Moulding Process

As mentioned in section 2.2, the various techniques for co-injection moulding process were investigated. However, those could be divided into two main groups: sequential and simultaneous technique. Brief descriptions of these techniques are described in the following section.

2.3.1 Sequential Co-injection Moulding Process [8-9]

It is common knowledge that one-channel nozzle co-injection or sandwich injection moulding machines has two cylinders in use. The melts are injected sequentially into the mould through the adjustable designed valve. The first injected melt forms the skin and conceals the core material which is injected afterwards.

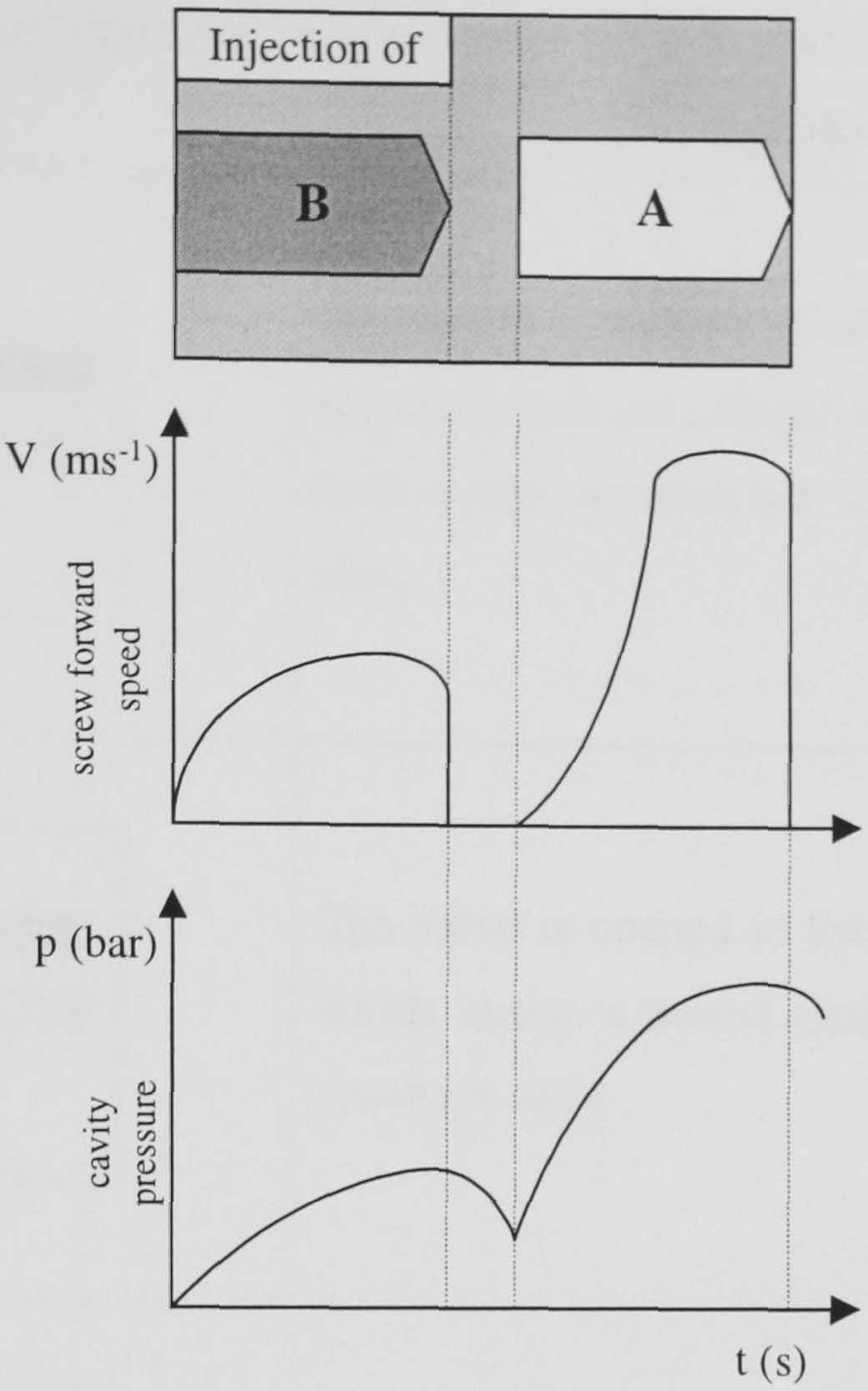

Figure 2.10 Diagram shows the mould filling principle of one-channel nozzle co-injection moulding process

When the core injection stroke is complete, the valve is switched over to the skin melt. As small amount of skin material as possible is injection first in order to ensure there is enough skin to cover the entire core. As a consequence of the flow behaviour of the melt along the flow path, the formation of skin frozen layer next to the mould wall occurs. A sandwich structure is accomplished. The mould filling principle and operating sequence of one-channel nozzle co-injection moulding are illustrated in Figure 2.10 and Table 2.1, respectively.

Table 2.1 Operating sequence of sequential co-injection moulding process

Stages	Details
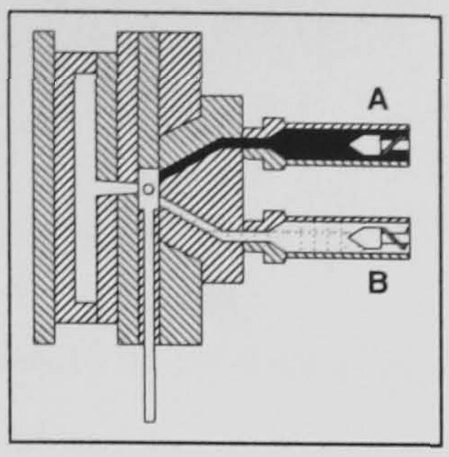 (1)	The mould is closed hydraulically, both injection units are charged with polymer, and both screws are retracted. The valve unit is shut.
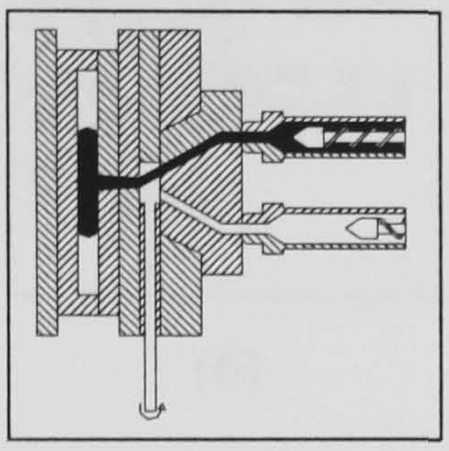 (2)	The valve is opened to the first injection unit, which injects a partial charge of skin material into the mould.
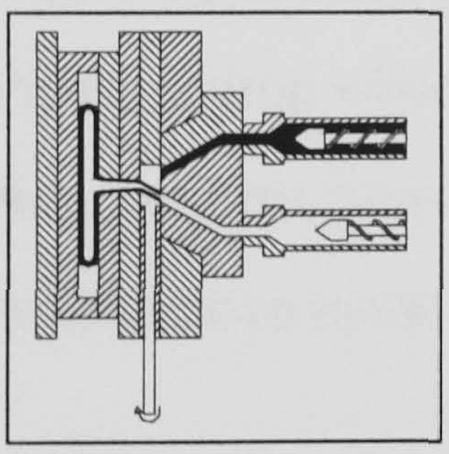 (3)	The valve is opened to the second injection unit, which injects core material into the mould, forcing the skin polymer outward.
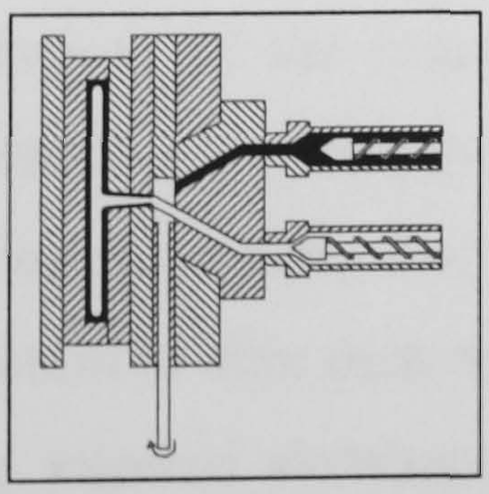 (4)	The full injection pressure of the second injection unit is applied to pack the mould and ensure a good surface finish.

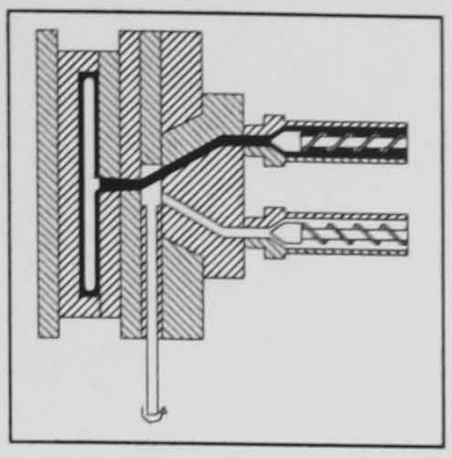 (5)	The valve is again opened to the first injection unit and a sufficient amount of skin polymer is injected into the mould cavity to clear the sprue of core polymer.
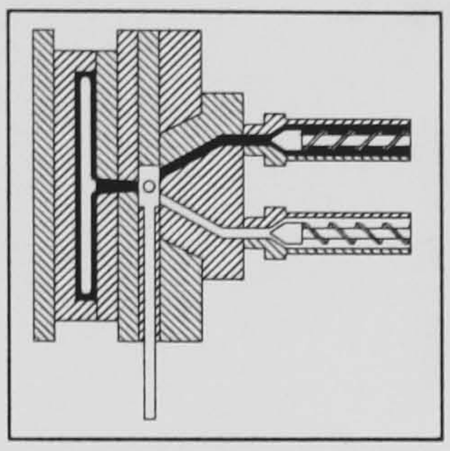 (6)	The valve unit is closed and full clamp pressure is held for a few seconds. While the component is cooling, the two injection units are recharged with polymer. At the end of the cooling time the mould is opened hydraulically and the sandwich moulded part was removed. The machine is then ready for the next moulding cycle.

However, there are several disadvantages of this technique as follows,

- Pressure drop when switching the melt
- Non-uniform core distribution
- A distinctive mark is left on a component (matt-ring around the gate)

2.3.2 Simultaneous Co-injection Moulding Process [8-9]

The limitations of the sequential co-injection moulding process are eliminated by application of the simultaneous phase, which can be produced by injecting skin overlap core materials. The filling of the mould with the two melts is commenced with injection of skin melt material, then core melt is admitted afterwards. Then both melts are injected simultaneously. The duration of simultaneous phase is usually about 5 to 25% of the metering stroke of skin material, dependent on the selected material and the geometry of the moulding. When the cavity is nearly filled, the core nozzle switches to shut off the core melt. A small amount of skin melt is then injected into the mould until end of injection stroke to ensure that the core melt is removed and does not contaminate the next cycle. The mould filling principal and details of

simultaneous co-injection moulding process are given in Figure 2.11 and Table 2.2, as follows.

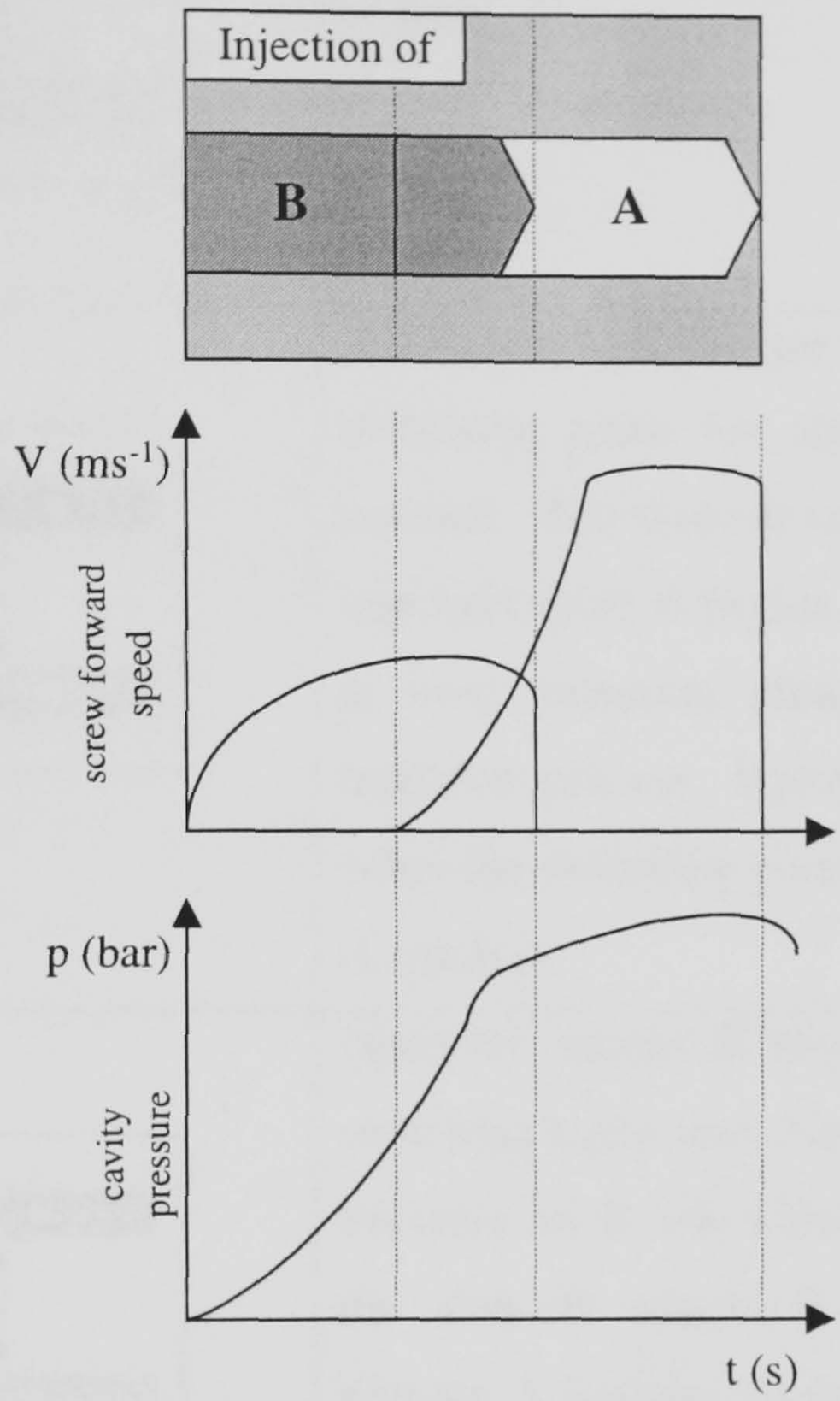

Figure 2.11 Diagram shows the mould filling principle of simultaneous co-injection moulding process.

Table 2.2 Operating sequence of simultaneous co-injection moulding process

Stages	Details
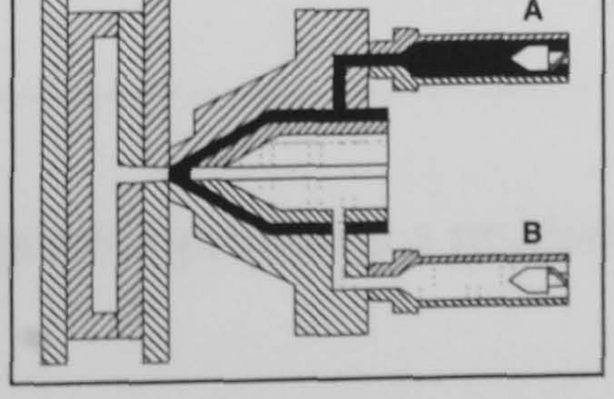 (1)	The nozzle contacts the mould, the shut-off nozzle A opens and the injection delay A begins.

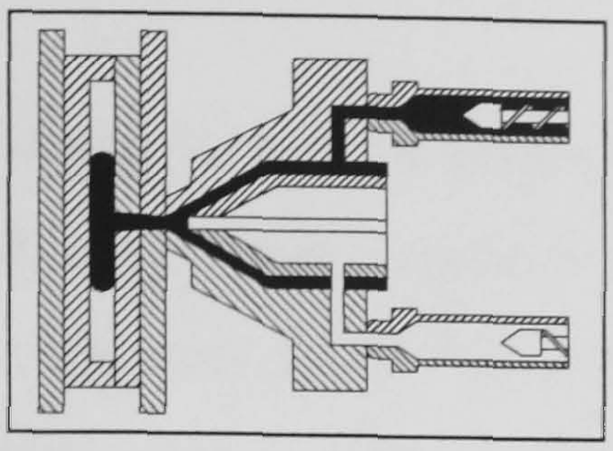 (2)	The injection plunger A adopts the injection process.
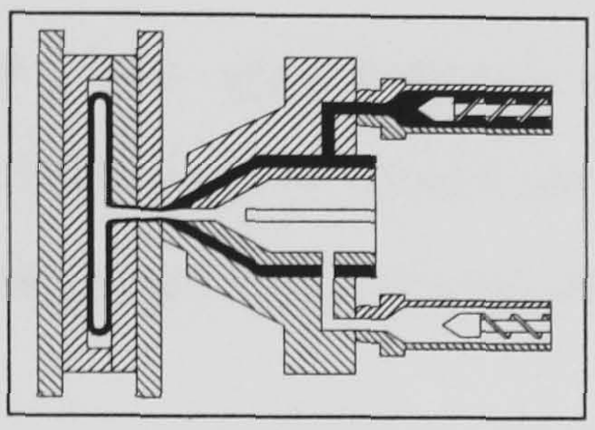 (3)	While injection plunger A is taking over, the switching point for starting injection B is reached. The shut-off nozzle B opens and the injection delay B begins. When the delay time is over, injection plunger B takes up the injection process. Injection plunger A stops when the switching point for holding pressure is reached.
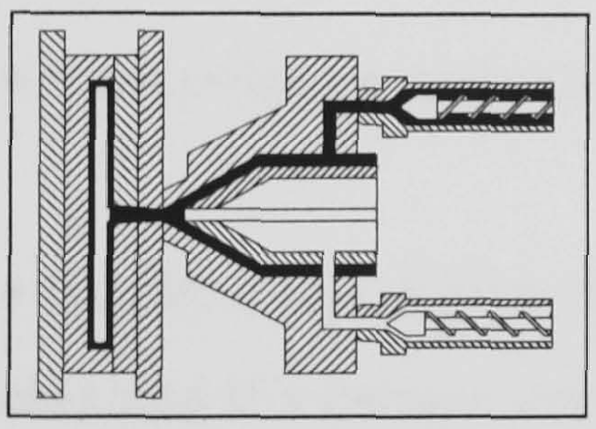 (4)	Injection plunger B runs until it reaches the switching point stop-injection 2nd component. Pressure on B side plunger is released. Then the shut-off nozzle B is closed. Injection plunger A imitates its activity once again and injects with holding pressure to continue to pack the mould.
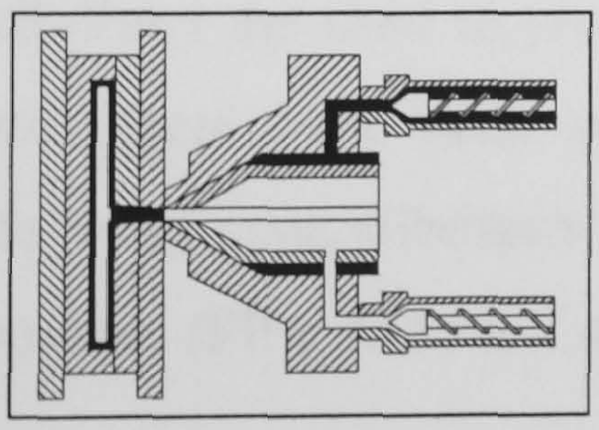 (5)	After the holding pressure time is over, the shut-off nozzle A closes and pressure on A side plunger is released. Cooling and metering time processes are then started.

The sequence produces a product which could be referred to as A-B-A or Skin–Core–Skin.

2.4 Material Selection [7-9]

The selection of raw materials for using as skin and core depends on the properties required of the final moulded part. Care has to be taken that the selected materials adhere with each other. Nevertheless, there are several criteria for process moulding from which good adhesion skin-core components, can be acquired. Therefore, for good adhesion, the materials should:

- Have approximately the same shrinkage and thermal expansion. A large difference in mould shrinkage and thermal expansion can give sink marks, warpage, and residual stresses.

- Adhesion between the raw materials must be good. This is particularly important when the component is exposed to mechanical load. If adhesion is poor, the core material could easily detach from the skin.

- Each polymer must have the same range of processing temperature.

- Exhibit same degree of bonding at the interface. A good bonding strength is obtained if a certain amount of interdiffusion occurs between the melts. It can be achieved when there is high compatibility or solubility between the melts.

Compatibilisers are used to promote bonding among the incompatible thermoplastic polymers. There have been several studies on the combination of incompatible polymers using compatibilisers [10-15, 22-23], such as utilising maleic anhydride grafted polypropylene (PP-g-MA) to interface polyamide (PA) with polypropylene (PP) [11-12, 22, 24].

The table of compatible and incompatible thermoplastic combinations is shown in Table 2.3.

Table 2.3 Combinations of some frequently used thermoplastics [7-9].

	ABS	ASA	EVA	PA6	PA66	PBT	PC	PE-HD	PE-LD	PET	PMMA	POM	PP	PPO.mod.	PS-GP	PS-HI	PVAC	PVC-W	SAN	TPU
ABS	+	+	+			+	+	-	-	+	+	-	-	-	*	*		+	+	+
ASA	+	+	+			+	+	-	-	+	+	-	-	-	*	-		+	+	+
EVA	+	+	+					+	+				+		+	+			+	
PA6				+	+	*	*	*	*			-	*	-	-	-			+	+
PA66				+	+	*	*	*	*			-	-	-	-	-			+	+
PBT	+	+		*	*	+	+	-	-	+	-	-	-	-	-	-		+	+	+
PC	+	+		*	*	+	+	-	-	+		-	-	-	-	-			+	+
PE-HD	-	-	+	*	*	-	-	+	+	-	*	*	-	-	-	-		-	-	-
PE-LD	-	-	+	*	*	-	-	+	+	-	*	*	+	-	*	-		-	-	-
PET	+	+				+	+	-	-	+	-	-		-	-	-				+
PMMA	+	+				-		*	*	-	+		*	-	-	-		+	+	
POM	-	-		-	-	-	-	*	*	-		+	-	-	-	-			-	
PP	-	-	+	*	-	-	-	-	+		*	-	+	-	-	-		-	-	-
PPO.mod.	-	-		-	-	-	-	-	-	-	-	-	-	+	+	+		-	*	-
PS-GP	*	*	+	-	-	-	-	-	*	-	-	-	-	+	+	+		-	-	-
PS-HI	*	-	+	-	-	-	-	-	-	-	-	-	-	+	+	+		-	-	-
PVAC																	+			
PVC-W	+	+				+		-	-		+		-	-	-	-		+	+	+
SAN	+	+	+	+	+	+	+	-	-		+	-	-	*	-	-		+	+	+
TPU	+	+		+	+	+	+	-	-	+			-	-	-	-		+	+	+

(-) : No adhesion, (*) : Poor adhesion, (+) : Good adhesion

2.5 Mould Technology for Co-injection Moulding Process

The injection moulding technology has been developed since 1869 [8, 25-30]. It is a very large subject on which much has been published and much discussed in a number of books. As mentioned, co-injection moulding process is similar to conventional single injection moulding. Such differences are the number of materials, a special designed nozzle, or auxiliary unit. However, mould designs and the technology of co-injection moulding is related to the conventional injection moulding. A brief review of the major types of injection mould tools associated with co-injection moulding process are given in the following section.

2.5.1 Types of Moulds [25-30]

Injection mould designs differ depending on the type of material being moulded; these necessitate various gating and ejection systems to achieve application with maximum economy.

2.5.1.1 Two-plate Mould (Standard mould)

This is the simplest mould design. Mould cavities are assembled to one plate and forced to the other plate. With the central sprue bushing placed into the stationary half of the mould, it is possible to have a direct runner system to a multi-impression mould or direct centre gate to a single-impression mould. The moving half of the mould basically contains the forces and the ejection mechanism. This is the fundamental design for injection moulding and all other designs are developed from this option which is illustrated in Figure 2.12.

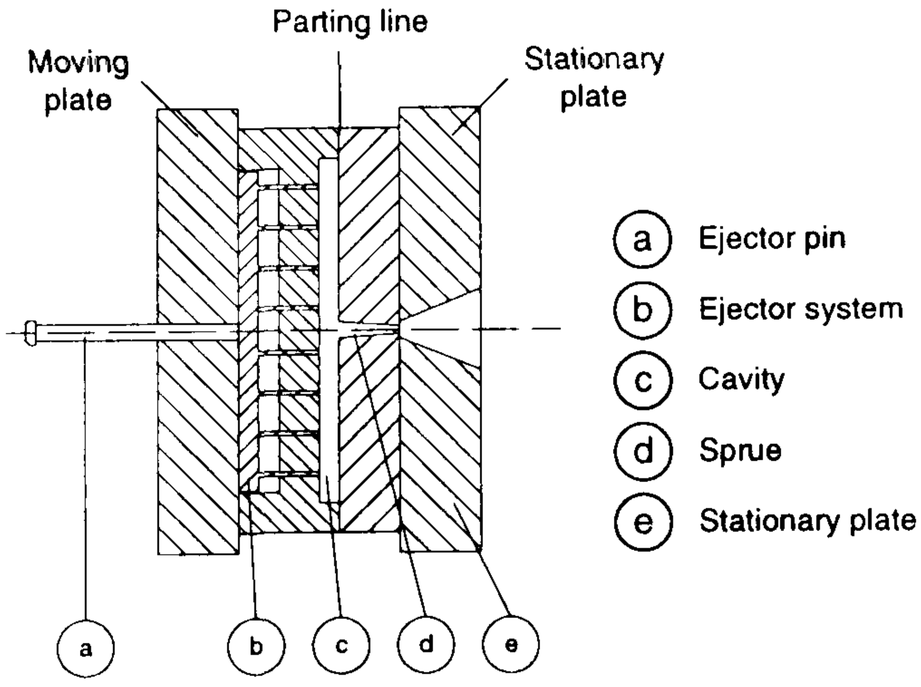

Figure 2.12 Two-plate injection mould

2.5.1.2 Stripper Mould

This type of mould is similar to the standard two-plate mould, only the ejection system is different. The stripper plate mould has a stripper plate for ejection, whereas the standard one has pins or sleeve as ejector. The cup-like shaped mould without undercut is suitable to be produced with this kind of mould.

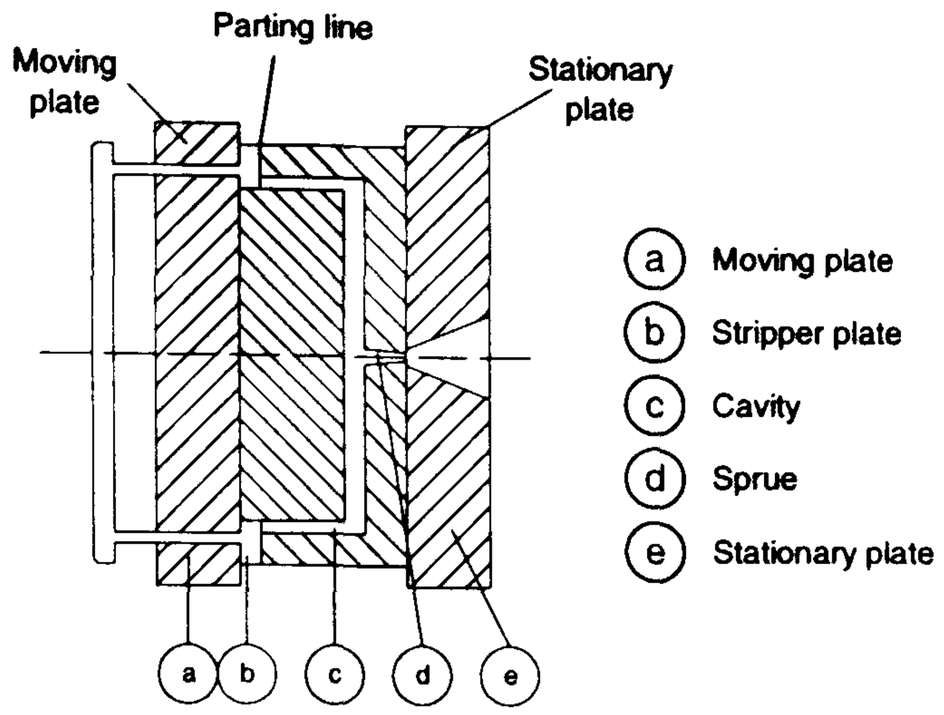

Figure 2.13 Mould with stripper plate

2.5.1.3 Slide Mould

This type is also the same as the standard two-plate mould, but with slides and cam pins for additional lateral movement. It is usually designed for producing parts with undercuts or external threads. The schematically design of the slide mould is given in Figure 2.14.

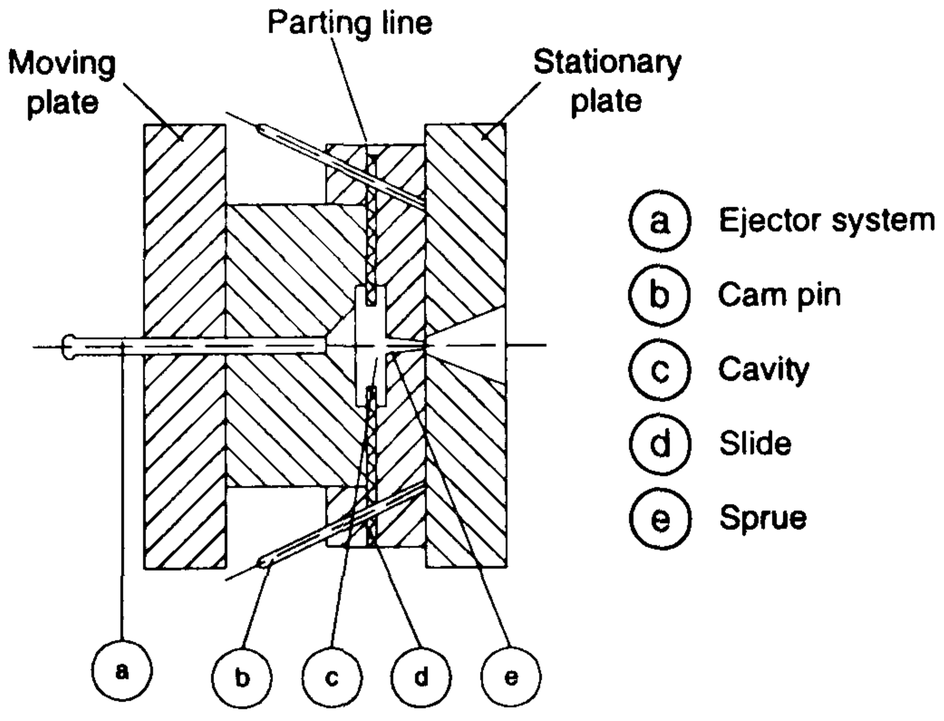

Figure 2.14 Slide mould

2.5.1.4 Split Cavity Mould

This is designed similar to the standard one but with split cavity block for moulding the undercut or external thread parts.

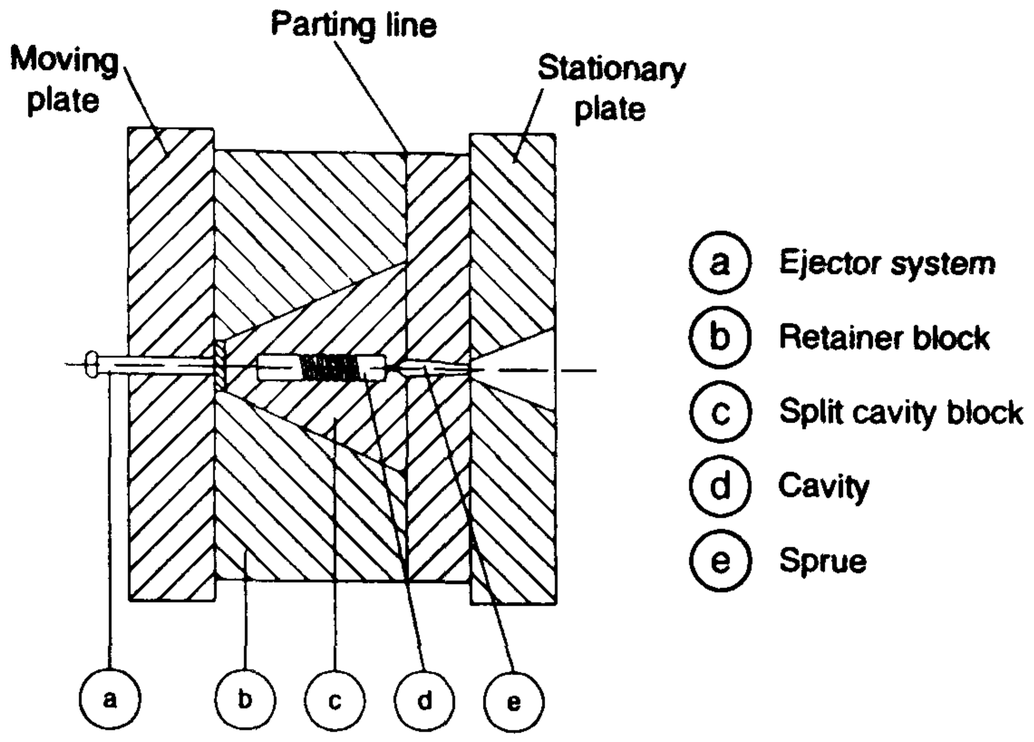

Figure 2.15 Split cavity mould

2.5.1.5 Three-plate Mould

This design is one of the popular moulds and widely used. By introduction of another intermediate and movable plate, which normally contains the cavities for the multi-impression moulds, it allows centre or offset gating of each cavity from the runner system and connects to the central sprue bushing. The three-plate mould design is illustrated in Figure 2.16.

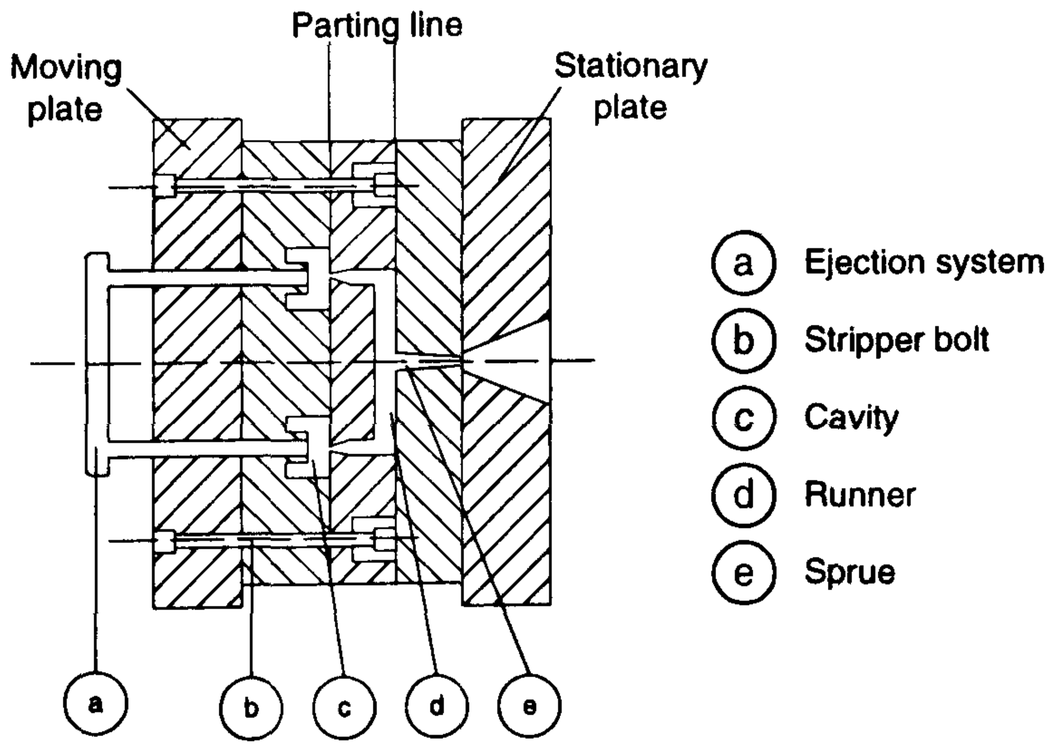

Figure 2.16 Three-plate mould

2.5.2 Cavity Designs [25-27]

If the component can be produced by any injection moulding process, the first thing to be decided for tool design, is whether or not to produce the component by either a single-impression or multi-impression mould. However, it is not only the number of

cavities, but the size and shape of the component that has to be taken into account. In general for the injection machine, the barrel is usually positioned in the central axis of the stationary platen. Thus, the cavities have to be arranged relative to the central sprue. There are some criteria to meet the condition as follows:

- All cavities should be filled at the same time with melt of the same temp.
- The flow length should be short to keep scrap to minimum.
- The distance between each impression should be sufficient to provide for placement of an efficient cooling line.
- The sum of all reactive forces should be in the centre of gravity of the platen.

Therefore, the possible option of the cavities layout can be arranged as shown in Table 2.4.

Table 2.4 The cavity layouts

Impression and Layout	Details
Single-impression 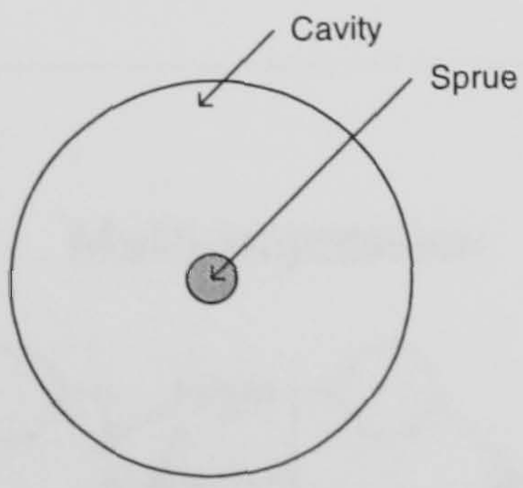 n= 1	No need to balance runner

Multi-impression 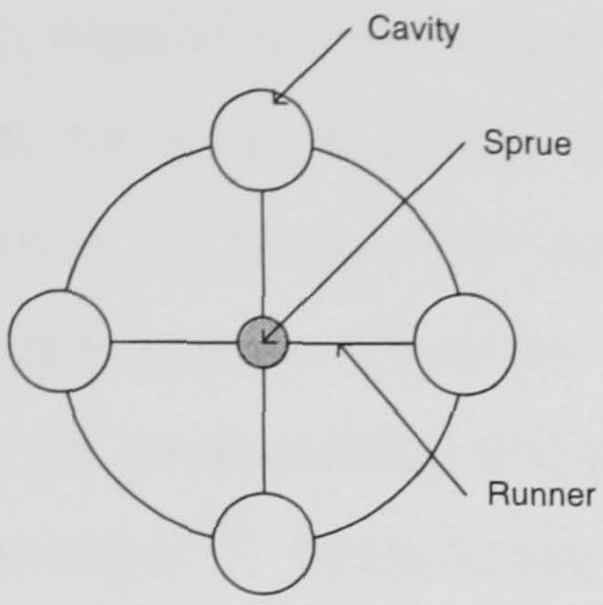 n= 2, 3, 4, ... Circular layout	Equal flow lengths to all cavities but only limited number of cavities can be accommodated.
Multi-impression 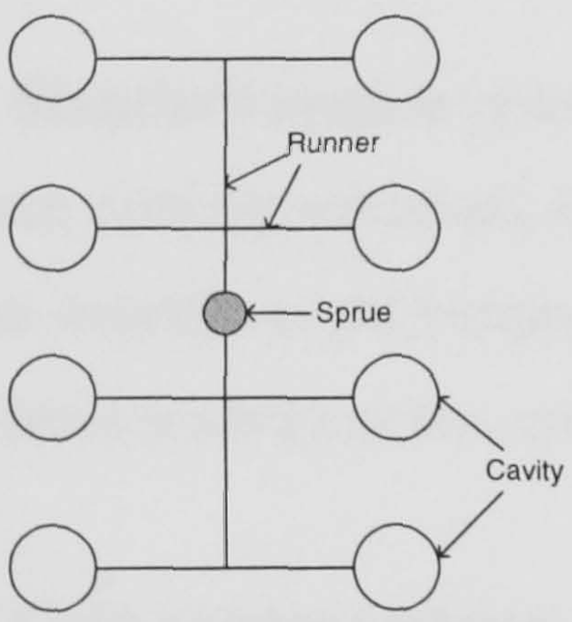 n= 2, 4, 6, ... Layout in series	Can place more cavities than the circular layout but need optimisation of the runner system to achieve uniform filling of the cavities.
Multi-impression 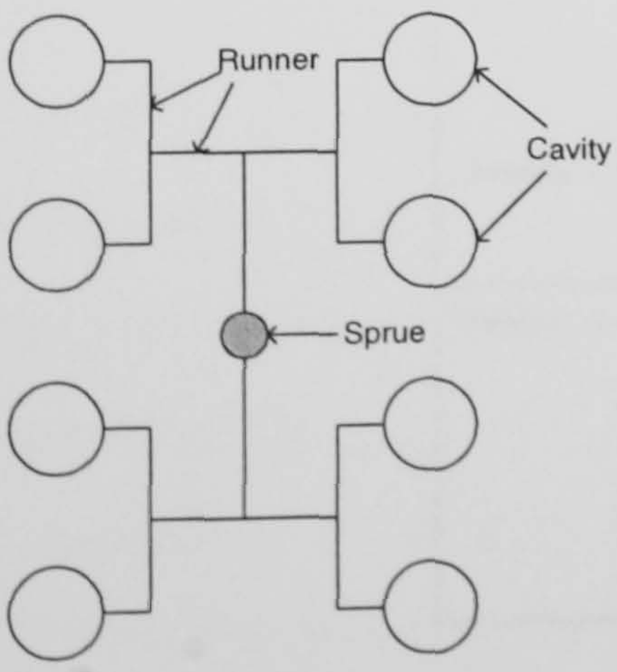 n= 2, 4, 8, ... Symmetrical layout	Equal flow lengths to all cavities without gate and runner correction. But leave a large number/volume (scrap) and produces rapid cooling of melt. That means it is more suitable for hot runner systems.

2.5.3 Runner Systems [25-28, 31]

Ideally, runners are to connect the sprue via the gate to the cavity. A runner acts as the path for material melt to flow evenly into the cavity at the same rate. When the melt enters the runner, heat can transfer from the melt close to the walls. Frozen layer of material occurs. Thus, the proper runner size, which can ensure the melt will not freeze off prematurely, should have a minimum value for its surface area-to-its volume ratio [25]. Several types of runner (cross section) are shown in Figure 2.17. It is found that the round and square runner shape are favourite types. However, the square runner is not very satisfactory because it is difficult to inject. Nevertheless, the runner systems can be divided into three main types; standard runner, cold runner and hot runner.

2.5.3.1 Standard runner systems

These are directly machined into the mould plates, so their temperature corresponds with the overall mould temperature, usually 20 to 120 °C. The material melt in the runner freezes after cavities are fully filled and packed by holding pressure.

2.5.3.2 Cold-runner systems

This type of runner system is suitable for reactive material such as thermosetting material or rubber. It can overcome the premature reaction of these materials in the runner by keeping the runner cold.

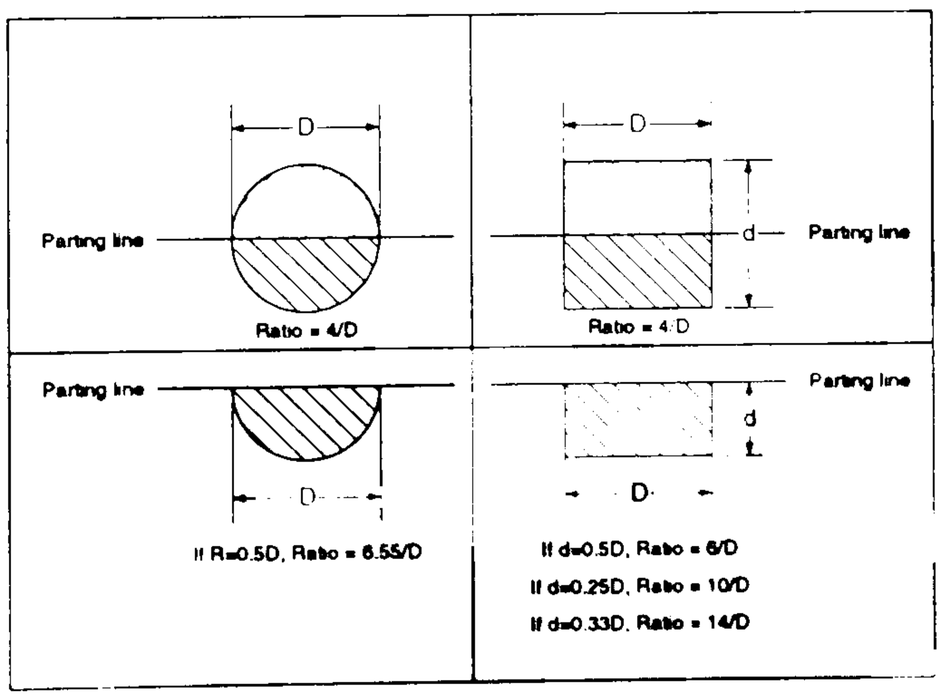

Figure 2.17 The surface area-to-volume ratios of various types of runner cross section.

2.5.3.3 Hot-runner systems

The hot-runner systems of a thermoplastic, used in typical injection moulding machines or co-injection moulding machines [31], have a heated manifold to keep the material melts from premature freeze off in the runner. Basically, the hot-runner system has a temperature of more than 180 °C which is in the range of melt temperature of thermoplastics and significantly higher than the standard runner system. In addition, the material can be saved because the runner content does not need to be demoulded and is available for the next shot. Moreover, it can be taken into account for the thin-part design. However, the disadvantages of the hot-runner system can be described as follows:

- More rejects at least during start-up.
- Higher mould cost from installation of auxiliary equipment such as heaters, temperature controllers and sensors.
- Material degradation occurs because of long flow paths and high shear velocity.
- Uneven melt temperature distribution results in non-uniform filling.

2.5.4 Mould Cooling Systems [25-28]

Mould cooling is essential to all types of the injection moulding process for both cost saving and quality control. The major purpose of the mould cooling system is to minimise cycle time and to minimise thermal differences in mould part cooling. Rapid cooling improves process economics while uniform cooling improves product quality by preventing differential shrinkage, high residual stress and mould release problems. In addition, uniform cooling can ensure a shorter moulding cycle. To meet these purposes, the coolant, size and layout of cooling channel play an important part in the production of a good moulding. A brief description of the coolant and its channel design is given as follows:

2.5.4.1 Coolant

Most thermoplastics moulding are produced using tool temperatures of 20 to 60 °C. For this range of temperature, water circulation is often employed. A water-base system may reach 140 °C in some case. Alternatively, an oil-base system is suitable for required tool temperatures of more than 160 °C up to 350 °C, whereas temperatures lower than 25 °C require water/glycol (anti-freeze) mixture system.

2.5.4.2 Cooling channel

To perform the uniform cooling of moulding, some guidelines [8, 25-27] can be followed:

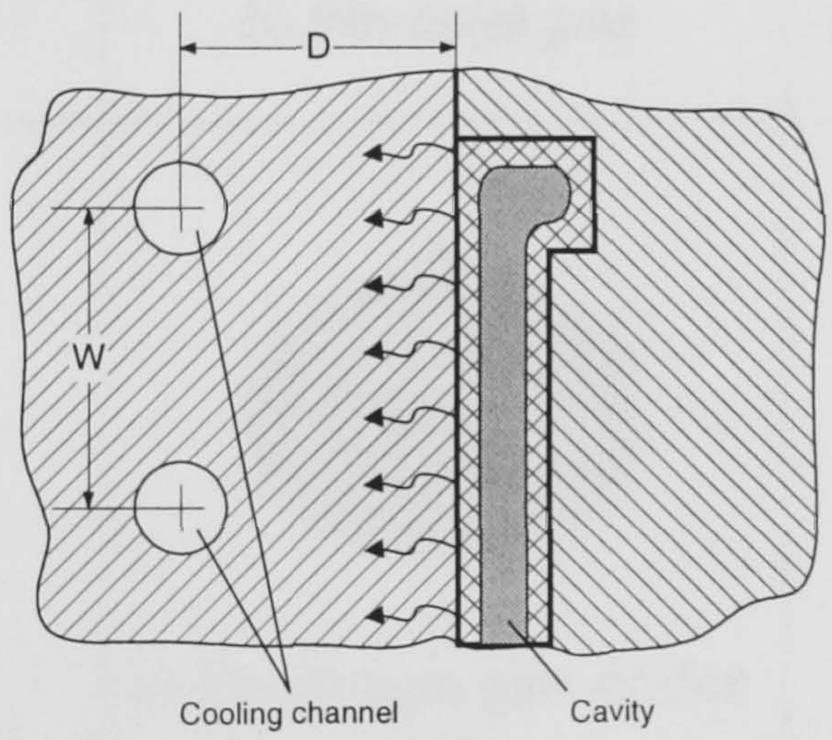

Figure 2.18 Layout of the cooling channel

Distances of cooling channel:

D lies between d_c to $5d_c$ and W lies between $2d_c$ and $5d_c$

Where d_c is diameter of cooling channel.

D is the depth of the cooling lines from the moulding surface.

W is the width of the pitch.

Increasing D reduces the heat transfer efficiency, and a large value of W results in a non-uniform tool temperature.

2.5.5 Gating Systems [25-28]

The standard gating systems are shown in Table 2.5, which have been used for conventional injection moulding and could be appropriate for co-injection moulding process as well. The gating systems are as follows,

Table 2.5 The standard gating system.

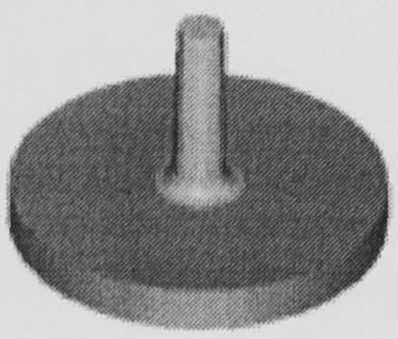 a) Sprue gate	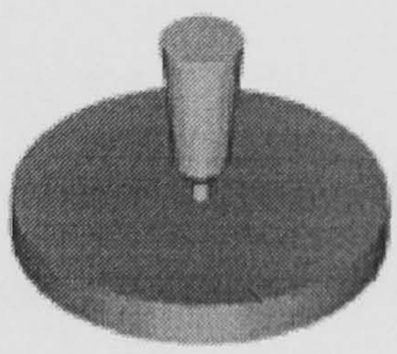 b) Pin-point gate	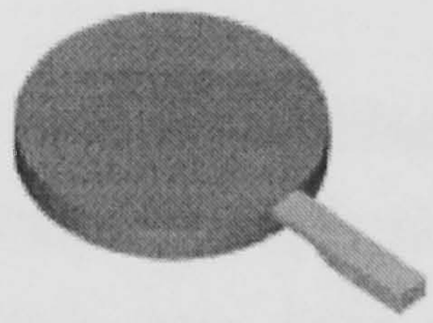 c) Side gate or edge gate
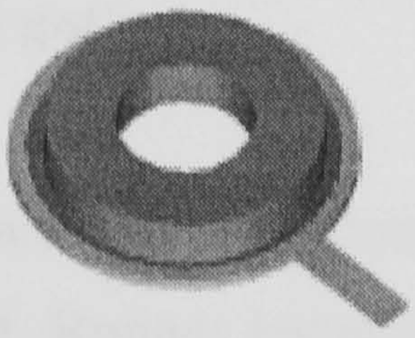 d) Ring gate	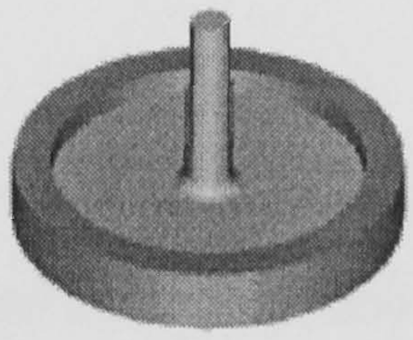 e) Diaphragm gate or disc gate	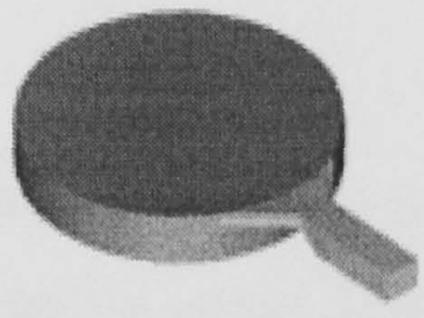 f) Fan gate
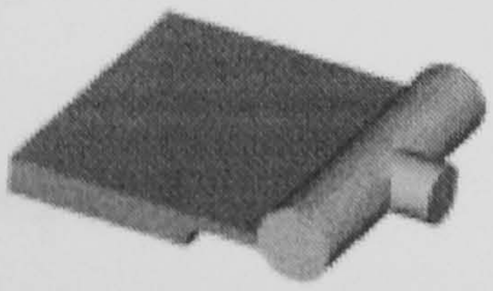 g) Film gate or flash gate	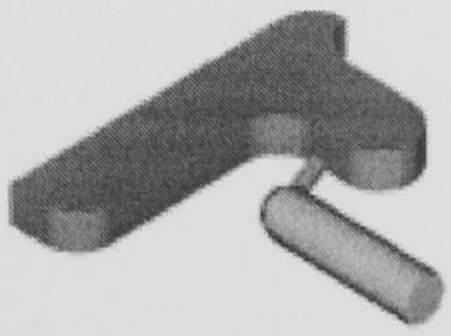 h) Tab gate	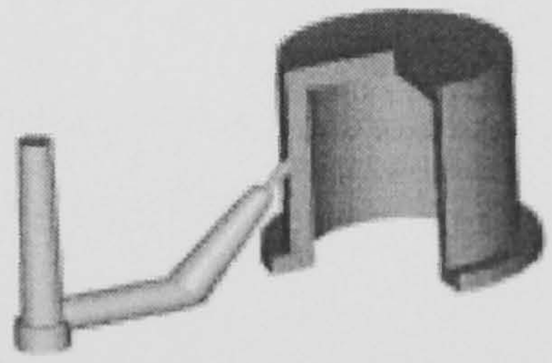 i) Tunnel gate or submarine gate

The function of these gating systems is described as follows:

a) Sprue gate

This is the most common gate system. The moulding is directly fed from a sprue. It is used for large single-impression mouldings as it is relatively easy to machine. By the way, this type of gate leaves a large gate mark on the moulding.

b) Pin-point gate

This is suitable for the three-plate moulds. The gate serves to ease of finishing and high shear rates can be generated near the gate. This means that there is a reduction in material viscosity and filling becomes easier. Such high shear rates have been employed so as to allow long cavities to be filled.

c) Side gate

This gate type is commonly used for multi-cavity tools. They feed the side of the product. Runner balancing is needed in case of multi-cavity tools to make sure that there is pressure distribution throughout the system. Unbalanced runners can give a moulding of unequal quality because the pressure and flow are not identical for the cavity area close to the sprue compared with the other points located far from the sprue.

d) Ring gate

A ring gate is employed for cylindrical parts, which requires the core to be supported at both ends because of its length. The melt passes through the sprue first into an annular channel, which is connected with the part by a land and this acts as a throttle during filling. In this gate system, a weld line in the ring gate occurs but is hardly visible or not at all.

e) Diaphragm gate or disc gate

This is used for single impression tubular shaped components on two-plate moulds. The sprue leads into a circular runner, smaller than the inside diameter of the tube. It forms a disc of material and allows material flow to radiate from the sprue to the gate.

f) Fan gate

This is a wide gate formed by opening the runner out so that it blends into the wide-thin impression. The gate cross-section is still relatively small, or restricted such that it leads to ease of finishing. The fan gate can help to distribute the melt into the cavity, thus, a weld-line can be minimised by this gate.

g) Film gate or flash gate

This gate provides oriental distribution and provides for flatness in a flat moulding. It is frequently used for transparent products like PMMA or PC. This gate can be used for minimising distortion in particular, in fibre-filled materials.

h) Tab gate

This gate is a particular gating technique for transparent materials where flow marks can be reduced to a minimum. It can eliminate jetting in large plane areas by breaking the flow. The melt is thereby caused to advance in a smooth steady flow resulting in a uniformly filled cavity.

i) Tunnel gate or submarine gate

This gate is a circular or oval gate, submerged and fed into the impression below the parting line of the mould. The gate is usually located in the moving half of the mould and, when the mould opens, the gate is sheared by the ejection action. This type of gate is usually used for small components in automatic moulds.

2.5.6 Ejection Systems

After a component has solidified and cooled down, it is removed from the mould cavity. It would be ideal if gravity could separate the part from cavity or core after mould opening. The moulding would then be kept in place. However, component with undercuts, adhesion and internal stresses have to be separated and removed from the mould by special means.

Ejection equipment is usually actuated mechanically by the opening stroke of the moulding machine. If this simple arrangement is insufficient, ejection can be performed pneumatically or hydraulicly. Manually actuated ejection can only be found in very small or prototype moulds and for small series if little force is necessary for actuating ejection and an exact cycle is of no matter. Another situation takes into account that large-components can be demoulded by pushing them out, when they must not be ejected. They are removed manually or by robot after being loosened.

The ejector system is normally housed in the movable mould half. Mould opening causes the mechanically actuated ejector system to move towards the parting line and to eject the moulding. Result of this procedure is that the moulding stays on or in the movable mould half. This can be achieved by undercuts or by letting the moulding shrink onto a core. Taper and surface treatment should prevent too much adhesion. However, this should be avoided or more complicated demoulding systems are needed.

A brief of ejection systems was given as following in Table 2.6,

Table 2.6 Several types of ejection systems.

Types	Ejection methods	Components of operation	Applications
Standard system for small parts	During opening stoke thrust in direction of demoulding, ejection with pins, sleeves or stripper plate.	Mechanical, hydraulic, pneumatic, manual, machine stop, lifting cylinder, cam, pivot, inclined plane, thrust plate.	Moulding of all kinds without undercut.
Direction of ejection towards movable side, stripping is used but usually for circular parts only.	During opening stroke pull in direction of demoulding, ejection with stripper plate.	Mechanical, hydraulic, pneumatic, stripper bolt, lifting cylinder, pin-link chain.	Cup-like mouldings with internal gate.
Demoulding at two parting lines for automatic operation including separation of gate)	During opening stroke thrust in direction of demoulding, ejection with pins, sleeves or stripper plate.	Mechanical, stripper bolt.	Mouldings with automatic gate separation.
Demoulding of parts with local undercuts (slide mould).)	During opening stroke thrust in direction of demoulding, ejection with pins, sleeves or stripper plate after release of undercut.	Mechanical, cam pins, slide mechanism.	Flat parts with external undercuts (threads).
Demoulding of large, full-side undercut (split-cavity mould).	During opening stroke thrust in direction of demoulding, ejection with pins.	Mechanical, hydraulic, springs, links, pins, cams.	Parts with external undercuts (ribs) or opening in side wall.
Air ejectors usually provide support. Breaking is done mechanically.	Thrust in direction of demoulding cause a first release followed by ejection with compressed air.	Mechanical-pneumatic in stages.	Cup-like, deep parts.

2.6 Previous Mould Filling Studies of Co-injection Moulding Process

Several investigations dealing with sandwich moulding has been published. Almost all deal with the one-channel technique. A brief review on these studies is given in the following section.

White and Dee [32] studied mould filling in thin rectangular plates. They found that the skin should have a significantly lower viscosity than the core to obtain a good skin-core structure.

A relatively investigation was performed by Young et al. [33]. Six polymers were studied. These polymers were two polystyrenes, two high-density polyethylenes, a low-density polyethylene, and a polypropylene. Their viscosities were measured as a function of shear stress. The ratio of zero shear viscosities was determined from these data measurements and varied between 0.04 to 24.0 (depending on the material that formed the skin). The process used a screw extruder and a ram injection moulding machine. An adjustable valve regulated the sequence of the melts entering the mould. The mould was a square plate with a gate positioned centrally on one of the long sides. It was equipped with a glass window so that mould filling could be observed. They found that the most uniform skin thickness occurred when the ratio of zero shear viscosities was between 1.5 and 2.0.

Mould filling studies on circular plates, diameter 180 mm, thickness 3 mm, gated at the centre, were also made by Schlatter et al. [9, 34]. Studies were performed with the mono sandwich technique on two polystyrene (PS) melts, one with a slightly higher viscosity. The parameters investigated were flow rate, melt temperature, and volume ratio skin/core. The core was coloured with a masterbatch for identification. The position of the interface was measured by cutting the plates along the radius and measuring layer thickness with a microscope. They found that when the core injection rate increased a lower skin thickness was obtained. Skin temperature also had some effect. And when the skin temperature was increased, a slightly thinner skin was obtained.

Donovan et al. [6] also studied mould filling. They used a two-shot nozzle with one polymer flowing axially through a cylindrical passage at the centre of the nozzle and the other surrounding the first polymer. Different mould geometries were studied, such as end-gated plaque moulds, centre-gated disc moulds, and in some cases also telephone housing and handle moulds. A variety of coloured acrylonitrile-butadiene-styrene (ABS) moulding compounds were used, including scrap ABS. Mould filling simulation was performed with a computer program described by Lord [35]. Interface shape was measured for plaque and disc moulds and compared with the simulation results. Skin thickness was measured by sectioning the parts and using an optical comparator attached to a microscope. Typical results for the disc mould were obtained with 52% and 62% core material by volume. In general there was a good agreement between experiments and the simulations.

Somnuk and Smith [36] using a Battenfeld co-injection machine performed mould-filling studies with the two-channel technique. The dimensions of the injected plates were 100 x 75 x 4 mm. Four grades of polypropylene with differing viscosities were studied. Viscosity data was obtained from the material supplier and the ratio of viscosity varied between 0.54 to 1.83, measured at a shear rate of 10^3 s^{-1}. Mould filling was studied with a mould equipped with a Pyrex-glass window. Optimum mould filling was obtained when the viscosity ratio between skin/core was 0.8-1.8. They claimed that, at approximately equal viscosity, good mould filling results were obtained by letting the duration of the simultaneous injection period correspond to almost 95% of the injection time for the skin. It was also found that by changing the skin/core volume ratio and their relative velocity a better skin core morphology could be obtained.

Lanvers et al. [37] performed extensive mould-filling studies with co-injection moulding machine at the IKV in Aachen, Germany. The Mould filling was examined starting from the viscosity ratios between skin and the core (η_{skin}/η_{core}). A relatively large number of materials were determined, such as PP, PS, HDPE, PBT, and PA 66, and variations of these, with and without filler. By cutting thin injection moulded plates along the flow direction, the shape of the interface between the melts at the flow front was studied. They found that the interface structure of the component had

in all cases a parabolic shape. A more sharp-angled, wedge-shaped profile was obtained if the core had a higher viscosity than the skin, a blunter profile was obtained if the core had a lower viscosity than the skin.

The previous works were summarised as below:

Workers	**Co-injection techniques**	**Claims**
White and Dee	Single channel (sequential)	$\eta_{skin} \leq \eta_{core}$ led good skin-core structure.
Young et al.	Single channel (sequential)	$1.5 \leq \eta_{skin}/\eta_{core} \leq 2.0$ led uniform skin thickness.
Schlatter et al.	Single channel (mono-sandwich)	Increasing core injection speeds led the lower skin thickness. Increasing skin melt temperatures led the slightly lower skin thickness.
Donovan et al.	Two channel (simultaneous)	Optimum conditions were achieved at 52% and 62% of core (by volume).
Somnuk and Smith	Two channel (simultaneous)	$\eta_{skin} \approx \eta_{core}$ and $V_{skin} \approx V_{core}$ produced good mould filling results.
Lanvers et al.	Two channel (simultaneous)	Interface shapes depended on η_{skin}/η_{core}.

The most successful parameters, which control the skin and core formations, were reported to be; skin and core viscosities, volume proportions of skin to core, injection velocities, melt temperatures of skin and core materials. The skin-core thickness fractions and their interface shapes were examined. If skin and core were compatible polymers, skin-core thickness had no effect on their adhesion. On the other hands, if skin and core were incompatible polymers, the skin-core thickness could be the critical parameter such that it introduced a good adhesion. However, the skin or core materials must contain an optimum amount of compatibiliser.

2.7 Computer Aids Engineering (CAE) for Co-injection Moulding Process

At the moment, a number of commercial CAE software for mould filling simulation of sequential co-injection moulding process have been developed, *although there is no existing commercial CAE software for simultaneous co-injection moulding process*. However, a few document papers have been published. The relatively scientific investigations of those CAE papers are given below.

Firstly, at the IKV in Germany, the mould filling simulation of sequential co-injection moulding had been implemented in a simulation programme named CADMOULD-3D [37]. This is based on a geometry description using shell-shaped finite elements. A model for describing the flow process in a two-phase system is presented in Figure 2.19.

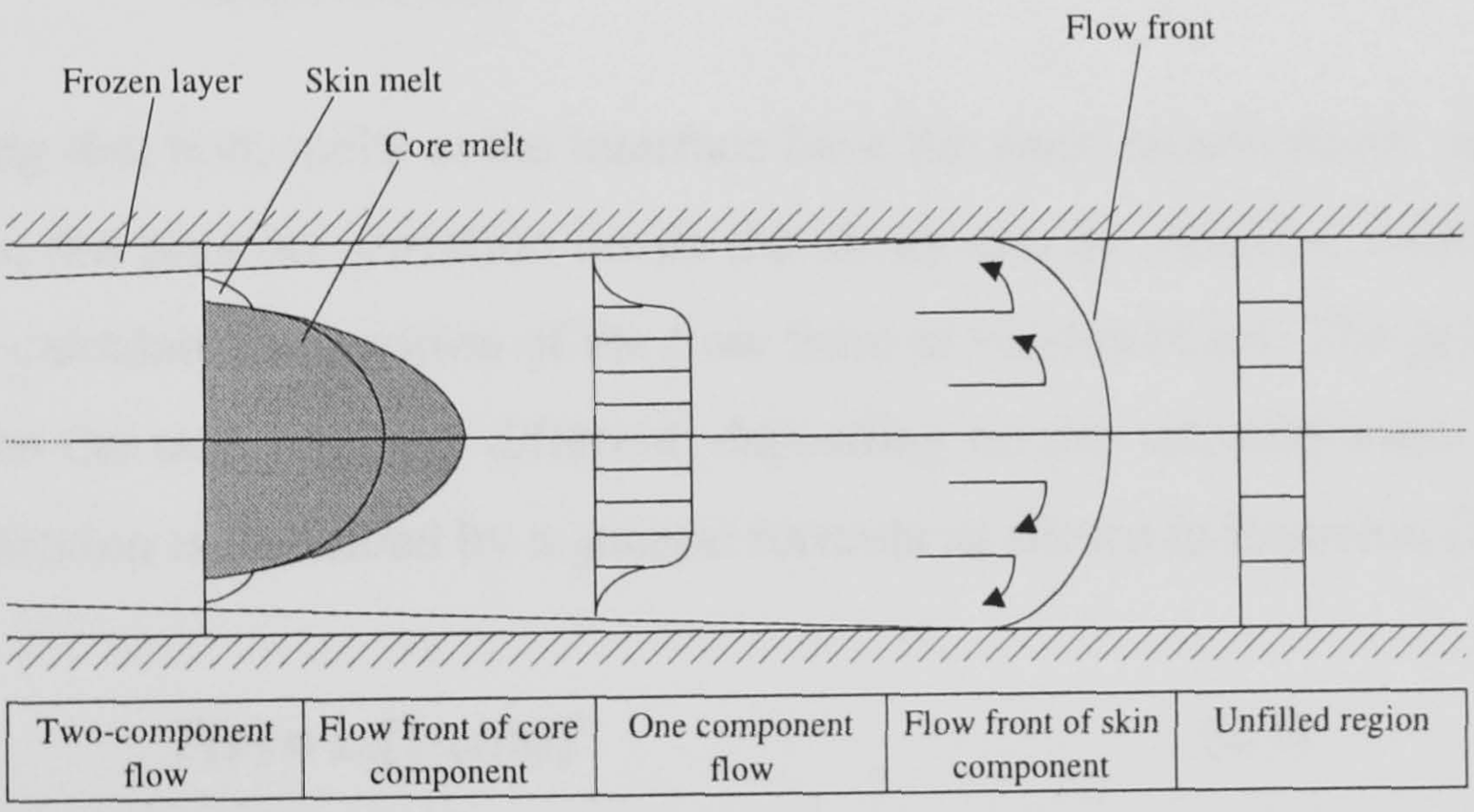

Figure 2.19 The computerised model of the cavity with co-injection moulding process

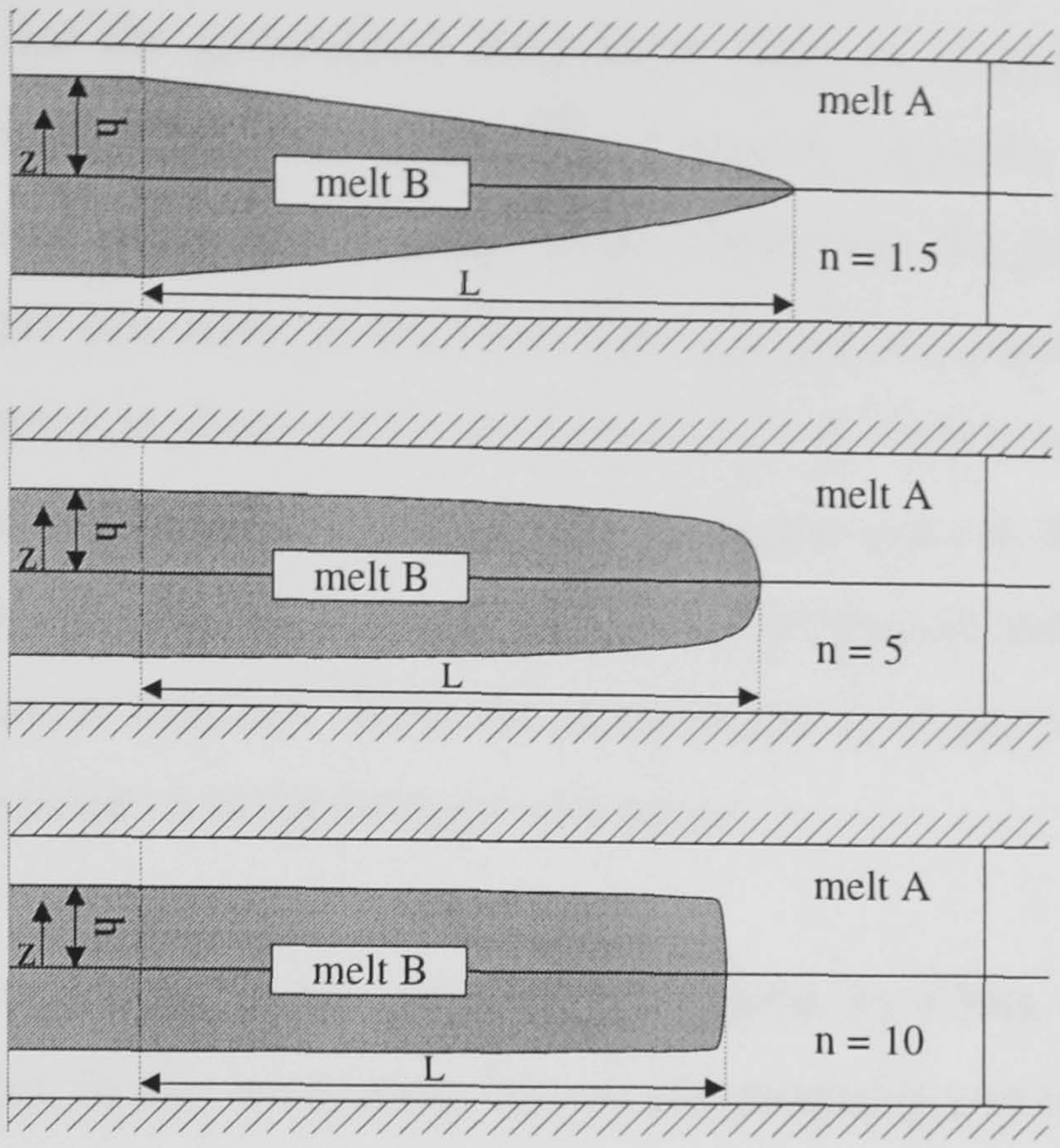

Figure 2.20 Numerical approximation of different penetration behaviour of skin and core material.

By assuming that both melts at the interface have the same temperature, velocity, and shear stress, the pressure variation inside the cavity can be obtained, which makes it possible to calculate the position of the flow front at various times. The penetration of the core into the skin can look different, depending on the viscosity ratio. The shape of the penetration is described by a general formula as shown in Equation (2.1).

$$F(z) = L.[1-(z/h)]^n \qquad (2.1)$$

Where n is the exponent which depends on the skin/core viscosity ratio and lies between 1 and ∞. L is the length of core penetration and h is half thickness of core.

As seen in Figure 2.20, the higher viscosity of the core material in relation to the skin material led to a reduced exponent (n), that made the interface a sharp-angled profile. In the reverse case, n is increased, making the interface shape more round.

Secondly, C-MOLD software package developed by AC Technology [38-39] is the numerical implementation of sequential co-injection moulding process. This three-dimensional mould filling program uses a hybrid finite element/finite difference

approach to solve for the generalised Hele-Shaw flow of inelastic, non-Newtonian fluids under non-isothermal conditions [38]. Viscosity, specific heat and thermal conductivity are parameters in this programme. Otherwise the programme accounts for the fountain flow occurring at the flow front. At the interface between skin and core, there is constancy in shear stress and heat fluxes. A routine in this programme is able to identify each material element and its residence time in the mould cavity. It allows the spatial distribution of skin and core to be recognised and represented by the core-polymer thickness fraction. With the programme it is also possible to predict under what circumstances a breakthrough will occur.

Thirdly and independently is the software developed by Chen et al. [40]. PS and PMMA were studied. In this evaluation, the mould geometry and their thickness were varied. In general, the skin-core distribution from experiment and simulation provided good correlation except in some parts of the geometry, such as corners, which were less in agreement.

The next one, a centre gated disc mould, with diameter of 180 mm and a thickness of 3 mm, was used in Schlatter's study [34]. Two polystyrenes with different viscosities were moulded. In this work, simulation and experimental results were compared at the interface of skin and core materials. They found that flow rate and viscosity ratio had an influence on skin-core distribution as mentioned.

Furthermore, the Ph.D. thesis, which was submitted by Somnuk [8], studied simultaneous sandwich injection moulding with various shapes and dimensions of moulds on a Battenfeld co-injection moulding machine of the BM series C2400/2x1000. Materials were the various grades of polypropylene and polystyrene. In this work, the mould-filling software for conventional injection moulding process from MoldFlow was simulated. Injection time and skin frozen layer thickness were obtained and compared with experimental results. Good mould-filling results were achieved by allowing the duration of simultaneous injection period to correspond to almost 95% of the injection time for the skin. He also claimed that, for good filling results, viscosities of skin and core melts should be the same or only differ slightly.

Recently, Lee et al.[41] attempted to develop a process model for simultaneous sandwich injection moulding. This work described a simulation approach based on the Hele-Shaw approximation to calculate the interface evolution between two phases during the cavity filling in simultaneous sandwich process. An experimental study had been performed in order to verify the simulation results for simple cavities. Three different polymers (LDPE, HDPE, and PS) were used in this study. It was found from results of simulation that relationships exist between the material properties and interface shape and between the process conditions and interface shape.

Chapter III
Compatibilisation

3.1 Definition

Any modification of a blend which increases its compatibility can be termed compatibilisation. For instance, one could quench the blend in a state of low degree of phase separation, which could be frozen in by crystallisation or vitrification of one or both components. Many factors could change and increase the region of miscibility in the phase diagram, and so influence the compatibility found under a certain set of conditions. However, the most successful method of compatibilisation has been the introduction of block or graft copolymers as compatibilisers.

3.2 Compatibility [10, 14-15]

Polymer-polymer compatibility had received much attention recently because many polymer blends performed well in attractive new applications for which the individual polymer components would not be suited. The ability to produce blends that had a better combination of properties than that of the individual components depended on the compatibility of the system. The term polymer blends referred to intimate mixtures of two or more polymers. The individual components might be melt-mixed, solution-blended and coprecipitated. Under microscopic inspection, it was possible to produce further classification into three types of polymer blends:

3.2.1 Miscible Polymer Blend

This blend consists of a single phase, on a molecular level, polymer-A molecules intermingle with polymer-B molecules as shown in Figure 3.1(a). Because a miscible polymer blend has only one phase, it is like a random copolymer in properties and processing. In order to be miscible, there has to be some interpolymer attraction resulting from specific interactions between functional groups on polymer A with different functional groups on polymer B.

3.2.2 Immiscible Polymer Blend

Polymer A forms a separate phase from polymer B. The polymer present in the lower concentration usually forms a discontinuous or discrete phase (domain), whereas the polymer present in the higher concentration forms a continuous phase as shown Figure 3.1(b).

3.2.3 Partially Miscible Polymer Blend

The mix might form completely miscible blends when either polymer is present in small amounts. At compositions where a partially miscible polymer blend is in two phases, the phases might not have a well-defined boundary, since polymer-A molecules can significantly penetrate into the polymer-B phase as depicted in Figure 3.1(c). The molecular mixing that occurs at the interface of a partially miscible two-phase blend can stabilise the domains and improve interfacial adhesion, which explains why these two-phase blends generally have good bulk properties.

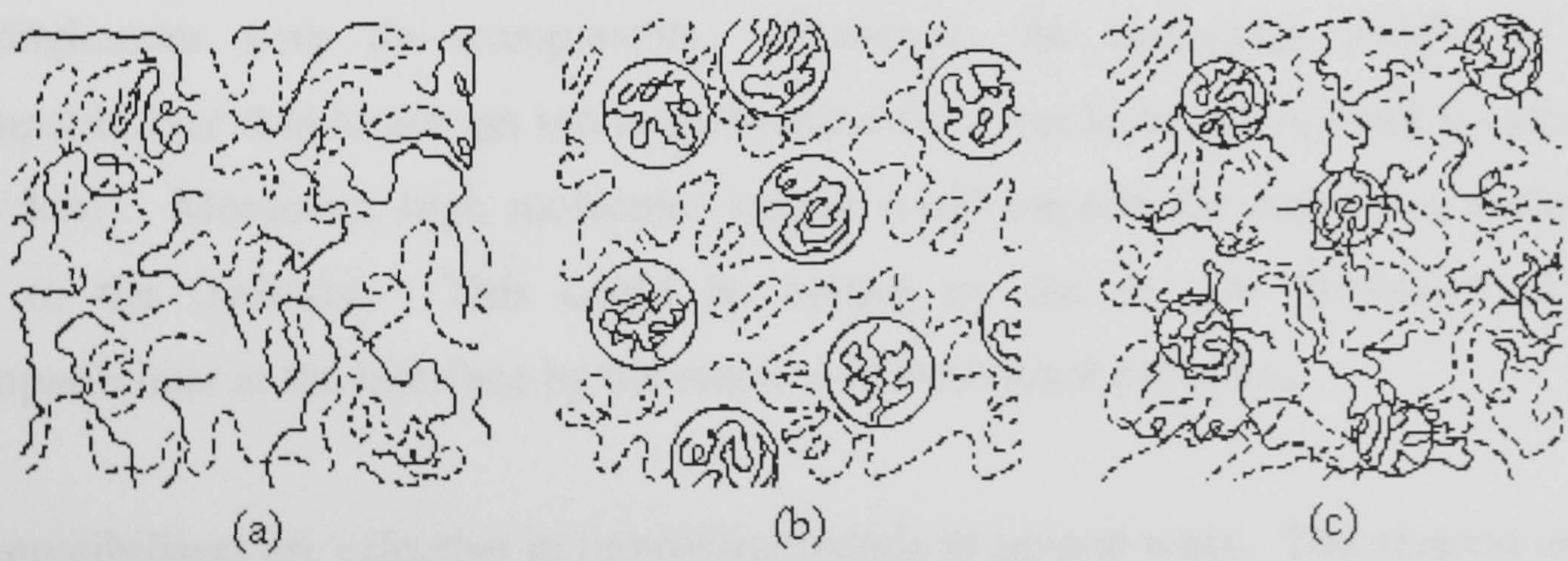

Figure 3.1 Morphologies of a blend of polymer A (solid lines) and polymer B (dashed lines); (a), miscible; (b), immiscible; and (c), partially miscible. [14-15]

The degree of intermolecular mixing might be affected as a consequence of thermal, mechanical, and solvent-exposure history.

3.3 Compatibiliser [10]

A compatibiliser needs to be a polymer that is made up of chemically distinct sections, some of which are miscible with one component and some with the other. This means that the compatibiliser must be some sort of a block or graft copolymer. The reason for this is that the compatibiliser must be at the interface to be effective, so it must have an amphiphilic nature. Since the blend components are by definition immiscible, this means that the blocks or arms of the compatibiliser must be chemically different. In fact, in most cases the sections of the compatibiliser are chemically identical to the individual components, but this is not necessary. The only exception to this rule is the case of a homopolymer, which is miscible with both of the two components even though they are not miscible with each other. However, in such a situation it is likely that the two components are nearly miscible and so in little need of compatibilisation.

The compatibiliser is most effective when its sections are of higher molecular weight than the corresponding components of the blend. This increases both from the desire to reduce interfacial tension as well as the need to achieve a high degree of entanglement with the components. However, the molecular weight of the compatibiliser should not get too large because these could be mixing and processing problems. Moreover, high molecular weight could impede the polymer's ability to get to the interface. This could be helped by the *in situ* formation of the compatibiliser at the interface by the reaction of functional polymers.

Compatibilisers are effective in improving blends in several ways. The clearest effect of compatibilisers is to control the sizes of the domains in a multiphase blend. There are two presumed mechanisms for this, which might both be operating in a particular system. The first is a thermodynamic mechanism in that it lowers the interfacial tension between the phases, while the second is a kinetic process in that the compatibiliser can reduce the agglomeration of domains by steric stabilisation. Moreover, it is likely that an important effect of the use of compatibilisers is the increase in the adhesion between the phases and consequently the mechanical strength of the blend. This multiplicity of effects can make the judgement of a compatibiliser's effectiveness hard to evaluate.

Types of compatibilisers are described as follows:

3.3.1 Block Copolymers

They are the most efficient forms of compatibiliser. For a given total molecular weight, adding a certain amount of a block copolymer will be more effective at improving the compatibility of a blend than the addition of a corresponding amount of graft copolymer. This is presumably because for the block copolymer there is only one linkage bond which is forced to be at the interface, allowing the rest of the chain to reach deeply into the homopolymer phases and entangle more strongly than for the other one (Figure 3.2).

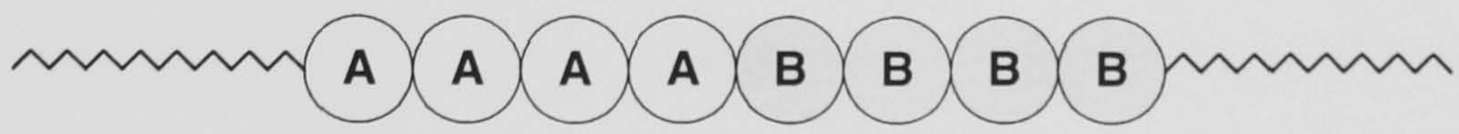

(a)

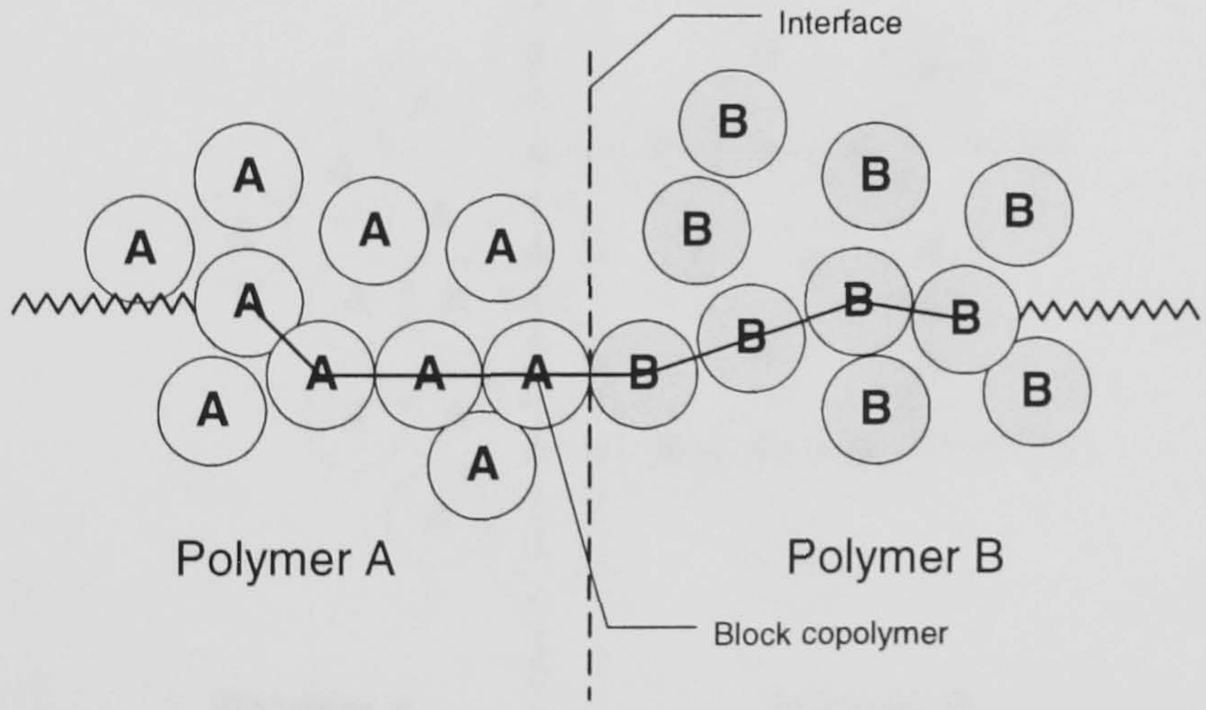

(b)

Figure 3.2 (a) Typical block copolymer and (b) interaction between polymer A and B in the presence of block copolymer

3.3.2 Graft Copolymers

They are the most commonly used compatibilisers. Despite the greater efficiency of block copolymers, they have only rarely been used in commercial applications. In fact, true block polymers have been made for only a small number of the possible pairs of monomers, so for most blends there is no corresponding block polymer. On the other hand, there is much more flexibility in the synthesis of graft polymers.

Moreover, the possibility of *in situ* graft polymer formation during the blending step by a polymer-polymer reaction has the advantages of simplifying the overall process and of placing the compatibiliser directly at the point where it is needed, that is at the interface (Figure 3.3).

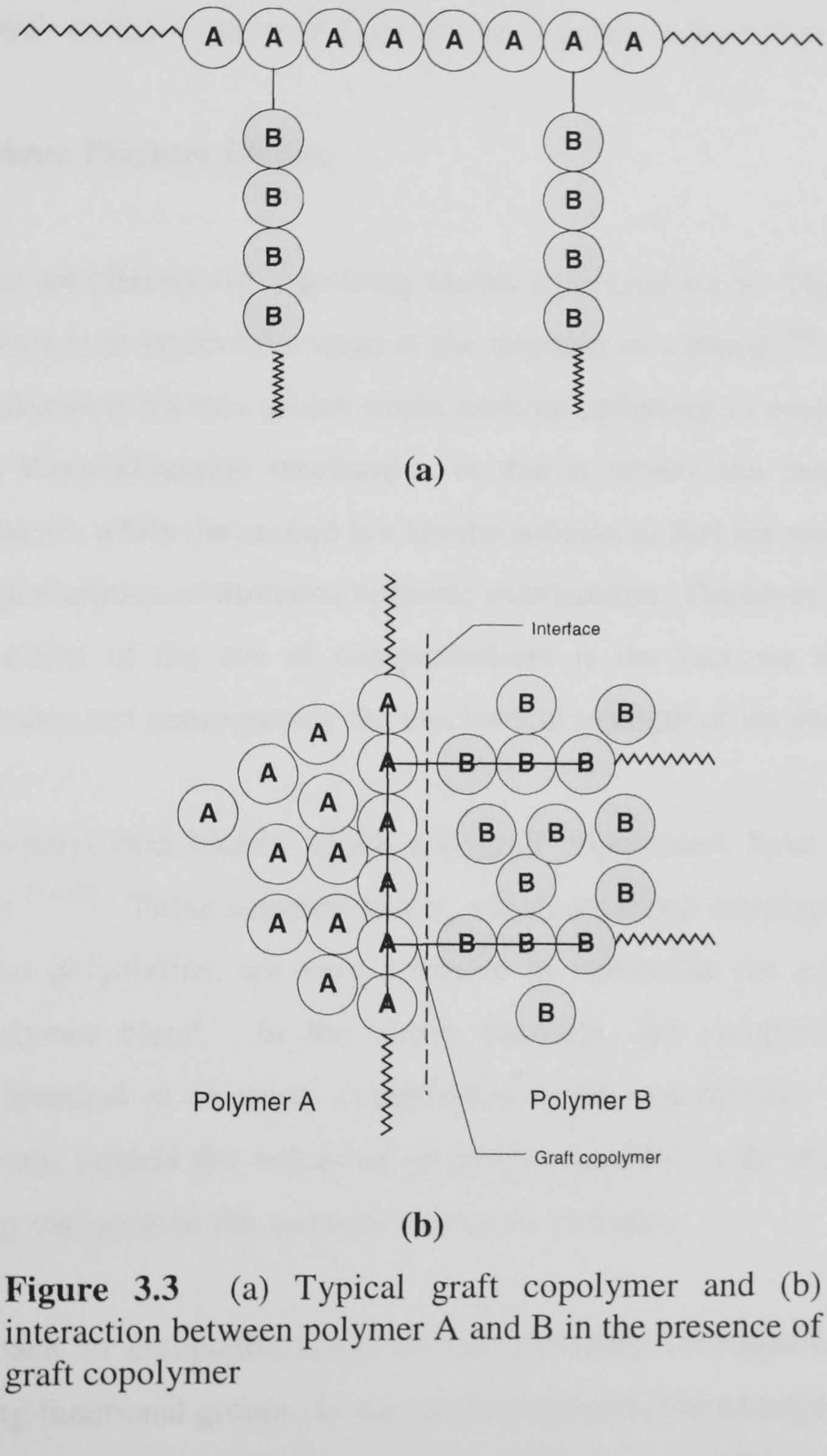

(a)

(b)

Figure 3.3 (a) Typical graft copolymer and (b) interaction between polymer A and B in the presence of graft copolymer

3.3.3 Combination between Block and Graft Copolymers

This type is the mixture of block and graft copolymer, so they can act as an efficient compatibiliser because of presentation of both types of copolymer.

3.4 Compatibilisers: Uses and Benefits in Polymer Blends

Several investigations dealing with utilising compatibilisers in polymer blends or alloys have been published. The application of compatibilisers in polymer blends or alloys can be divided into two-main groups: single-phase and multi-phase polymer blends (or alloys). A brief review on these studies is given in the following sections.

3.4.1 Single-phase Polymer Blends

Compatibilisers are effective in improving blends in several ways. The clearest effect of compatibilisers is to control the sizes of the domains in a blend [10]. There are two presumed mechanisms for this, which might both be operating in a particular system. The first is a thermodynamic mechanism in that it lowers the interfacial tension between the phases, while the second is a kinetic process in that the compatibiliser can reduce the agglomeration of domains by steric stabilisation. Moreover, it is likely that an important effect of the use of compatibilisers is the increase in the adhesion between the phases and consequently the mechanical strength of the blend.

In polystyrene-polyolefin blends, block and graft copolymers have been added as compatibilisers [14-15]. These compatibilisers, which are block copolymers or grafts of polystyrene and polyolefins, are very effective in enhancing the properties of the immiscible polymer blend. In the above example, the compatibiliser polymer segments are identical in chemical composition to the components of the polymer blend. The main criteria for enhanced properties appears to be miscibility of the compatibilising segments in the respective polymer domains.

Another approach to compatibilisation of two normally incompatible polymers is through grafting functional groups on one of the polymers. For example, after grafting a small amount of maleic anhydride, polypropylene is compatible with polyamides such as PA6 [12, 22]. The grafted functional polymer (PP-g-MA) can be bonded with a PA6-polymer chain. Using SEM, it can be observed that sizes of the domains in a blend are decreased. It is suggested that some chemical reactions can occur in the combination of PA6 and PP in the presence of MA-g-PP under certain conditions, and

that a graft polymer is formed between MA in PP and the terminal amino groups of PA6.

The PE/PET blend system has been studied by Champagne [42]. Copolymers of ethylene and glycidyl methacrylate are added to PE/PET blends. It is assumed in this scheme that a reaction involving PET end-groups and GMA units can lead to an ethylene-PET copolymer acting as interface modifier for the blend.

The addition of GMA-based copolymers in PE/PET blends is very effective in reducing the segregation scale of the blends, as shown in Figure 3.4. Replacing ¼ PE by E-GMA copolymer in a 10 wt% PE/PET blend decreased the PE particle size from 2-3 microns range down to the sub-micron level. The *in situ* generated graft copolymer of E-GMA and PET is assumed to be the compatibilizing species in the system. This assumption implicitly supposes that PE molecules interact favorably with the E-GMA backbone of the E-GMA-PET graft copolymer.

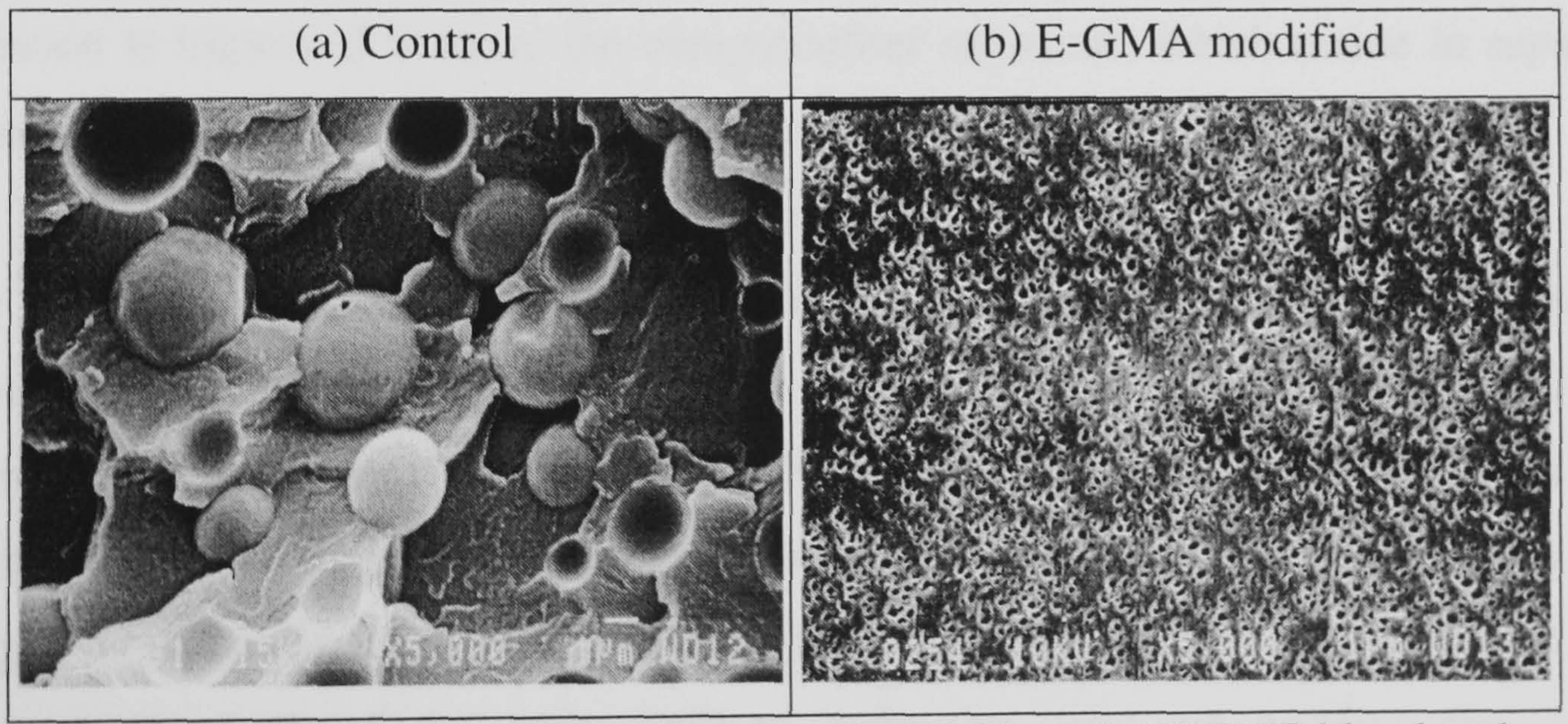

Figure 3.4 Scanning electron micrographs of 10 wt% PE/PET blends taken from: (a) freeze-fractured surface of the unmodified blend and (b) microtomed and etched blend compatibilized by replacing ¼ PE by E-GMA copolymer.

3.4.1.1 Applications

Basically, compatibilisers can create chemical bonds at the interface of two dissimilar polymers. These alloys or blends have superior physical properties compared to noncompatible systems. They can be used to coating the pipe, and limit the emission of vapours into the atmosphere. Blends of polyamide and EVOH (ethylene vinyl

alcohol) are used as oxygen barrier polymers. It is highly useful in many sectors. i.e., food and medical packaging, and automobiles (fuel tank) [43].

3.4.2 Multi-phase Polymer Blends

Stable polymer blends might be produced from immiscible polymers by using compatibilisers. It should be possible to enhance the stability and properties of an immiscible polymer blend by adding a compatibilising polymer, usually a block or graft copolymer.

The compatibilisers can penetrate both phases of an immiscible blend when mixed, as shown in Figure 3.5. In the examples, it is assumed that the A segment of the block or graft copolymer is identical to polymer A and the B segment identical to polymer B. The working hypothesis is that segment A penetrates polymer A and segment B penetrates polymer B. Stabilised, more uniformly dispersed domains should result because of reduced interfacial energy between phases. In addition, the interfacial adhesion is improved because the compatibiliser segments, which reside in separate phases, are linked by covalent bonds.

The molecular weights of the segments in the block or graft copolymer appear to influence the efficiency of the compatibilisation strongly. If the molecular weight of compatibiliser segments is low, the depth of penetration into the domains by the compatibiliser is also low, resulting in poor interfacial adhesion. If the molecular weight of the compatibiliser segments is very high, the penetration might be high, although the bulk of the compatibiliser molecules limit the number that could penetrate the domain.

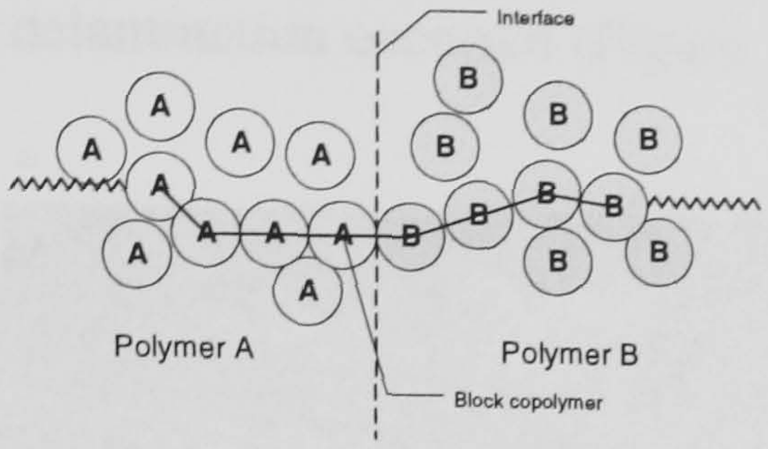

(a)

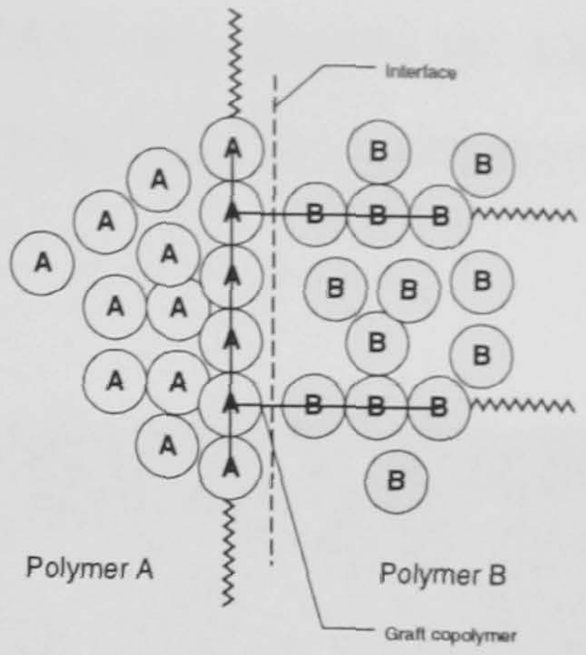

(b)

Figure 3.5 Penetration of block- or graft-copolymer compatibilisers into the A and B phases of a polymer blend: (a) block-copolymer compatibiliser; (b) graft-copolymer compatibiliser.

The linkage between phases is called a "tie layer". The tie layer is found to be reported in several works [42-45] as follows:

3.4.2.1 Hot Melt Adhesive Components

Solid state adhesion between PET sheets have been prepared using thin films (30-50 microns thick) of GMA-based copolymers [42]. These thin GMA copolymer films were used in joining two 0.5 mm thick PETG (glycol-modified PET) sheets in a compression molding press at the bonding temperature ranged from 175°C, up to 275°C with holding time being varied from 5 to 20 min. It was found that the GMA copolymer films acted as a tie layer dispersion between the PET sheets and held them together.

3.4.2.2 Coextrusion

The effect of a thin tie layer on the adhesion of polypropylene (PP) and polyamide-66 (PA) was studied by delamination of microlayers. The microlayers consisted of many alternating layers of PP and PA separated by a thin layer of a maleic treated PP (PP-g-MA). Microlayer sheets were coextruded using the three-component layer multiplying process [44]. The peel toughness and delamination failure mode were determined using the T-peel test. Without a tie layer, there was no adhesion between PP and PA. A tie layer with 0.2% MA provided some adhesion; however, delamination occurred by interfacial failure. Increasing the maleic anhydride (MA) content of the tie layer

increased the interfacial toughness. With 0.5% MA, the interfacial toughness exceeded the craze condition of PP, and a transition from interfacial delamination to craze delamination occurred (Figure 3.6).

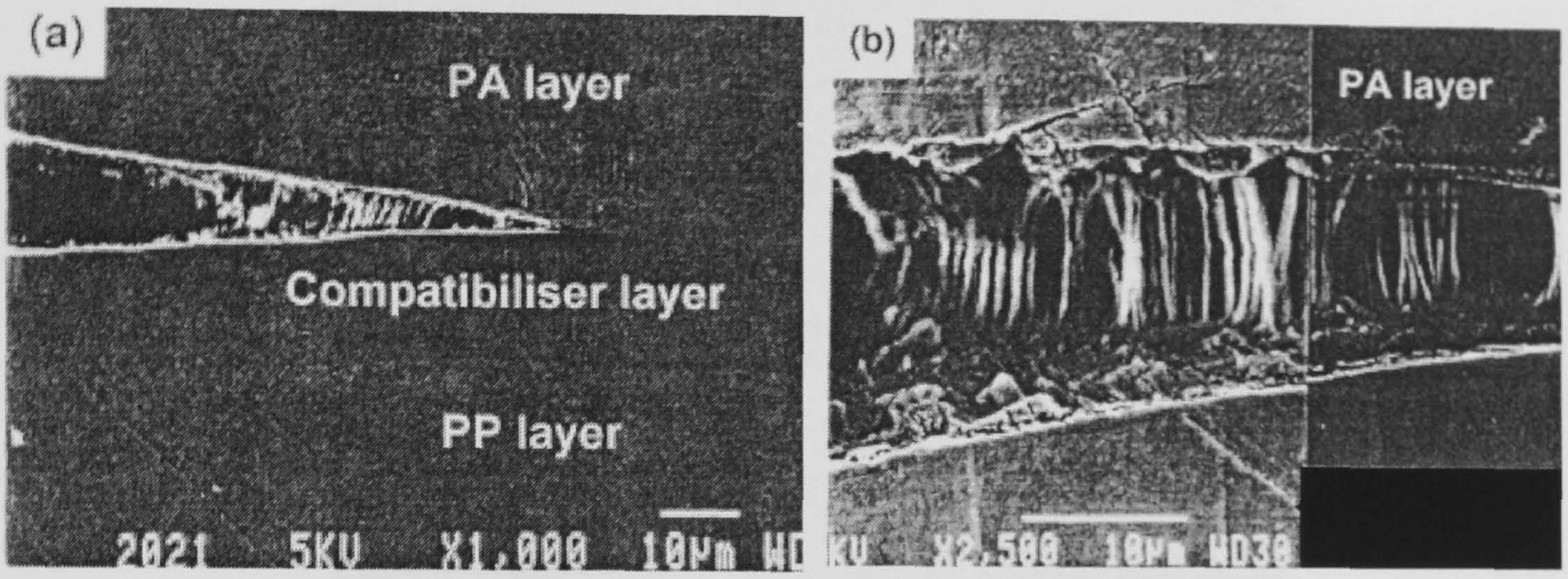

Figure 3.6 Peel crack tip of PP/0.5 MA/PA: (a) low magnification; (b) higher magnification.

3.4.2.3 Co-injection Moulding

A Battenfeld co-injection moulding machine series BMT-1100/2x300 controlled with the UNILOG 9000 system was used in this study [45]. Three grades of polypropylene (PP/Novolen) with compatibiliser and two grades of polyamide 6 (PA6/Durethan) were used as core and skin materials, respectively. The compatibiliser was maleic anhydride grafted polypropylene (PP-g-MA), named Polybond 3150 with 0.5% by weight of maleic anhydride level in this copolymer. The modified core materials were prepared by dry-blend mixing unmodified polypropylene with 10% by weight of the compatibiliser. Then, square-plaque specimens were prepared by using co-injection moulding process [2-6]. The peel tests were also performed to determine the level of adhesion of each specimen. Moreover, optical and scanning electron micrograph were used for determination of the interface layer of skin and core of the peel test specimens. It was found that the tie layers between the polymer phases were observed by SEM (Figure 3.7).

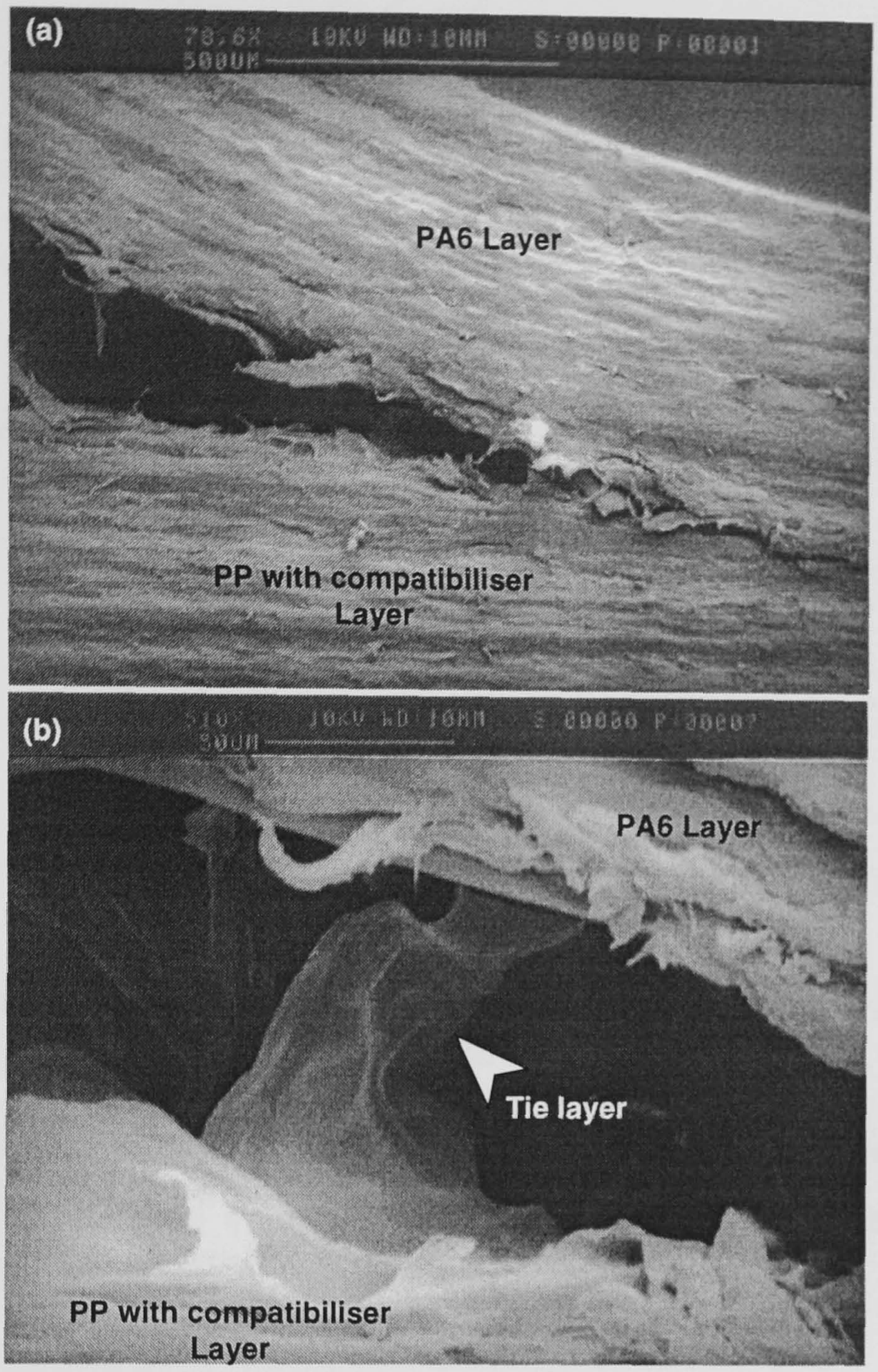

Figure 3.7 SEM of the peel crack tip of the skin and core layers : (a) low magnification (b) higher magnification.

These layers acted like the linkage between skin and core surfaces as seen in Figure 3.7. However, the mechanical interlocks of skin and core interface which can be introduced by 'Fountain flow'[38, 46-47] of the core melts also provided the peel strength and component adhesion [45].

However, it is suggested that some chemical reactions can occur in the combination of PA6 and PP in the presence of MA-g-PP under certain conditions, and that a graft polymer is formed between MA in PP and the terminal amino groups of PA6 as shown below [12, 24, 48],

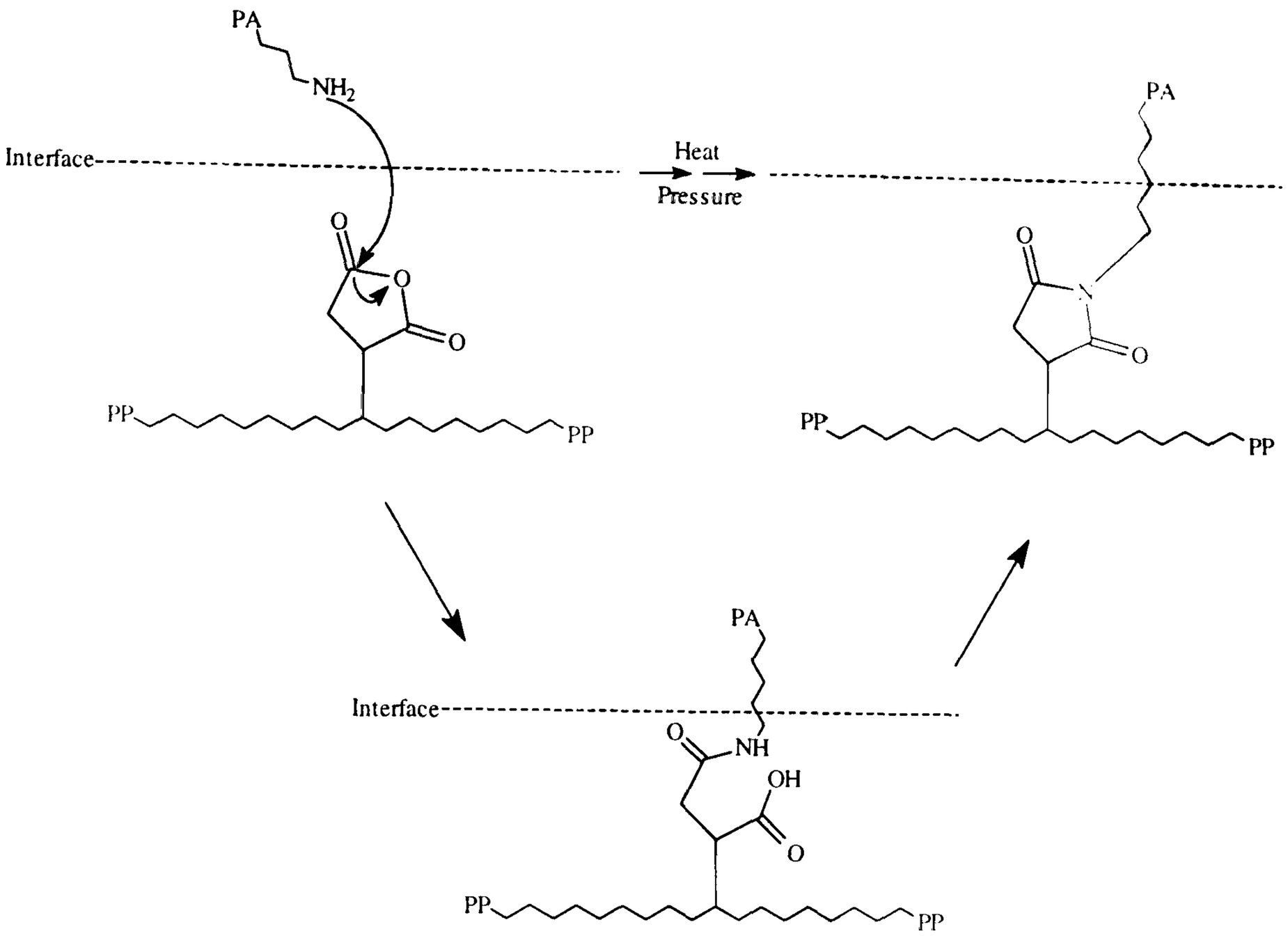

Figure 3.8 The chemical reaction between PA6 and MA-g-PP

Moreover, in the review documents [10-15, 22, 49-50] of compatibilisation, there is an investigation of the utilised compatibilisers for incompatible thermoplastics blend systems, some of them are illustrated as show in Table 3.1.

Table 3.1 Some recommended compatibilisers for incompatible thermoplastics

Blend systems	**Compatibilisers**
PP/PA6	PE-*g*-methyl NBDCA PP-*g*-MA / EP-g-MA PP-*g*-MA / (E,VA,GMA) PP-*g*-MA* PP-*b*-PA6 PP-*g*-NBDCA / EP-*g*-NBDCA PP-*g*-GMA
PP/PA66	PP-*g*-MA / (E,VA,GMA) PP-*g*-MA PP-*g*-MA / EP-g-MA
PP/PBT	PP-*g*-MA / (E,VA,GMA) PP-g-P(St-*co*-GMA) PP-*g*-GMA
PP/PS	St-*co*-MAA

* To be used in this work.

3.5 Determination of Compatibilisation [10, 14-15]

Most incompatible polymers can be promoted for compatibility by using grafted functional groups on one of the polymers or using block or graft copolymers. In the case of a simultaneous co-injection process, the skin and core materials are injected simultaneously. So in the presence of compatibiliser, it can lead to the formation of a two-phase polymer blend. Thus, it is necessary to determine how the structure and morphology of a compatibiliser can affect the polymer blend properties (mechanical and physical properties).

3.5.1 Structure and Morphology

It is necessary to determine the structure of a compatibiliser in order to assess its ability to affect the morphology and properties of blend. This is certainly true in the case of the presence of block or graft polymers which act as compatibilisers. However, for a good understanding, the compatibiliser has to be made with different amounts of each reactant and under various process conditions. The most useful techniques [14-15] for characterising compatibility was presented as follows:

3.5.1.1 Spectroscopy [14-15]

In many case of compatibilisation, the compatibiliser was formed "*in situ*" either during polymerisation or during the blending process. Clearly one of the most direct ways to tell whether grafting had occurred was to determine, if a bond between the two portions of the graft copolymer had been formed. The most direct ways to do this was by spectroscopy, either infrared (IR), or Raman.

3.5.1.2 Microscopy [10, 14-15]

The main measure of degree of compatibility in a blend was the size scale of the phase domains under a given set of conditions. In the interested range of interest from 0.01 μm to 10 μm, the techniques that were useful for determination of the domain sizes were those of microscopy, especially electron microscopy and scattering.

3.6 Mechanical Properties [10]

The most common reason for compatibilisation is to modify and control mechanical properties. In fact, changes in mechanical properties are often used as evidence for compatibilisation, for instance, the critical amount of compatibiliser is the concentration which becomes effective to increase interfacial adhesion and decrease interfacial particle sizes.

Two incompatible polymers, in which one or both had the compatibiliser present, were injected simultaneously using a co-injection unit. Under a set of conditions, this introduced the two-phase polymer blend component and involved partial compatibilisation. There were many ways to determine compatibility of these blends[10]:

3.6.1 Glass Transition Temperature (T_g) [10]

The glass transition temperature of a polymer is the temperature at which the molecular chain has sufficient energy to overcome attractive forces and moves vibrationally, and translationally. The number and locations of the glass transition temperatures provides much insight into the nature of a polymer blend. For example, a miscible one-phase blend should have only one T_g, whereas a two-phase blend should have two glass transitions, one for each phase. However, it is also applicable in the case of a partial polymer blend, which is involved with a co-injection moulding process. The analytical techniques, which can be used for determining glass transition temperature, are given as follows.

- Thermomechanical method, such as differential scanning calorimeter (DSC), or thermomechanical analysis (TMA)
- Dynamic mechanical method, such a dynamic mechanical analysis (DMA)

3.6.2 Mechanical Testing

Most mechanical analysis is based on determining the number and location of T_gs. Nevertheless, in terms of mechanical testing, tensile testing (peel test), or impact testing, these are based on measuring the strength [10] of a component which could be related to compatibility of the blends. In fact, the mechanical properties of two-phase polymer blends are more difficult to predict than the single-phase blend. This is especially so in the case of a partial polymer blend where the level of phase adhesion is very important to control the strength of the blend.

3.6.3 Other Techniques [10]

In addition to the more common approaches of spectroscopy, microscopy, thermomechanical methods, and dynamic mechanical methods, a variety of experimental techniques have been used to determine the compatibility of polymer blends. The other techniques, such as light, x-ray, and neutron scattering, they are aimed at the determination of domain size which affects their properties. However, nuclear magnetic resonance (NMR) technique is also used to obtain the compatibility information.

Chapter IV

Flow of The Molten Polymers

In Co-injection Moulding Process

4.1 Introduction

This chapter intends to discuss briefly the basic process of injection moulding as an example of a flow field which depends on rheology and heat transfer, and is very complex. Injection moulding involves two processes: production of the flow of molten polymer, and shaping the product in the die [51-53].

A stream of molten polymer is forced into the mould under pressure from the ram action of the moulding machine. The flow is through the sprue, runner, and gate system into the mould cavity; heat transfer to the mould, which is cool i.e. below the melt (T_m), then solidifies the molten polymer. Initially flow rates are high, but freezing of a skin of the melt next to the mould surface slows the flow towards the end of the mould-filling cycle. If cooling is too rapid, the mould might not be properly filled. After the cavity has been filled, the pressure is kept on the melt to compact it securely into the cavity and compensate for contraction during the cooling phase. The component is then ejected, thus, completing the cycle.

In fact, the basis of injection moulding process can be applicable for fill in the co-injection moulding process, in which is injected two or more polymer melts into the mould. Basically the melt streams are forced by pressure from the special nozzle through the runner, gate system, to the cavity.

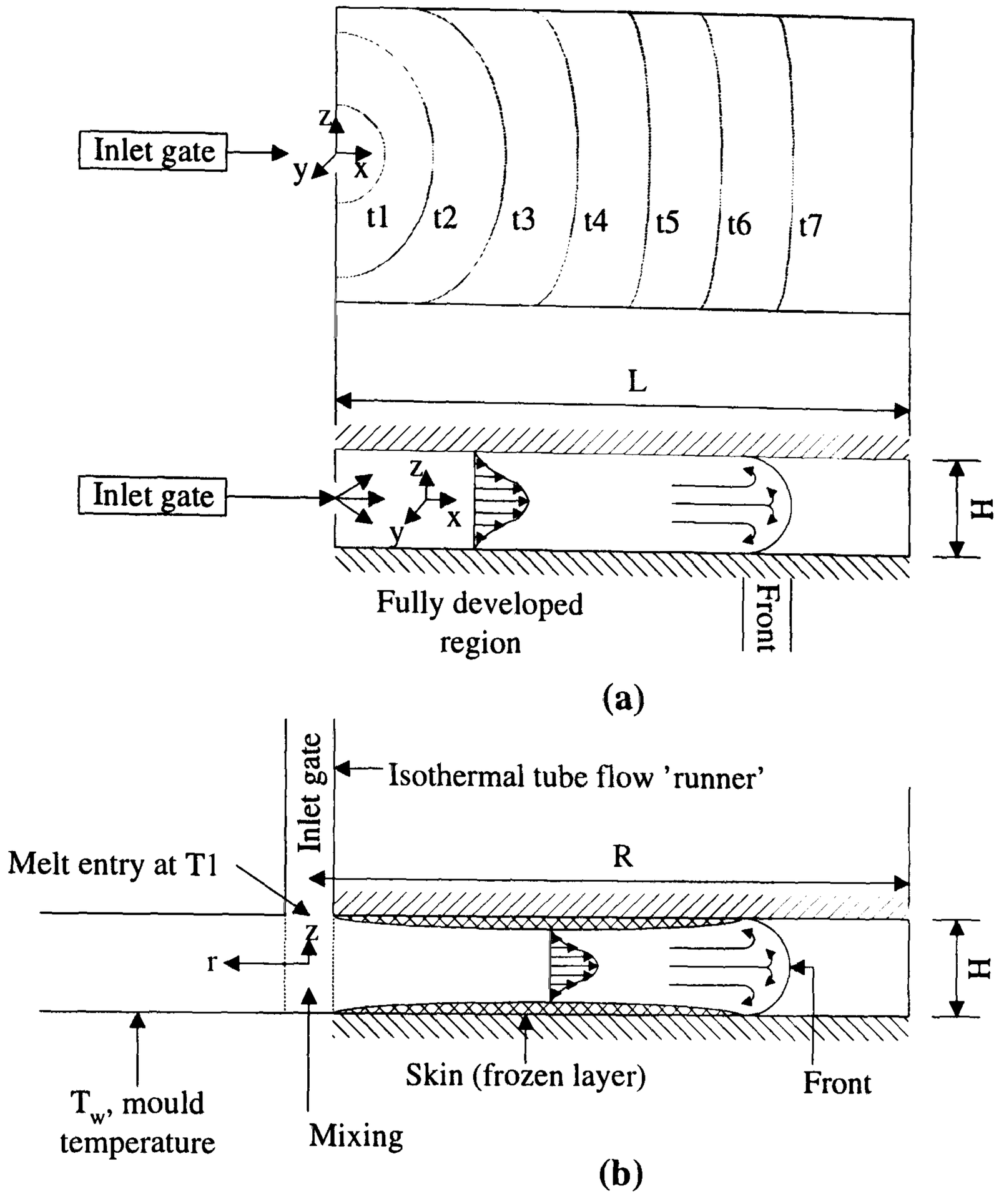

Key:
T = temperature
t = time
H = thickness of the cavity
R and L= Flow length from the centre of sprue to the edge of the cavity

Figure 4.1 Filling schematic [52]

In Figure 4.1(a), t_n shows the position of the polymer melt front at different times during the filling. Figure 4.1(b), shows the frozen 'skin' which constricts the flow. Near the entry there is enough heat transfer to keep the skin thin; further into the mould, it first gets thicker and is thin near the polymer melt front.

In view of the complexity, material properties are needed, especially those properties which relate to flow behaviour. In addition, the rheological properties of the polymer

melts are very important. A brief review of the basis of melt flow behaviour is given in the following section.

4.2 Classification of Fluid Behaviour [54-56]

Imagine a fluid, at fixed temperature, placed between two plates that are a small distance apart. Suppose the bottom plate is stationary and the top plate moves with a constant speed V_x in the x-direction due to application of a force F as illustrated in Figure 4.2. This flow is called steady simple shear flow. The shear stress (τ), acting on the top plate is given by,

$$\tau = \frac{F}{A} \qquad (4.1)$$

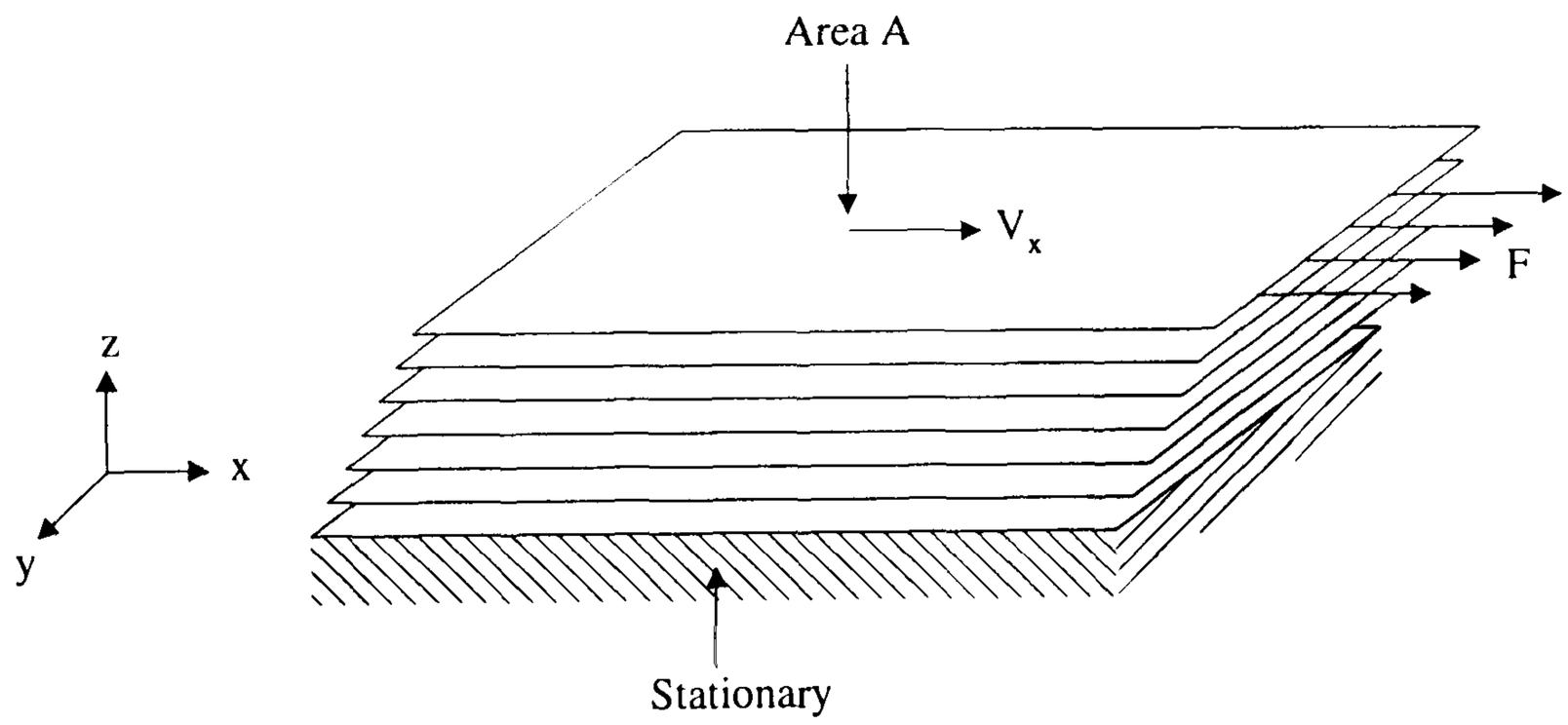

Figure 4.2 Steady simple shear flow

Where A is the area of the plate. The dimension of shear stress is force per unit area. It has been determined empirically that the shear stress is proportional to the velocity gradient of the fluid, dV_x/dz. That is,

$$\tau_{zx} = \mu \frac{dV_x}{dz} \qquad (4.2)$$

The velocity gradient dV_x/dz is called the shear rate and is denoted by $\dot{\gamma}$. It has units of reciprocal seconds. The shear rate is a measure of how fast the layers slide over each other. Therefore,

$$\tau_{zx} = \mu \dot{\gamma} \qquad (4.3)$$

The constant of proportionality μ, is called the viscosity of the fluid, η. It relates the shear stress to the rate of deformation of the fluid. From Equation (4.3), this fluid is known as Newtonian type, the viscosity is a property of the fluid and is not altered or changed by the shear rate, $\dot{\gamma}$. For Newtonian fluid, only temperature and pressure has an effect on viscosity.

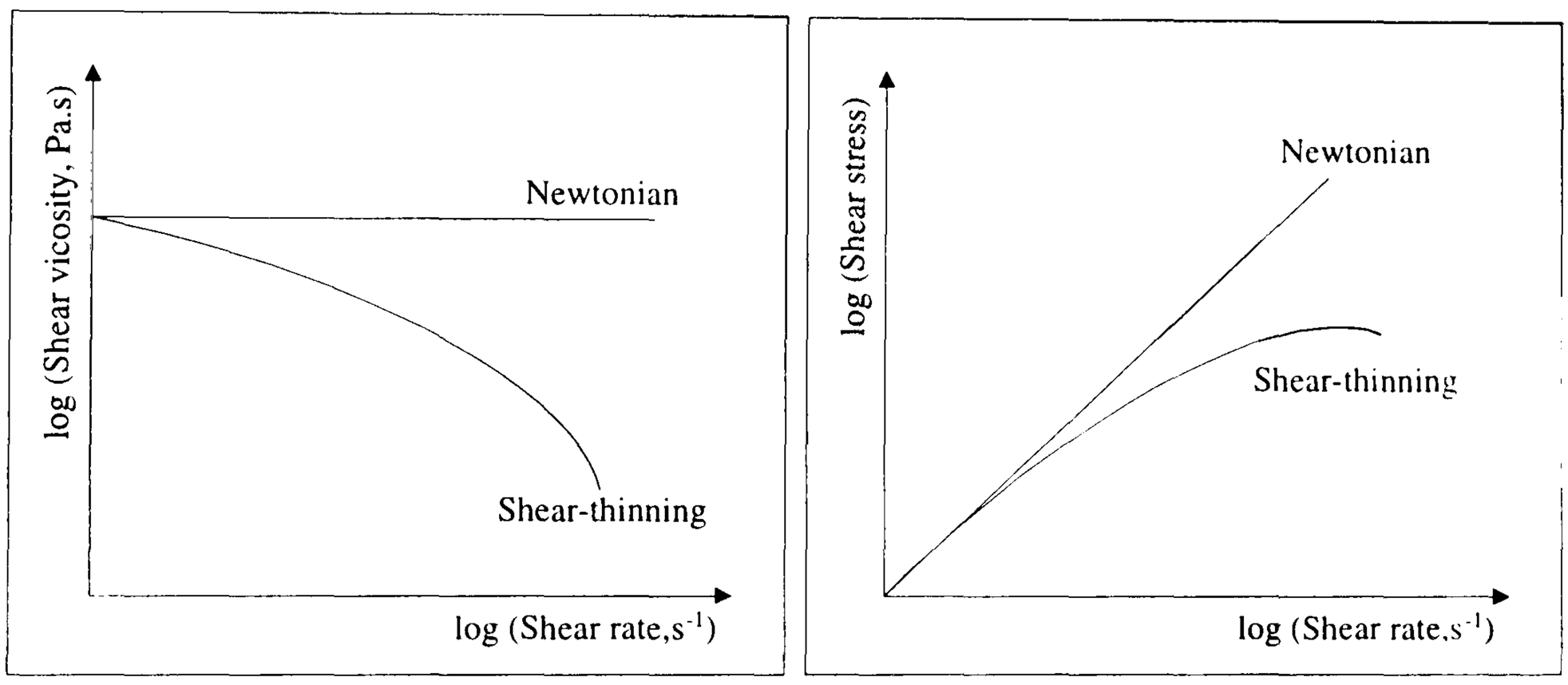

Figure 4.3 Relationship between shear stress and apparent viscosity against shear rate of Newtonian and Non-Newtonian fluid (shear thinning).

In polymer melt systems, there is an another fluid system, which is called non-Newtonian. As can be seen in above figure (Figure 4.3), the apparent viscosity, η_{app} for a Newtonian fluid is a constant whereas non-Newtonian fluid show a decreasing apparent viscosity with increasing shear rate, sometimes called shear-thinning fluid. Shear-thinning fluid is also called pseudoplastic. Modification of Equation (4.3) is made to allow the viscosity to be a function of shear rate.

Therefore, Equation (4.3) becomes:

$$\eta = \eta_0 \dot{\gamma}^{n-1} \qquad (4.4)$$

Where η_0 is the zero-shear viscosity and n is a constant, lie between 0 and 1.

4.3 Viscosity Models for Flow Analysis [38-40, 54-56]

Some plots of viscosity against shear rate at the different temperatures are shown in Figure 4.4. The curves are typical for materials commonly used in injection moulding. The aim of the viscosity model is to match the observed behaviour of the material as closely as possible.

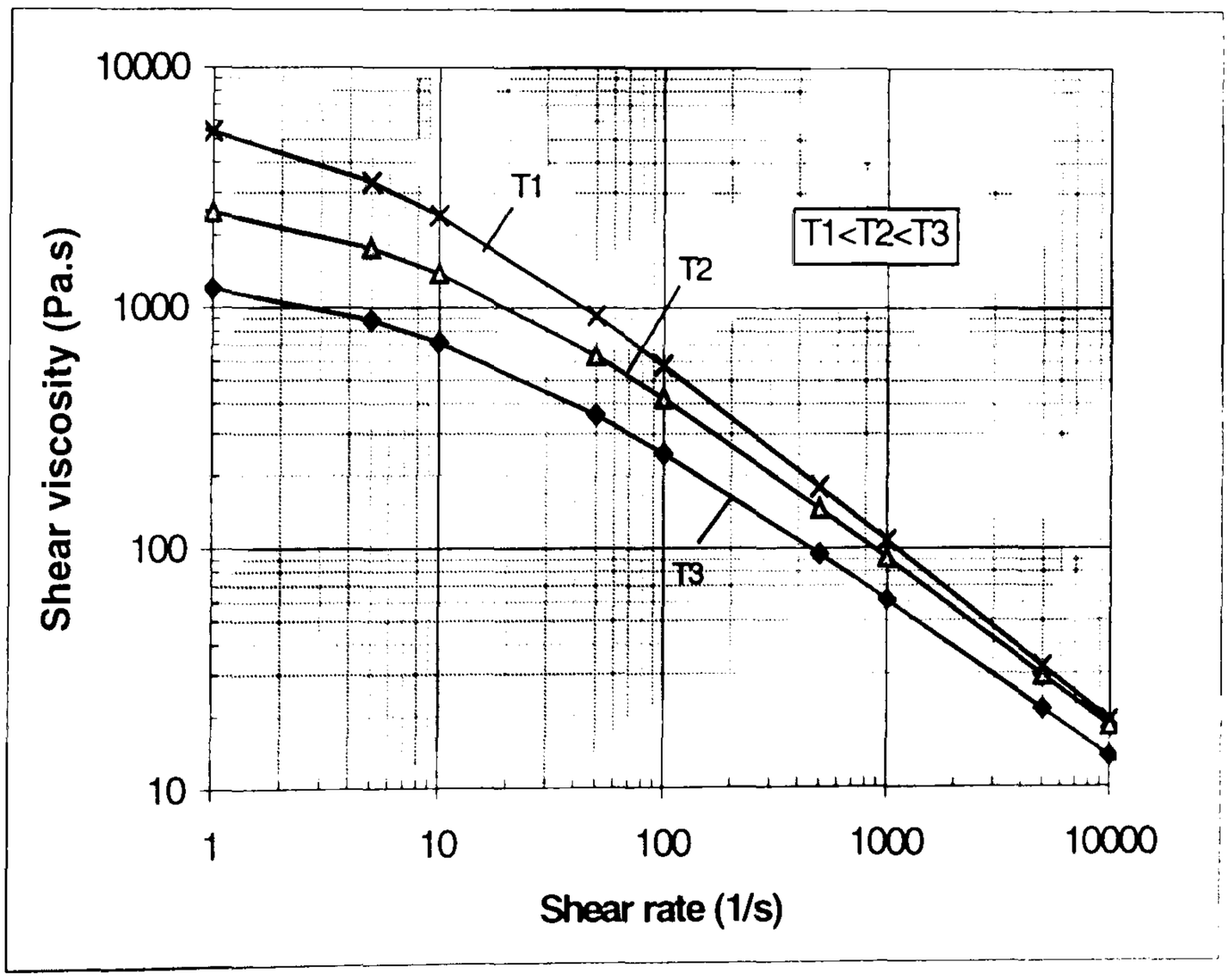

Figure 4.4 Plots of viscosity against shear rate at the various temperatures.

To model the injection moulding process, a viscosity function (or model) is required. A number of well-known models are available. It is important to choose a model,

which is both accurate over the processing range and for which data can be readily obtained. Some common viscosity functions are:

- Power law model
- MoldFlow second order model
- Ellis model
- Carreau model
- Cross-WLF model
- Cross-exp model (C-MOLD)

4.3.1 Power Law Model

This model has the form:

$$\eta = \eta_0 \dot{\gamma}^{n-1} \qquad (4.5)$$

Where η_0 is the zero-shear viscosity and constant.

n is a constant and lies between 0 and 1.

4.3.2 MoldFlow Second Order Model

For improving the viscosity model in the low shear rate region, the following model has been developed by MoldFlow.

$$\ln \eta = A_0 + A_1.\ln \dot{\gamma} + A_2.T + A_3.(\ln \dot{\gamma})^2 + A_4.T.\ln \dot{\gamma} + A_5.T^2 \qquad (4.6)$$

Where the A_i are constants.

4.3.3 The Ellis Model

The Ellis model expresses the viscosity as a function of shear stress, τ. It has the form:

$$\frac{\eta_0}{\eta} = 1+\left(\frac{\tau}{\tau_{1/2}}\right)^{\alpha-1} \qquad (4.7)$$

Where $T_{1/2}$ is the value of shear stress for which $\frac{\eta_0}{\eta} = 2$ and α-1 is the slope of the graph ln $[\frac{\eta_0}{\eta} - 1]$ versus ln $[\frac{\tau}{\tau_{1/2}}]$.

4.3.4 The Carreau Model

The Carreau model has the form:

$$\eta = \frac{A.a_T}{(1+Ba_T\dot{\gamma})^C} \qquad (4.8)$$

Where A, B, C are polymer-dependent constants.

η is apparent viscosity.

a_T is the influence of temperature on viscosity.

The influence of temperature on viscosity can be taken into account by the shift factor.

For crystalline polymers this can be expressed as:

$$a_T = b_1(T_a)\exp(\frac{b_2}{T}) \qquad (4.9)$$

Where b_1 and b_2 are resin-dependent constants.

T and T_a are temperature (K) and reference temperature (K), respectively.

The shift factor a_T for amorphous polymers is determined from the Williams, Landel, and Ferry (WLF) equation, given as

$$\log a_T = -\frac{C_1(T-T_a)}{C_2+(T-T_a)} \qquad (4.10)$$

Where C_1 and C_2 are resin-dependent constant.

T and T_a are temperature (K) and reference temperature (K), respectively.

Polymer melt at low shear rate is accurate with this model [37].

4.3.5 Cross-Exp Model (C-MOLD Filling Stage Model)

To incorporate the dependence of melt viscosity on shear rate, temperature, and pressure, the following 5-constants (n, τ^*, B, T_b, β), together with the cross-exp model is adequate for simulating the filling stage in injection moulding;

$$\eta(T,\dot{\gamma},p) = \frac{\eta_0(T,p)}{1+\left(\frac{\eta_0\dot{\gamma}}{\tau^*}\right)^{1-n}} \qquad (4.11)$$

With

$$\eta_0(T,p) = B.\exp(\frac{T_b}{T}).\exp(\beta p) \qquad (4.12)$$

Where n is power law index

τ^* is shear stress of resin at which shear-thinning behaviour begins to manifest itself.

T_b is Temperature-sensitivity factor.

B is resin-dependent constant.

β characterises the pressure dependence of η_0.

η_0 is zero-shear viscosity.

The Corss-exp model can handle both the Newtonian and shear-thinning flow regions found in polymer rheology.

4.3.6 Cross-WLF Model (C-MOLD Post-Filling Stage Model)

To extend the modelling into the post-filling stage, it is necessary to employ the following 7-constants (n, τ^*, D_1, D_2, D_3, A_1, $\tilde{A}$), in the Cross-WLF model, which still represent the shear-thinning behaviour according to Equation (4.11), but replaced Equation (4.12) with a more extensive model based on the WLF functional form:

$$\eta_0(T,p) = D_1 \exp\left[-\frac{A_1(T-T_a)}{A_2+(T-T_a)}\right] \qquad (4.13)$$

Where $T_a = D_2 + D_3.p$, and $A_2 = \tilde{A} + D_3.p$.

D_1 is resin-dependent constant.

4.4 Flow of Two-Phase Melts

Basically, co-injection moulding is a process, which involves injection of a skin polymer followed by injection of a different core polymer at a specified switchover time. Imagine each molten polymer that is injected into the mould, take advantage of a characteristic of injection moulding called "Fountain flow" [37, 49-50], that is, as the cavity is filled, the polymer at the melt front moves from the centre line of the stream to the cavity walls. Because the wall temperatures are below the transition temperature (freeze temperature) of the melt, the material that is against the walls cools rapidly and freezes in place. This provides insulating layers (frozen layers) on each cavity wall and new melt then made its way to the melt front. The Fountain flow schematic diagram is shown in Figure 4.5.

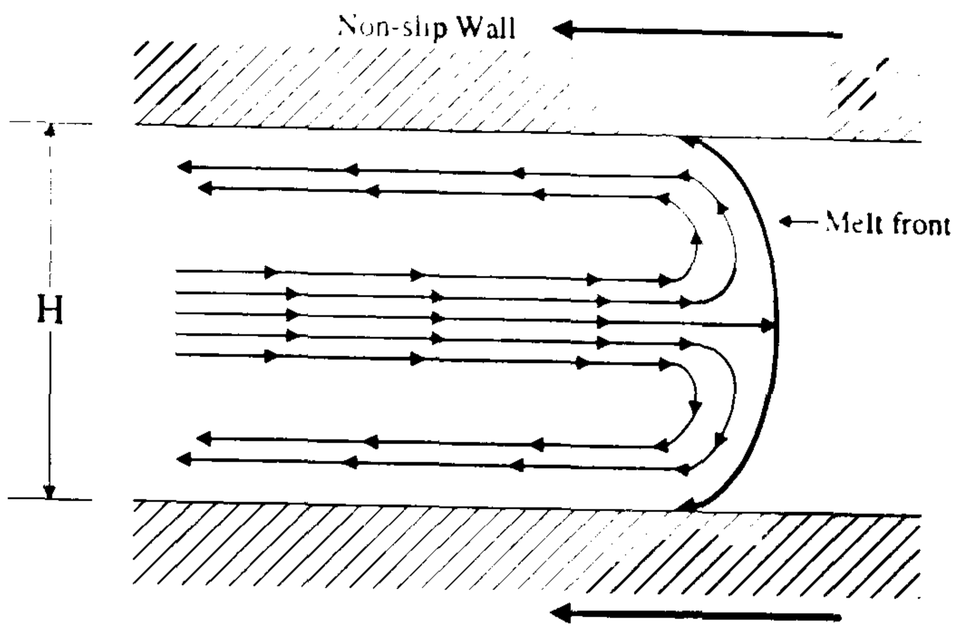

(a)

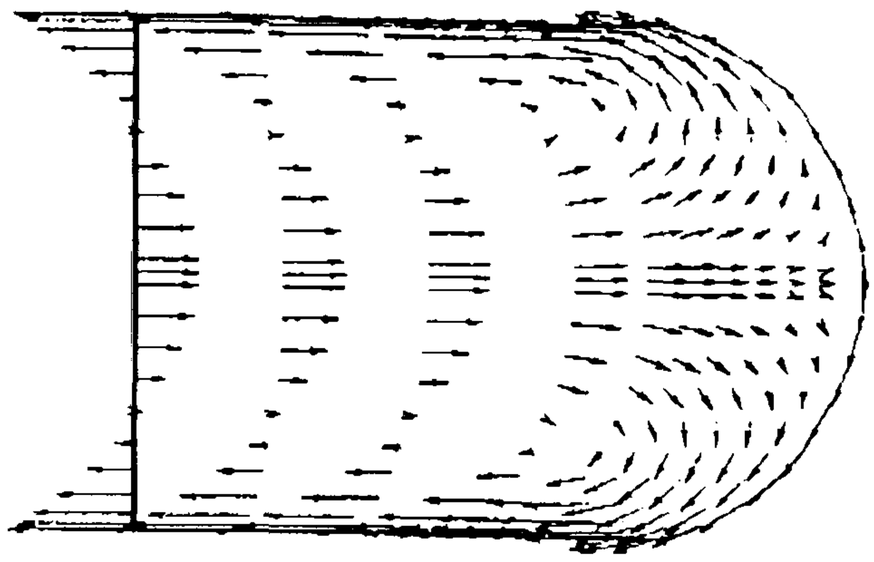

(b)

Figure 4.5 Fountain flow pattern; (a) schematic diagram (b) stream line of melt [49-50].

4.5 Co-Injection Modelling and Mathematical Formulations

At the moment, *there is not an existing commercial CAE software for simultaneous co-injection moulding process* as reviewed in Chapter II. There are several CAE packages, which represent the sequential co-injection moulding process released to the plastics industrial market place. However, it is advantageous to use those sequential co-injection moulding package for simulating the simultaneous co-injection moulding process which can achieve acceptable results [38, 40, Chapter 7.2 (page 93)] from those simulation packages.

A brief review of process modelling and mathematical formulations is given as follows:

4.5.1 Modelling Scheme of the Co-injection Moulding Process

In the case of the co-injection moulding process, the melt flow dynamics depends on the corresponding properties of the skin and core materials. It is no longer suitable to use a hybrid FEM/FDM/Control-Volume [57-58] numerical implementation, which is similar to conventional injection moulding analysis. Nevertheless, the basic theory can still be applied to the individual material regions. The major difference is that the theory is based upon the time and location that the material element enters the mould cavity. That time is called residence time. The residence time is defined as the duration that a particular material element has spent in the cavity since it entered the cavity [38, 57-58]. These means have enabled the simulation of the sequential co-injection moulding process.

By knowing the total injection time and the switchover time from skin to core injection, this analysis model can identify the skin/core materials and trace the skin/core interface during the entire moulding process. Such distribution is called core-polymer thickness fraction, which is defined in Figure 4.6 (a) and (b).

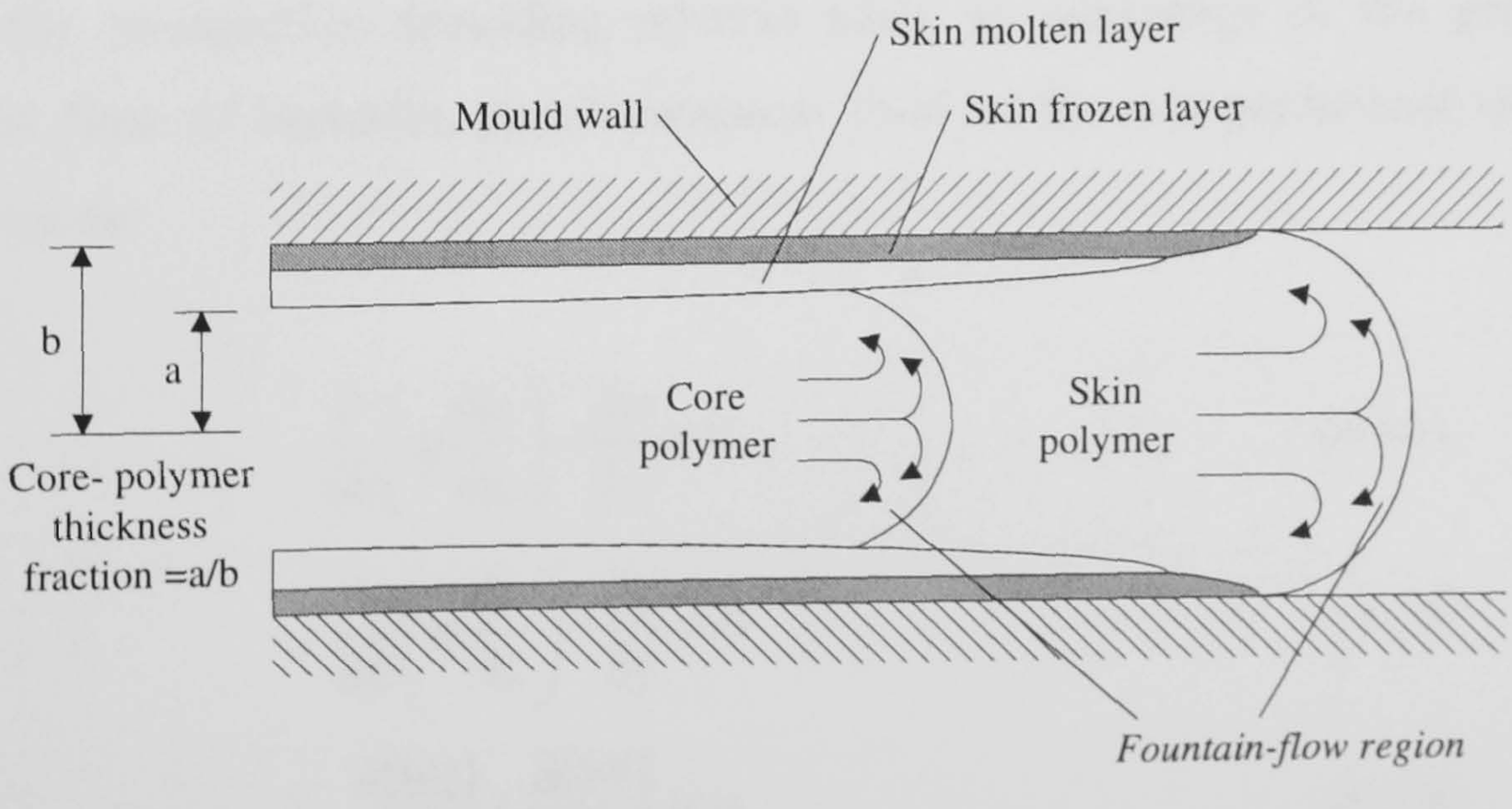

(a)

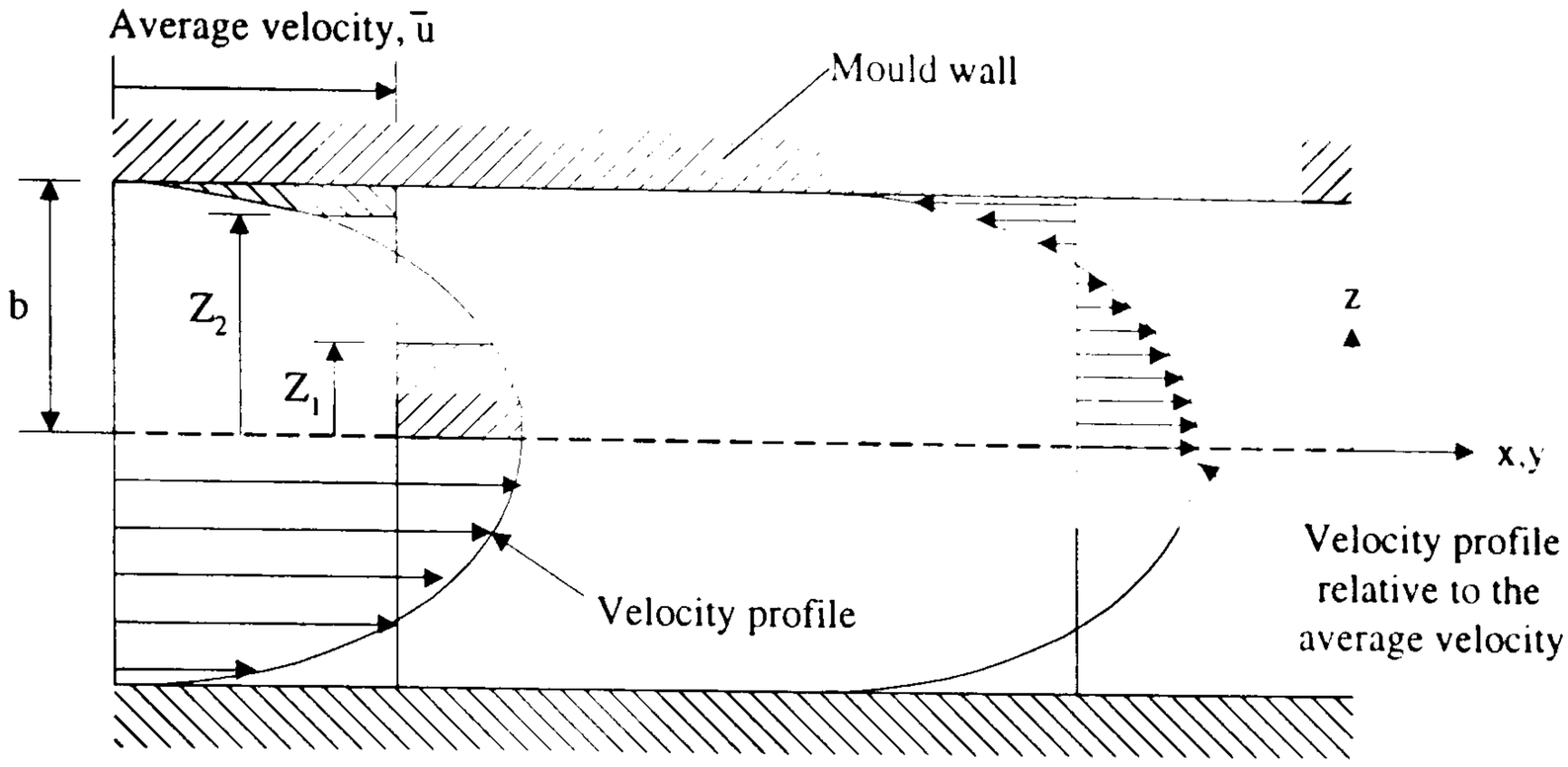

(b)

Figure 4.6 Simulation of core-polymer thickness fraction [38]

However, it should be a concern that the numerical implementation for solving the residence time distribution is not straightforward for complicated structural parts.

4.5.2 Numerical Implementation of the Co-injection Moulding Process [57-58]

The solving of the problem requires a simplification of the co-injection moulding part; in this model, a sheet-like geometry is selected. Each flow dynamics of polymer melts in the co-injection moulding process takes an advantage of the generalised Hele-Shaw flow of inelastic, non-Newtonian fluid under non-isothermal conditions and is given as;

$$\frac{\partial}{\partial z}\left(\eta\frac{\partial u}{\partial z}\right)-\frac{\partial p}{\partial x}=0 \qquad (4.14)$$

$$\frac{\partial}{\partial z}\left(\eta\frac{\partial v}{\partial z}\right)-\frac{\partial p}{\partial y}=0 \qquad (4.15)$$

$$\frac{\partial(b\bar{u})}{\partial x}+\frac{\partial(b\bar{v})}{\partial y}=0 \qquad (4.16)$$

$$\rho C_p\left(\frac{\partial T}{\partial t}+u\frac{\partial T}{\partial x}+v\frac{\partial T}{\partial y}\right)=k\frac{\partial^2 T}{\partial z^2}+\eta\dot{\gamma}^2 \qquad (4.17)$$

Where b is the half-gap thickness.

$\bar{x}$ is denotes an average.

z is the gap wise co-ordination.

t is time.

x, y are the planar co-ordinates.

p is pressure.

T is temperature.

$\dot{\gamma}$ is the shear rate.

η is the shear viscosity.

ρ is the polymer density.

C_p is the specific heat

k is the thermal conductivity.

From those governing Equations (4.14)-(4.17), it is necessary to achieve a sharp interface (no mixing) between skin and core materials. The shear stress and heat are continuous. It has to make assumptions such as:

$$\left(\eta\frac{\partial u}{\partial z}\right)_{skin} = \left(\eta\frac{\partial u}{\partial z}\right)_{core} \qquad (4.18)$$

$$\left(\eta\frac{\partial v}{\partial z}\right)_{skin} = \left(\eta\frac{\partial v}{\partial z}\right)_{core} \qquad (4.19)$$

$$\left(k\frac{\partial T}{\partial z}\right)_{skin} = \left(k\frac{\partial T}{\partial z}\right)_{core} \qquad (4.20)$$

The initial parameters (temperature, residence time, etc.) are then given at start-up. Advancing the melt front, leads to obtaining information such as advancement of melt front, pressure temperature, velocity profile and the residence time of each nodes of the geometry.

At the present time, several CAE developers apply this model and numerical implementation for simulating the sequential co-injection moulding process. One of these is AC technology that develops C-MOLD software, which represents the solution of a sequential co-injection moulding process.

Chapter V
Objectives

As mentioned previously, this work is related to the development of granular injection paint technology, which aims to coat thermoplastic components in the mould by paint. This technique is designed to meet industrial painting requirements with the co-injection moulding process. The technique uses one material in a layered combination with another to achieve an appropriate combination of properties, thus, selection of raw materials for use as skin or core of the sandwich moulding depends on the properties required of the final component.

Therefore, the overall aim of this work is to provide a realistic process technology for skin-core formation of incompatible thermoplastic polymer melts in the thin-walled co-injection moulding. The main problem to be overcome is interfacial adhesion when moulding incompatible material. Compatibilisers are used to promote this bond in alloys (polymer blends) and this methodology can be applied to the dual injection process. There have been several studies on combination of incompatible polymers incorporating compatibilisers [10-15, 22-23], such as utilising maleic anhydride grafted polypropylene to interface polyamide with polypropylene [11-12, 22, 24]. Unfortunately, the compatibilisers were only one of the important factors, which were employed to achieve good interfacial adhesion between polymers. The processing conditions, such as machine setting data, amount of skin and core and rheological properties of moulding materials are also major parameters.

Therefore, the summarised aims of this work were shown as follows.

- To study the filling model for co-injection moulding process.
- To determine the correlation which exists between the viscosity ratios of skin to core materials and the moulding parameters.

- To study the effects of the moulding conditions on the skin-core formations of the incompatible skin and core materials.

- To determine interfaces between phases of each of the polymers and the mechanical properties of the moulding components.

- To investigate the chemical and physical mechanism, which produces good adhesion of incompatible skin and core materials.

Chapter VI
Experiments

A Battenfeld co-injection moulding machine series BMT-1100/2x300 controlled with the UNILOG 9000 system was used in this study. The specification of this machine is given in Table 6.1,

Table 6.1 The Battenfeld co-injection moulding machine series BMT-1100/2x300 specification [21]

Machine Design	Two-stage, hydraulic clamping system with swing disc	
Clamping unit	Clamping force, max. Opening force, max. Space between tie-bars	1100 kN 94 kN 470 mm
Hydraulic ejector	Ejection force, max. Ejection stroke, max.	44 kN 160 mm
Injection unit	Injection force, max. Screw stroke, max. Nozzle contact force, max. Nozzle stroke, max.	238 (2x) kN 125 (2x) mm 187.6 kN 270 mm
Hydraulic unit	Hydraulic oil, tank capacity Oil temperature, min. Oil temperature, max. Switch-on temperature for oil cooling system	380 lit. 35 °C 70 °C 45 °C
Screw drive	Gear box, oil content Thrust bearing, oil content Shift gear box, oil content Electromagnetic clutch, oil content	-- lit. -- lit. -- lit. -- lit.
Mould height adjustment	Reducer gear box, oil content	-- lit.
Central lubricating system	Tank capacity Oil quantity for each lubricating pulse	2.7 lit. 0.1 cm^3
Weight		6,300 kg
Dimensions (length x width)		6.13 x 1.37 m
Cooling water inlet		¾ inch
Cooling water outlet		1 inch

From the mentioned specification, the most important part of this machine is its specially designed nozzle. The representation of this nozzle is shown as follows,

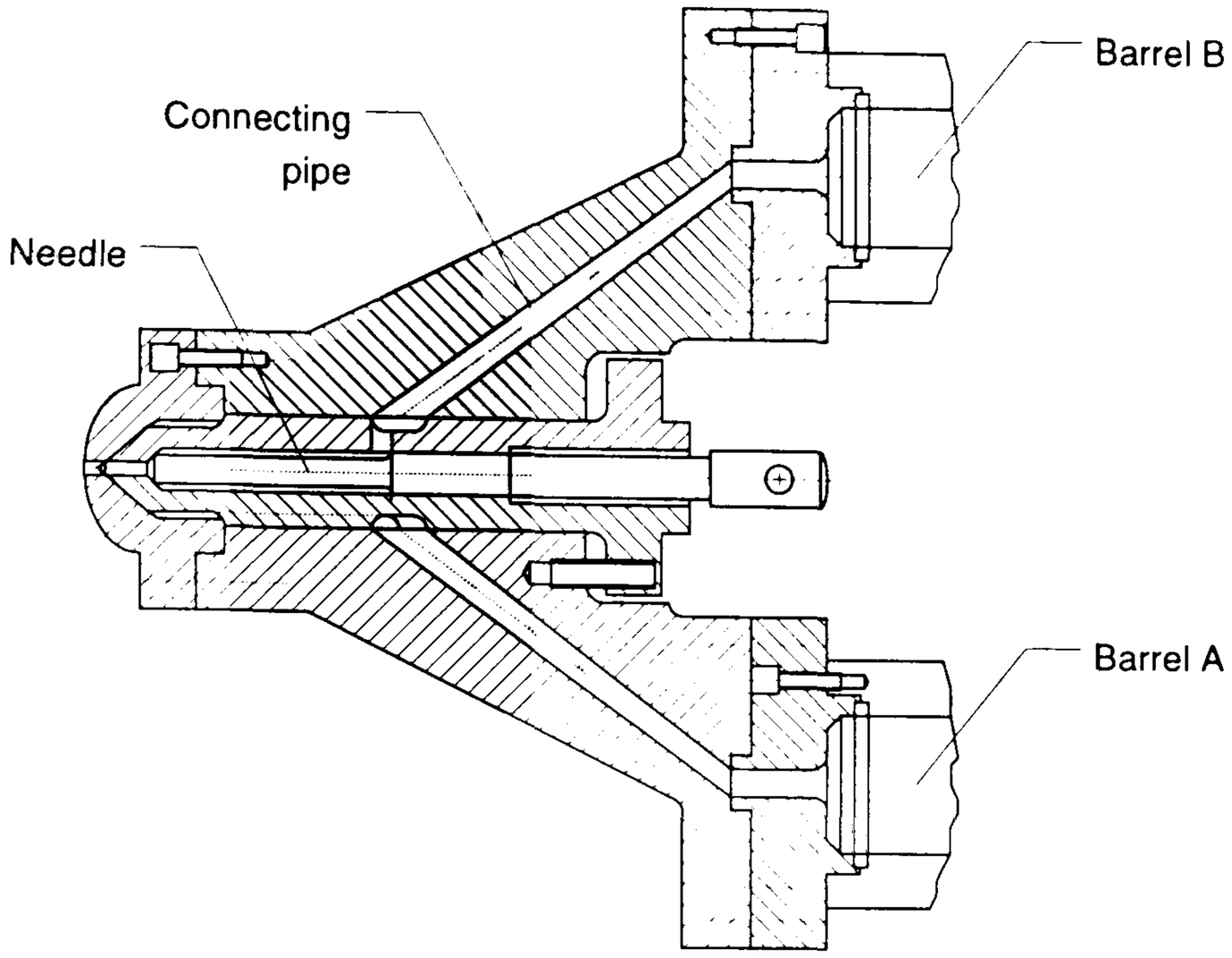

Figure 6.1 The nozzle of the Battenfeld series BMT-1100/2x300 co-injection machine.

6.1 Experimental No.1: PP (Skin)/PP (Core) Moulding Components

6.1.1 Mould

A rectangular plaque mould with cavity dimension 200 x 200 x 3 mm fed via a conventional centred sprue-gate (see Figure 6.2) which was readily available was used in these and other studies.

6.1.2 Materials

Three grades of polypropylene with different viscosities, but with similar thermal conductivity were used in these studies. Their viscosity's are depicted in Figure 6.2 and their values are shown in Table API.2.

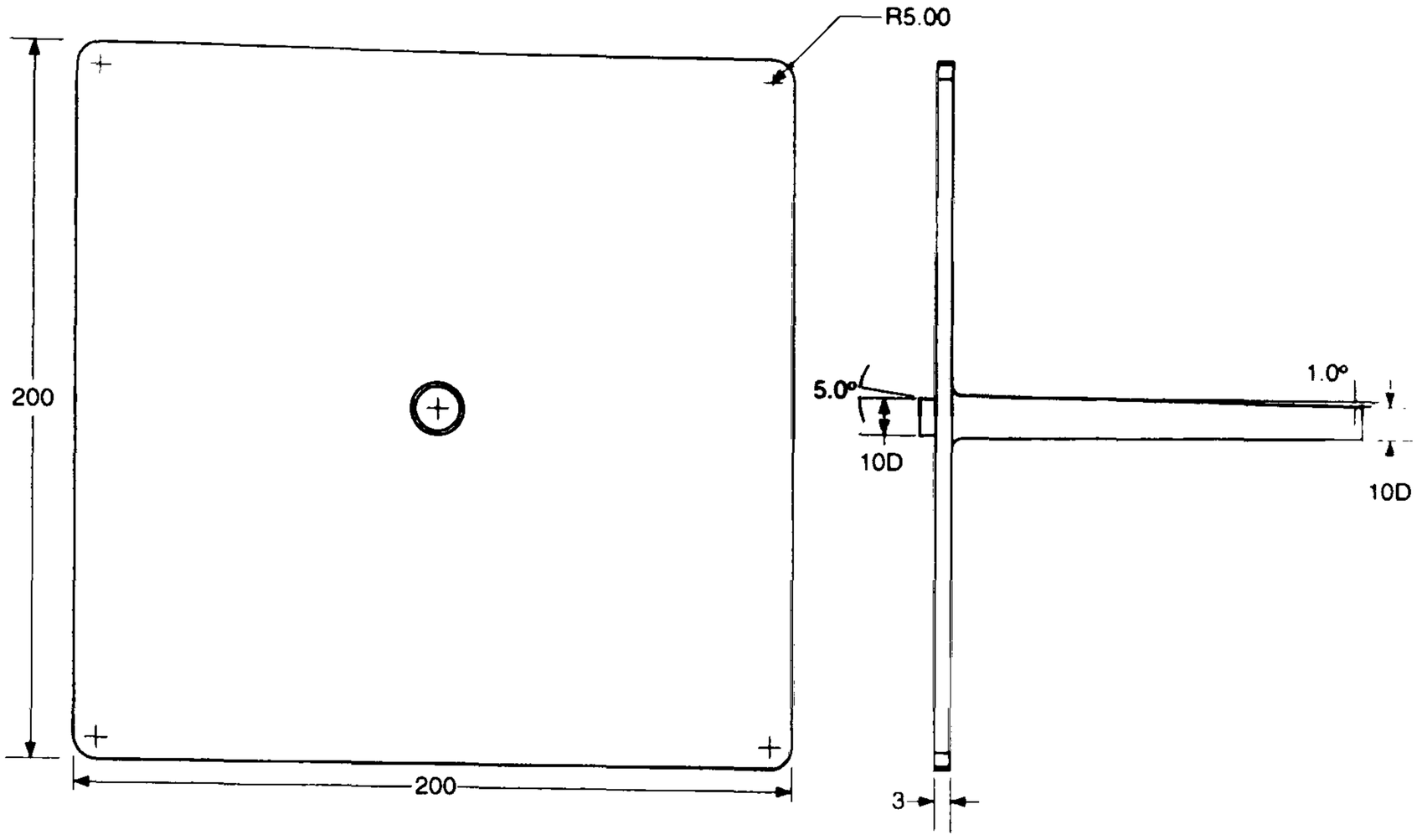

Figure 6.2 Square plaque plate moulding

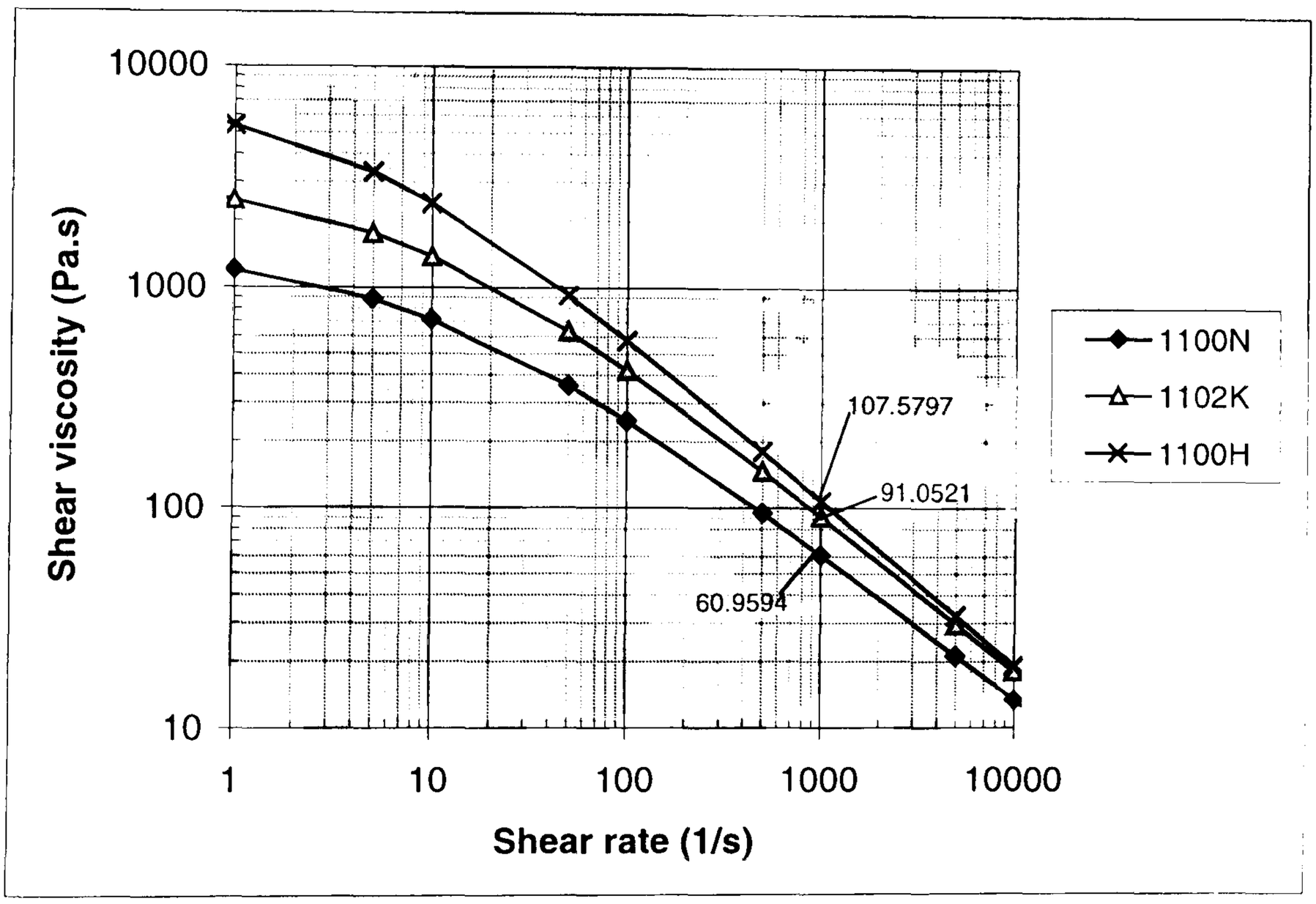

Figure 6.3 Relationship between shear viscosity and shear rate of the three grades of polypropylene (Novolen) at temperature of 235 °C

As shown in Figure 6.3, the skin/core viscosity ratios of all combinations are summarised in Table 6.2

Table 6.2 The skin/core viscosity ratios

No.	Combinations	η_{Skin}/η_{core}
1	1100N/1100H	0.5666
2	1100N/1102K	0.6695
3	1102K/1100H	0.8464
4	1100N/1100N	1.0000
5	1100H/1100H	1.0000
6	1100H/1102K	1.1815
7	1102K/1100N	1.4937
8	1100H/1100N	1.7648

6.1.3 Procedure

The combinations of each polypropylene were simultaneously injected in different volume proportion between skin materials (semi-transparent) and core materials (colour) until the optimum conditions of skin-core were obtained. To achieve the optimum condition of the moulding components, firstly, the metering strokes of skin and core polymer melts were varied until the flow front of the core polymer (colour) approached to the edge of the moulding component with no core breakthrough. Then, switch-over point for injecting core polymer (SWB) and injection speeds of skin (VA) and core (VB) were varied to adjust the flow front of the core polymer and avoid the core breakthrough. The machine control setting data are shown in Table 6.3.

Table 6.3 The moulding condition for experimental no.1

Skin melt temperature (A barrel)	235	°C
Core melt temperature (B barrel)	235	°C
Nozzle temperature	235	°C
Mould temperature	40	°C
Injected A side before B side		
Injection delay time on A side	0.1	s
Injection delay time on B side	0.2	s
Holding pressure on A side	40	MPa
Holding time	15	s
Cooling time	40	s

C-MOLD software was used for simulating the injection time and predicting the skin frozen layer fraction and core polymer thickness fraction. Simulations of conventional injection and co-injection mould moulding process are illustrated in Appendix III.

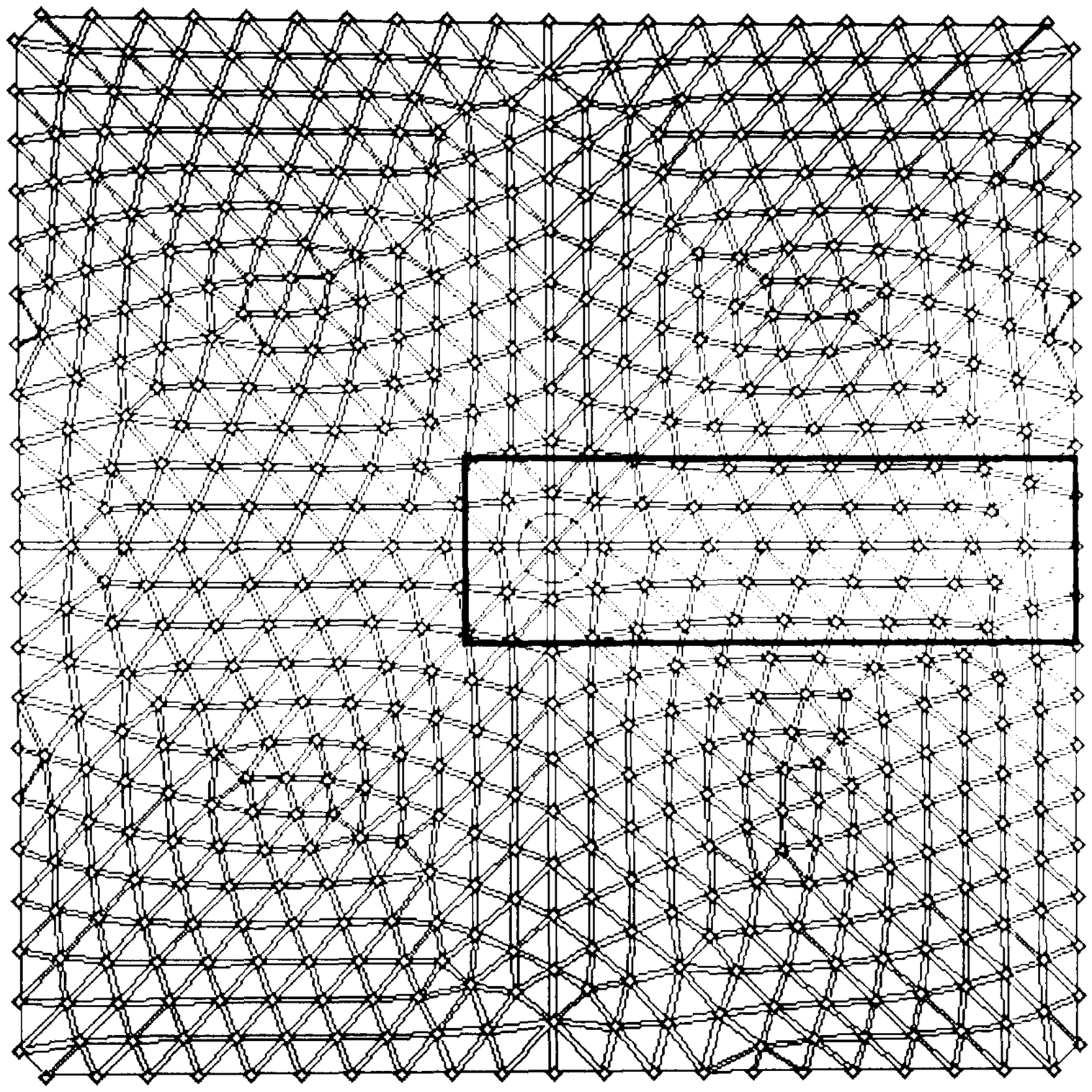

(a)

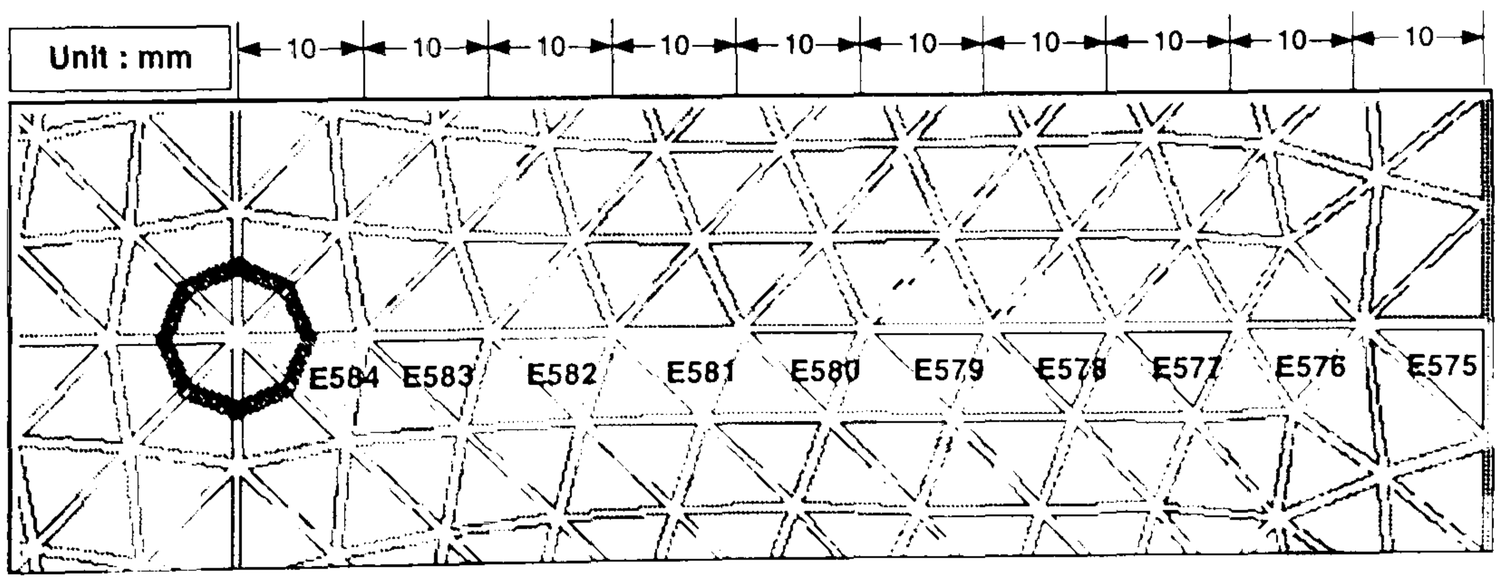

(b)

Figure 6.4 The locations of selected element from C-MOLD filling analysis for square plaque moulding: (a) position of selected elements, and (b) magnified view showing exact location of the elements

After moulding, these components from experiment no.1 were collected and the skin thickness measured. Figure 6.4 shows the geometry element meshes and the selected elements for determining skin information.

The components from co-injection moulding were sectioned as seen in Figure 6.4. The skin thickness fractions were determined using Image processing software (see Appendix IV). The beginning of measured distance was found to be at the edge of component, and increased up to the centre of the moulding component. The specimen is shown as follows:-

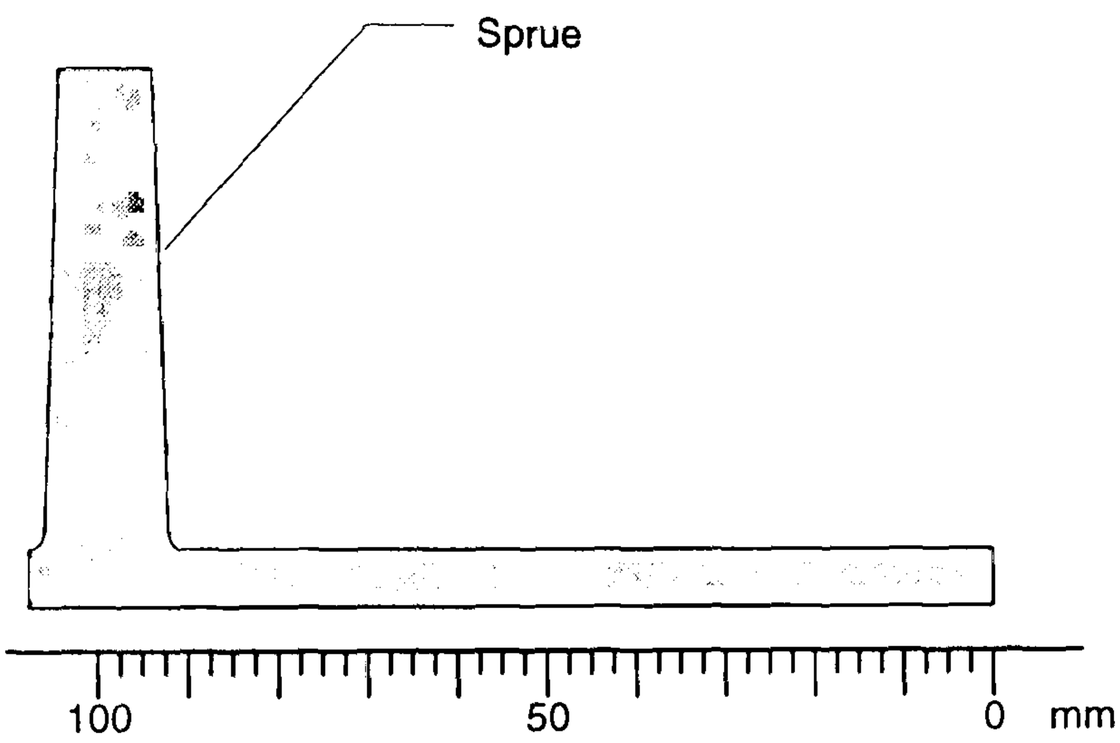

Figure 6.5 Cross section of the specimen from the square plaque moulding.

6.2 Experimental No.2: PA6 (Skin)/PP (Core) Moulding Components

6.2.1 Materials

In this section, three grades of polypropylene (PP)* and three grades of polyamide 6 (PA6)** were used as core and skin materials, respectively. Their viscosity data was obtained from the materials supplier database (C-MOLD) and shown in Table 6.4.

---

* Polypropylene Novolen (1100H, 1102K, 1100N) obtained from Targor

** Polyamide 6 Durethan (B30S, B31SK) obtained from Bayer

Table 6.4 Shear viscosity data of polypropylene and polyamide 6 at the various temperatures.

Temperature (°C)	Shear viscosity (η) at shear rate (γ) of 10^3 s^{-1}, (Pa.s)				
	Polypropylene (Novolen)			Polyamide 6 (Durethan)	
	1100N	1102K	1100H	B31SK	B30S
190	85.1601	126.8097	139.6493		
195	81.6334	121.6051	135.0899		
200	78.3674	116.7842	130.8360		
205	75.3360	112.3082	126.8590		
210	72.5160	108.1433	123.1338		
215	69.8874	104.2594	119.6378		
220	67.4324	100.6304	116.3513	332.4289	231.3575
225	65.1351	97.2329	113.2564	284.5636	215.4223
230	62.9816	94.0462	110.3373	244.2015	200.5876
235	60.9594	91.0521	107.5797	210.0534	186.7895
240	59.0575	88.2342	104.9709	181.0799	173.9678
245	57.2660	85.5778	102.4994	156.4361	162.0652
250	55.5758	83.0699	100.1548	135.4293	151.0263
255				117.4876	140.7975
260				102.1362	131.3269
265				88.9787	122.5643
270				77.6829	114.4611
275				67.9696	106.9710
280				59.6032	100.0496

Note: Viscosity data were obtained from C-MOLD materials database and calculated using Cross-WLF viscosity model as shown in Appendix I.

In this experiment, the skin melt temperature of 260 °C and the core melt temperature of 235 °C were selected for moulding. Therefore, from Table 6.4, the combinations of skin/core and their viscosity ratios were shows as follows.

Table 6.5 The skin/core viscosity ratios of PA6 (Durethan) and PP (Novolen)

No.	Combinations	η_{Skin}/η_{core}
1	B31SK/1100H	0.9494
2	B31SK/1102K	1.1217
3	B30S/1100H	1.2207
4	B30S/1102K	1.4423
5	B31SK/1100N	1.6755
6	B30S/1100N	2.1543

6.2.2 Procedures

The mould and machine setting data were similar to experiment no.1, except barrel, nozzle, and tool temperature were varied (see Table 6.6). Both of skin and core polymer melts were injected in different volume proportion. All parameters were

recorded when the skin-core configuration was optimised by changing skin and core metering strokes, injection speed of skin and core, switch-over point for injecting core polymer, etc. After the moulding was removed from the mould, the component was cut at the mid-point along the centre line of the moulding part. The skin-core thickness fractions were then obtained using Image processing software.

Additionally, the skin frozen layer and core polymer thickness fractions were simulated using the co-injection moulding module from C-MOLD software package. It was able to simulate flow and temperature profiles. Also by using rheological data of skin and core materials, the skin frozen layer and core polymer thickness fractions were predicted. However, the conventional injection moulding module, which is also available in C-MOLD software package, was used for simulating the skin frozen layer fraction (thickness) and then both skin frozen layer information were compared.

Table 6.6 Moulding conditions for experimental no.2

Skin melt temperature (A barrel)	260	°C
Core melt temperature (B barrel)	235	°C
Nozzle temperature	247	°C
Mould temperature	80	°C
Injected A side before B side		
Injection delay time on A side	0.1	s
Injection delay time on B side	0.2	s
Holding pressure on A side	40	MPa
Holding time	15	s
Cooling time	40	s

6.3 Experimental No.3: PA6 (Skin)/PP with Compatibiliser (Core) Moulding Components

6.3.1 Materials

The materials were the same grades as in experimental no.2, including compatibiliser. In this study, the compatibiliser is maleic anhydride grafted polypropylene (PP-g-MA), named Polybond 3150 with 0.5% by weight of maleic anhydride level in this copolymer. The modified core materials were prepared by dry-blend mixing

unmodified polypropylene with 10% by weight of the compatibiliser (see Appendix II, the optimum amount of compatibiliser for incompatible skin (PA6) and core (PP)).

However, the rheological data of the unmodified core and modified core materials were acquired using ROSAND Advance Extrusion Capillary Rheometer (ASTM D3835 test method [59]), then the results were compared to determine the effect of compatibiliser on the core viscosity. The rheometer schematic is shown in Figure 6.6.

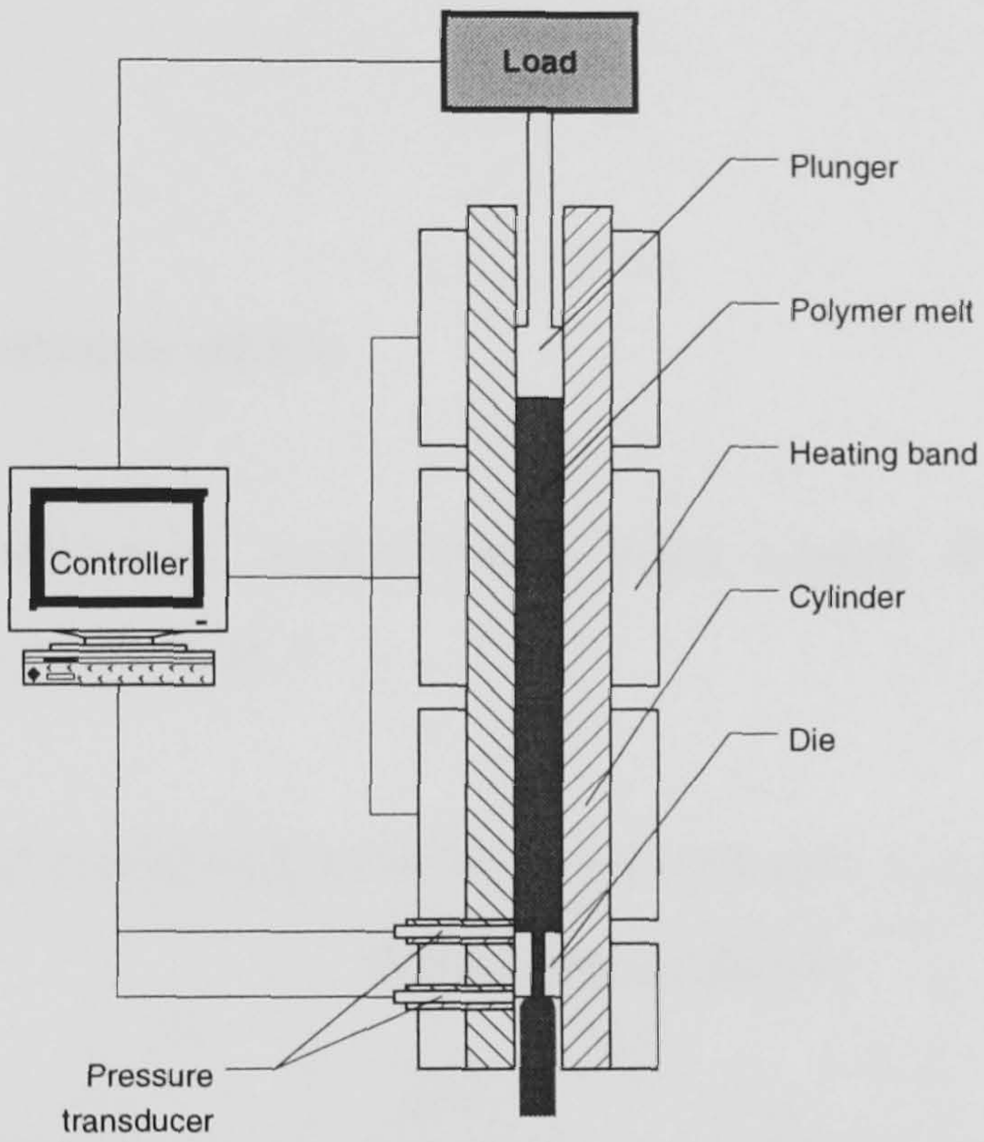

Figure 6.6 Diagram of capillary rheometer.

6.3.2 Procedure

By using the same moulding conditions as experimental no.2, the skin-core distribution of this experiment (experiment no. 3) could be compared to experiment no.2. Both skin and core polymer melts were injected in different volume proportion. The parameters were changed until the optimum skin-core condition was obtained. After the removal of the moulding parts from the mould, the components were cut at the mid-point along of the moulding part (see Figure 6.4 and 6.5). The skin-core thickness fractions was then determined using Image processing software.

6.4 Experimental No.4: Effects of Moulding Conditions on Skin-Core Thickness Fractions and Adhesion.

6.4.1 Materials

The polyamide 6 (Durethan/B31SK) and the polypropylene (Novolen/1100H) with and without 10 % of compatibiliser were used in these studies. Their viscosity data is shown in Table 6.4, experimental no.2.

6.4.2 Procedures

6.4.2.1 Effect of melt temperatures

In this section, the skin-core temperatures were varied. Their combinations of temperatures are given in Table 6.7

Table 6.7 The combinations of temperatures and viscosity ratios.

	No.	Melt temperatures (°C)		η_{Skin}/η_{core}
		Skin	Core	
Variation in core melt temperature	1	260	225	0.9018
	2	260	235	0.9494
	3	260	245	0.9965
Variation in skin melt temperature	4	250	235	1.2589
	5	260	235	0.9494
	6	270	235	0.7221

*Viscosity data see also Table 6.4

The moulding conditions of this experiment, such as volume proportion of skin, core materials, their injection speeds were the same as the one's used in experimental no.2, combination no.1 (Table 6.5).

6.4.2.2 Effect of tool temperatures

As mentioned in experimental no.2 (combination no.1), the machine setting data and moulding conditions were duplicated. However, various temperatures of tool were installed. These were set at the temperatures of 40, 60, 80, and 100 °C, respectively.

6.4.2.3 Effect of injection speeds

The moulding conditions and machine setting data were the same as mentioned in experimental no.2 (V_{core} = 135 mm/s and V_{skin} = 114 mm/s). Nevertheless, the injection speeds of skin and core melts were varied as follows.

a) Various skin injection speeds and constant core injection speed

V_{core} = 135 mm/s

V_{skin} = 64, 94, 114, 134, 164 mm/s

b) Various core injection speeds and constant skin injection speed

V_{skin} = 114 mm/s

V_{core} = 85, 115, 135, 155, 185 mm/s

After the moulded components were removed, the samples were sectioned then the skin-core thickness fractions were measured.

6.4.2.4 Effect of lengths of simultaneous injection phase

In this case study, it was proposed to investigated the length of time of the simultaneous phase (TOL)* and its effect on the skin-core penetration. Materials, machine setting data, and moulding conditions were similar to the combination no.1 in experiment no.2.

---

* Calculation of investigated the length of time of the simultaneous phase (TOL) will be discussed in chapter VII (equation 7.5).

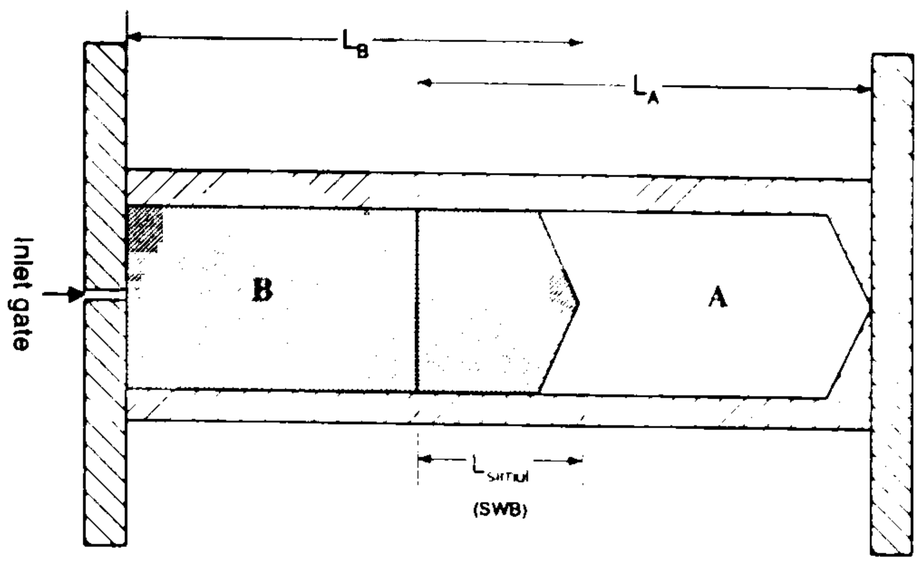

Figure 6.7 The simultaneous injection phase.

As seen in Figure 6.7, lengths of simultaneous injection phase (L_{simul})* were varied by two options; one is injection core polymer (B) sooner, and another one was injection core polymer (B) later.

Therefore, this experiment was divided into two subsections as follows.

a) Variation in the length of simultaneous injection phase (L_{simul}) by injecting B sooner. This was achieved by setting the switch-over points of B-side (SWB) at 35 mm, and 25 mm of A-side metering stroke, respectively.

b) Variation in the length of simultaneous injection phase (L_{simul}) by injecting B later. This was achieved by setting the switch-over points of B-side (SWB) at 15 mm, and 6 mm of A-side metering stroke, respectively.

6.4.2.4 Effect of skin/core metering stroke ratios

In this case study, it was proposed to investigate the skin and core metering strokes and the effect on the skin-core penetration. Materials, machine setting data, and moulding conditions were similar to the combination no.1 in experimental no.2. The metering stroke of skin and core were set at 65/60, 70/55, 75/50, and 80/45 mm/mm, respectively.

---

* Calculation of the length of simultaneous injection phase (L_{simul}) will be discussed in chapter VII (equation 7.6).

6.5 Analysis

6.5.1 Instruments

- Optical Microscope
- Scanning Electron Microscope (SEM)
- Instrumented Impact Tester (ICI Australia Operation Pty Ltd)
- Universal Testing Machine (Lloyd Instruments model M30K)

6.5.2 Sample preparations and procedures

6.5.2.1 Impact test

In this section, the components from experimental no. 2, 3, and 4 were cut with the dimension of 100x100 mm along the centre line. They were then marked for the impact point (Figure 6.8). Impact strength of the components was determined and is illustrated in Appendix VII, Table APVII.1.

6.5.2.2 Peel test

The components from experimental no.4 were also cut with the dimension of 90x20 mm along the centre line. The specimens thickness were 3.0±0.1 mm. Before performing the peel test, the specimens had to have a peel skin layer of 10 mm initiate for clamping with the grip (Figure 6.9), then the load could be applied to measure the peel strength.

Moreover, the minimum skin thickness fractions which provided a good skin-core adhesion were obtained from the correlation between the peel strengths and the thickness fractions of the moulding components.

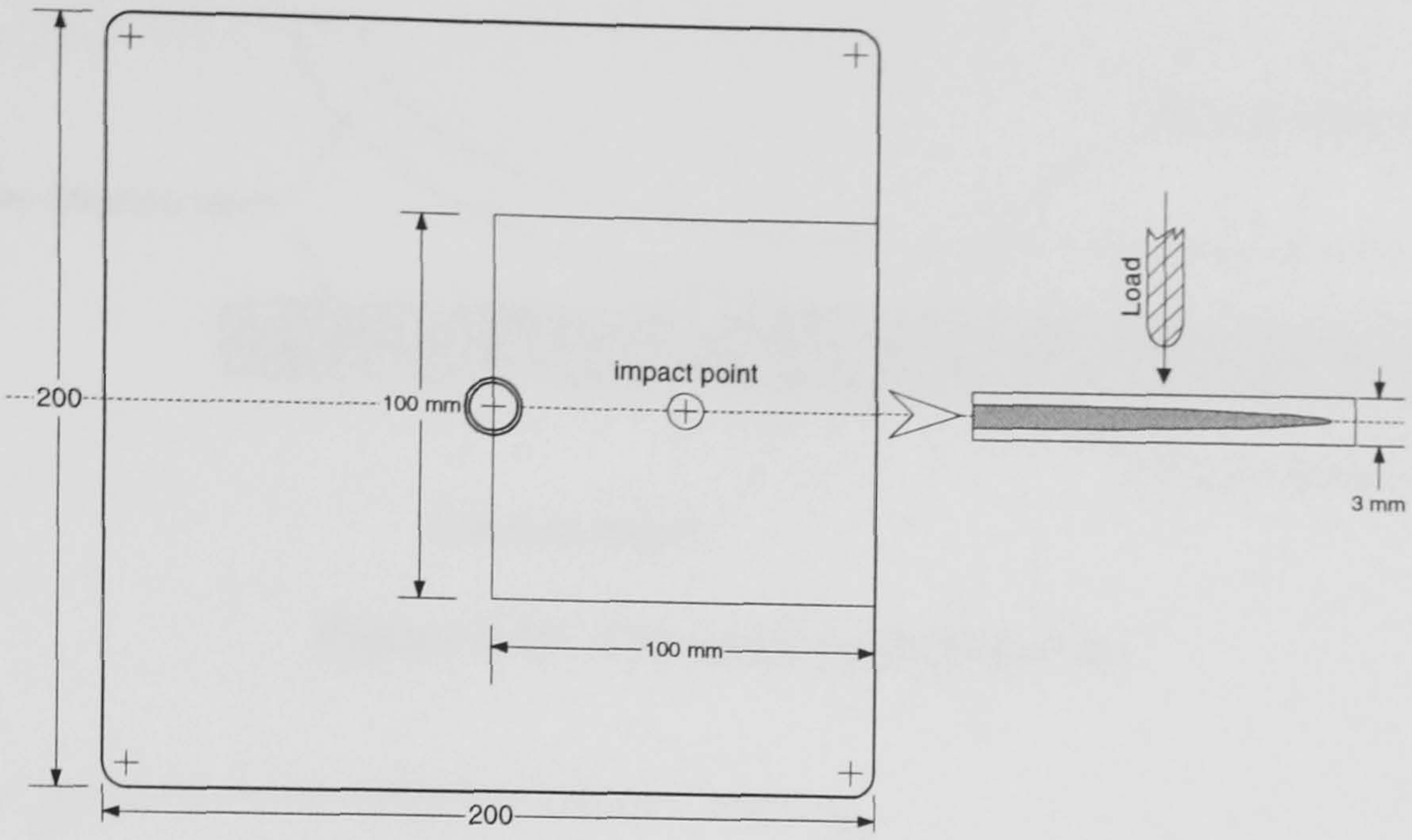

Figure 6.8 Impact test specimen

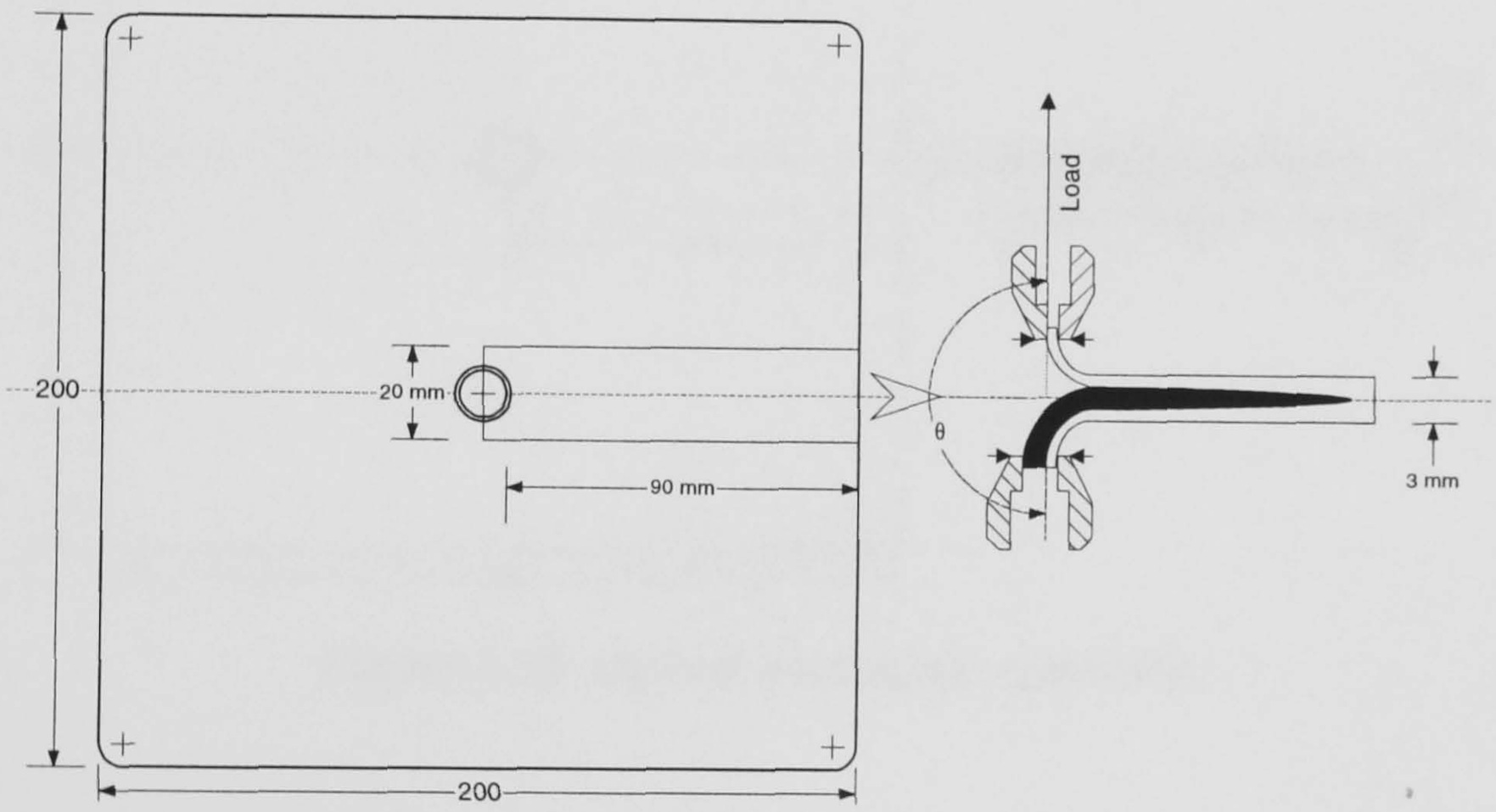

Figure 6.9 Peel test specimen

6.5.2.3 Scanning electron microscope (SEM)

In this analysis, the components were also from experiment no.4 (Durethan B31SK (Skin)/Novolen 1100H with 10% of Uniroyal Polybond G3150 (Core)). The crack tip was prepared by using a fresh razor blade inserted into the mid-plane of interface between skin and core as seen in Figure 6.10. The crack tip regions were investigated using SEM. The results will be described in Chapter VII.

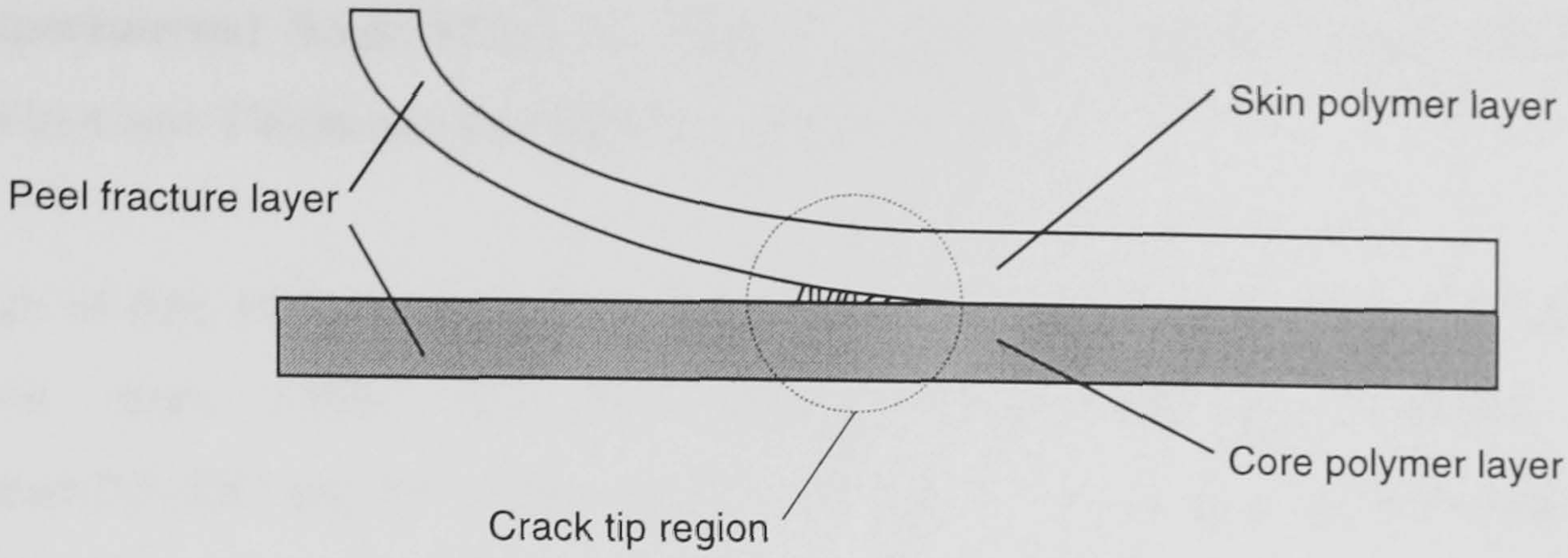

Figure 6.10 The crack tip propagation

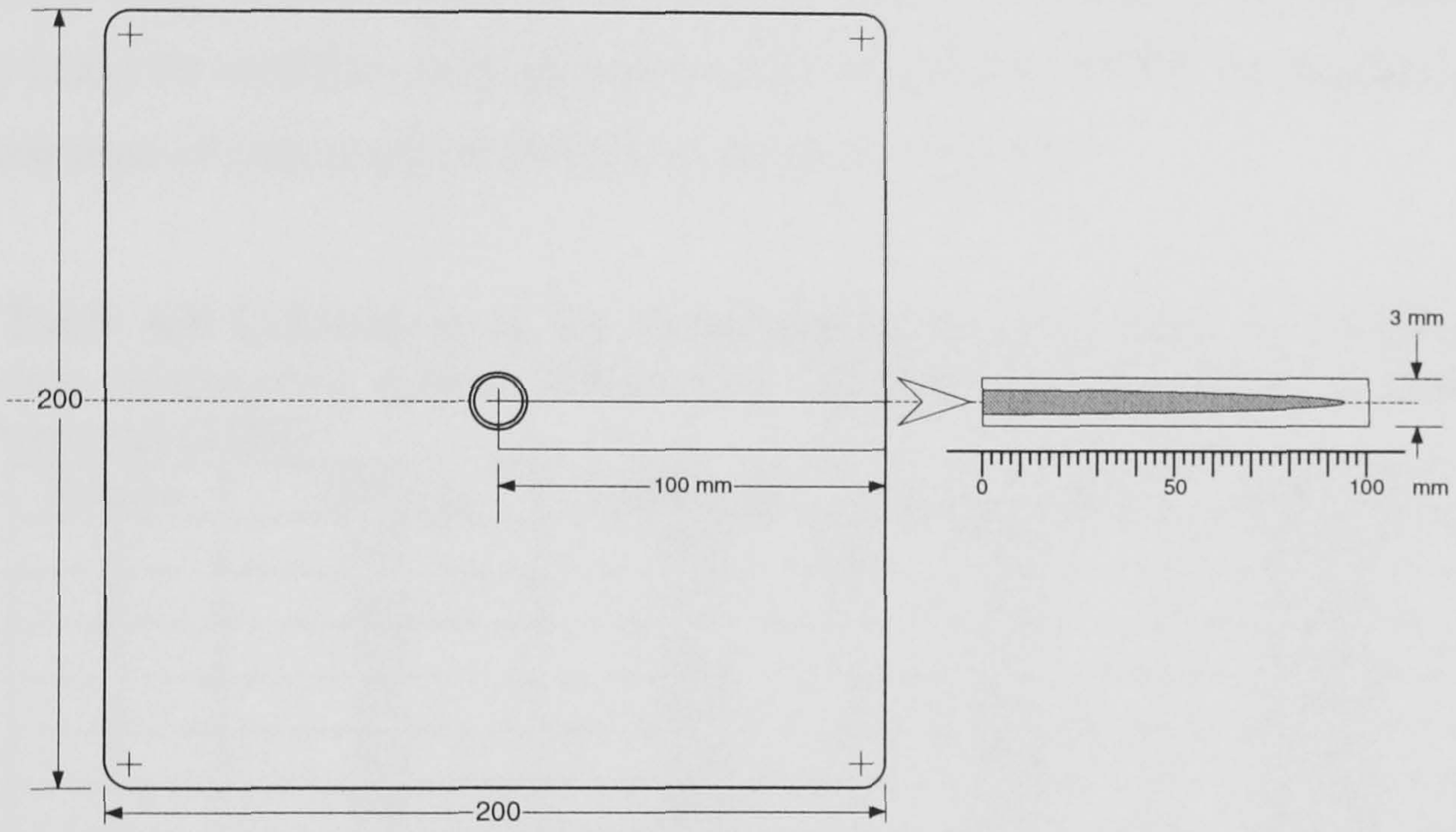

Figure 6.11 Optical microscope specimen

6.5.2.4 Optical microscope

In this analysis, the interfaces between polymer phases were studied. Specimens were prepared by sectioning along the centre line as seen in Figure 6.11. The specimens were then polished using a soft material polishing technique. At the locations of 20, 50 and 70 mm from the central gate, an optical microscope attached with camera was used for determination of the interfaces between polymer phases. After performing the peel test, the peel fractures of the specimens were also determined by a microscope at the same location.

6.6 Experimental No.6: Effect of The Simultaneous Injection Times (TOL) on The Skin-Core Thickness Formations and Adhesion.

The aim of this study was to investigate the relationship between the simultaneous injection times (TOL) and the minimum skin thickness fractions. PA6 (Durethan/B31SK) and PP with compatibiliser were used as skin and core materials. Unfortunately, the grade of PP was changed from Novolen/1100H to Novolen/1102K, because Novolen/1100H was no longer in existence in the market place and Novolen/1102K is very similar to Novolen/1100H. The simultaneous injection times (TOL) could be varied by varying core switch-over points (SWB) and by delaying the injection time of core material (TDB) as shown in Table 6.8.

Table 6.8 Calculation of the simultaneous injection times by varying core switch-over points (SWB) and delaying injection time of core material (TDB)

Data no.	TDB (s)	SWB (mm)	Lsimul* (mm)	TOL** (s)
1	0.0	70.0	70.0	0.6140
2	0.0	60.0	60.0	0.5263
3	0.0	50.0	50.0	0.4386
4	0.0	40.0	40.0	0.3509
5	0.0	30.0	30.0	0.2632
6	0.0	20.0	20.0	0.1754
7	0.0	10.0	10.0	0.0877
8	0.1	30.0	18.6	0.1632
9	0.1	20.0	8.6	0.0754
10	0.1	10.0	-1.4	-0.0123
11	0.2	30.0	7.2	0.0632
12	0.2	20.0	-2.8	-0.0246
13	0.2	10.0	-12.8	-0.1123
14	0.3	40.0	5.8	0.0509
15	0.3	30.0	-4.2	-0.0368
16	0.3	20.0	-14.2	-0.1246
17	0.3	10.0	-24.2	-0.2123
18	0.4	50.0	4.4	0.0386
19	0.4	40.0	-5.6	-0.0491
20	0.4	30.0	-15.6	-0.1368
21	0.4	20.0	-25.6	-0.2246
22	0.4	10.0	-35.6	-0.3123
23	0.5	30.0	-27.0	-0.2368
24	0.5	20.0	-37.0	-0.3246
25	0.5	10.0	-47.0	-0.4123

Other constant parameters: skin metering stoke (SOA) = 70.0 mm, core metering stoke (SOB) = 55.0 mm, skin melt cushion (SCA) = 5.0 mm, core melt cushion (SCB) = 0.0 mm, skin injection speed (VA) = 114 mm/s, and core injection speed (VB) = 135 mm/s.

---

* Lsimul =TOL*VA (7.6)

** TOL= (SWB/VA) – TDB (7.5)

After the moulding components were removed from the mould, the peel tests were performed. Their skin-core thickness fractions were also investigated. The minimum skin thickness fractions were then obtained from the correlation between the peel strength and skin-core thickness fraction curves.

Chapter VII

Results and Discussions

7.1 The Filling Model for The Co-injection Moulding Process

The co-injection moulding (sometimes called sandwich injection moulding) is the process, which injects two or more different polymer melts sequentially or simultaneously into a moulded cavity. A multilayered structure is then formed by the first injected polymer melt which forms the skin and the subsequently injected polymer forms the core. Thus, a filling model is deemed necessary in order to understand how these skin and core melts form a multilayered structure and to understand the effect of the co-injection moulding machine on the process. A typical filling model schematic is shown as follows.

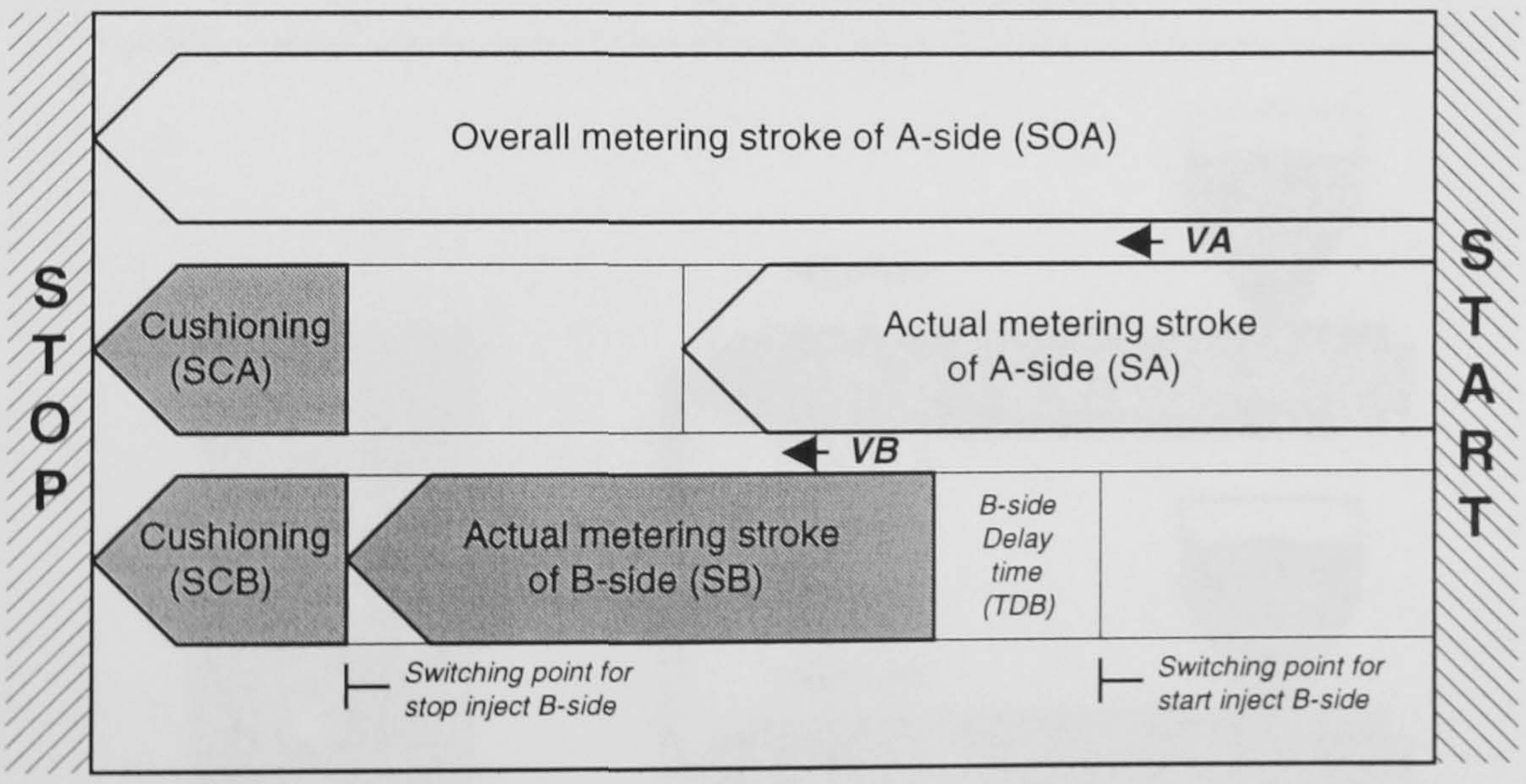

Figure 7.1 Sequence of the co-injection moulding process

The guidelines for finding mould conditions and parameters is, therefore, available. The schematic diagram of this model has been investigated [8] as shown in Figure 7.2.

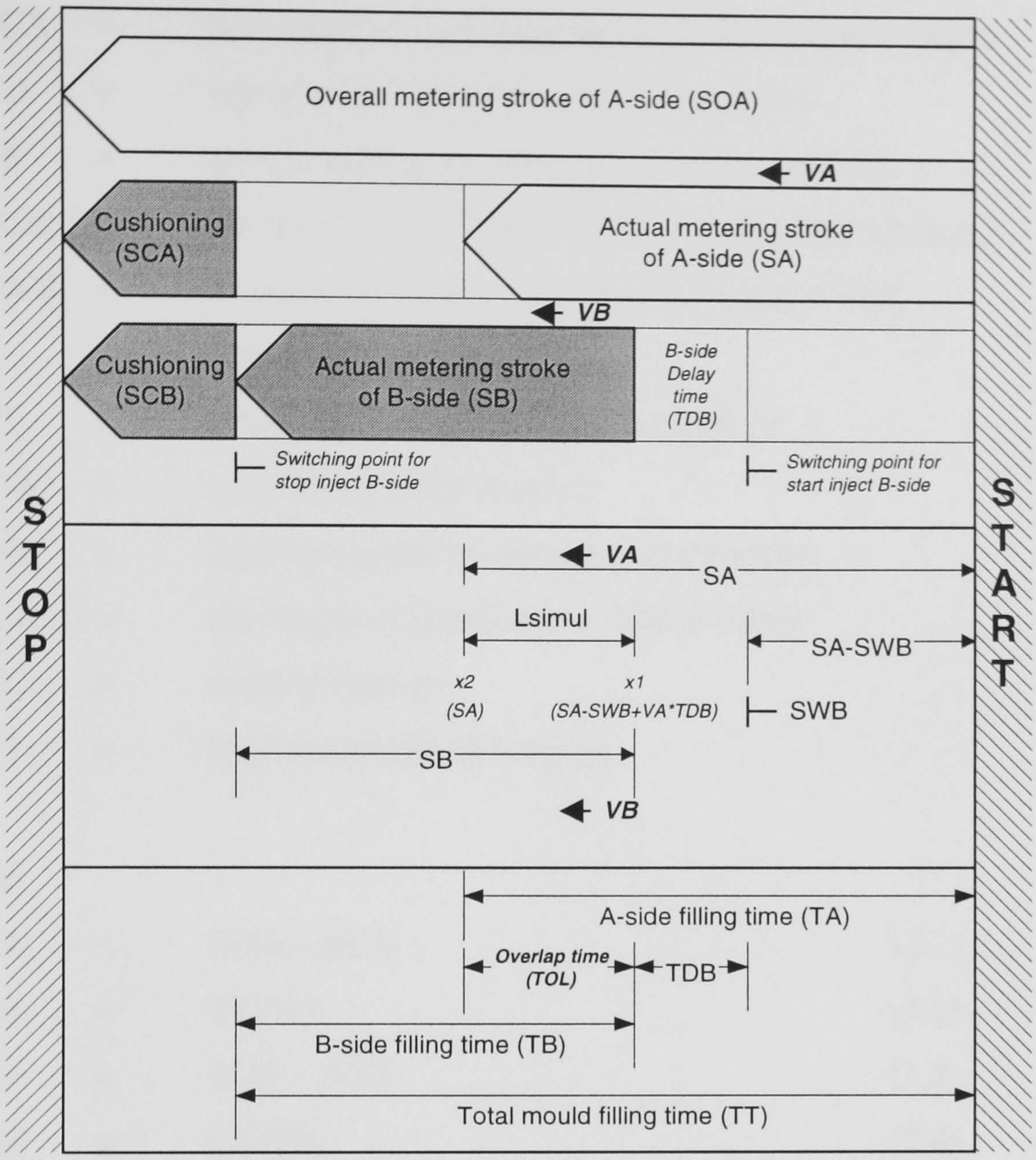

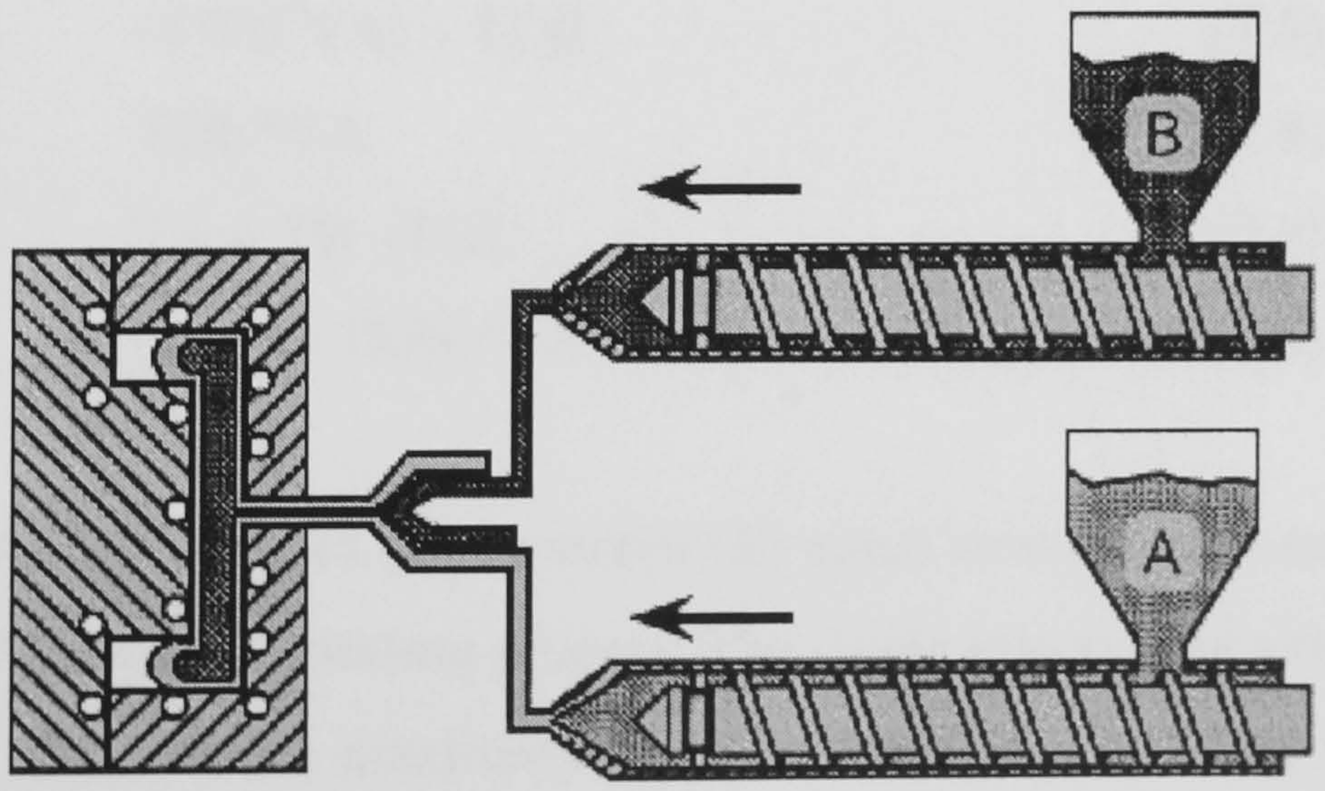

Figure 7.2 The mould filling model for co-injection moulding process.

From above diagram, all parameters were assigned as follows:

SOA = overall metering stroke of skin material (mm)

SA = actual metering stroke of skin material (mm)

TA = actual filling time for skin material (s)

SCA = the length of melt cushioning of skin material (mm)

VA = injection speed for skin material (mm/s)

SB = overall metering stroke of core material (mm)

SCB = the length of melt cushioning of core material (mm)

SWB = switch-over point to start filling stroke of core material (mm)

TB = actual filling time for skin material (s)

TDB = core filling delay time (s)

VB = injection speed for core material (mm/s)

Lsimul = the length of simultaneous phase (mm)

TOL = overlap time (s)

TT = total mould filling time (s)

Therefore;

$$SA = SOA - SCA \quad (7.1)$$

$$TA = SA/VA \quad (7.2)$$

$$SB = SOB - SCB \quad (7.3)$$

$$TB = SB/VB \quad (7.4)$$

$$TOL = (SWB/VA) - TDB \quad (7.5)$$

$$L_{simul} = TOL*VA \quad (7.6)$$

$$TT = TA + TB - TOL \quad (7.7)$$

$$SWB = (TOL + TDB)*VA \quad (7.8)$$

By letting the metering stoke of core material (B) equal zero, the process is simplified to a conventional injection moulding process. The single injection of skin material (A) is introduced to obtained the maximum cavity volume (S_{max}). Then, the maximum injection velocity (V_{max}) is obtained from the following relationship.

$$V_{max} = S_{max}/t_{pred} \quad (7.9)$$

Where t_{pred} is the filling time for injecting the skin material into the cavity. This was simulated using the C-mold software.

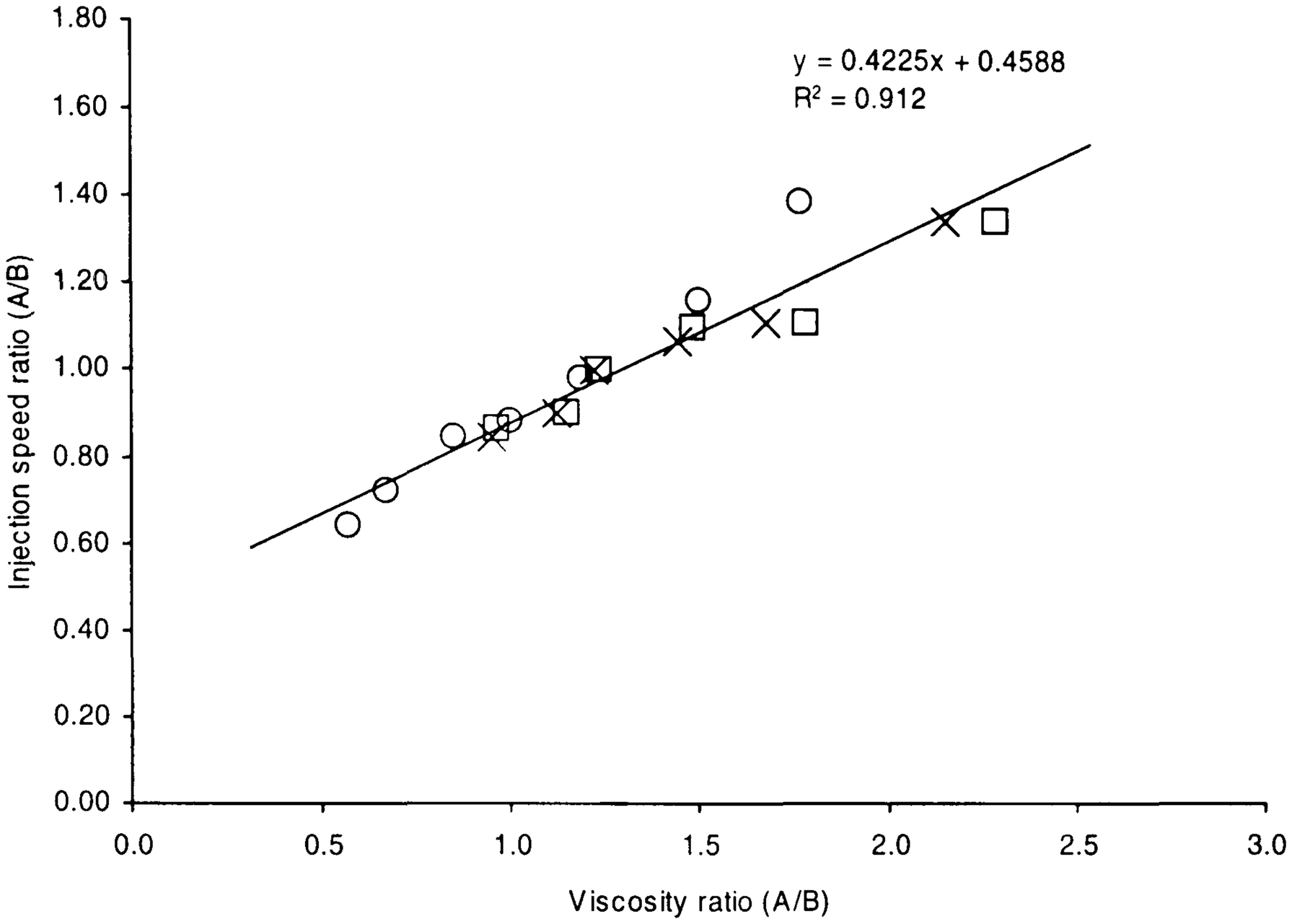

Figure 7.3 Relationship between viscosity ratios of skin to core (η_A/η_B) and skin/core injection speed (VA/VB): (○)PP(skin)/PP (core), (□) PA6(skin)/PP(core), and (x) PA6(skin)/PP with 10% Polybond 3150(core), respectively. The correlation between η_A/η_B and VA/VB is,

$$y = 0.4225x + 0.4588$$

where x is skin/core viscosity ratios and y is skin/core injection speed ratios. R^2 is 0.912, which mean 91.2% of data are applicable.

In this section, it is aimed to determine the correlation which exists between the viscosity ratios of skin to core materials (η_A/η_B) and the moulding parameters, such as the skin to core injection speed (VA/VB) and the simultaneous time (TOL). Firstly, polypropylenes (PP) were used as skin and core material. Secondly, the core polymer was still the same as experiment no.1, but the skin polymer was polyamide 6 (PA6). Then, the skin was PA6 and the core was PP but mixed with 10% of compatibiliser. All combinations between skin and core material were investigated by changing the various viscosity ratios of skin to core. Afterwards, the optimum conditions for each combination were recorded. Three groups of data were investigated by constructing a plot as in Figure 7.3. The relationship between η_A/η_B and VA/VB was found to be a

linear trend overall range of viscosity ratios. It was found that a correlation existed between the skin/core viscosity ratios and skin/core injection velocity ratios and was determined in Figure 7.3.

Comparison between Somnuk's work [8] and current work was investigated and is compared by the slope equations from Figure 7.3,

Somnuk's model: $y = 0.4104x + 0.4723$ (7.10)

Current model: $y = 0.4225x + 0.4588$ (7.11)

It can be seen from the correlation (equation 7.10 and 7.11) that the equations were slightly different. From the equation 7.11, it was possible to predict the injection velocity for skin and core material if its skin/core viscosity ratio was known. The prediction of VA and VB is described as follows:

$$\frac{VA}{VB} = 0.4225\frac{\eta_A}{\eta_B} + 0.4588 \quad (7.11)$$

If $\frac{VA}{VB} \geq 1.00$ then,

$$VA = \frac{S_{max}}{t_{pred}} \quad (7.12)$$

$$VB = \frac{S_{max}}{t_{pred}\left[0.4225\frac{\eta_A}{\eta_B} + 0.4588\right]} \quad (7.13)$$

Else if $\frac{VA}{VB} \leq 1.00$ then,

$$VB = \frac{S_{max}}{t_{pred}} \quad (7.14)$$

$$VA = \frac{S_{max}}{t_{pred}\left[0.4225\frac{\eta_A}{\eta_B} + 0.4588\right]} \quad (7.15)$$

However, the simultaneous injection time (sometime called overlap time, TOL) was found to be an important parameter. The skin-core thickness fraction and their sandwich structure were controlled by varying the switch-over point to start the filling stroke of core material (SWB). In the experimental study of the simultaneous co-injection moulding process, which was investigated by Somnuk [8], it was claimed that the good filling results were achieved by letting the duration of simultaneous injection period correspond to almost 95 % of the injection time for the skin. Thus, it could be concluded that the suitable overlap time or simultaneous injection time for optimum moulding components was 5.0 % of the total injection time, approximately.

In fact, the simultaneous injection time for the optimum moulding components was related to the viscosity ratio of skin to core. The relationship between simultaneous injection times and the skin/core viscosity ratios is depicted in Figure 7.4 (page 90).

If the viscosity ratios of skin to core (η_A/η_B), the actual metering stoke of skin and core (SA and SB), the maximum metering stoke (S_{max}), the predicted filling time (t_{pred}), and the core filling delay time (TDB) were known, then the moulding parameters are therefore obtained and summarised as shown in Table 7.1 and 7.2 (page 91-92).

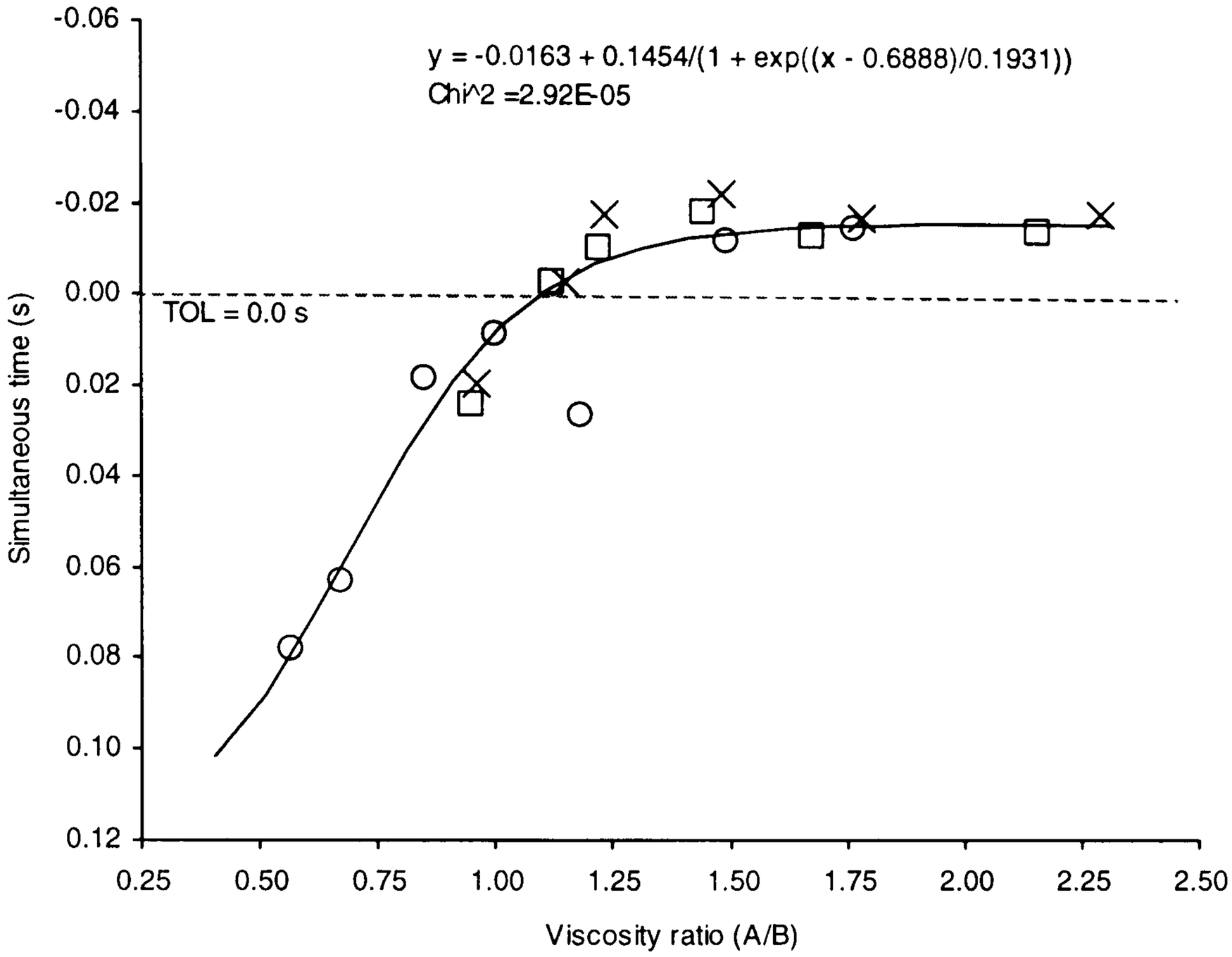

Figure 7.4 Relationship between viscosity ratios of skin to core (η_A/η_B) and simultaneous injection times (TOL): (○) PP(skin)/PP(core), (□) PA6(skin)/PP(core), and (x) PA6(skin)/PP with 10% Polybond 3150(core), respectively. The correlation between η_A/η_B and TOL was found to be:

$$y = -0.0163 + \frac{0.1454}{1 + e^{\left[\frac{x-0.6888}{0.1931}\right]}} \qquad (7.16)$$

where x is skin/core viscosity ratios and y is simultaneous injection times. χ^2 (chi-square) was established as 2.92×10^{-5}. (χ^2 is the sums of the differences of actual values from expected values power second then divided by the expected values)

Table 7.1 The moulding parameters for the co-injection moulding process obtained from machine setting data of experimental no.1, 2 and 3.

Skin/ Core	Combinations	η_A/η_B	Overall Metering A (SOA, mm)	Overall Metering B (SOB, mm)	A-Cushion (SCA, mm)	B-Cushion (SCB, mm)	SA/SB (%)	VA (mm/s)	VB (mm/s)	VA/VB	B-Delay (TDB, s)	Switch-over (SWB, mm)
PP(skin)/PP(core)	1100N/1100H	0.5666	68.0	57.0	5.0	0.0	54.40	90	140	0.6429	0.2	25.0
	1100N/1102K	0.6695	65.0	60.0	5.0	0.0	52.00	95	131	0.7252	0.2	25.0
	1102K/1100H	0.8464	64.0	61.0	5.0	0.0	51.20	110	130	0.8462	0.2	24.0
	1100N/1100N	1.0000	63.0	62.0	5.0	0.0	50.40	115	130	0.8846	0.2	24.0
	1100H/1100H	1.0000	62.0	63.0	5.0	0.0	49.60	115	130	0.8846	0.2	24.0
	1100H/1102K	1.1815	66.0	59.0	5.0	0.0	52.80	115	117	0.9829	0.2	26.0
	1102K/1100N	1.4937	67.0	58.0	5.0	0.0	53.60	128	110	1.1636	0.2	24.0
	1100H/1100N	1.7648	70.0	55.0	5.0	0.0	56.00	130	93	1.3978	0.2	24.0
PA6(skin)/PP(core)	B31SK/1100H	0.9494	69.0	56.0	5.0	0.0	55.20	114	135	0.8444	0.2	25.5
	B31SK/1102K	1.1217	70.5	54.5	5.0	0.0	56.40	122	135	0.9037	0.2	24.0
	B30S/1100H	1.2207	70.0	55.0	5.0	0.0	56.00	132	132	1.0000	0.2	25.0
	B30S/1102K	1.4423	71.5	53.5	5.0	0.0	57.20	138	129	1.0698	0.2	25.0
	B31SK/1100N	1.6755	73.0	52.0	5.0	0.0	58.40	134	120	1.1167	0.2	25.0
	B30S/1100N	2.1543	75.0	50.0	5.0	0.0	60.00	135	100	1.3500	0.2	25.0
PA6(skin)/PP with 10 % polybond 3150 (core)	B31SK/1100H	0.9589	70.5	54.5	5.0	0.0	56.40	114	185	0.6162	0.2	25.0
	B31SK/1102K	1.1504	71.5	53.5	5.0	0.0	57.20	122	135	0.9037	0.2	24.0
	B30S/1100H	1.2330	71.0	54.0	5.0	0.0	56.80	132	132	1.0000	0.2	24.0
	B30S/1102K	1.4792	72.5	52.5	5.0	0.0	58.00	138	125	1.1040	0.2	24.5
	B31SK/1100N	1.7787	74.0	51.0	5.0	0.0	59.20	134	120	1.1167	0.2	24.5
	B30S/1100N	2.2871	76.0	49.0	5.0	0.0	60.80	135	100	1.3500	0.2	24.5

Table 7.2 The predicted moulding parameters for the co-injection moulding process.

Skin/ Core	Combinations	η_A/η_B	t_{pred} (s)	S_{max} (mm)	VA/VB	VA (mm/s)	VB (mm/s)	TA (s)	TB (s)	TOL (s)	Simultaneous phase (%)	TDB*VA (mm)	SWB (mm)	Total filling time (TT, s)
PP(skin)/PP(core)	1100N/1100H	0.5666	0.90	125.0	0.6982	93	133	0.68	0.43	0.0787	11.62	18.6	25.9	1.03
	1100N/1102K	0.6695	0.90	125.0	0.7417	99	133	0.61	0.45	0.0600	9.89	19.8	25.7	1.00
	1102K/1100H	0.8464	0.90	125.0	0.8164	109	133	0.54	0.46	0.0283	5.22	21.8	24.8	0.97
	1100N/1100N	1.0000	0.90	125.0	0.8813	118	133	0.49	0.47	0.0079	1.60	23.5	24.4	0.95
	1100H/1100H	1.0000	0.90	125.0	0.8813	118	133	0.49	0.47	0.0079	1.63	23.5	24.4	0.95
	1100H/1102K	1.1815	0.90	125.0	0.9580	128	133	0.48	0.44	-0.0058	-1.21	25.5	24.8	0.93
	1102K/1100N	1.4937	0.90	125.0	1.0899	133	122	0.47	0.47	-0.0141	-3.03	26.7	24.8	0.95
	1100H/1100N	1.7648	0.90	125.0	1.2044	133	111	0.49	0.50	-0.0157	-3.23	26.7	24.6	1.00
PA6(skin)/PP(core)	B31SK/1100H	0.9494	0.90	125.0	0.8599	115	133	0.56	0.42	0.0136	2.44	22.9	24.5	0.96
	B31SK/1102K	1.1217	0.90	125.0	0.9327	124	133	0.53	0.41	-0.0023	-0.44	24.9	24.6	0.94
	B30S/1100H	1.2207	0.90	125.0	0.9745	130	133	0.50	0.41	-0.0076	-1.52	26.0	25.0	0.92
	B30S/1102K	1.4423	0.90	125.0	1.0682	133	125	0.50	0.43	-0.0134	-2.69	26.7	24.9	0.94
	B31SK/1100N	1.6755	0.90	125.0	1.1667	133	114	0.51	0.46	-0.0154	-3.02	26.7	24.6	0.98
	B30S/1100N	2.1543	0.90	125.0	1.3690	133	97	0.53	0.51	-0.0162	-3.09	26.7	24.5	1.05
PA6(skin)/PP with 10 % polybond 3150 (core)	B31SK/1100H	0.9589	0.90	125.0	0.8639	115	133	0.56	0.38	0.0125	2.25	23.0	24.5	0.93
	B31SK/1102K	1.1504	0.90	125.0	0.9449	126	133	0.52	0.37	-0.0041	-0.79	25.2	24.7	0.90
	B30S/1100H	1.2330	0.90	125.0	0.9797	131	133	0.50	0.38	-0.0081	-1.63	26.1	25.1	0.88
	B30S/1102K	1.4792	0.90	125.0	1.0838	133	123	0.50	0.39	-0.0139	-2.79	26.7	24.8	0.91
	B31SK/1100N	1.7787	0.90	125.0	1.2103	133	110	0.51	0.43	-0.0158	-3.10	26.7	24.6	0.95
	B30S/1100N	2.2871	0.90	125.0	1.4251	133	94	0.53	0.48	-0.0163	-3.10	26.7	24.5	1.02

It was found that the relationship between simultaneous injection times and skin/core viscosity ratios was a non-linear regression, in which the best fitting curve is governed by sigmoidal (growth) curve fitting. This curve fitting function is shown as follow:

$$y = A_2 + \frac{(A_1 - A_2)}{1 + e^{\left[\frac{x - x_0}{dx}\right]}} \qquad (7.17)$$

Where A_1 is initial value.

A_2 is final value.

x_0 is centre of the curve.

dx is the time constant.

Thus, the correlation between the simultaneous injection times (TOL) and the skin/core viscosity ratios (η_A/η_B) can be determined as shown in equation 7.16.

Nevertheless, Figure 7.4 (page 90) shows that when skin/core viscosity ratio was decreased, the simultaneous co-injection moulding process resulted in TOL > 0 s. On the other hand, increasing skin/core viscosity ratio resulted in a process trend to sequential co-injection moulding techniques where TOL $\leq$ 0 s.

7.2 Comparison of Skin-Core Thickness between Experimental and Simulated Mould Filling Analysis Results

7.2.1 PP (skin)/PP (core)

In this study, polypropylenes are used as skin and core polymers. The core thickness fraction of the moulding components were obtained from measurements using ***Image processing software*** as seen in appendix IV. At the same moulding conditions and parameters such as injection speeds of skin and core, viscosity data, metering strokes of skin and core, etc., the core thickness fraction were also simulated using C-mold software. Moreover, the skin frozen layer thickness fraction of the conventional injection moulding process (1k) and co-injection moulding process (2k) were obtained using the same simulation package (C-mold).

In other cases of skin-core combinations (Table 6.2, page 70), the experimental and simulated results of a skin frozen layer thickness fraction and a core thickness fraction were also investigated and shown in Appendix V. The skin frozen layer thickness fractions which were obtained from the filling analysis of the conventional injection moulding process (1k) and co-injection moulding process (2k) are compared (Figure 7.5(a)). It was found that the skin frozen layer thickness fractions of 1k and 2k process are 0.10 and 0.09, respectively. From the previous work [8], the skin frozen layer thickness fraction was simulated using the filling analysis of the conventional injection moulding process (1k) from Moldflow because at that time the filling analysis for co-injection moulding process (2k) did not exist. Thus, it was only possible to simulate this thickness fraction by a filling analysis using a 1k process.

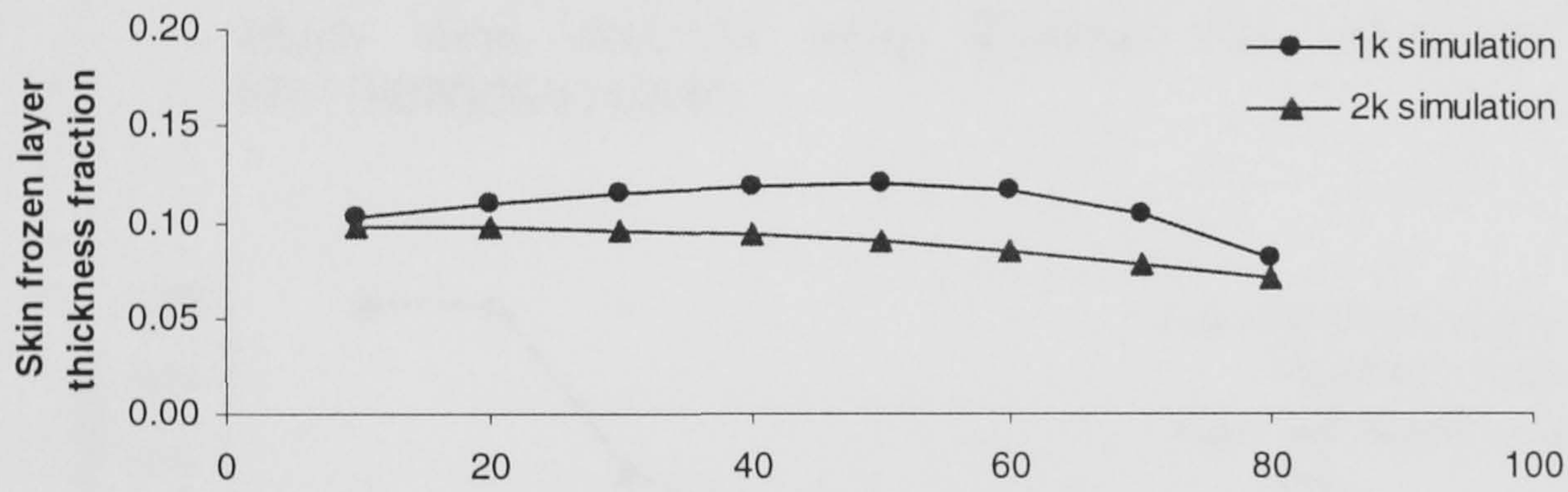

Figure 7.5(a) Plot of skin frozen layer thickness fraction against distances from the edge of moulding component.

Basically, the core thickness fraction was obtained using the filling analysis for a co-injection moulding process. Then, the skin thickness fraction was calculated as following:

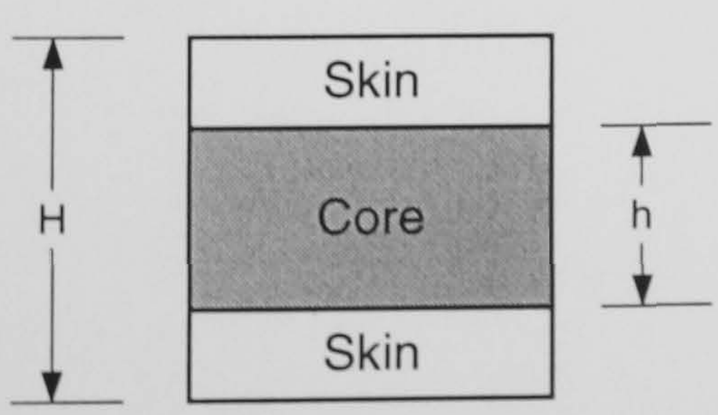

Skin thickness fraction (STF) = 1 - Core thickness fraction (CTF) (7.18)

It was found that the simulated result of a skin thickness fraction which was obtained using the filling analysis for a co-injection moulding process is ca. 0.29*(range from 0.13 to 0.70).

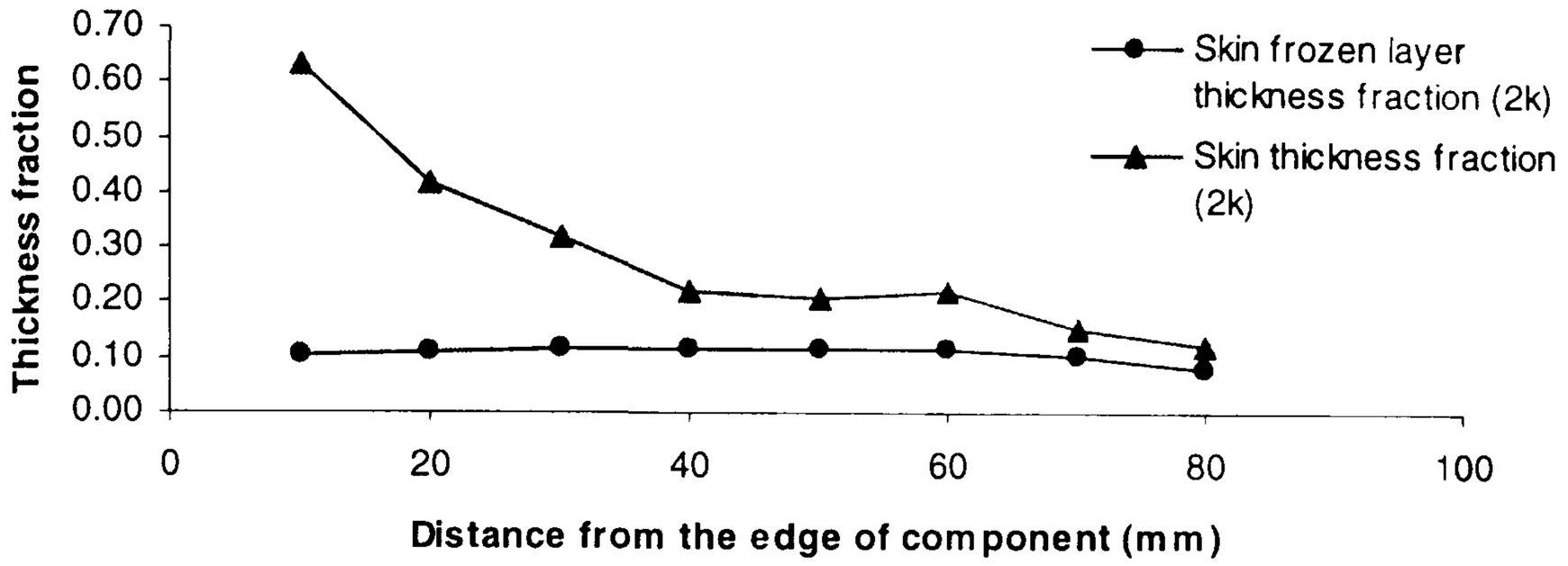

Figure 7.5(b) Comparison between the simulated results of the skin frozen layer thickness fraction and the skin thickness fraction which were obtained using C-mold (2k). Skin/core was PP(1100N)/PP(1100H).

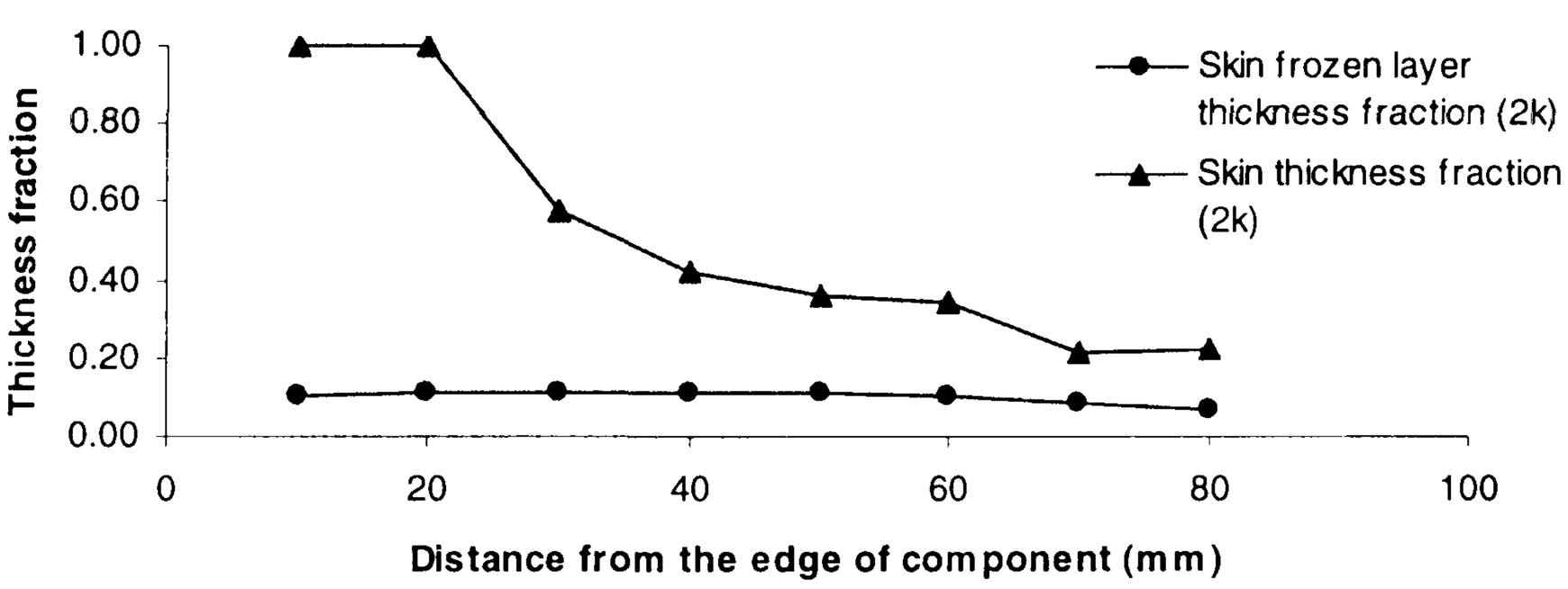

Figure 7.5(c) Comparison between the simulated results of the skin frozen layer thickness fraction and the skin thickness fraction which were obtained using C-mold (2k). Skin/core was PP(1100H)/PP(1100N).

---

* Calculated by using data points at the distances from the edge of the moulding component of 10, 20, 30, ..., 90 mm

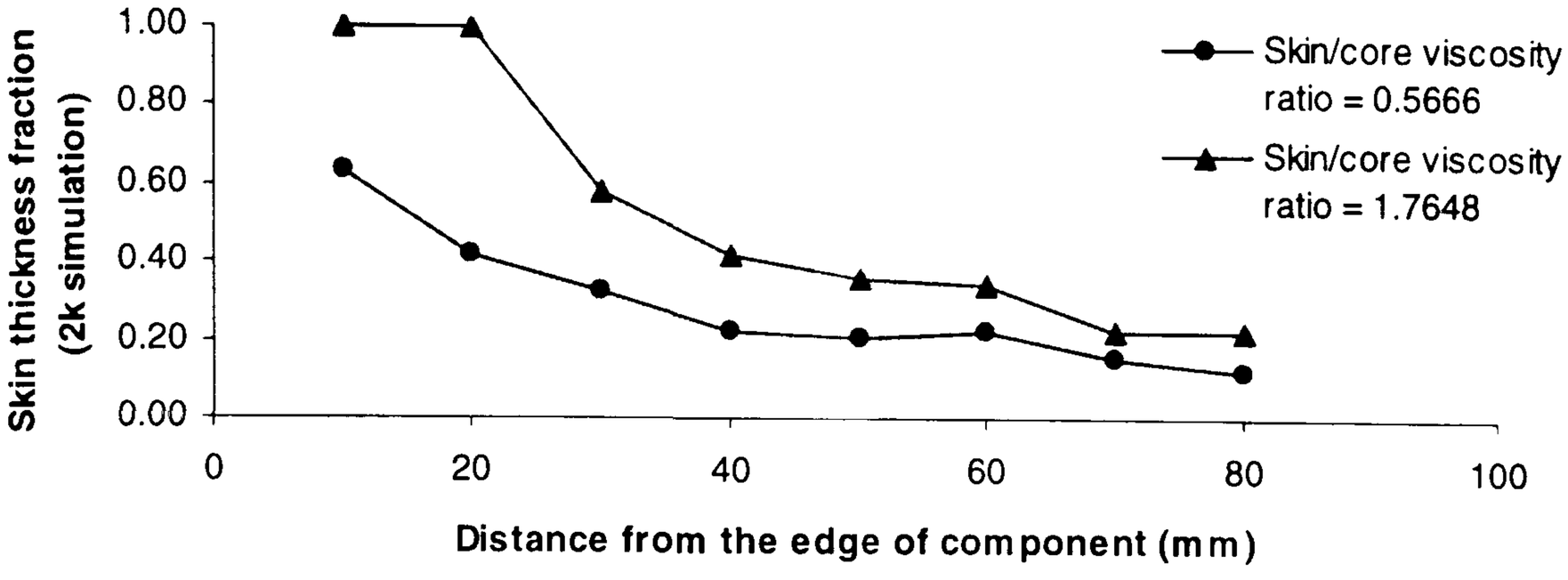

Figure 7.5(d) Comparison between the simulated results of the skin thickness fraction which were obtained for different viscosity ratios using C-mold (2k): (•)PP(1100N)/PP(1100H) and (Δ)PP(1100H)/PP(1100N).

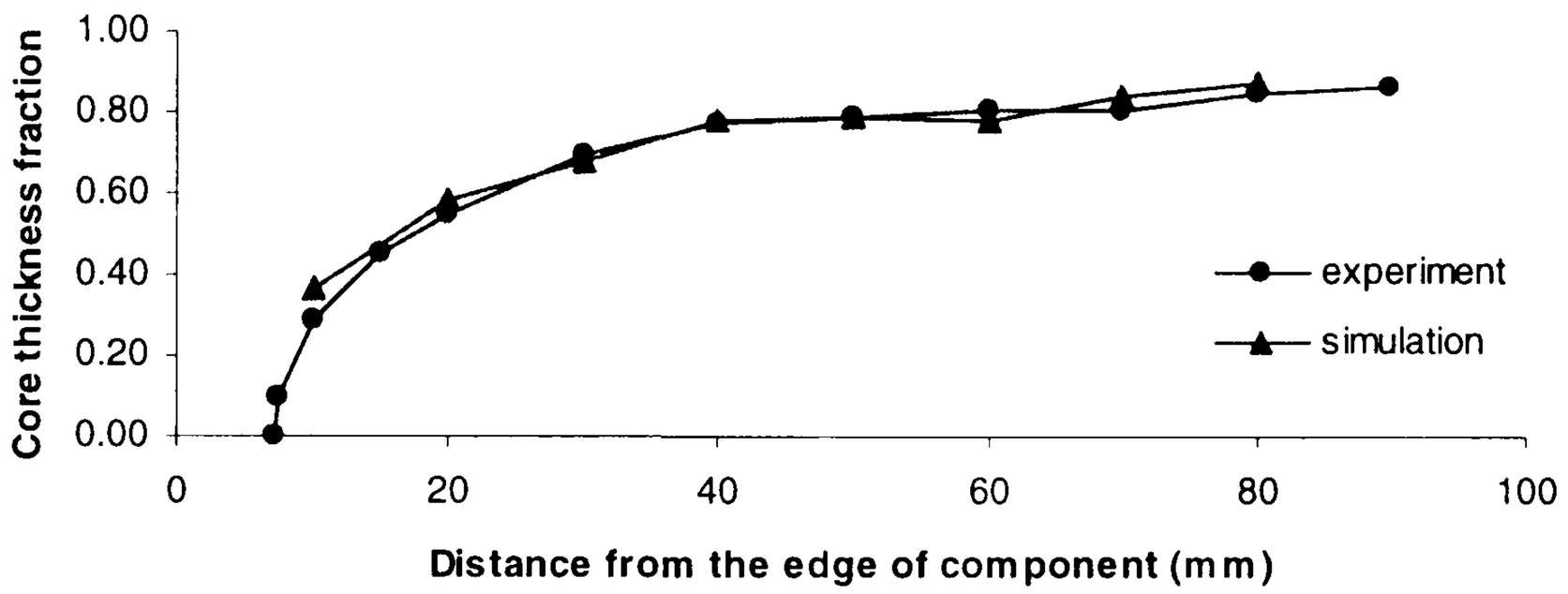

Figure 7.5(e) Comparison between the experimental and simulated results of a core thickness fractions. Skin/core was PP(1100N)/PP(1100H).

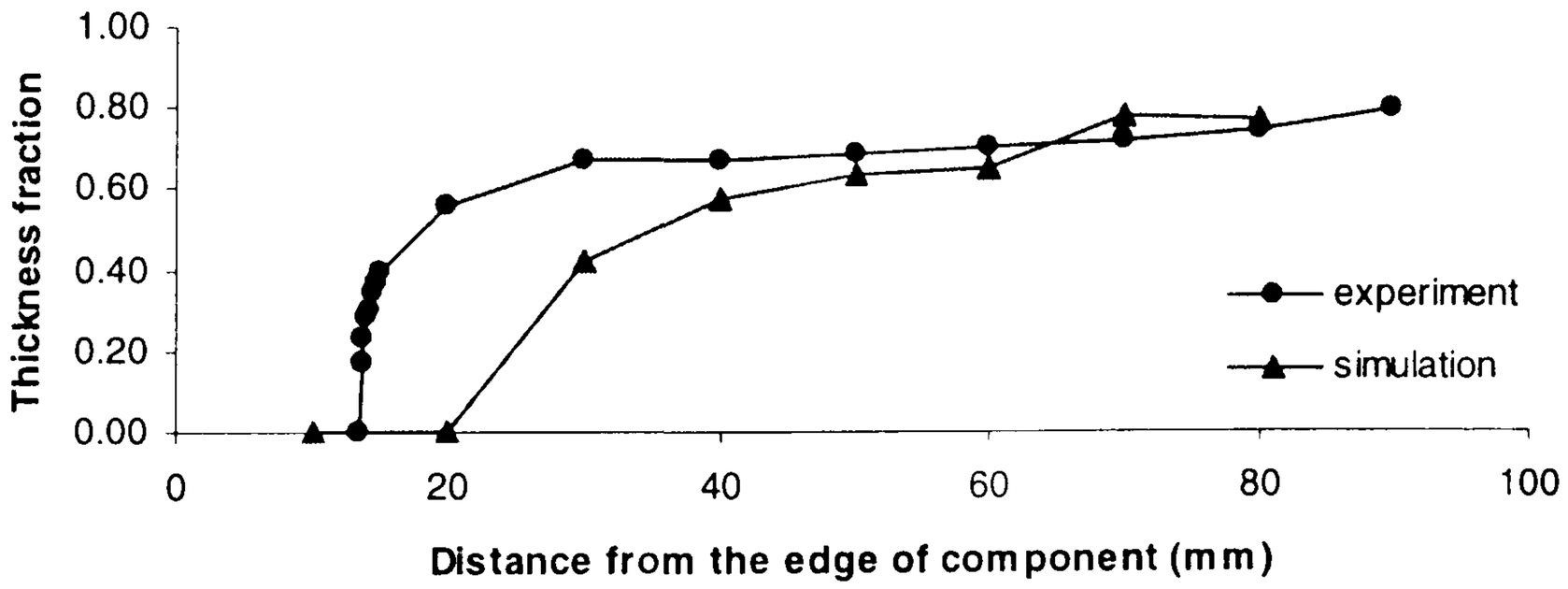

Figure 7.5(f) Comparison between the experimental and simulated results of a core thickness fractions. Skin/core was PP(1100H)/PP(1100N).

As seen in Figure 7.5(b), the comparison of the simulated results between the skin frozen layer thickness fraction and the skin thickness fraction which were obtained using filling analysis for co-injection moulding process (2k) are shown in Figure

7.5(c) and 7.5(d), respectively. Note that skin fronzen layer when simulated shows a uniform thickness throughout the length of the moulding. However, the simulated skin thickness fraction is not uniform throughout the length of moulding and will later be shown to be more realistic of the experimental results. Previously, Somnuk had been obliged to use the skin frozen layer as the appropriate skin thickness as defined by the Moldflow 1k route. This work shows how it can be refined using C-Mold filling analysis for co-injection moulding (2k).

However, the simulated results of skin and core thickness fractions are in good agreement with one of the lower skin/core viscosity ratio as shown in Figure 7.5(e), Figure 7.5(f), and Figure 7.6. It could be explained that under the certain conditions an instable two-component flow could develop during the filling stage. The mechanism causing the formation of an instability during the displacement of a highly viscous skin polymer by less viscous core polymer was reported as connected to changes in viscosity and thus local pressure differences [60].

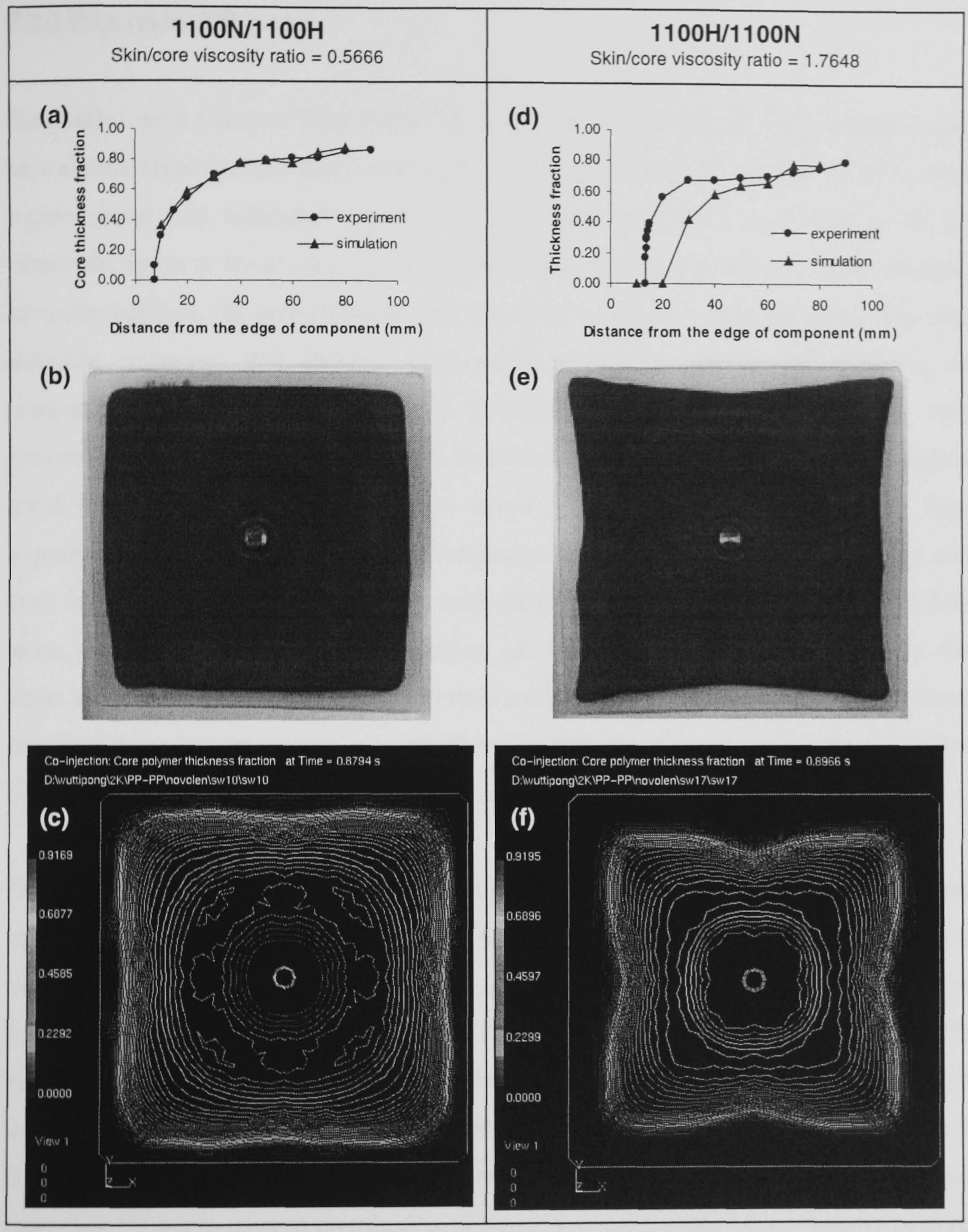

Figure 7.6 Comparison of the simulated and experimental (core thickness fractions) results: (a)-(c) low skin/core viscosity ratio ($\eta_A/\eta_B<1.0$) and (d)-(f) high skin/core viscosity ratio ($\eta_A/\eta_B>1.0$).

From above figure, it could be concluded that the simulated results of skin and core thickness fractions are in good agreement with one of the lower skin/core viscosity ratio using the filling analysis for co-injection moulding process (C-mold).

7.2.2 PA6 (skin)/PP (core)

Generally, most cases of PA6 (skin)/PP (core) resulted in higher skin thickness and skin frozen layer fraction than in the case of PP (skin)/PP (core), and occurred in both experimental and simulated results*. In fact, skin thickness was found to be an important factor in the production of a good skin-core adhesion results. In the absence of compatibiliser, the skin thickness has no effect on the skin-core adhesion. The two different polymers still showed poor adhesion results, but in the presence of compatibiliser a chemical reaction between functional group of skin and compatibiliser in the core occurred [48]. Suitable conditions were necessary to produce good bonding between skin and core active sites. Unfortunately, a greater than expected thickness of skin layer was necessary to allow more time for the skin and core active functional groups to react with each other. Otherwise, in the case of thin skins, the skin became the no-flow layer, i.e. solid and prevented reaction. On the other hand, if skin thickness was lower than a minimum requirement, high shear stress occurred between skin and core layers, then the skin layers were easily detached from core material after the moulding was ejected or a load was applied to the components.

As seen in a typical figure (Figure 7.7(a)-7.7(f)), the frozen layer thickness fraction results at filling time of 0.90 second is ca. 0.14. The simulated skin thickness fractions can be shown to vary in the range of 0.27 to 0.61 (ca. 0.36), where the skin/core viscosity ratios and their metering stroke ratios vary from 0.9494 to 2.1543 and 0.55 to 0.60, respectively. It was found that the skin thickness fractions of experimental and simulated results are in good agreement when skin/core viscosity ratios are low (Figure 7.7(e) and Figure 7.8). It could be explained that interfacial instabilities of core melt [60] led to uneven distribution of the core polymer when the viscosity of core polymer was lower than skin polymer ($\eta_A/\eta_B > 1.0$).

---

* Experimental and simulated results of skin thickness and skin frozen layer fraction were shown in Appendix V

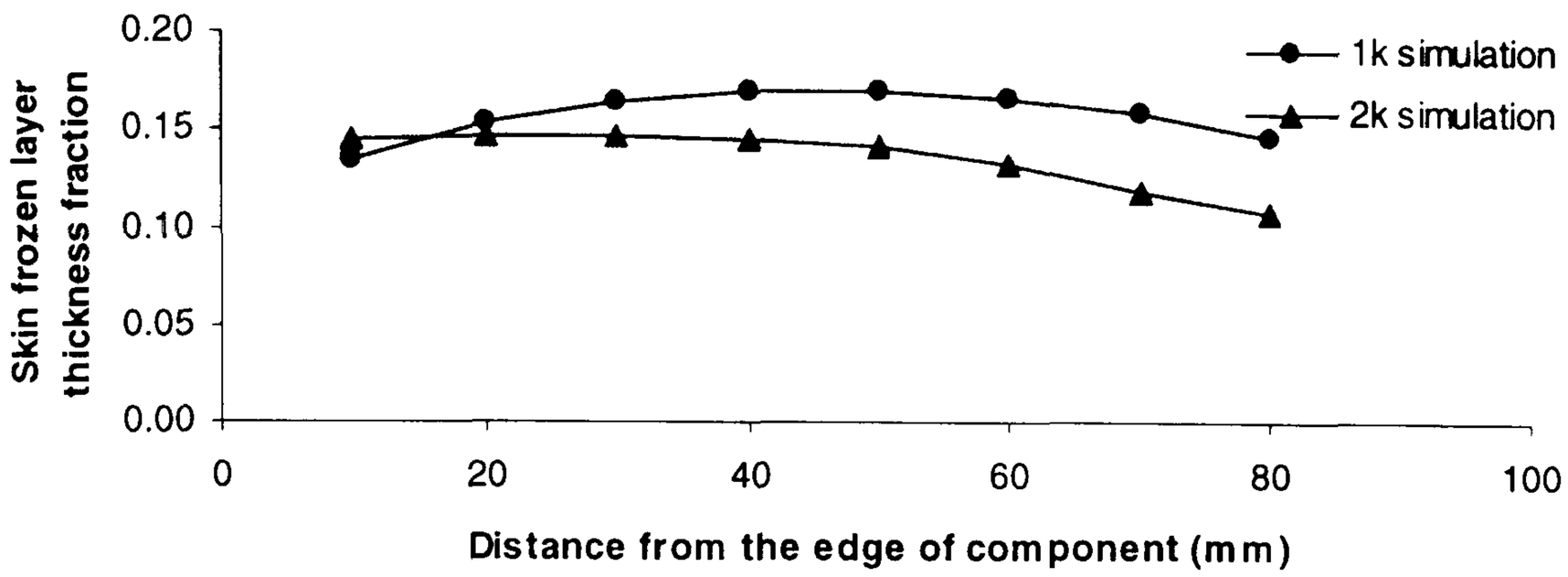

Figure 7.7(a) Plot of skin frozen layer thickness fraction against distances from the edge of moulding component.

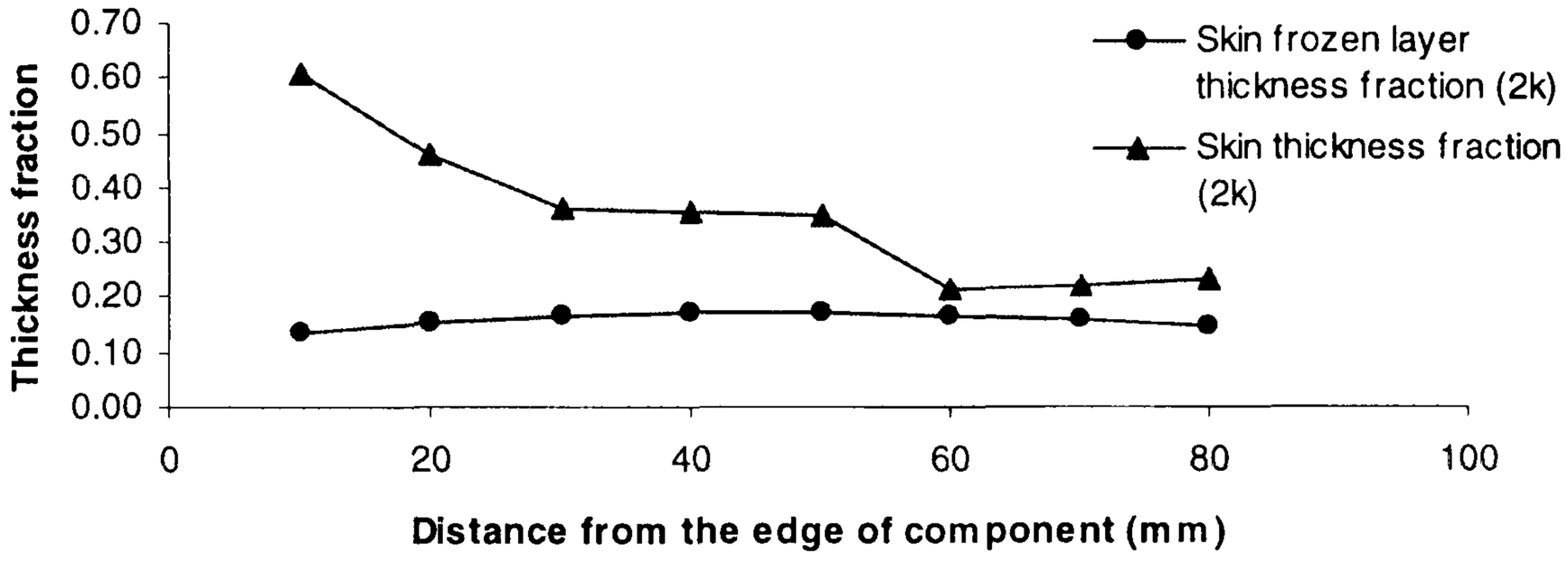

Figure 7.7(b) Comparison between the simulated results of the skin frozen layer thickness fraction and the skin thickness fraction which were obtained using C-mold (2k). Skin/core was PA6(B31SK)/PP(1100H).

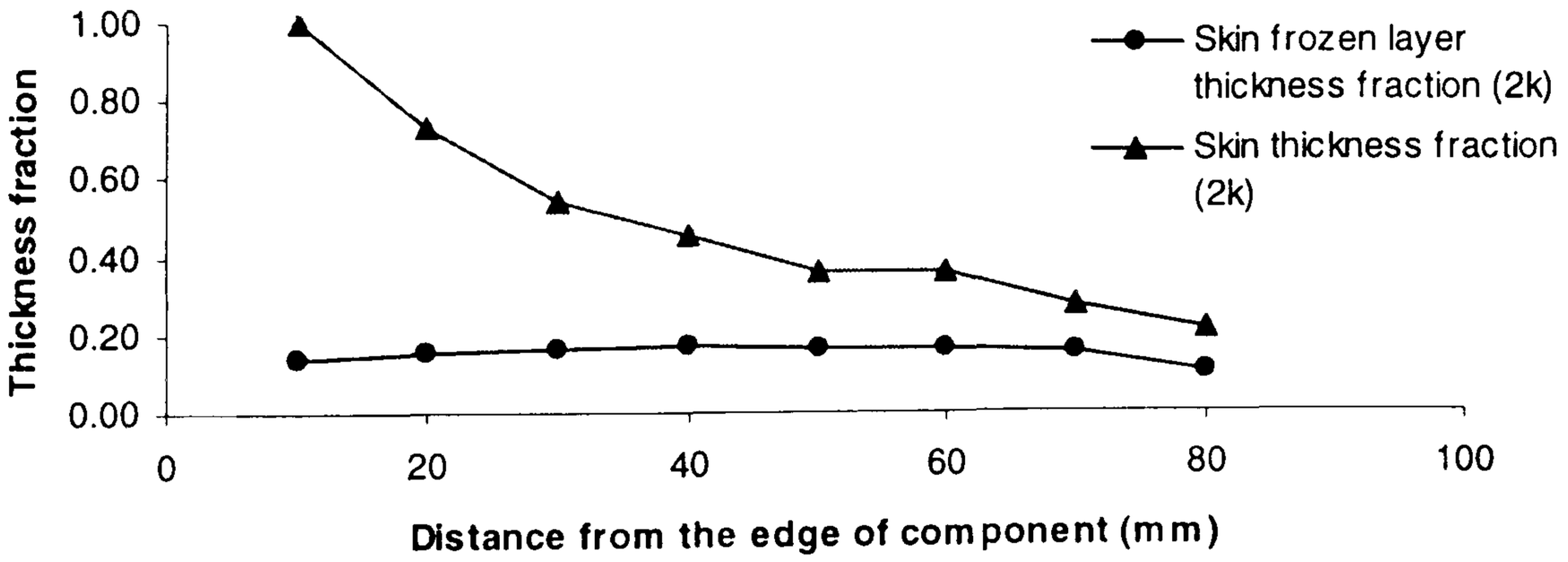

Figure 7.7(c) Comparison between the simulated results of the skin frozen layer thickness fraction and the skin thickness fraction which were obtained using C-mold (2k). Skin/core was PA6(B30S)/PP(1100N).

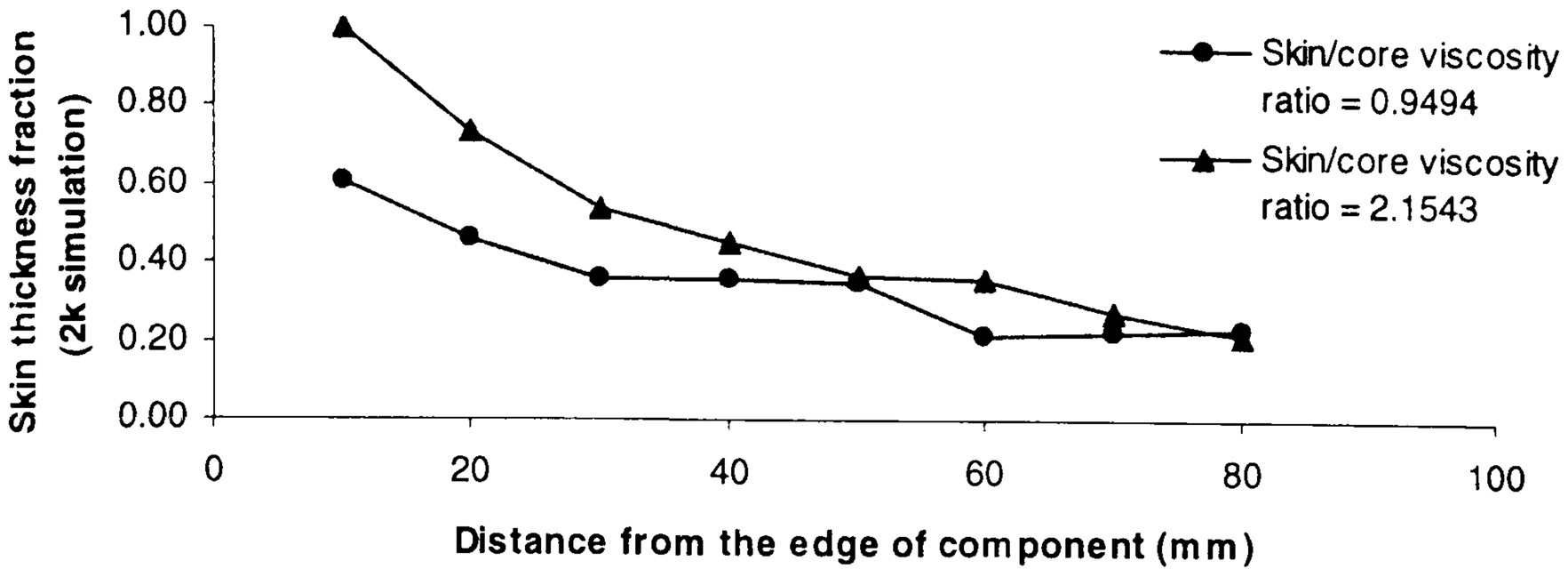

Figure 7.7(d) Comparison between the simulated results of the skin thickness fraction which were obtained for different viscosity ratios using C-mold (2k): (•)PA6(B31SK)/PP(1100H) and (Δ)PA6(B30S)/PP(1100N).

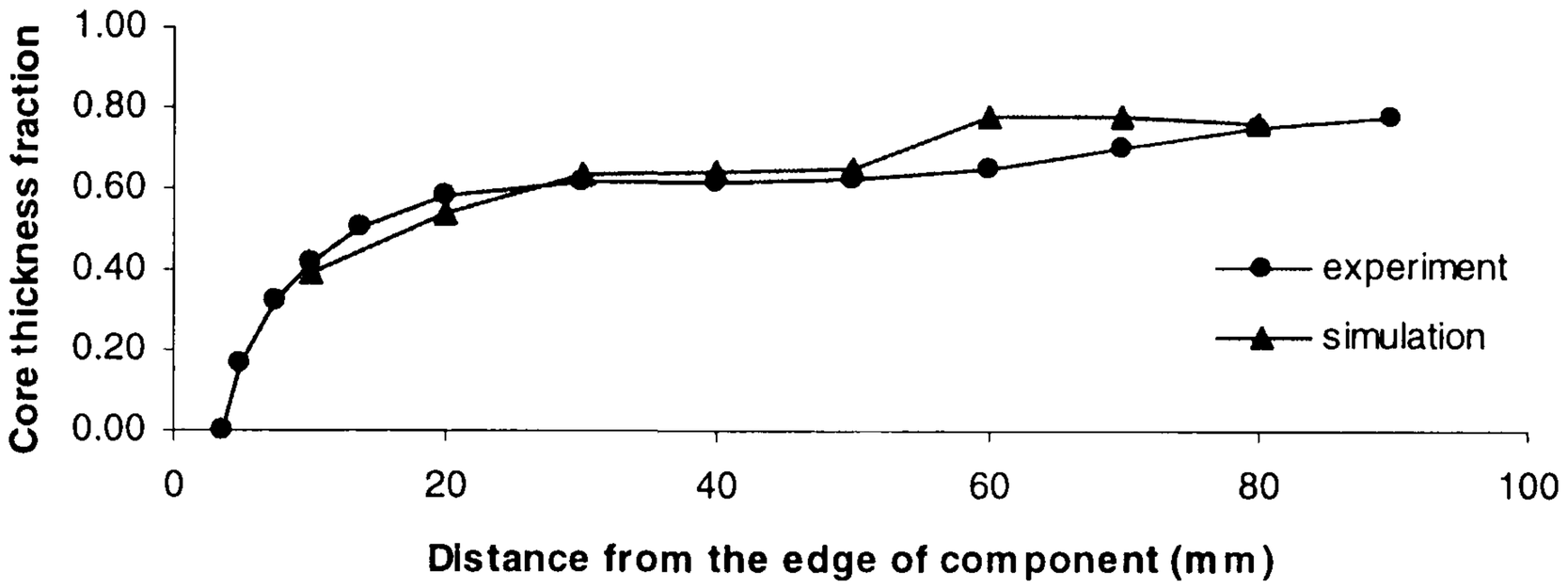

Figure 7.7(e) Comparison between the experimental and simulated results of a core thickness fractions. Skin/core was PA6(B31SK)/PP(1100H).

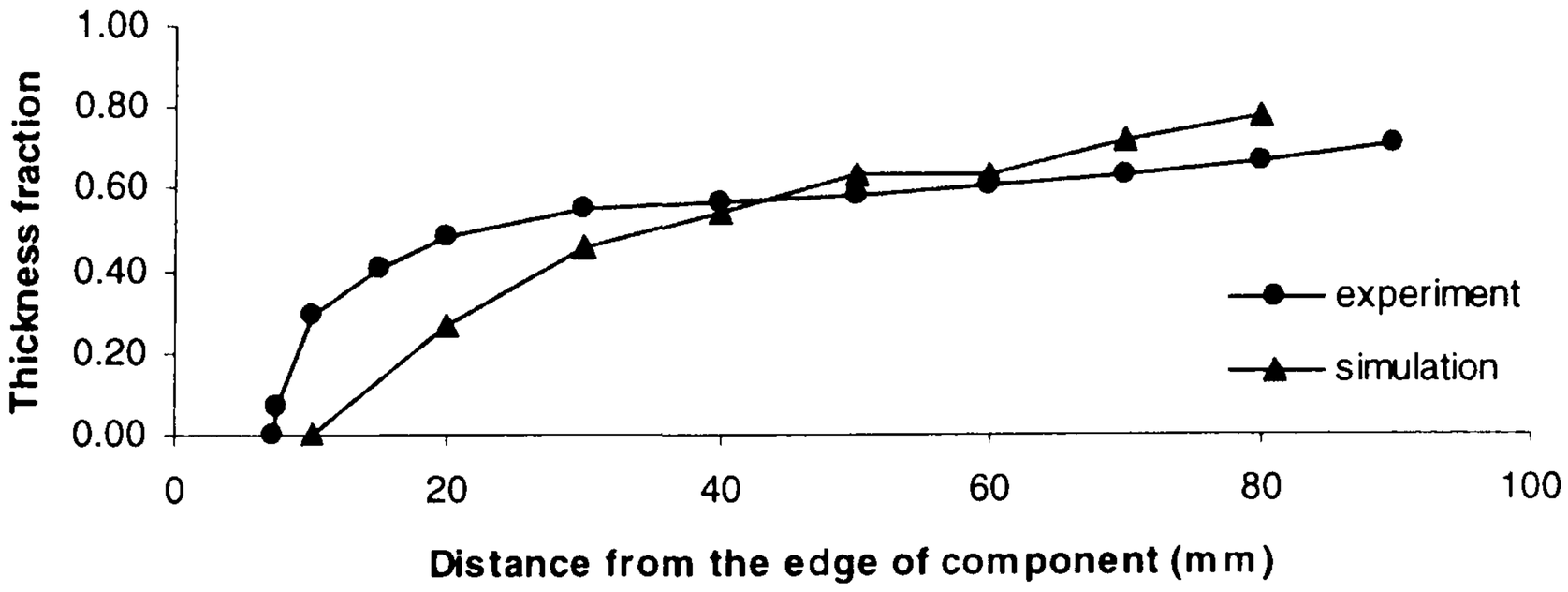

Figure 7.7(f) Comparison between the experimental and simulated results of a core thickness fractions. Skin/core was PA6(B30S)/PP(1100N).

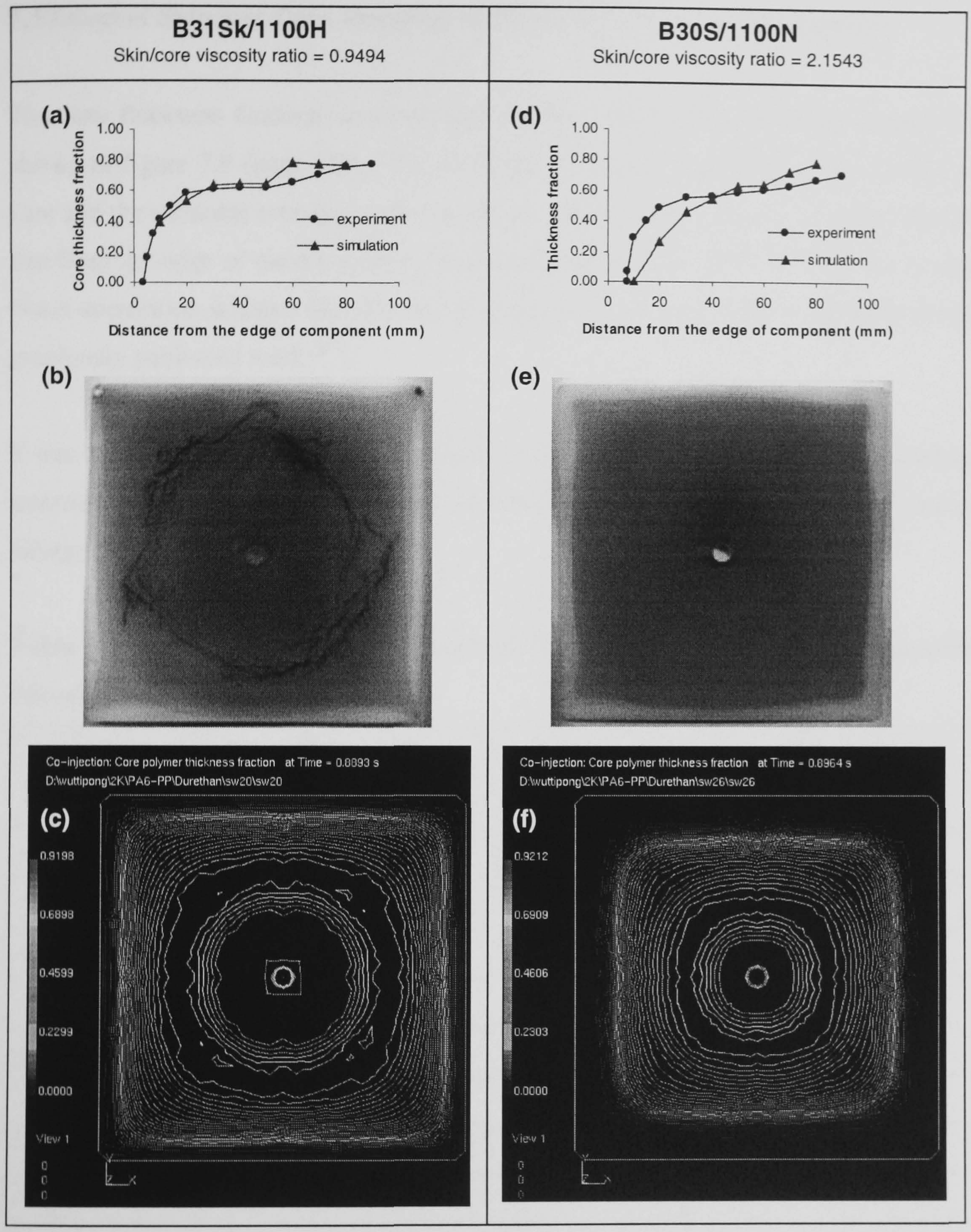

Figure 7.8 Comparison of simulated and experimental (core thickness fractions) results: (a)-(c) low skin/core viscosity ratio ($\eta_A/\eta_B<1.0$) and (d)-(f) high skin/core viscosity ratio ($\eta_A/\eta_B>1.0$).

In case of PA6(skin)/PP(core) system, it could be concluded that the simulated results of skin and core thickness fractions are in good agreement with one of the lower skin/core viscosity ratio using the filling analysis for co-injection moulding process (C-mold). It is similar to PP(skin)/PP(core) system.

7.3 Effect of Skin and Core Viscosity on Skin-Core Thickness Formations

The core thickness fractions corresponded to their cross-section interface shapes as shown in figure 7.9 (page 104). The relationship between viscosity ratios of skin to core and the sectional core thickness fractions at each location of core along the centre line from the edge of the components was confirmed in Figure 7.10-7.15 to be a non-linear correlation whether the skin was polypropylene or polyamide 6 as presented in previously published work [37].

It was found that when the skin/core viscosity ratio decreases, there is corresponding increase in the thickness of the core melt into the skin polymer at the end of cavity filling (Table 7.3).

Table 7.3 Average core thickness fraction (CTF_{avg})* at the variation of the skin/core viscosity ratios.

$\eta_{A,PP}/\eta_{B,PP}$	**CTF_{avg} of PP(skin)/PP(core) components**	$\eta_{A,PA6}/\eta_{B,PP}$	**CTF_{avg} of PA6(skin)/PP(core) components**
0.5666	0.7244	-	-
0.6695	0.7249	-	-
0.8464	0.7170	0.9494	0.6388
1.0000	0.7146	1.1217	0.6110
1.0000	0.7016	1.2207	0.6097
1.1815	0.6382	1.4423	0.5956
1.4937	0.6274	1.6755	0.5793
1.7648	0.6201	2.1543	0.5683

It was also found that near the gate, the core thickness fraction was a high fraction and decreased as the length of flow path was increased (Figure 7.10(c) and 7.10(d)). It could be described that when the viscosity of skin polymer was lower than the core polymer ($\eta_A/\eta_B<1.0$), the advancing front of the core polymer melts were pulled into a sharp-angle. This led to a deeper penetration of core polymer and also led to a

---

* Calculated by using data points at the distances from the edge of the component from 0 to 90 mm.

higher core thickness fraction as well. If the viscosity relationships were reversed ($\eta_A/\eta_B>1.0$), this would lead to the interface shape becoming more round.

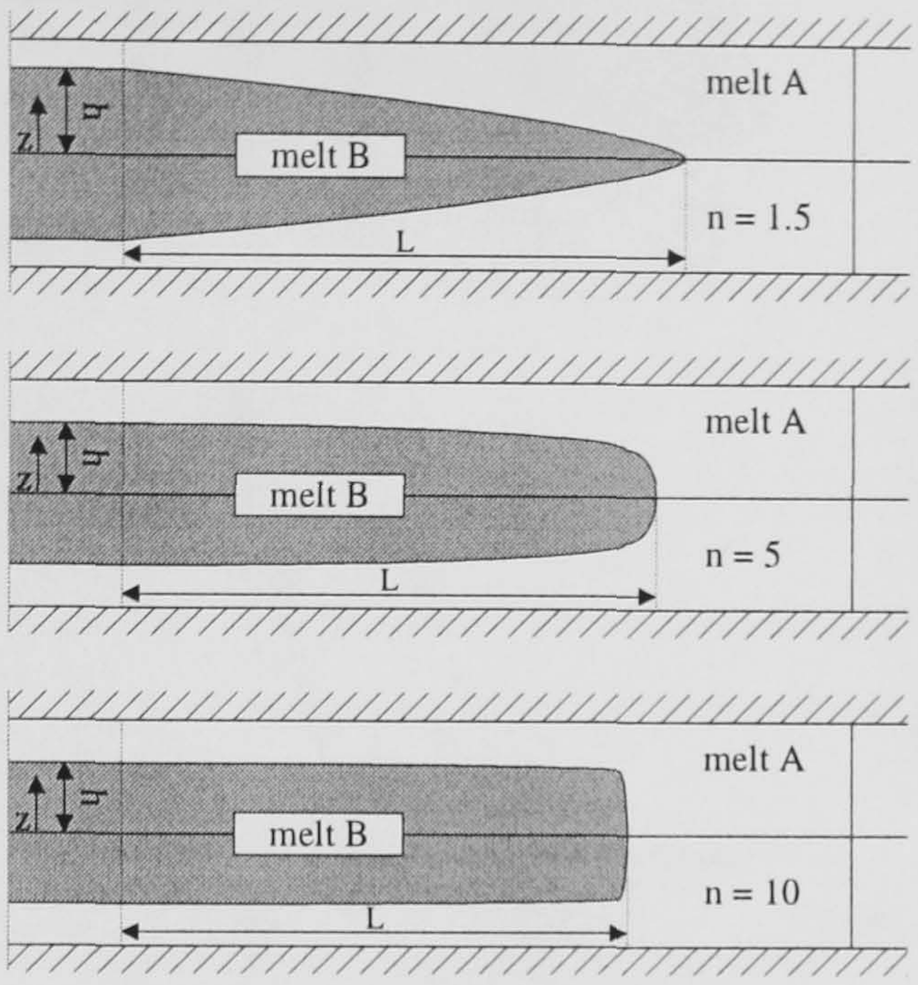

Figure 7.9 Shapes of core penetration: (a) low skin/core viscosity ratio, (b) moderated skin/core viscosity ratio, and (c) high skin/core viscosity ratio, respectively.

7.4 The Shapes of Core Penetration

As mentioned in the previous section, the extent of core penetration was related to the core thickness fraction. In this case study, the results were divided into two sections; PP(skin)/PP(core) and PA6(skin)/PP with and without compatibiliser (core), respectively.

7.4.1 The shapes of PP (skin)/PP (core) core penetration

In the case of PP(skin)/PP(core), the core penetrated shapes (Figure 7.9 and 7.10(a)-(h)) were in good agreement with results from the previous work [36]. It was found that a lower skin/core viscosity ratio led to an interface with sharp-angle profile whereas the higher skin/core viscosity ratio introduced a more rounded interface shape.

(a) Effect of PP/PP viscosity ratios on core thickness fractions at various sectional location of core

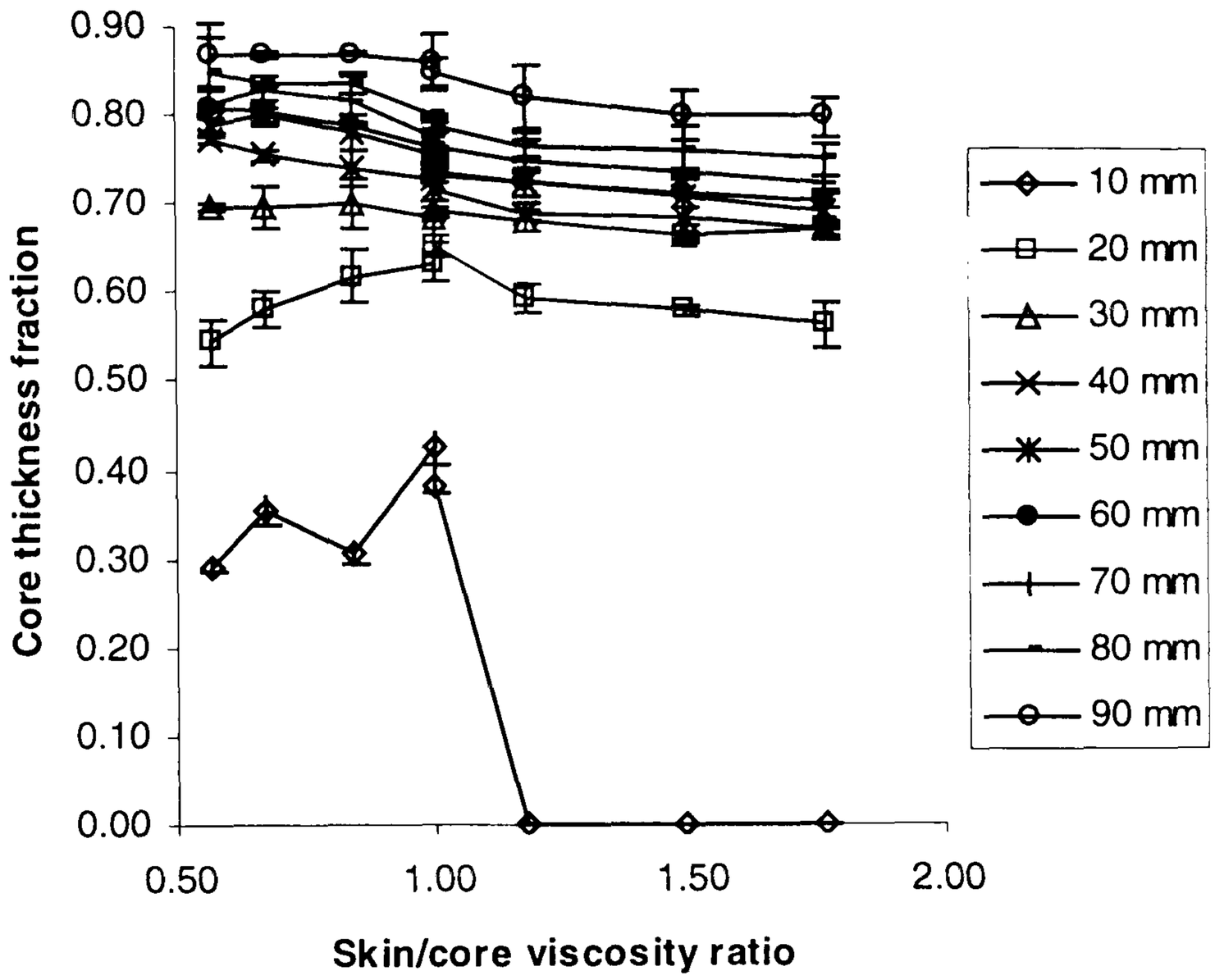

(b) Effect of PA6/PP viscosity ratios on core thickness fractions at various sectional location of core

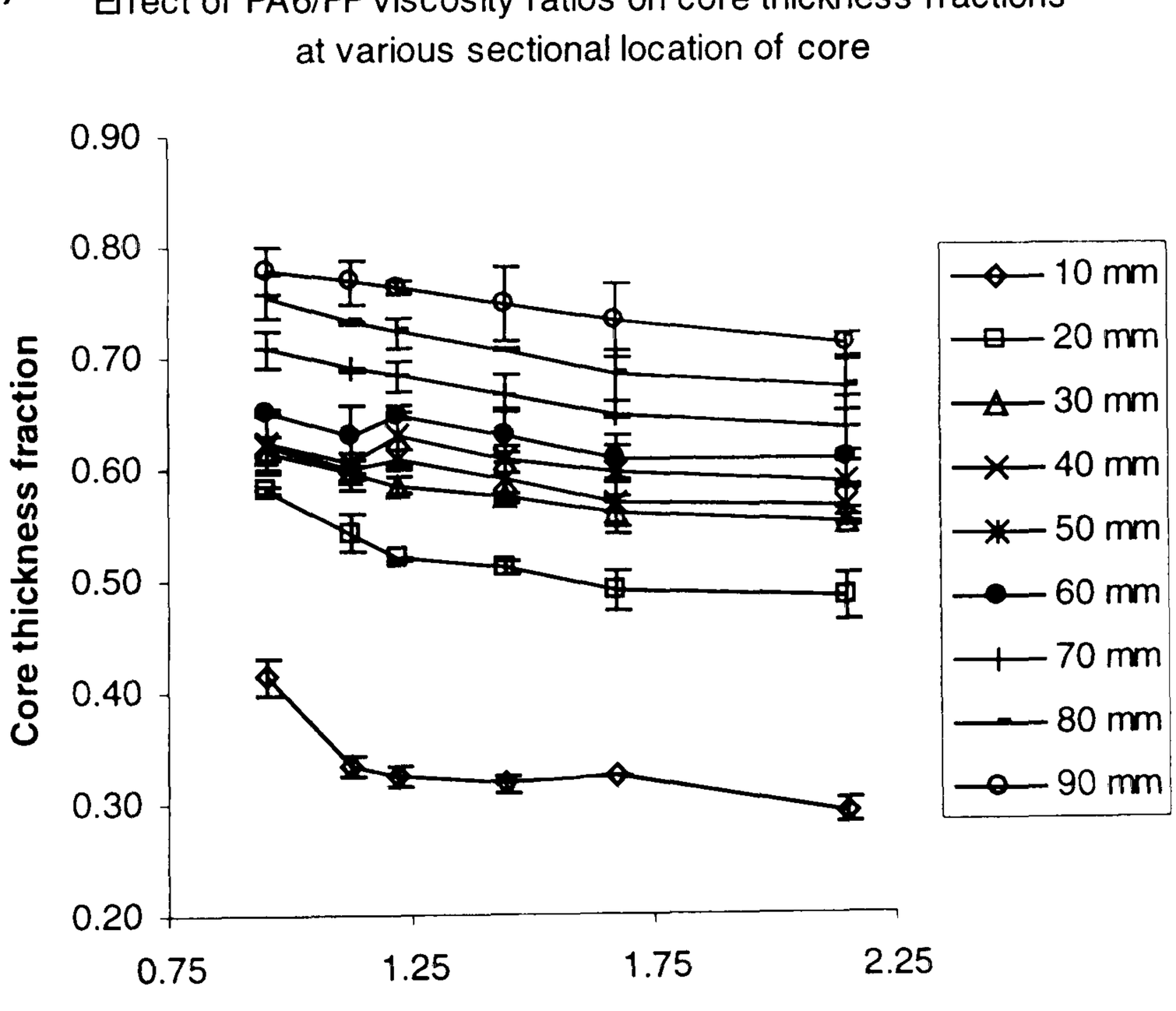

Figure 7.10 (a)-(b)

(c)

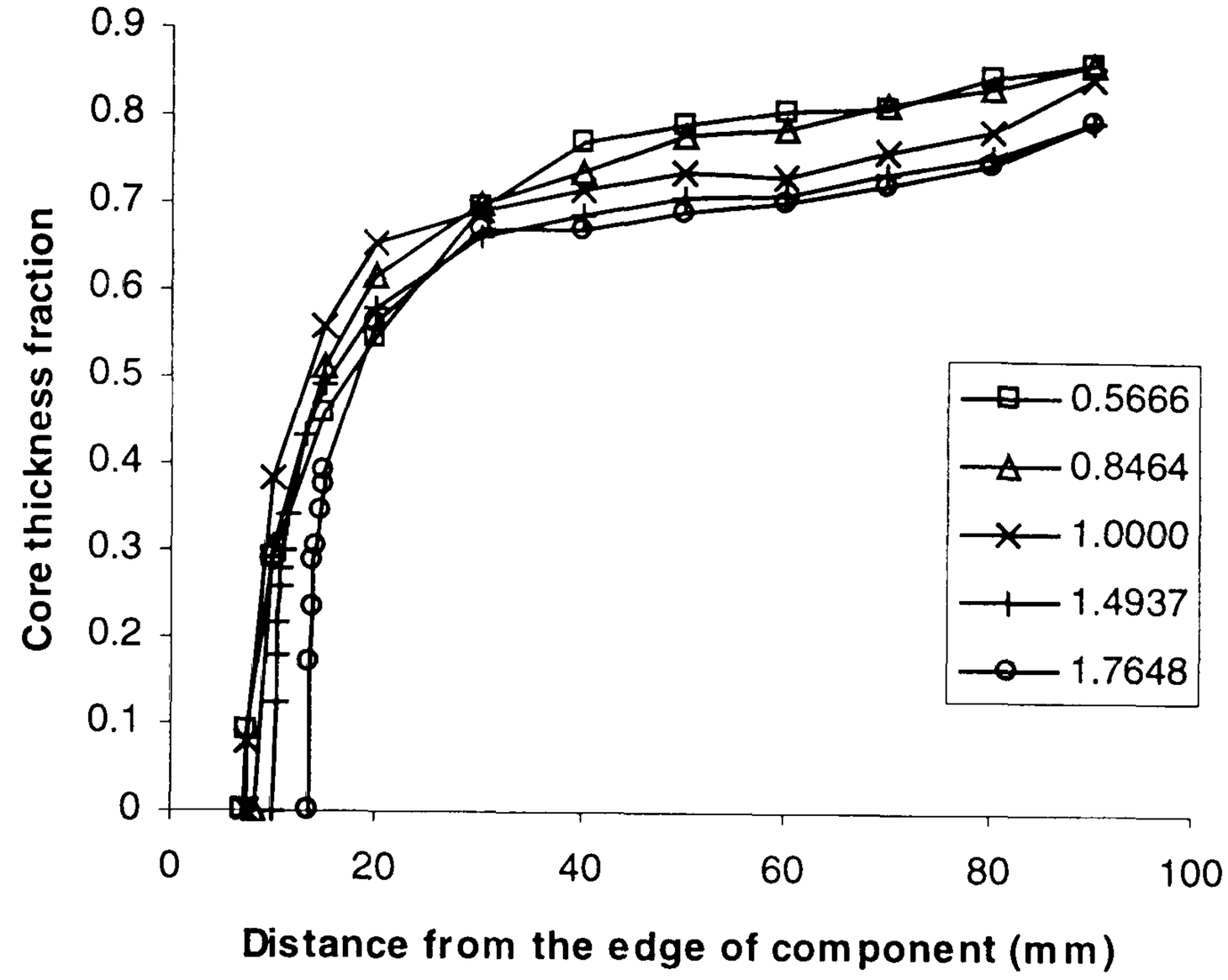

(d)

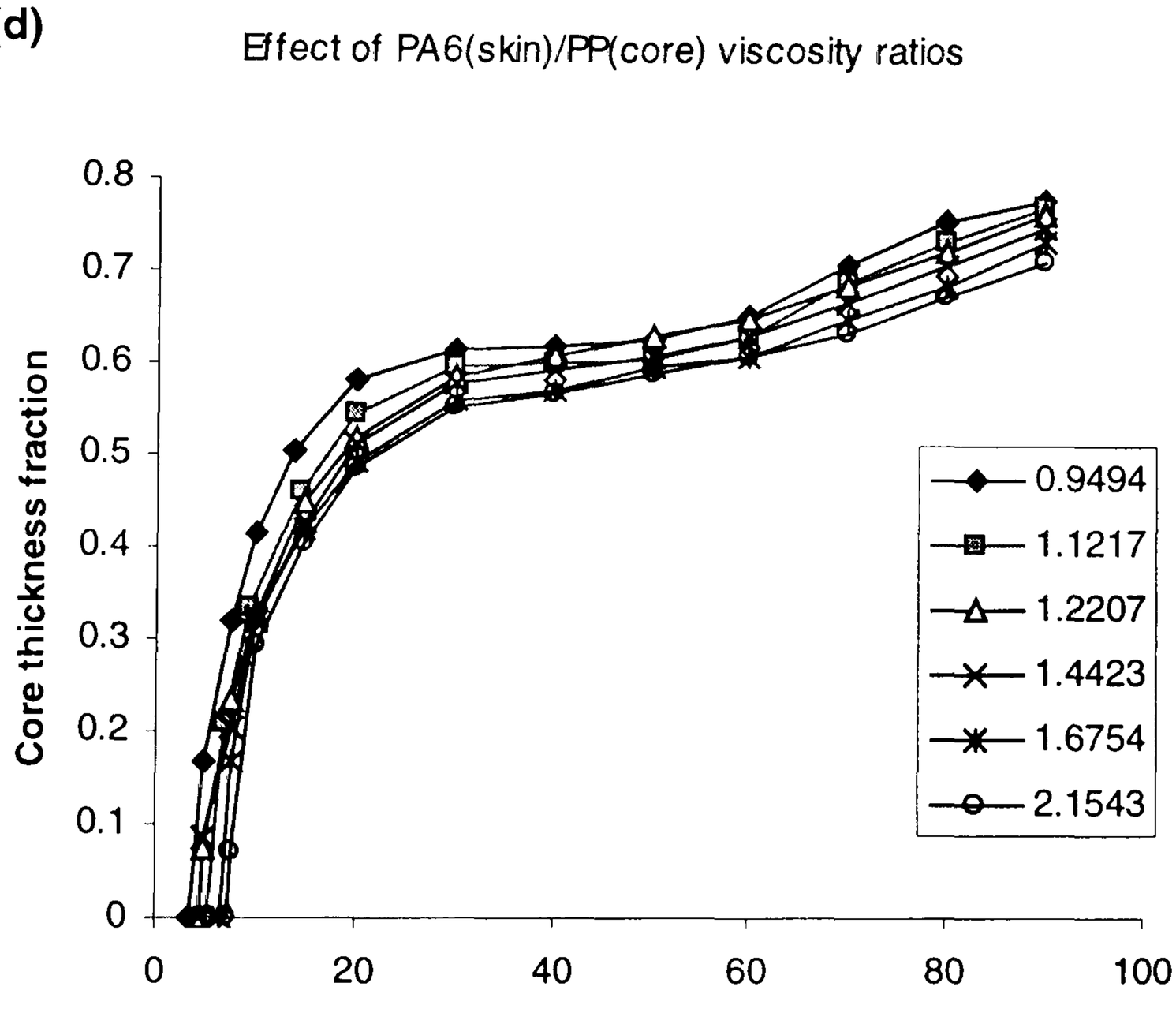

Figure 7.10(a)-(d) Relationship between the sectional core thickness fraction and skin/core viscosity ratios at the various location of core on the component taking zero as the edge of the plaque (Figure 6.5).

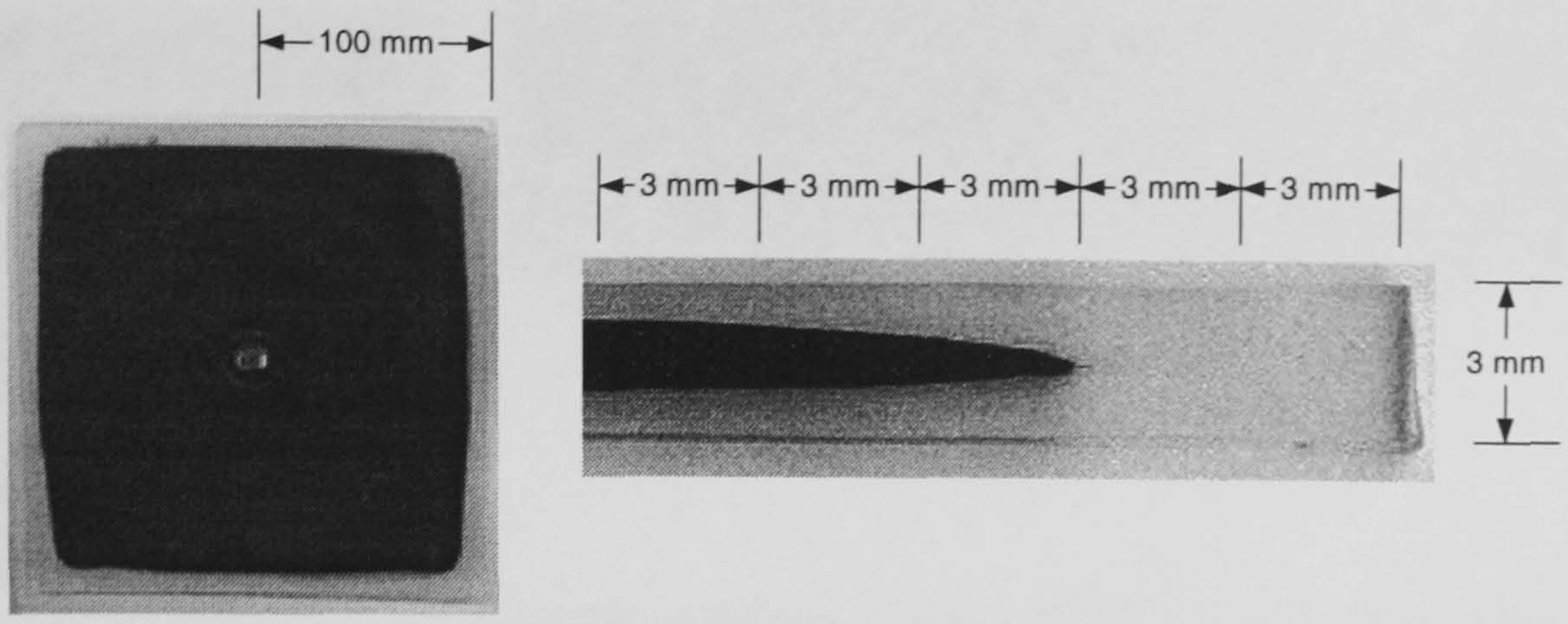

Shows scale of the component

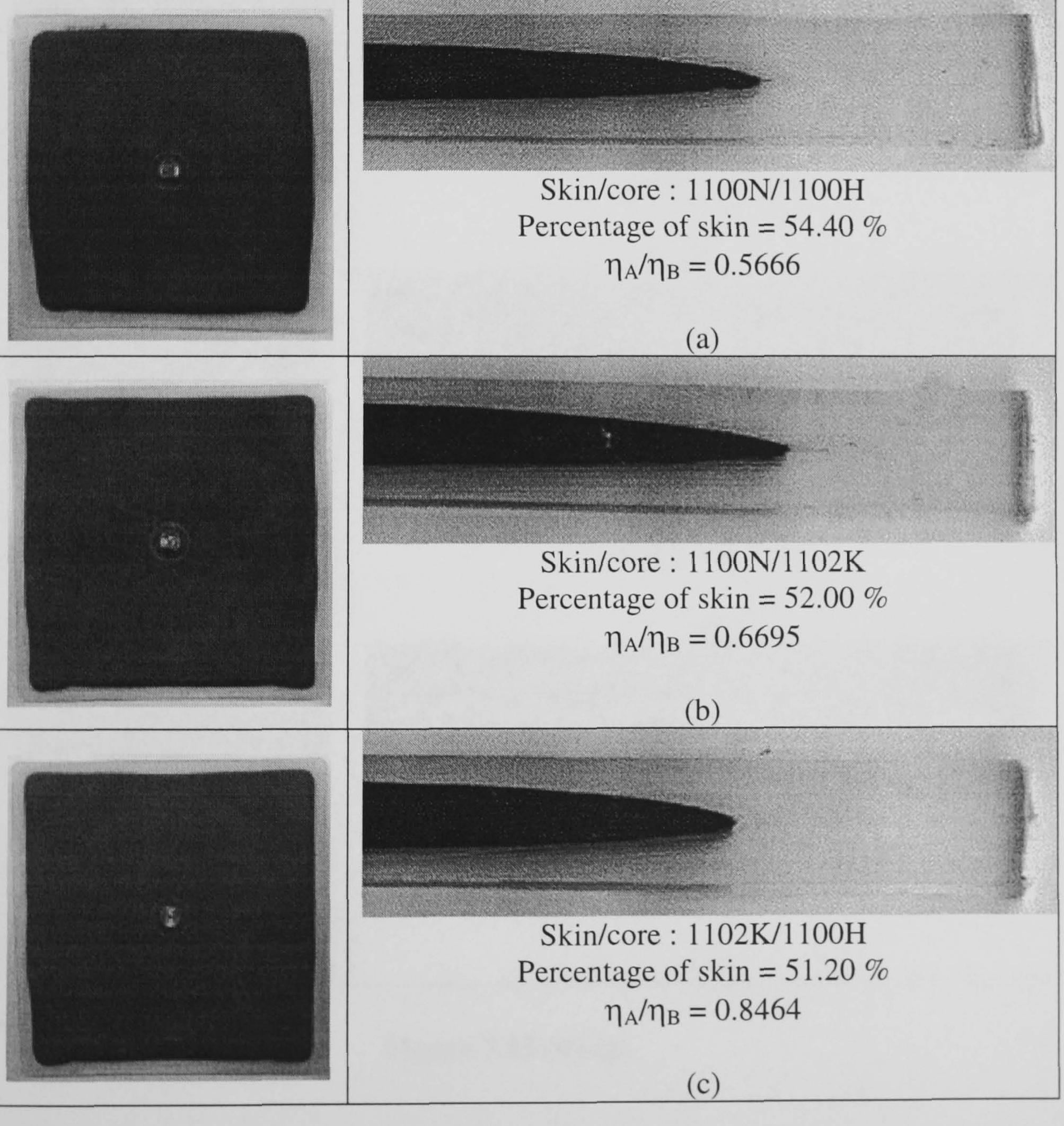

Skin/core : 1100N/1100H
Percentage of skin = 54.40 %
$\eta_A/\eta_B = 0.5666$

(a)

Skin/core : 1100N/1102K
Percentage of skin = 52.00 %
$\eta_A/\eta_B = 0.6695$

(b)

Skin/core : 1102K/1100H
Percentage of skin = 51.20 %
$\eta_A/\eta_B = 0.8464$

(c)

Figure 7.11 (a)-(c)

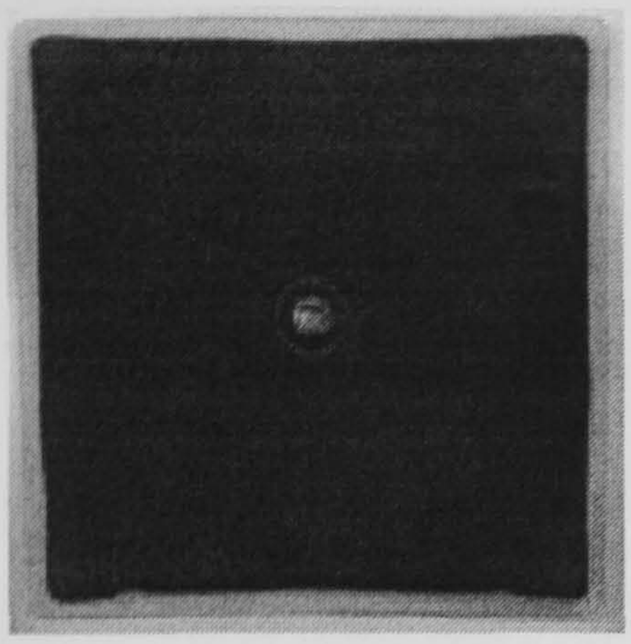

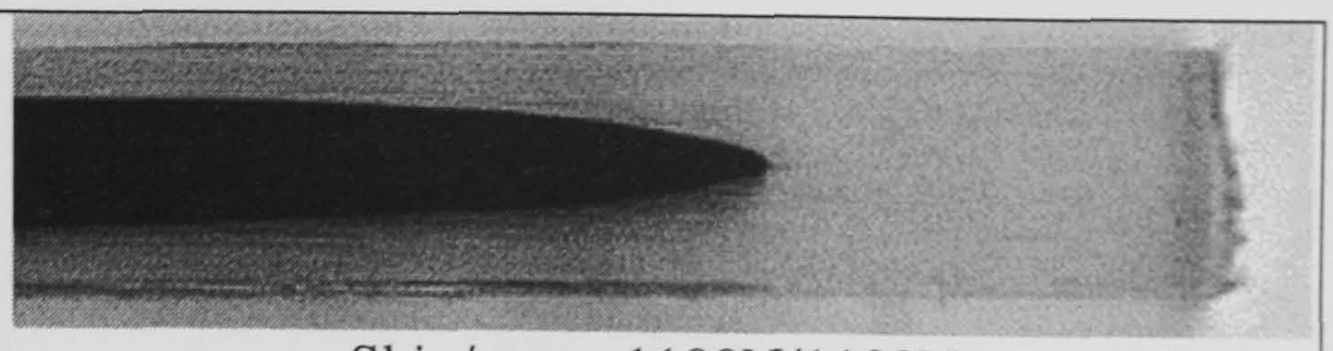

Skin/core : 1100N/1100N
Percentage of skin = 50.40 %
η_A/η_B = 1.0000

(d)

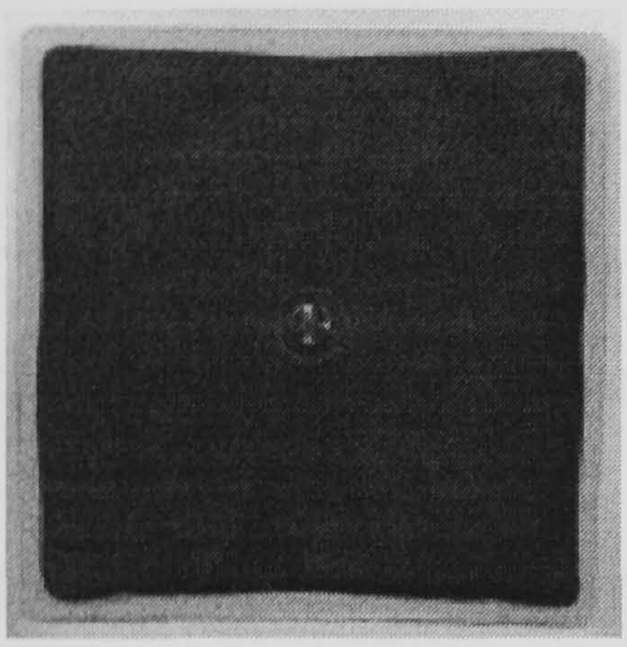

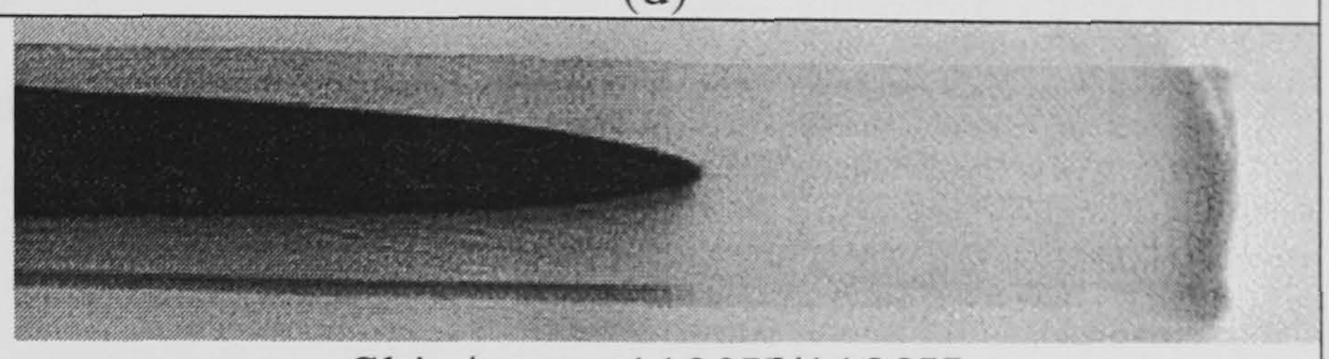

Skin/core : 1100H/1100H
Percentage of skin = 49.60 %
η_A/η_B = 1.0000

(e)

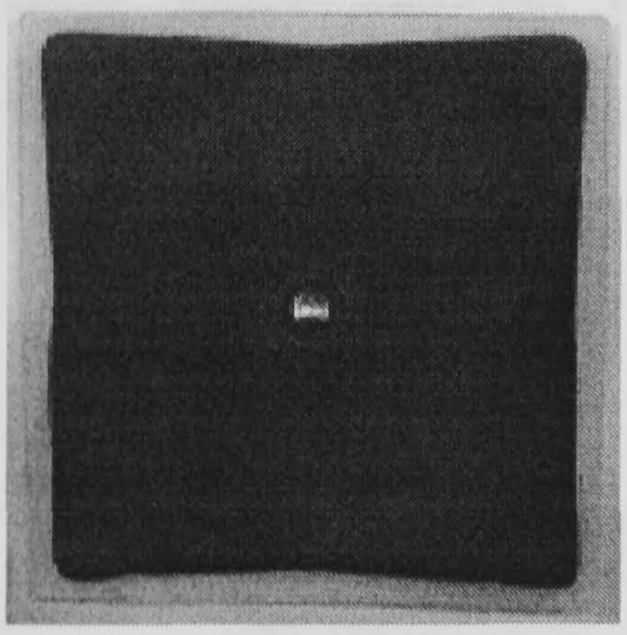

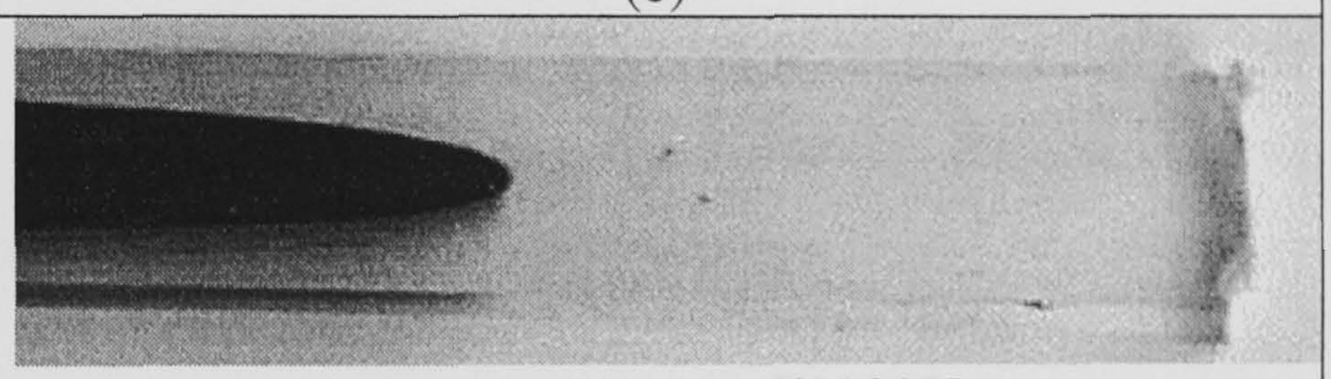

Skin/core : 1100H/1102K
Percentage of skin = 52.80 %
η_A/η_B = 1.1815

(f)

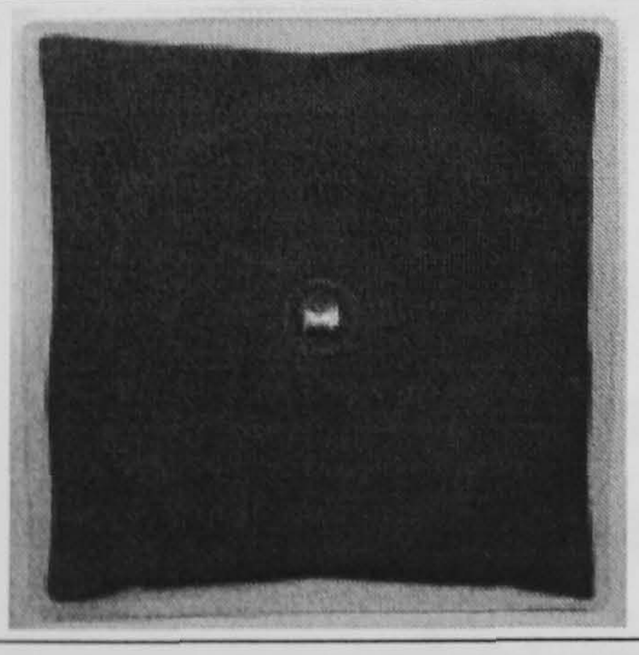

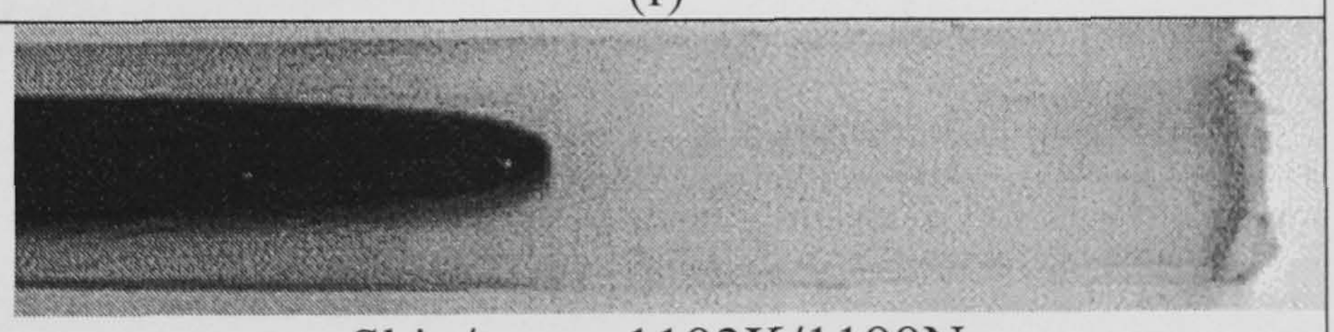

Skin/core : 1102K/1100N
Percentage of skin = 53.60 %
η_A/η_B = 1.4937

(g)

Figure 7.11 (d)-(g)

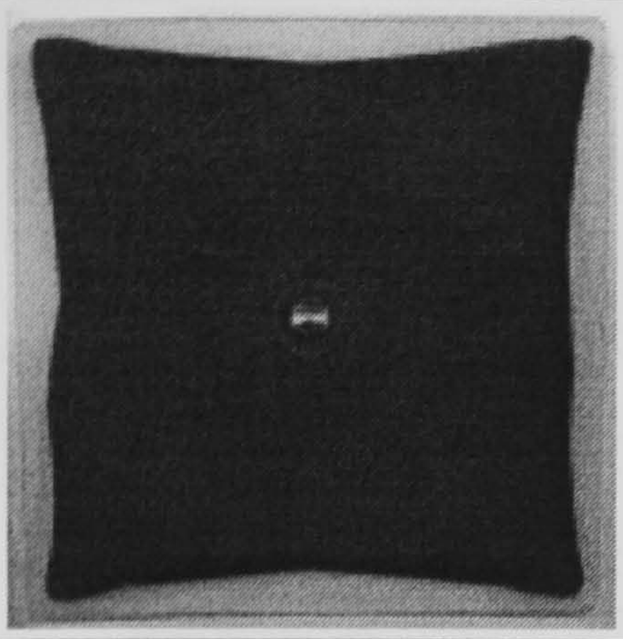

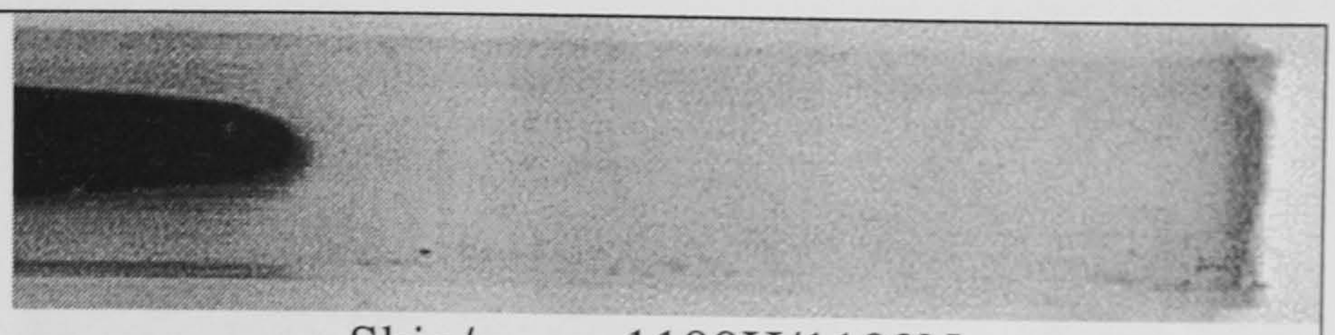

Skin/core : 1100H/1100N
Percentage of skin = 56.00 %
η_A/η_B = 1.7648

(h)

Figure 7.11 The moulding components and the shapes of core penetration: (a)-(h) skin/core viscosity ratios were increased, sequentially.

7.4.2 The shapes of PA6 (skin)/PP (core) core penetration

In this section, the relationship between the core penetrated shapes and the skin/core viscosity ratios showed a similar trend to the lower viscosity ratio of PP(skin)/PP(core) combinations. However, they were completely different when skin/core viscosity ratios were high (Figure 7.12(b)).

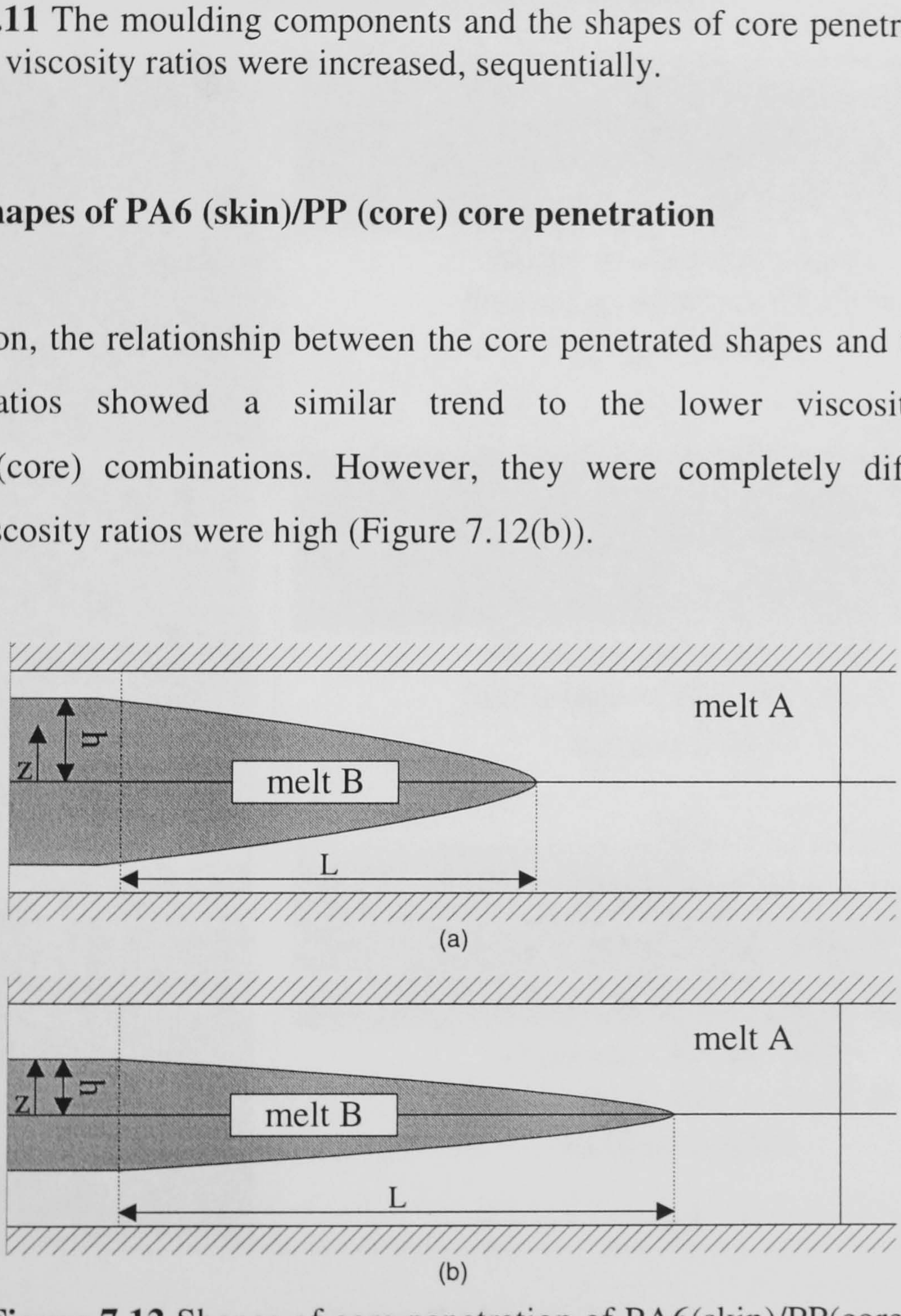

Figure 7.12 Shapes of core penetration of PA6(skin)/PP(core): (a) low skin/core viscosity ratio, and (b) high skin/core viscosity ratio, respectively.

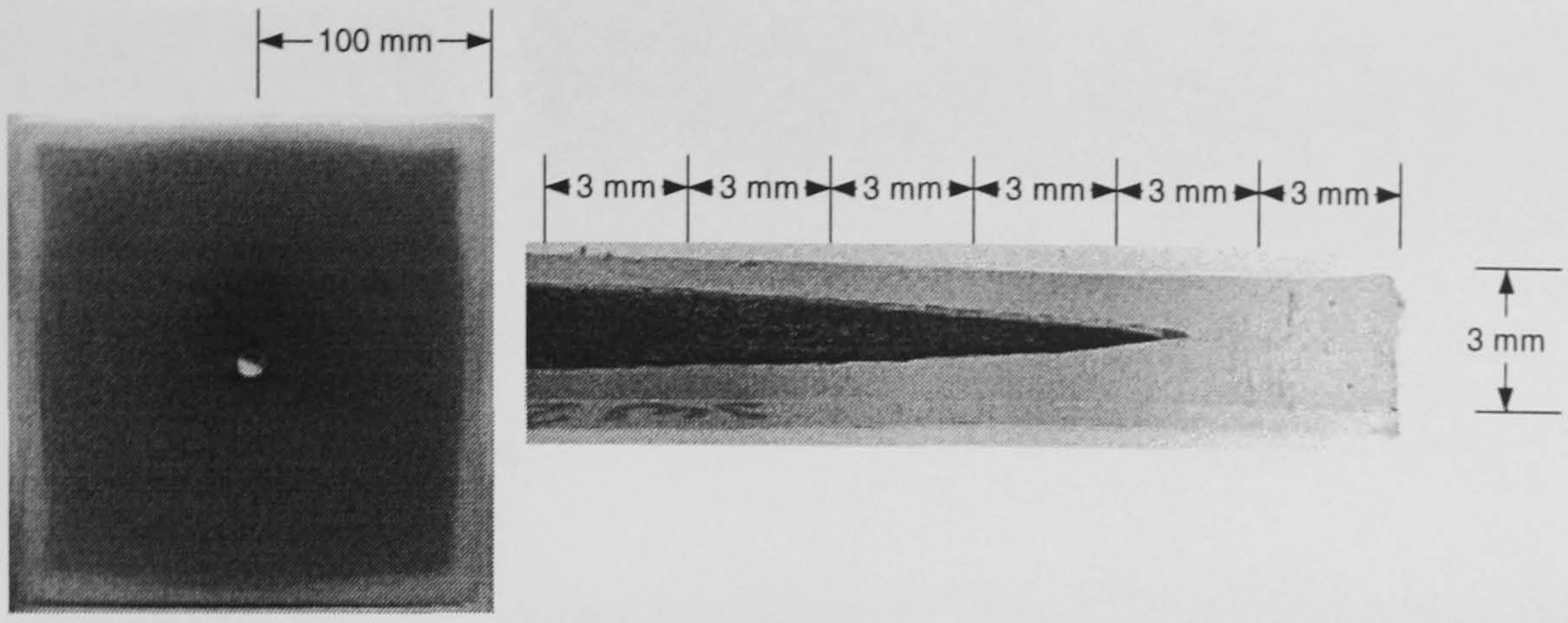

Shows scale of the component

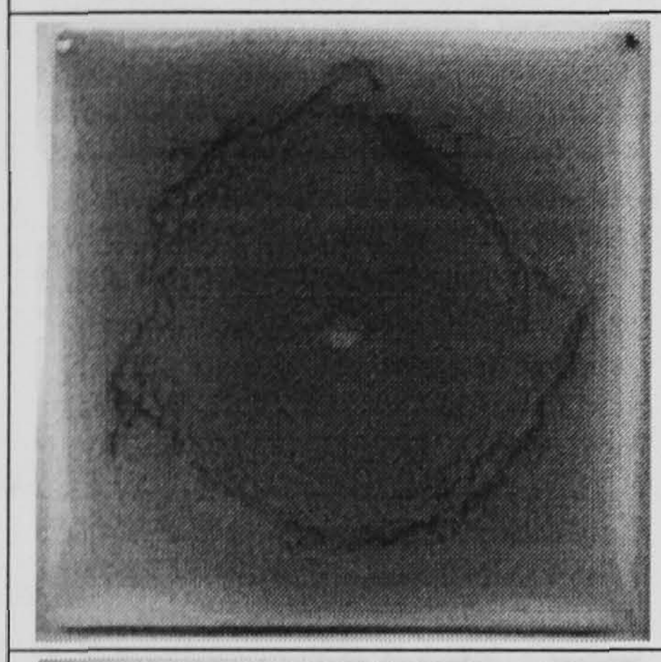

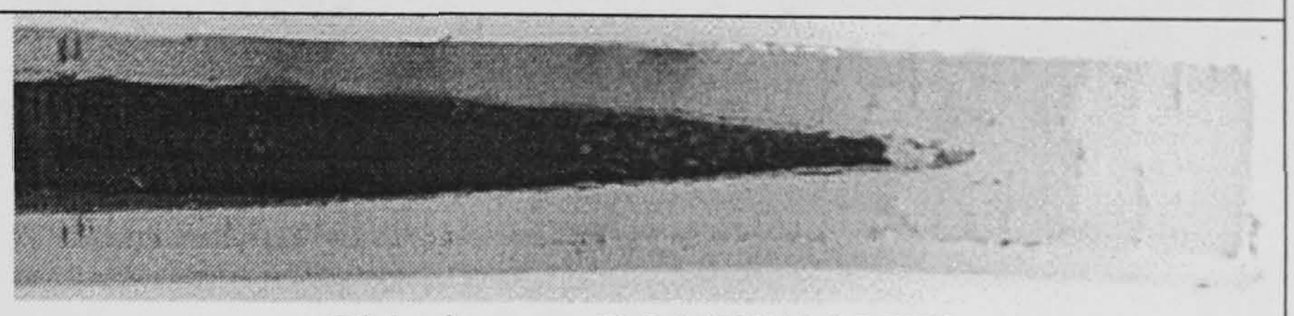

Skin/core : B31SK/1100H
Percentage of skin = 55.20 %
$\eta_A/\eta_B = 0.9494$

(a)

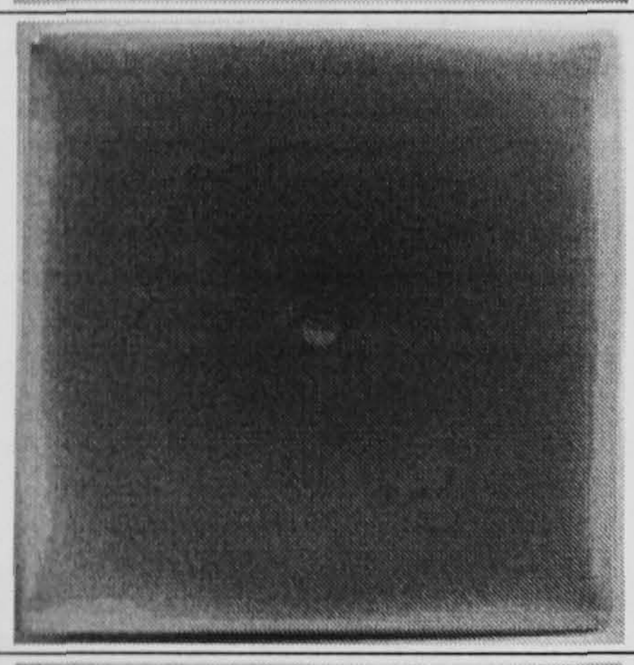

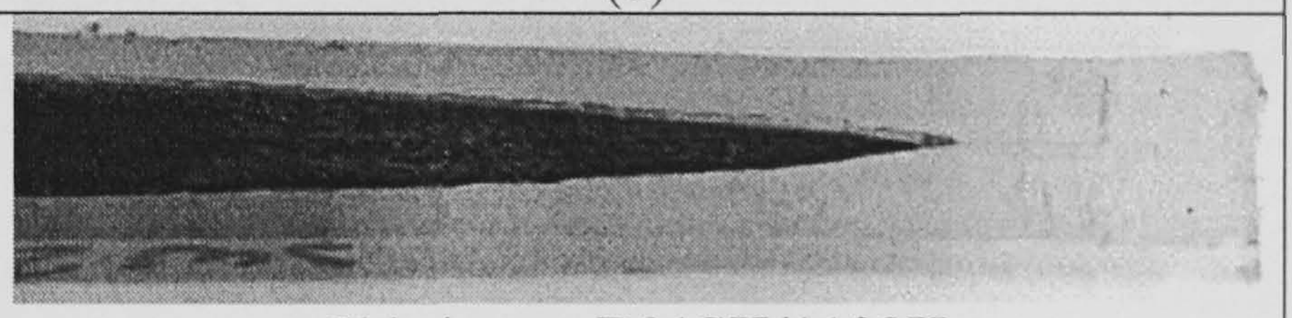

Skin/core : B31SK/1102K
Percentage of skin = 56.40 %
$\eta_A/\eta_B = 1.1217$

(b)

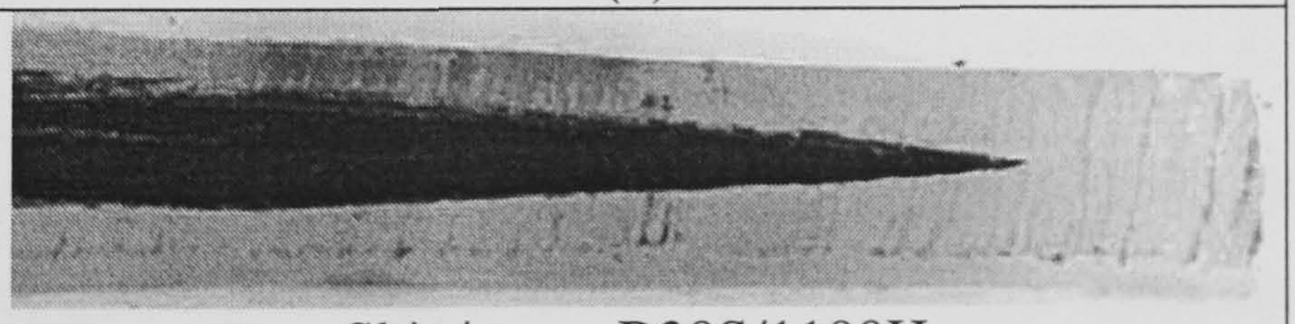

Skin/core : B30S/1100H
Percentage of skin = 56.00 %
$\eta_A/\eta_B = 1.2207$

(c)

Figure 7.13 (a)-(c)

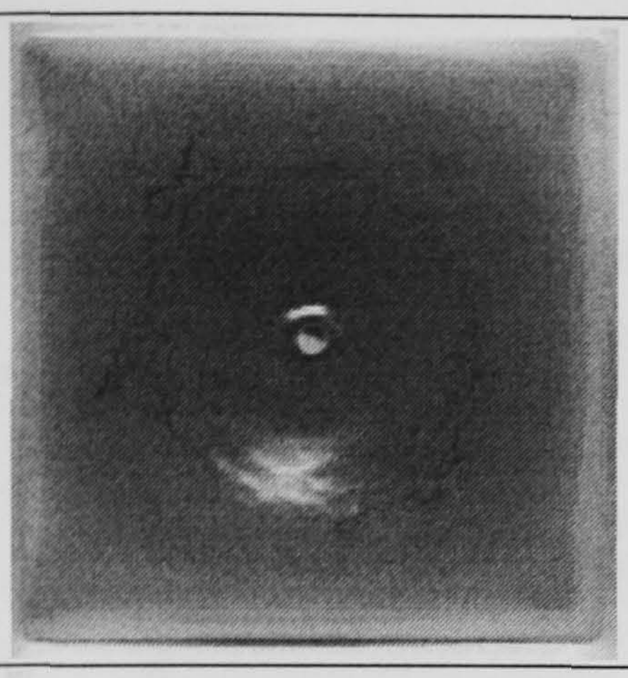

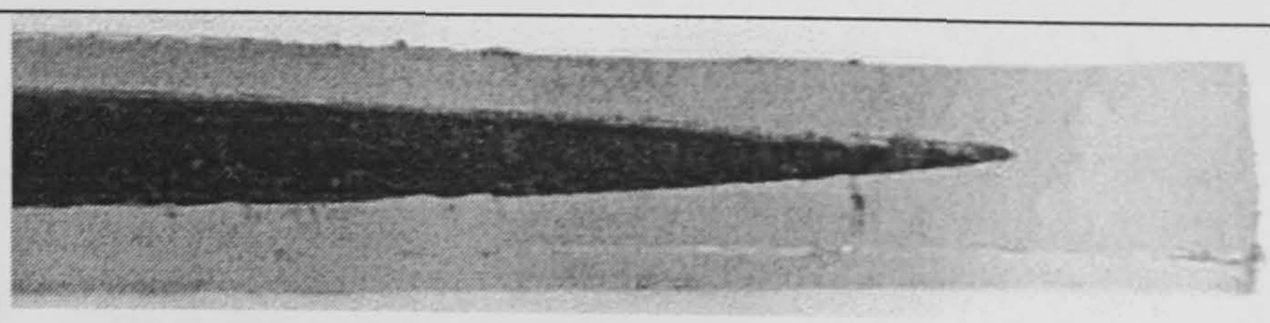

Skin/core : B30S/1102K
Percentage of skin = 57.20 %
η_A/η_B = 1.4423

(d)

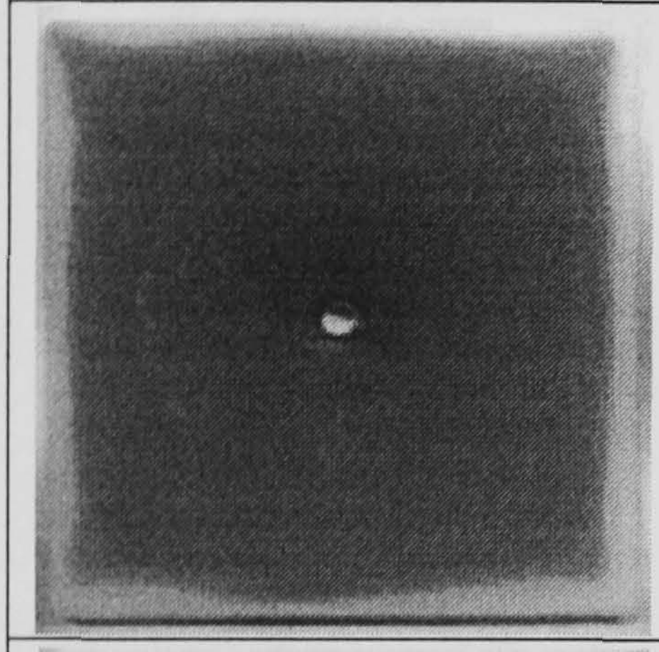

Skin/core : B31SK/1100N
Percentage of skin = 58.40 %
η_A/η_B = 1.6755

(e)

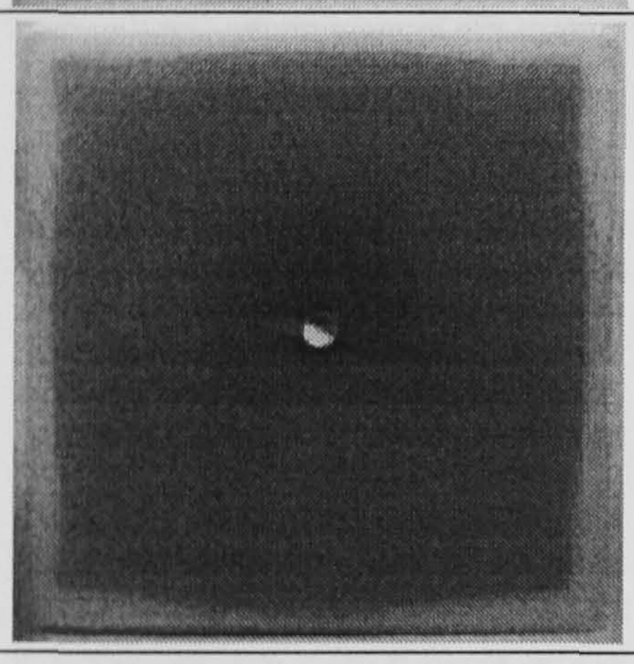

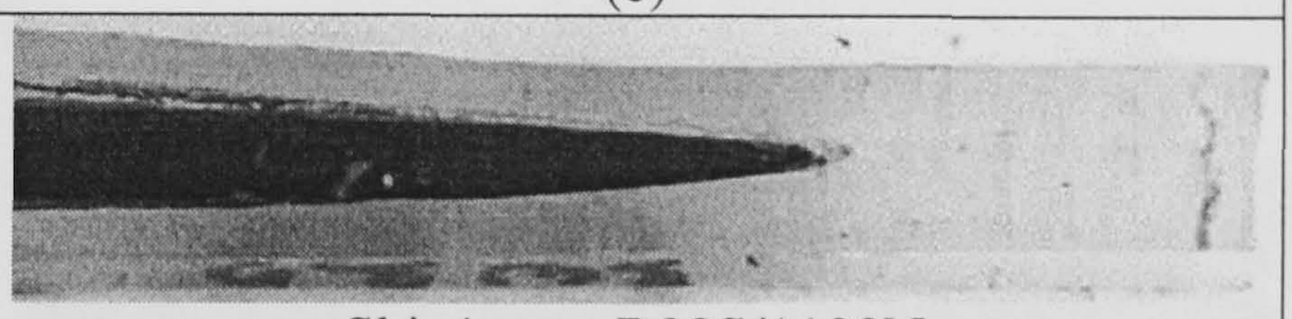

Skin/core : B30S/1100N
Percentage of skin = 60.00 %
η_A/η_B = 2.1543

(f)

Figure 7.13 The moulding components and the shapes of core penetration: (a)-(f) PA6 (skin)/PP (core) viscosity ratios are increased sequentially.

Unfortunately with no compatibiliser, poor skin-core adhesion components are achieved. After mixing 10 % compatibiliser (Polybond 3150) into the core materials, adhesion levels of skin and core were improved (test by peel test). The cross-section photos of PA6(skin)/PP with compatibiliser (core) were examined [Figure 7.14(a)-(f)]. The core thickness fractions were also measured and plotted against the distances from the edge of component (Figure 7.15). It was found that in both cases of the moulding, the components (with and without compatibiliser) are quite similar. The effect of compatibiliser on the core thickness fraction will be investigated in section 7.5.7, page 125.

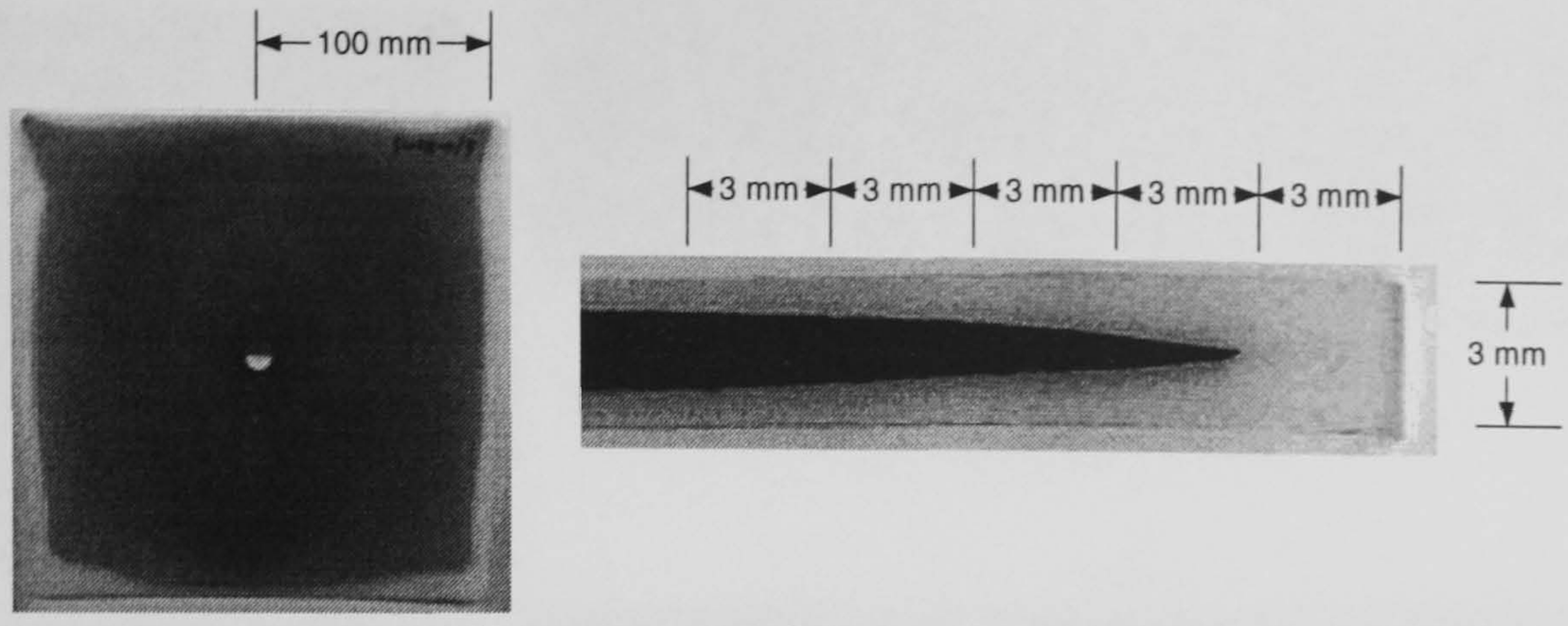

Shows scale of the component

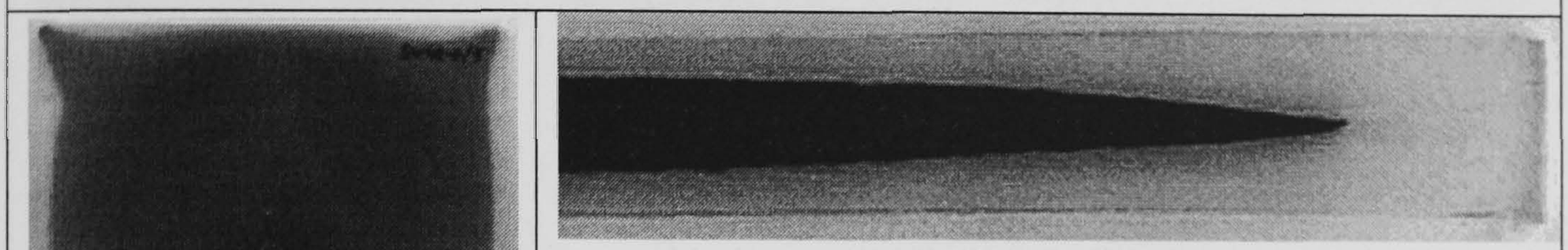

Skin/core : B31SK/1100H + 10% Polybond
Percentage of skin = 56.40 %
$\eta_A/\eta_B = 0.9589$

(a)

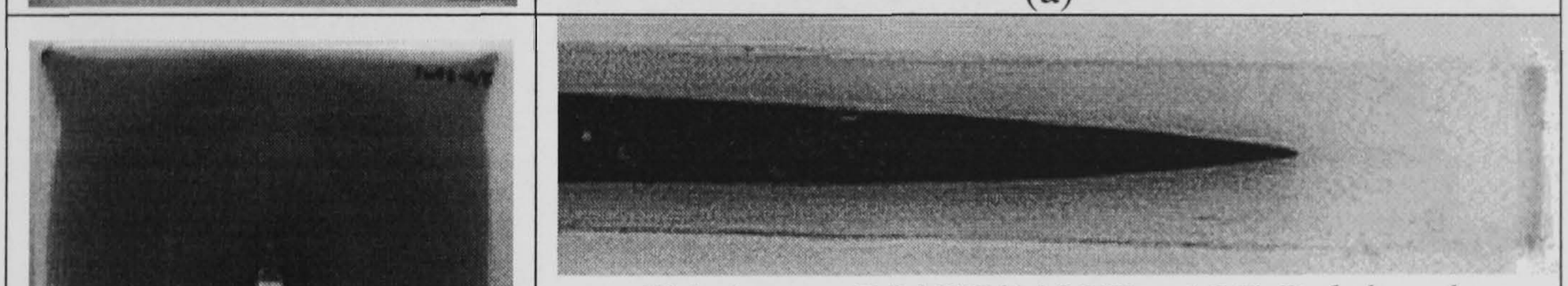

Skin/core : B31SK/1102K + 10% Polybond
Percentage of skin = 57.20 %
$\eta_A/\eta_B = 1.1504$

(b)

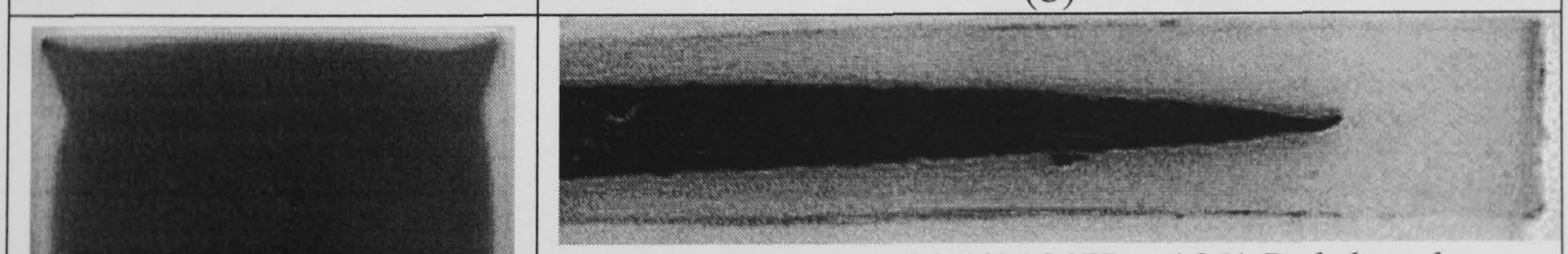

Skin/core : B30S/1100H + 10% Polybond
Percentage of skin = 56.80 %
$\eta_A/\eta_B = 1.2330$

(c)

Figure 7.14 (a)-(c)

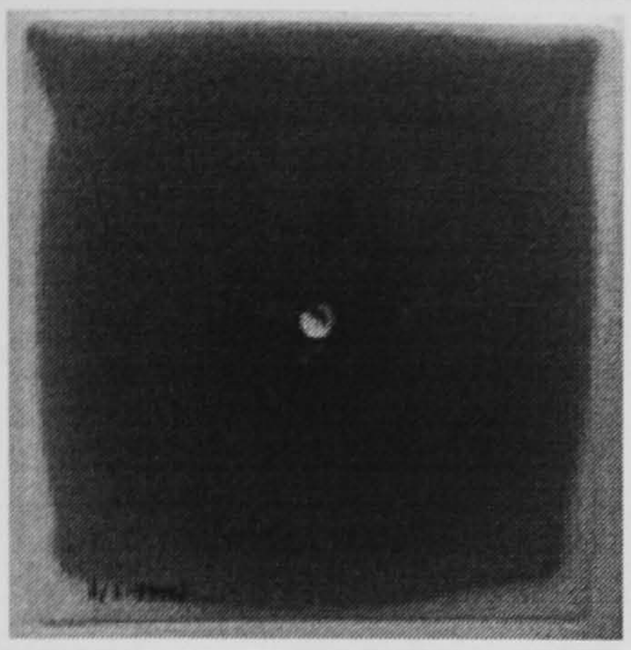

Skin/core : B30S/1102K + 10% Polybond
Percentage of skin = 58.00 %
η_A/η_B = 1.4792

(d)

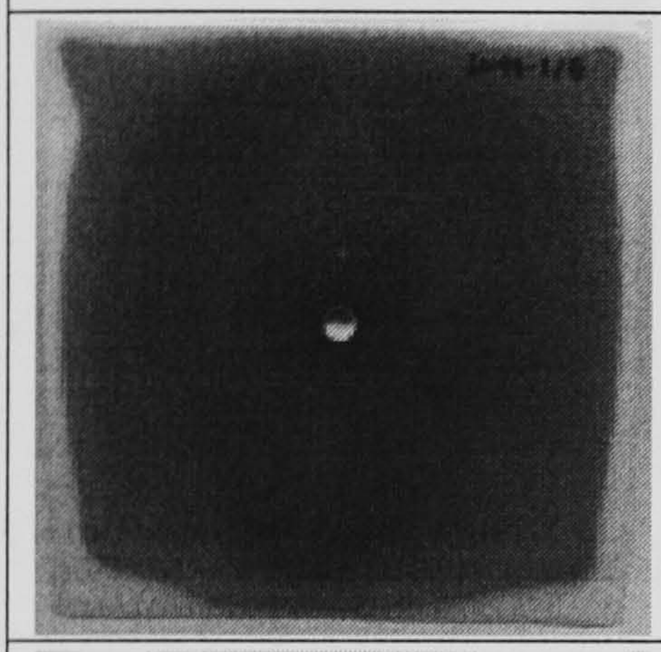

Skin/core : B31SK/1100N + 10% Polybond
Percentage of skin = 59.20 %
η_A/η_B = 1.7787

(e)

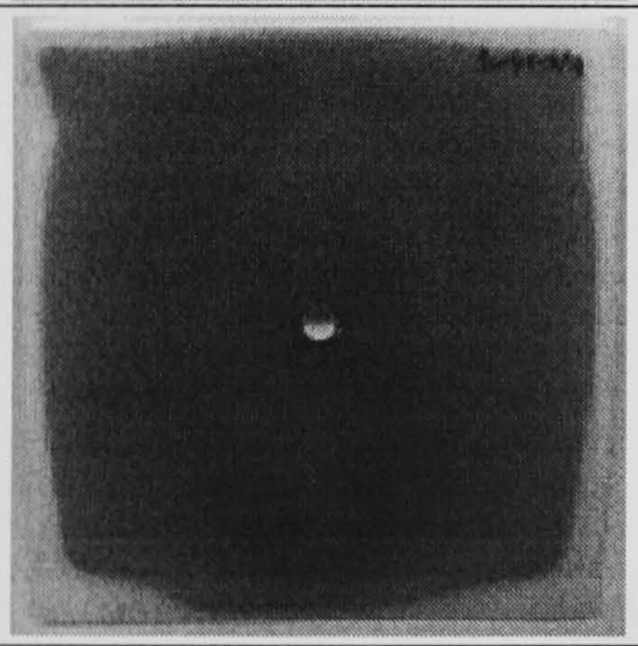

Skin/core : B30S/1100N + 10% Polybond
Percentage of skin = 60.80 %
η_A/η_B = 2.2871

(f)

Figure 7.14 The moulding components and the shapes of core penetration: (a)-(f) PA6 (skin)/PP + 10% Polybond 3150 (core) viscosity ratio are increased sequentially

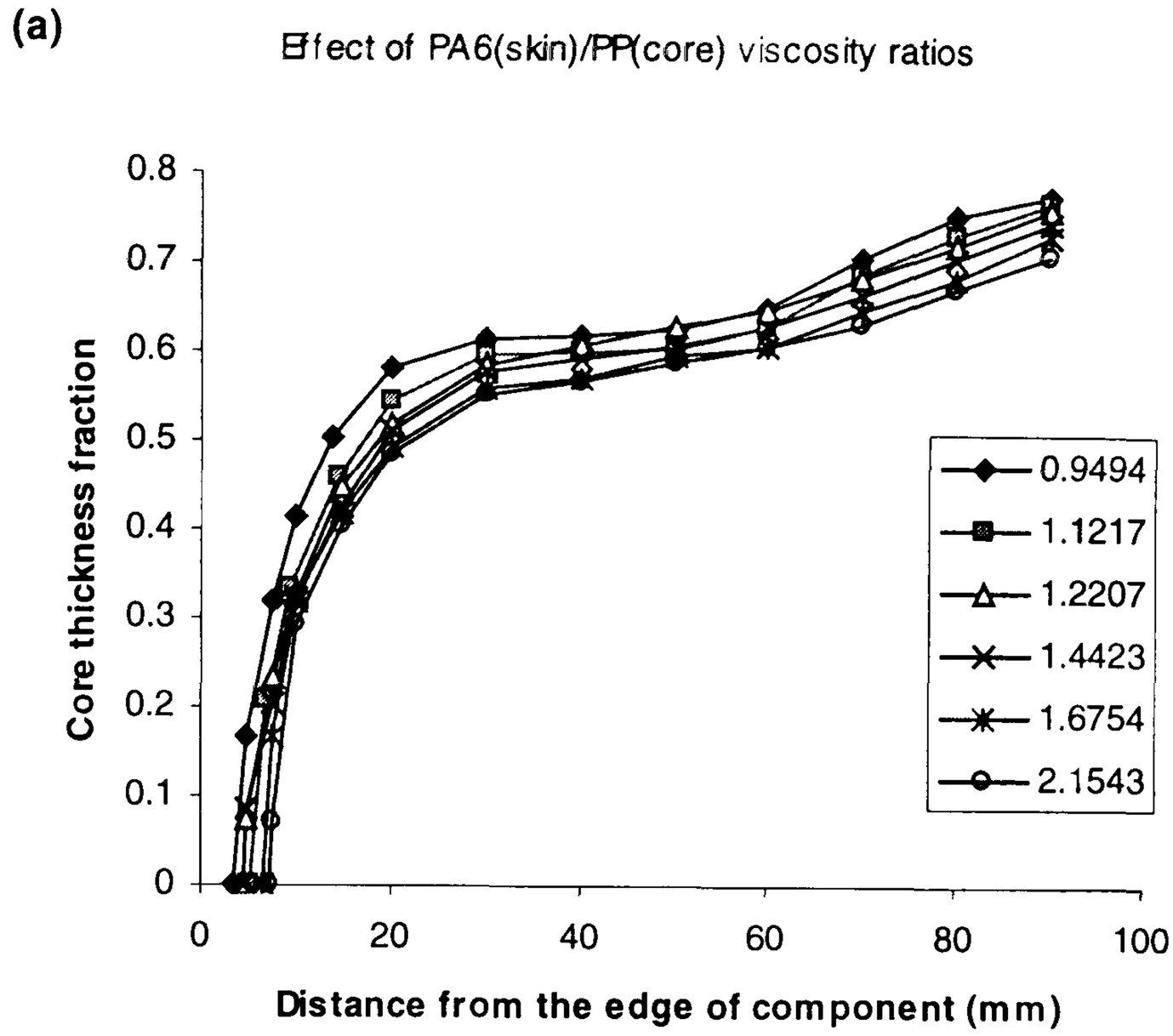

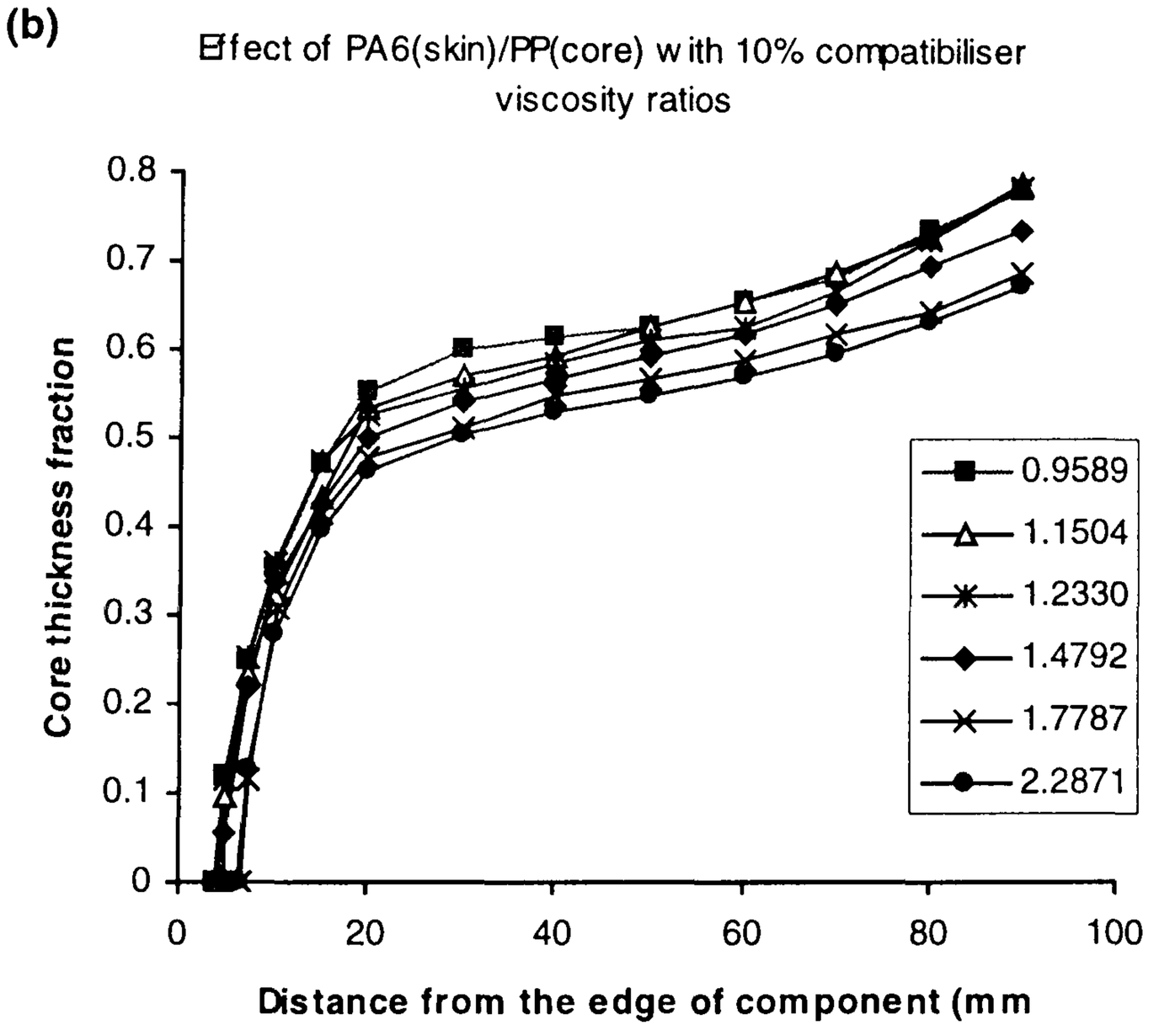

Figure 7.15 Relationship between the sectional core thickness fraction and skin/core viscosity ratios: (a) PA6/PP and (b) PA6/PP+10%compatibiliser.

In the case of PA6 (skin)/PP (core) with and without compatibiliser, shapes of core penetration always show the sharp-angle caused by their thermal properties. The melt temperature (T_m) of PA6 and PP were 216 °C and 148 °C, respectively*. Comparison

---

* Data from C-mold software

between T_m of PA6 and PP shows that $T_{m,\,PA6}$ is higher than $T_{m,\,PP}$, significantly. At the same condition of tool temperature, the solidification rate of PA6 (skin) was evidently faster than PP (core), thus, the frozen layer of skin polymer was being formed when the core polymer melt was still in the molten stage. Therefore, the advancing front of core melt compensated and formed the sharp-angled shape of core penetration.

7.5 Effect of Moulding Conditions on Skin-Core Formation

The aims of this section are to understand the influence of moulding conditions such as melt temperatures, tool temperatures, injection speeds, length of simultaneous phases and compatibiliser on skin and core thickness formation.

7.5.1 Effect of melt temperatures

The skin formation and core penetration were not significantly affected by skin and core melt temperatures. In the case of increasing skin melt temperature, a lower skin viscosity resulted, thus, the skin material could flow easier than one in which the lower melt temperature led to a higher skin thickness (Figure 7.16). It was found that the skin thickness fractions of them varied but not to a great extent (see Table 7.4, Data no. 4, 5, 6). Also, decreasing the core viscosity by increasing core melt temperature could lead to a thicker skin thickness but not significantly (Figure 7.17). It can be explained by the fact that increasing melt temperatures (skin or core) results in a decrease in viscosities of both skin and core polymer melts.

Table 7.4 Average core thickness fraction (CTF_{avg}) with variation of the skin and core melt temperatures.

Data no.	Melt temp. (°C)		η_{Skin}/η_{core}	CTF_{avg}	% Change of CTF_{avg}	
	Skin	Core				
(1)	260	225	0.9018	0.5687		
(2)	260	235	0.9494	0.5797	100*[(2)-(1)]/(1)	1.94
(3)	260	245	0.9965	0.5896	100*[(3)-(1)]/(1)	3.68
(4)	250	235	1.2589	0.5483		
(5)	260	235	0.9494	0.5783	100*[(5)-(4)]/(4)	5.47
(6)	270	235	0.7221	0.5576	100*[(6)-(4)]/(4)	1.70

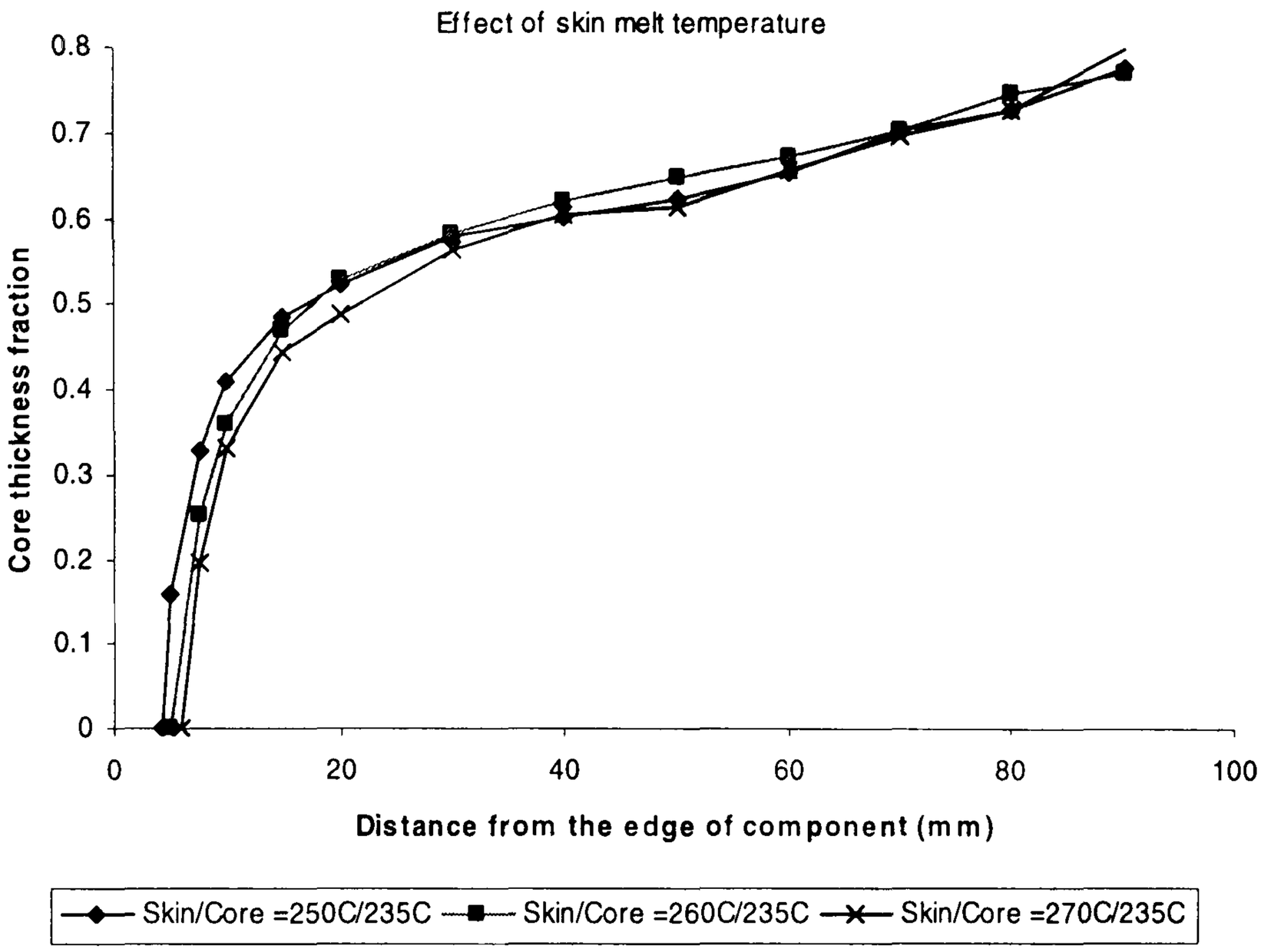

Figure 7.16 Effect of skin melt temperatures on core thickness fraction.

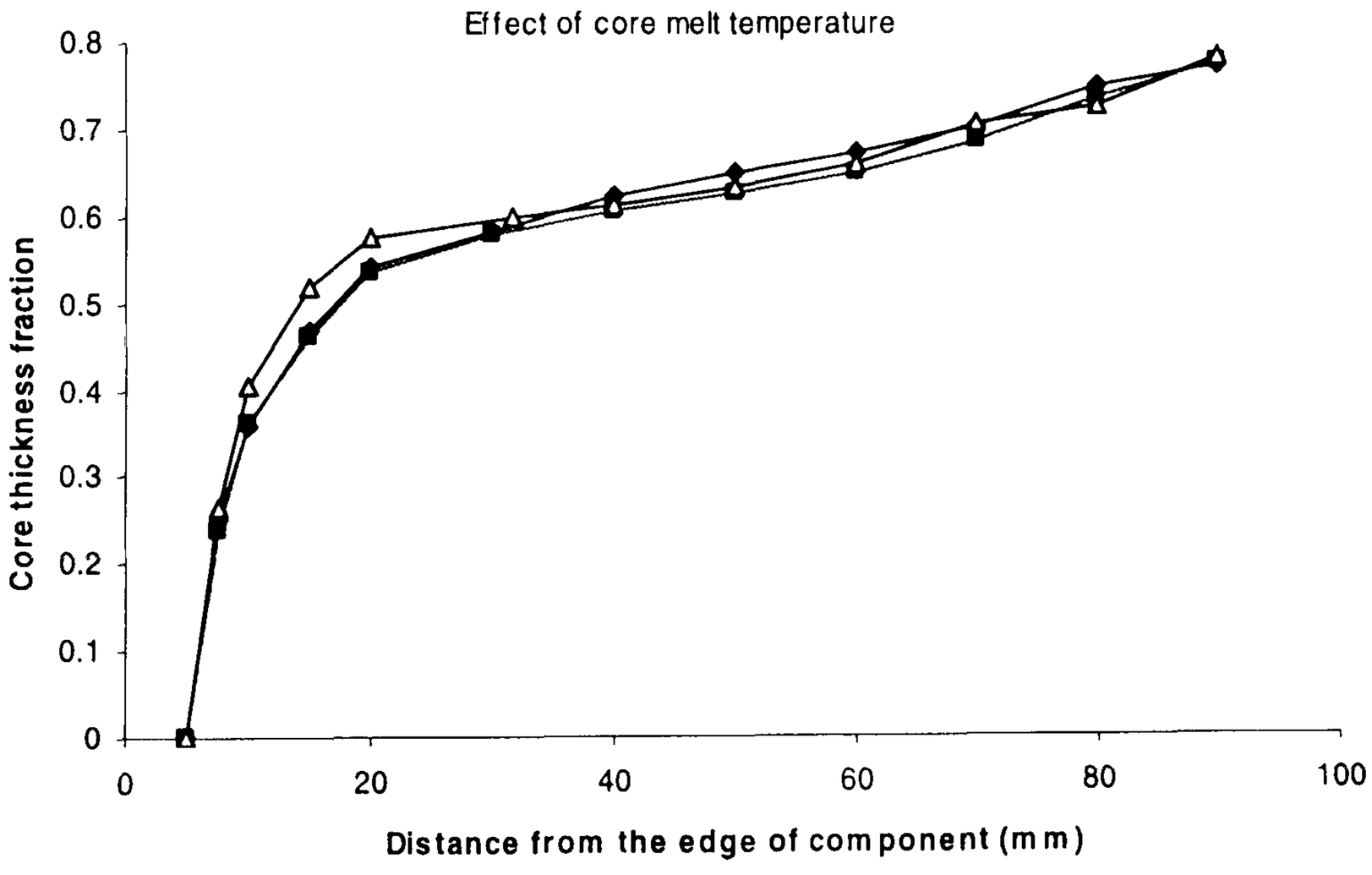

Figure 7.17 Effect of core melt temperatures on core thickness fraction.

7.5.2 Effect of tool temperatures

Basically, unsuitable tool temperatures can cause residual stress in component parts. This parameter however, was shown to have only a slight effect on skin formation (see Table 7.5, Data no. 1, 2, 3, 4). As seen in Figure 7.18, it was found that core penetration and skin thickness fractions were only slightly changed as the tool temperatures was altered significantly. It could be concluded that tool temperature had negligible contribution to skin and core viscosity which consequently affected skin-core formation.

It was a fact that the highest tool temperature of this experiment (98 °C) was still much lower than melt temperature (T_m) of skin and core polymers*. Therefore, the viscosities of skin and core did not change at this tool temperature.

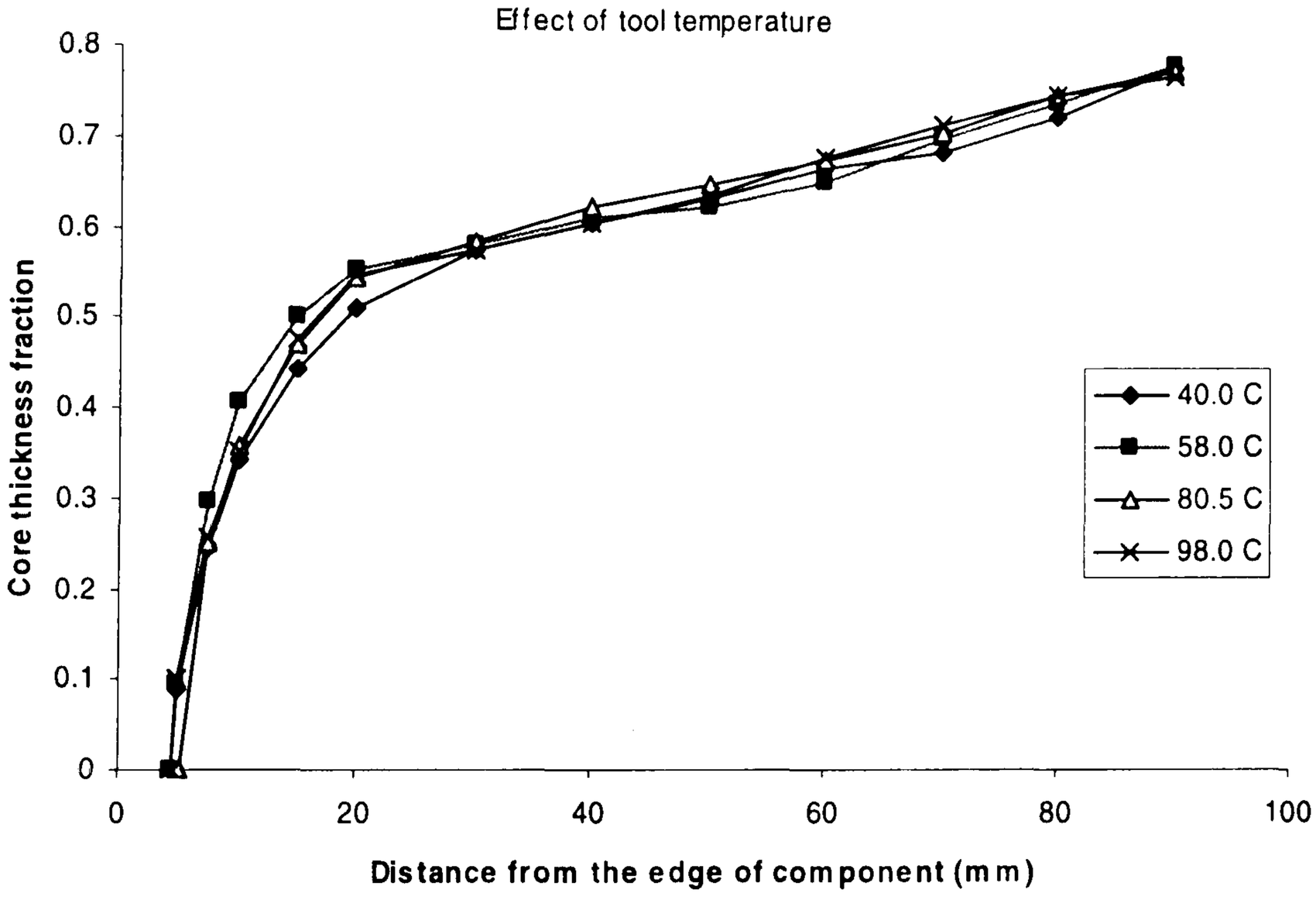

Figure 7.18 Effect of tool temperatures on core thickness fraction.

---

* $T_{m,PA6}$ = 216 °C, $T_{m,PP}$ = 148 °C, Data from C-mold software

Table 7.5 Average core thickness fraction (CTF_{avg}) with variation of the tool temperatures.

Data no.	Tool temp. (°C)	CTF_{avg}		% Change of CTF_{avg}	
(1)	40.0	0.5239			
(2)	58.0	0.5448		100*[(2)-(1)]/(1)	3.98
(3)	80.5	0.5314		100*[(3)-(1)]/(1)	1.43
(4)	98.0	0.5381		100*[(4)-(1)]/(1)	2.71

7.5.3 Effect of injection speeds

As seen in Figure 7.19 and Table 7.6, It was found that when skin injection speeds are lower than core injection speed (VA = 64 and 114 mm/s, VB = 135 mm/s), the core thickness fractions are not significantly different. This is because skin and core polymer were injected simultaneously (in this study, TOL at VA = 64, 114, and 164 mm/s were 0.1906, 0.0193, and – 0.1985 s, respectively*). On the other hand, the sequential process (TOL = – 0.1985 s) took place when the injection speed of skin polymer was too high (VA=164 mm/s, VB=135 mm/s). This led to a higher skin thickness fraction. In addition, faster core injection speeds could lead to higher core thickness fractions. The higher that the injection speed is, so the higher is the pressure.

Table 7.6 Average core thickness fraction (CTF_{avg}) with variation of the skin and core injection speeds.

Data no.	Injection speeds (mm/s)		CTF_{avg}		% Change of CTF_{avg}	
	Skin (VA)	Core (VB)				
(1)	64	135	0.5317			
(2)	114	135	0.5265		100*[(2)-(1)]/(1)	0.98
(3)	164	135	0.4838		100*[(3)-(1)]/(1)	9.02
(4)	114	85	0.5172			
(5)	114	135	0.5312		100*[(5)-(4)]/(4)	2.72
(6)	114	185	0.5558		100*[(6)-(4)]/(4)	7.47

* Calculated by using equation (7.5), where SWB = 25.5 mm and TDB = 0.2 s

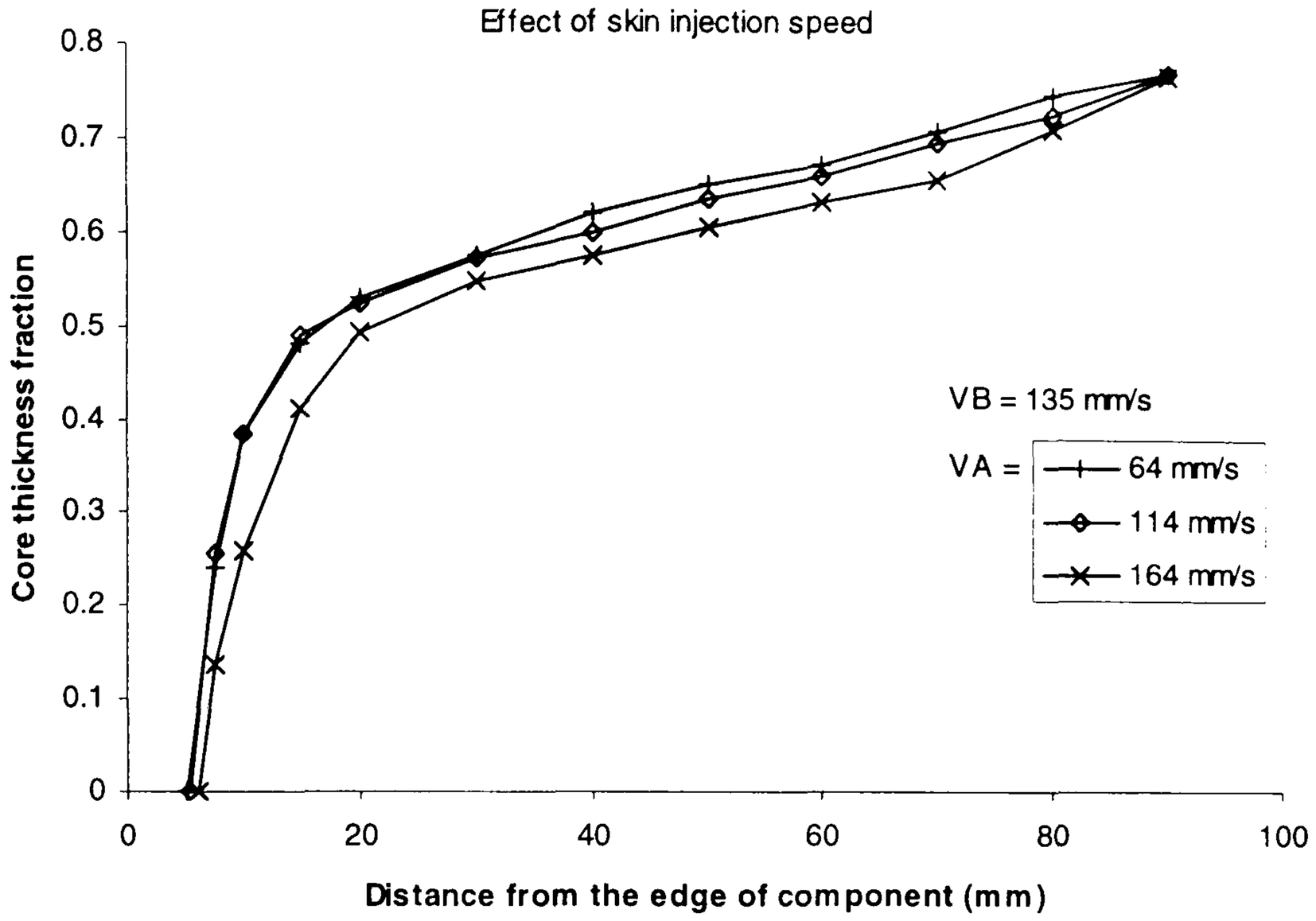

Figure 7.19 Effect of skin injection speeds on core thickness fraction.

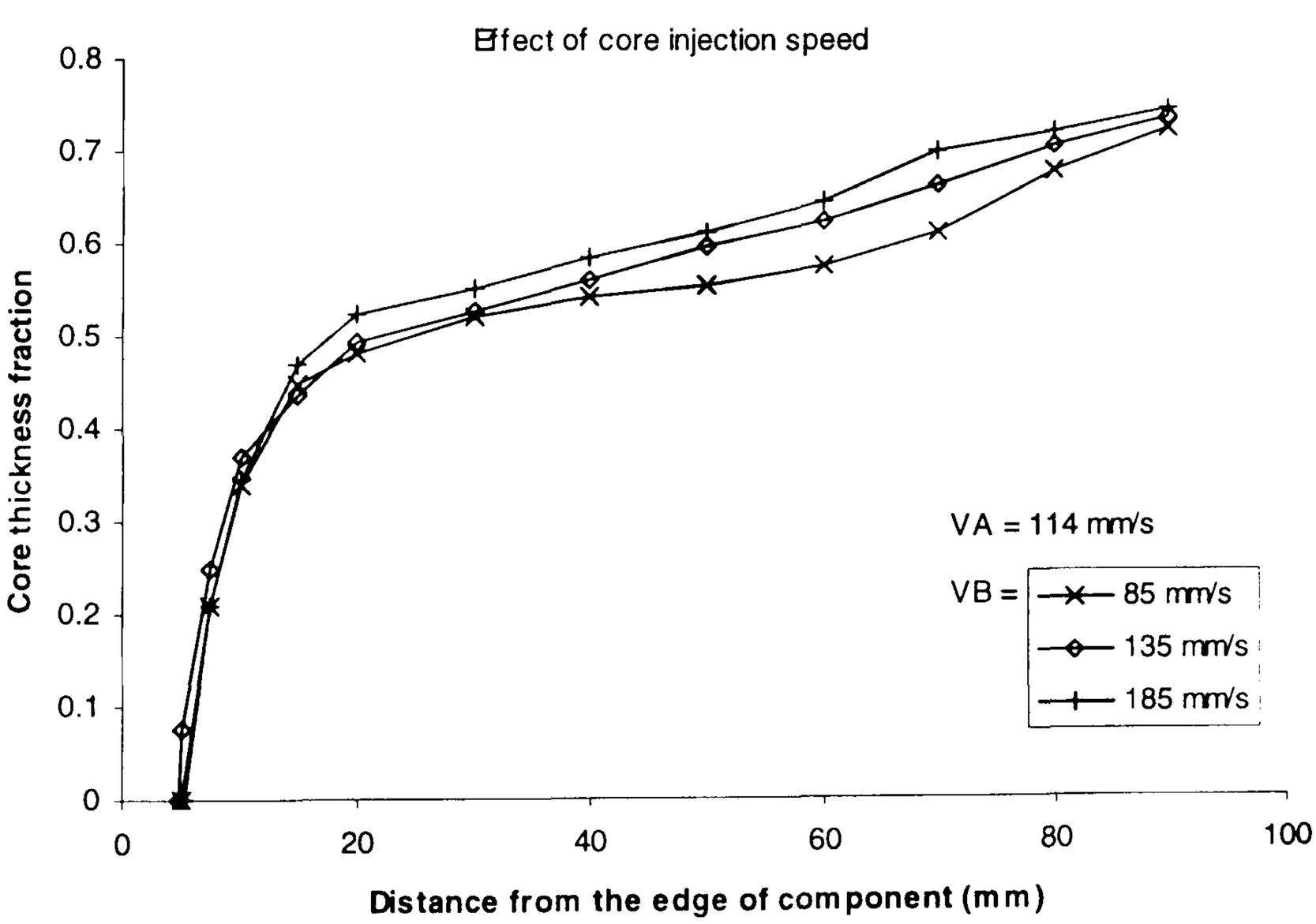

Figure 7.20 Effect of core injection speeds on core thickness fraction.

7.5.4 Effect of lengths of simultaneous phase

The simultaneous injection times (or overlap time, TOL) and lengths of simultaneous phase (L_{simul}) were obtained as shown in Table 7.7.

Table 7.7 Effect of the length of simultaneous phase.

	(a)	(b)	(c)	(d)	Unit
Core switch-over at	35	25	15	6	mm
Core injection speeds	135	135	135	135	mm/s
Skin injection speeds	114	114	114	114	mm/s
Overlap time	0.107	0.019	-0.068	-0.147	s
L_{simul}	12.20	2.20	-7.80	-16.80	mm
Simultaneous phase ($100*L_{simul}/SA$)	17.68	3.20	-11.30	-24.35	%
Filling results					

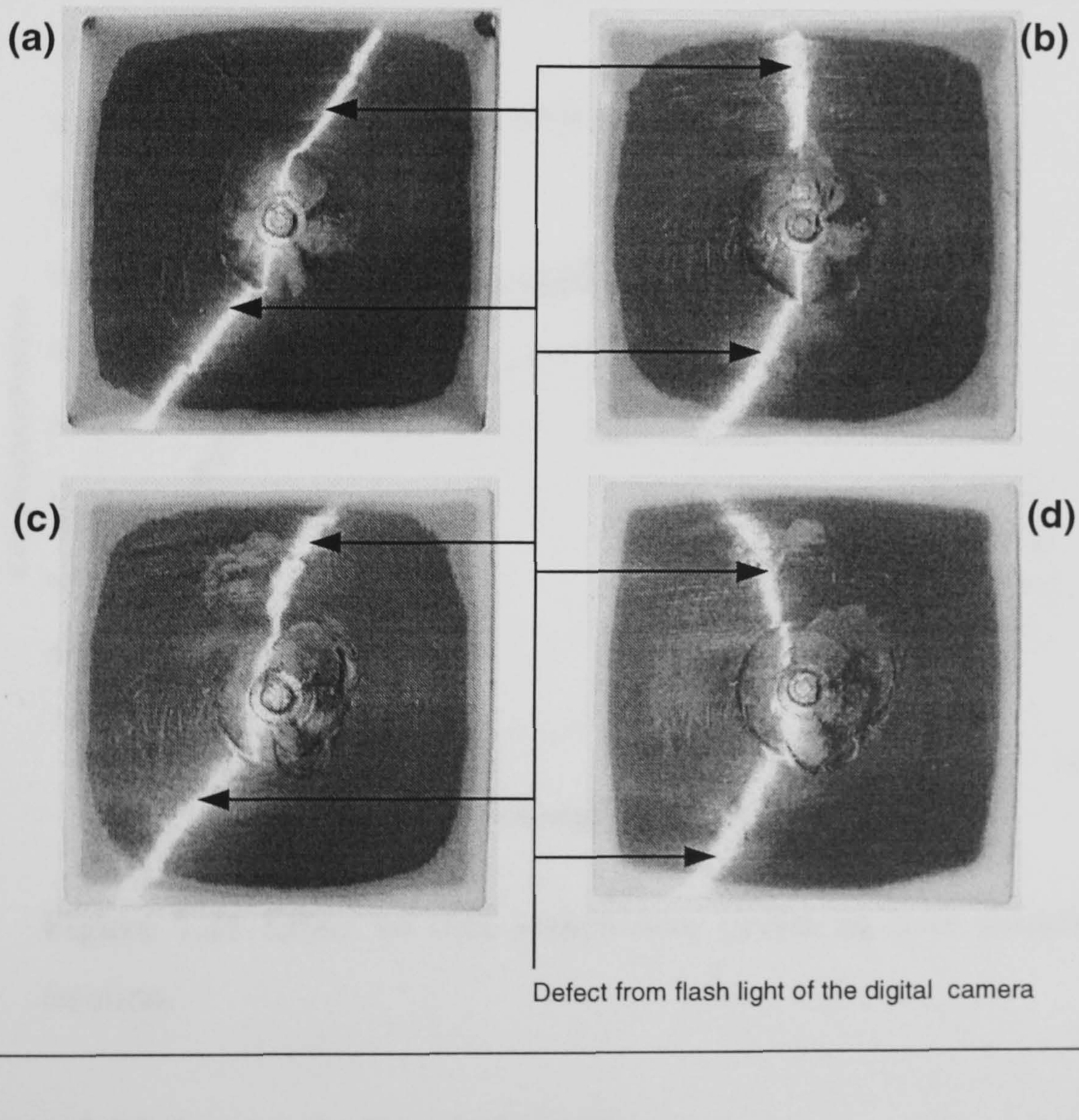

As previously mentioned in section 6.4.2.4 (page 77-78), the length of simultaneous phase (L_{simul}) was related to the switch-over points of the B-side (SWB) and calculated using equation (7.5). It was found that when the length of simultaneous phase was too high (L_{simul} = 12.20 mm), it caused poor filling of the component (core breakthrough, Table 7.7 (a)). On the other hand, the optimum filling of the component

was not achieved if the length of simultaneous phase was too low as seen in Table 7.7(d) (L_{simul} = -16.80 mm). It was also found that the higher L_{simul} led to a greater core thickness fraction whereas the lower L_{simul} resulted in a lower core thickness (Table 7.8). Therefore, a lower skin thickness of the moulding component could be obtained by increasing the length of the simultaneous phase.

Table 7.8 Average core thickness fraction (CTF_{avg}) with variation of the switch-over points of B-side (SWB).

Data no.	SWB (mm)	CTF_{avg}		% Change of CTF_{avg}	
(1)	35	0.5534			
(2)	25	0.5023		100*[(2)-(1)]/(1)	9.24
(3)	15	0.4892		100*[(3)-(1)]/(1)	11.60
(4)	6	0.4486		100*[(4)-(1)]/(1)	18.95

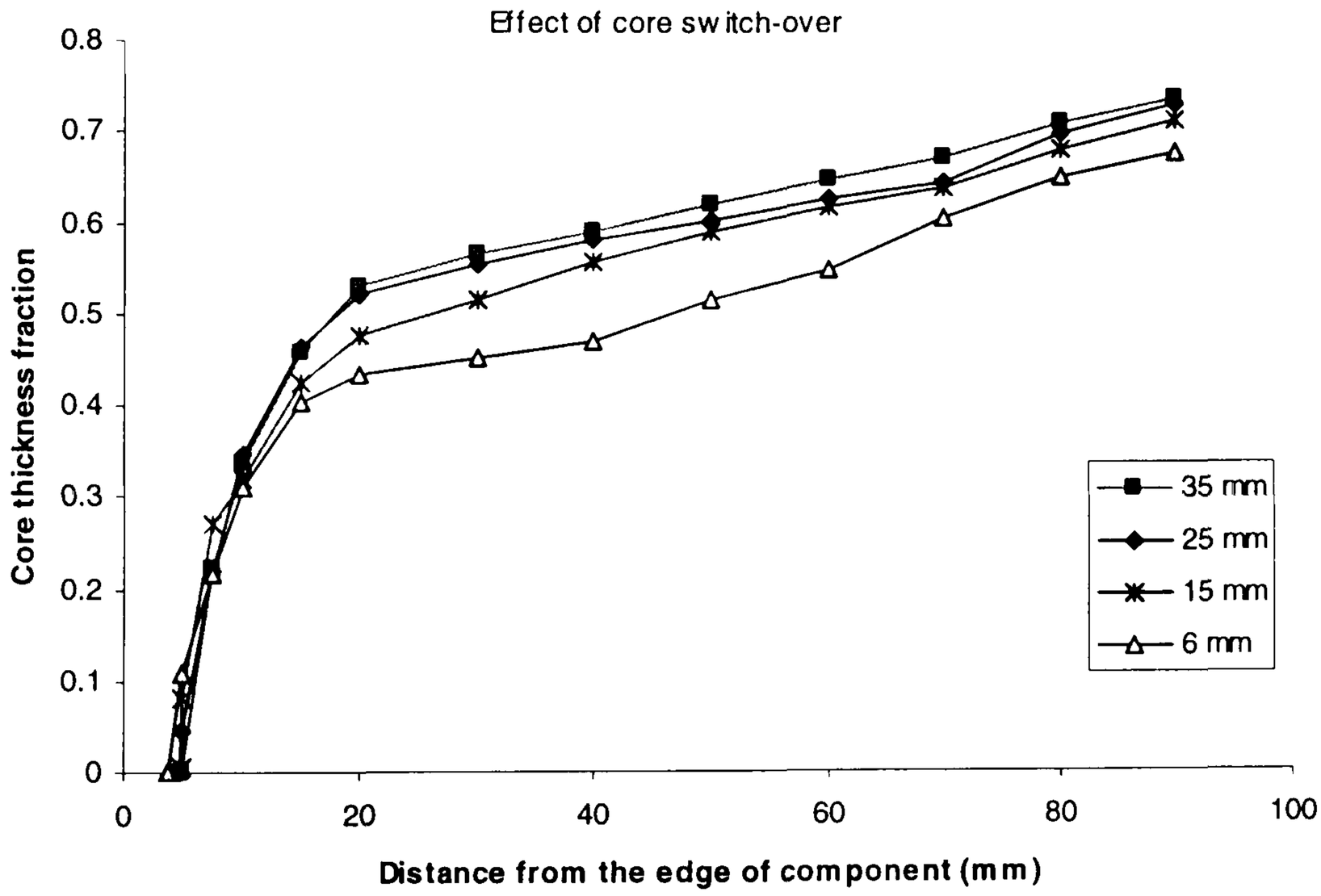

Figure 7.21 Effect of core switch-over points on core thickness fraction.

7.5.5 Effect of skin/core metering stroke ratios

In this case, it was found that the average core thickness fraction (CTF_{avg}) was 0.5707, 0.5419, 0.5000, and 0.4768 when skin/core metering stroke ratios (100*SA/SB) were 52%, 56%, 60%, and 64%, respectively. The change of CTF_{avg} of each skin/core

metering stroke ratios was significant (Table 7.10 and Figure 7.22). It was also found that at SA/SB = 0.52, core breakthrough was observed. On the other hand at SA/SB = 0.64, the optimum condition was not achieved (the flow front of core polymer was far from the edge of the component). It was concluded that in both cases, a too high or a conversely a too low proportion of skin to core metering stroke led to a non-optimum moulding component.

Table 7.9 Effect of skin/core metering stroke ratios

	(a)	(b)	(c)	(d)	Unit
Skin/Core metering stroke of	65/60 (52%)	70/55 (56%)	75/50 (60%)	80/45 (64%)	mm
Core injection speeds	135	135	135	135	mm/s
Skin injection speeds	114	114	114	114	mm/s
Overlap time	0.0193	0.0193	0.0193	0.0193	s
L_{simul}	2.200	2.200	2.200	2.200	mm
Simultaneous phase ($100*L_{simul}/SA$)	3.38	3.14	2.93	2.75	%

Filling results

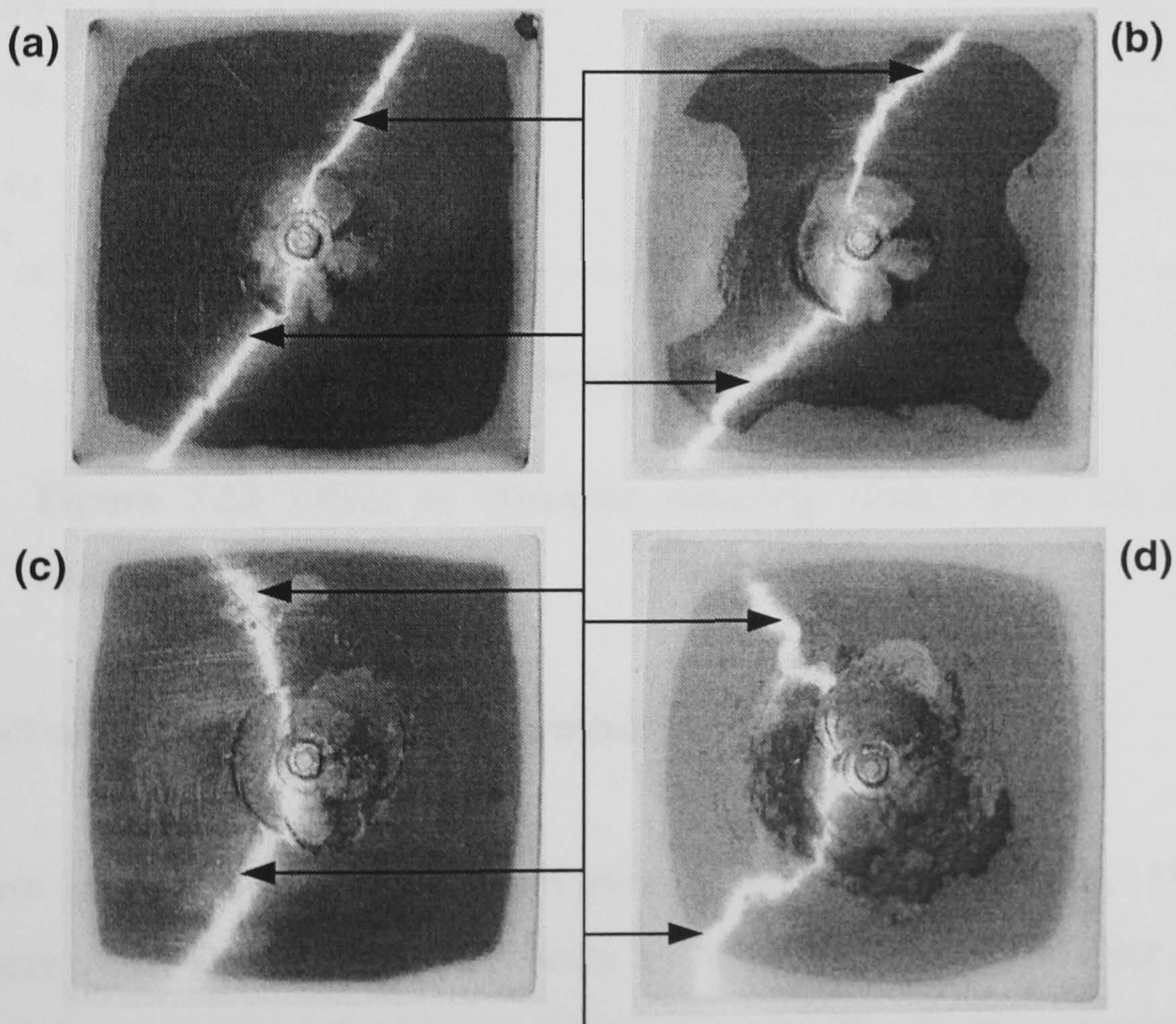

Defect from flash light of the digital camera

Table 7.10 Average core thickness fraction (CTF_{avg}) with variation of the switch-over points of B-side (SWB).

Data no.	SA/SB (%)	CTF_{avg}		% Change of CTF_{avg}	
(1)	52	0.5707			
(2)	56	0.5419		100*[(2)-(1)]/(1)	5.04
(3)	60	0.5000		100*[(3)-(1)]/(1)	12.38
(4)	64	0.4768		100*[(4)-(1)]/(1)	16.46

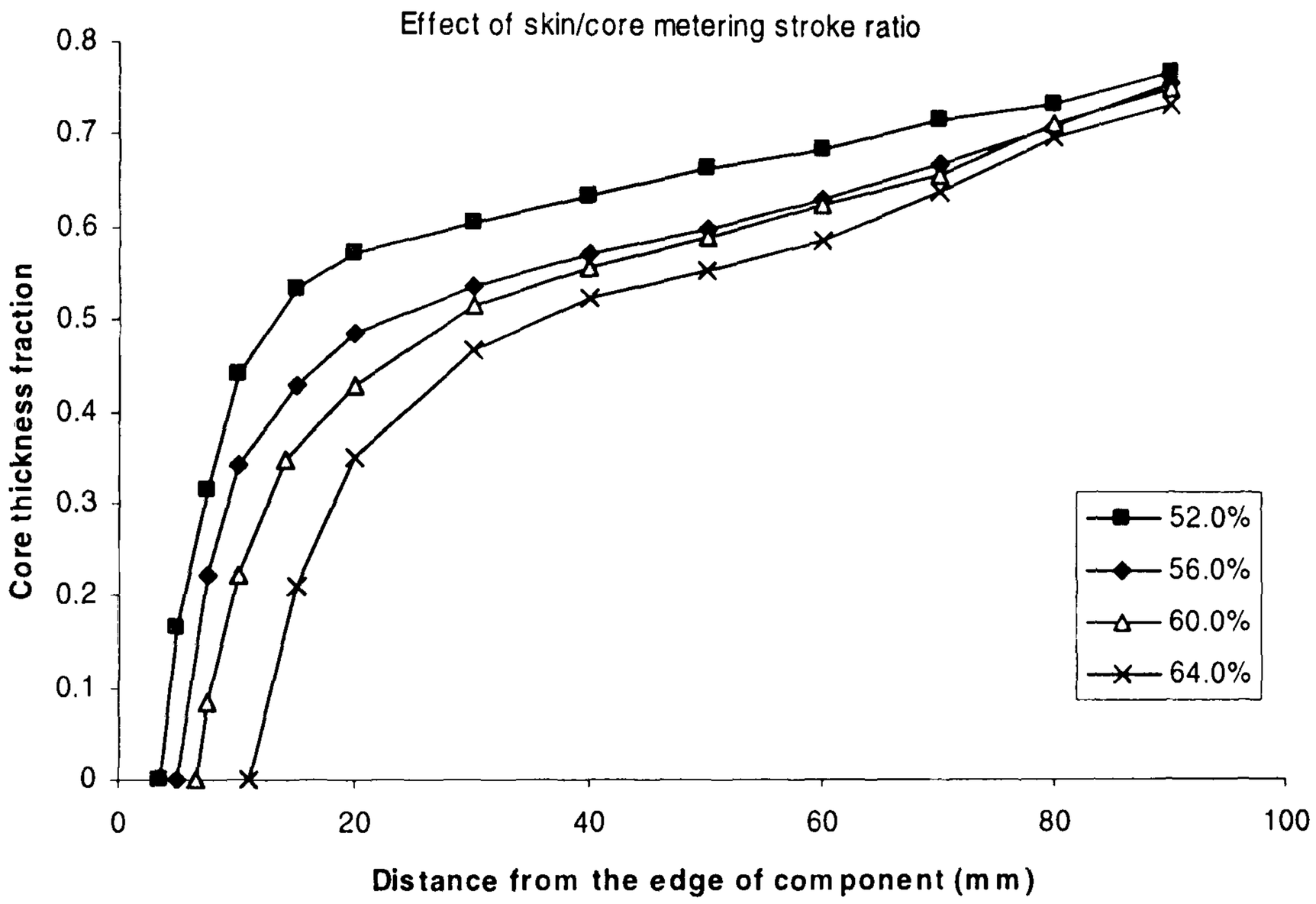

Figure 7.22 Effect of skin/core metering stroke ratios on core thickness fraction

7.5.6 Effect of compatibiliser on core viscosities

In this case study, three grades of polypropylene (Novolen: 1100H, 1102K, and 1100N) were used. To these polymers were added, 10% of compatibiliser (Polybond G3150) and this was then mixed in the injection screw. The blends were injected into the mould with melt temperature of 180 °C. The moulding components were removed and reground. The viscosity of the modified PP and unmodified PP were measured using a ROSAND Advance Extrusion Capillary Rheometer (ASTM D3835 test

method [59]), then the results were compared to determine the effect of compatibiliser on core viscosities.

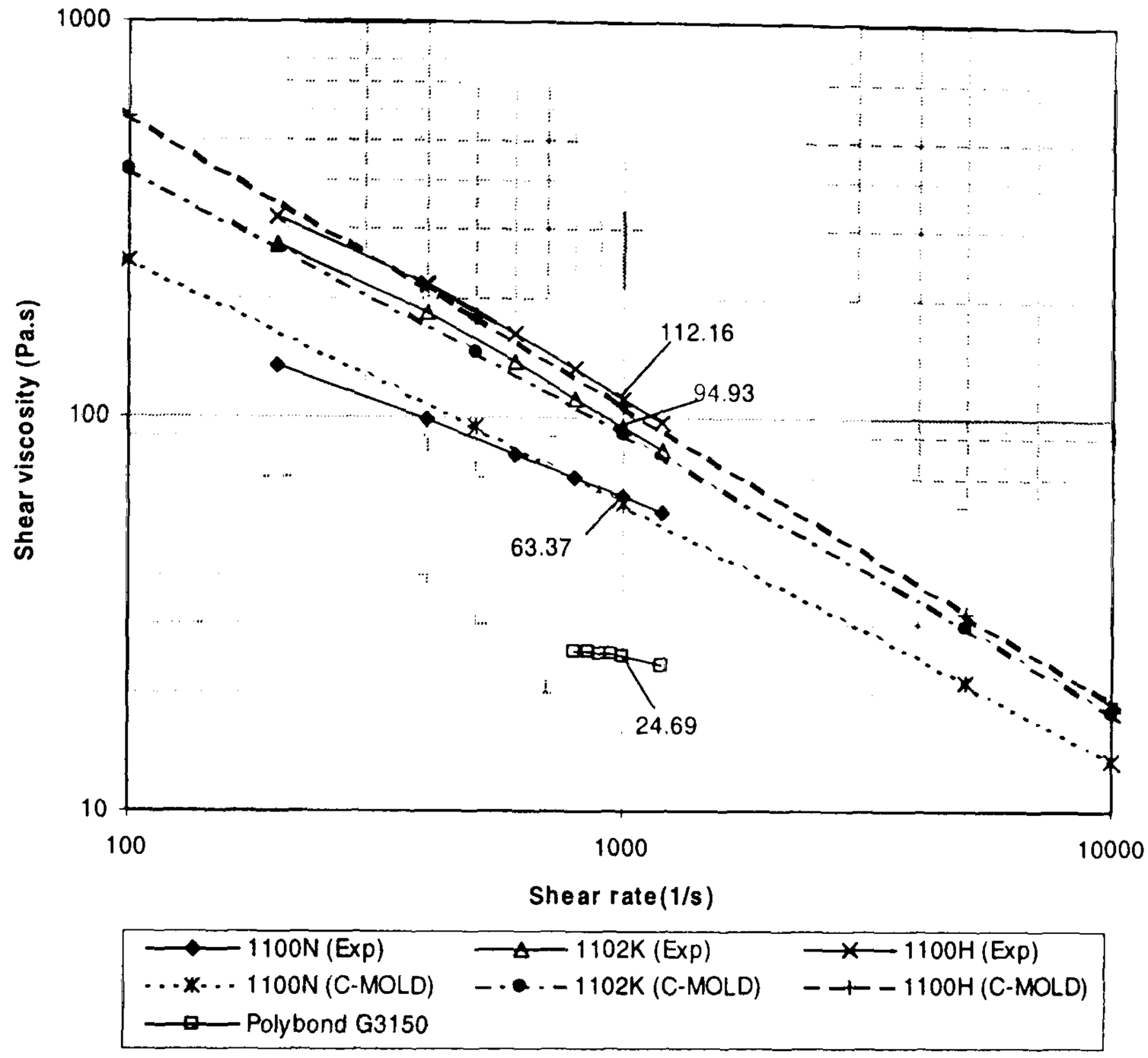

Figure 7.23 Comparison of three grades of unmodified PP(Novolen) and Polybond G3150 to C-MOLD viscosity data.

It was found that Polybond G3150 plays the role of both a compatibiliser and plasticiser. In each case, the viscosity was reduced by addition of Polybond G3150. It had the effect of influencing viscosity of each polymer to different levels. In the case of the higher viscosity material such as Novolen/1100H, the effect of Polybond was slight, but adding the same amount of compatibiliser into the lower viscosity material such as Novolen/1100N, the viscosity was decreased significantly (Table 7.11).

Table 7.11 Percentage of viscosity change with addition of 10% Polybond G3150.

Polymer grade	Shear viscosity (η) at shear rate (γ) of 10^3 s^{-1}, (Pa.s)		Change (%)
	Without G3150	With 10% G3150	
1100H	112.16	106.51	5.03
1102K	94.93	85.16	10.29
1100N	63.37	55.23	12.84

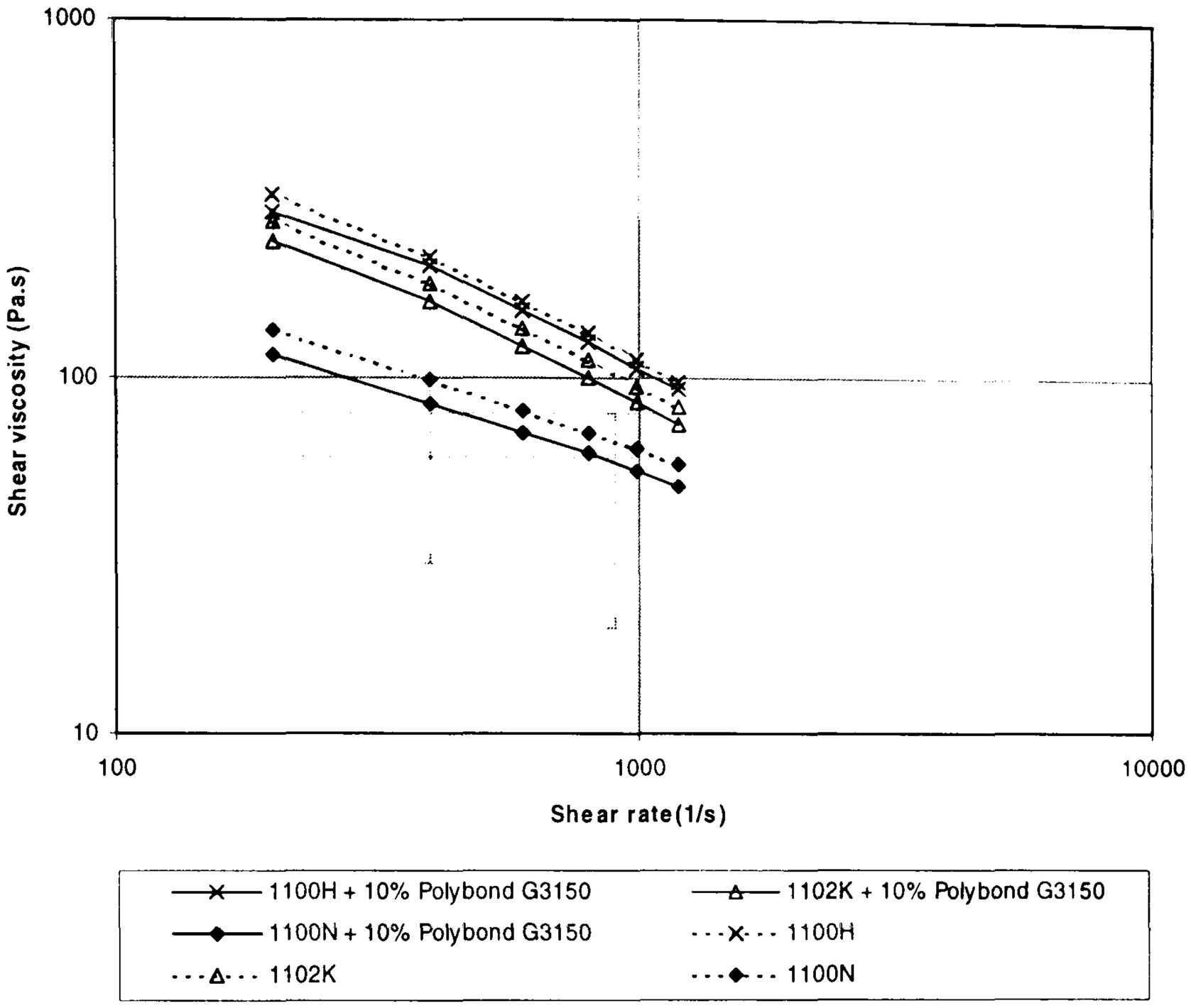

Figure 7.24 Viscosity data of three grades of modified and unmodified PP(Novolen)

7.5.7 Effect of compatibiliser on core thickness fraction

As mentioned, the addition of compatibiliser to the core material caused a decrease in core viscosity and affected the skin-core thickness formation. It was found that it did not significantly effect the skin-core thickness when there was only a slight change in the modified core viscosity (Figure 7.25(a), CTF_{avg} was changed 3.72%.). But if the modified core viscosity was substantially reduced, it showed a more effective thickness formation as shown in Figure 7.25(f) (CTF_{avg} was changed 5.86%.).

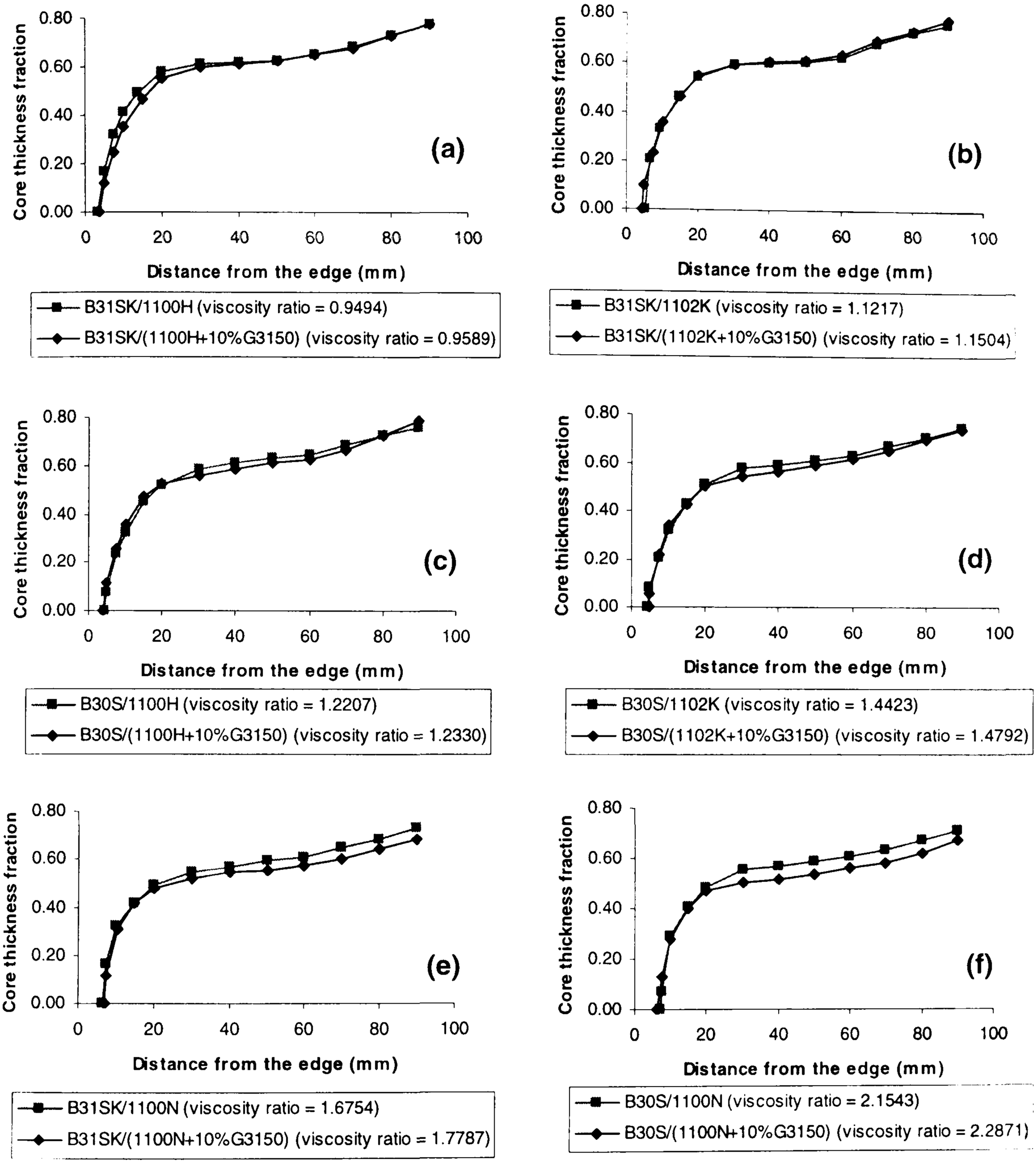

Figure 7.25 Effect of compatibiliser on skin-core thickness fractions

Furthermore, the moulding conditions such as skin/core viscosity ratios, melt temperatures, tool temperatures, injection speeds, and the length of simultaneous phase, were found to have an effect on the skin-core formation in a similar way to PA6/PP in the absence of compatibiliser system as shown in Figure 7.26 (a)-(h).

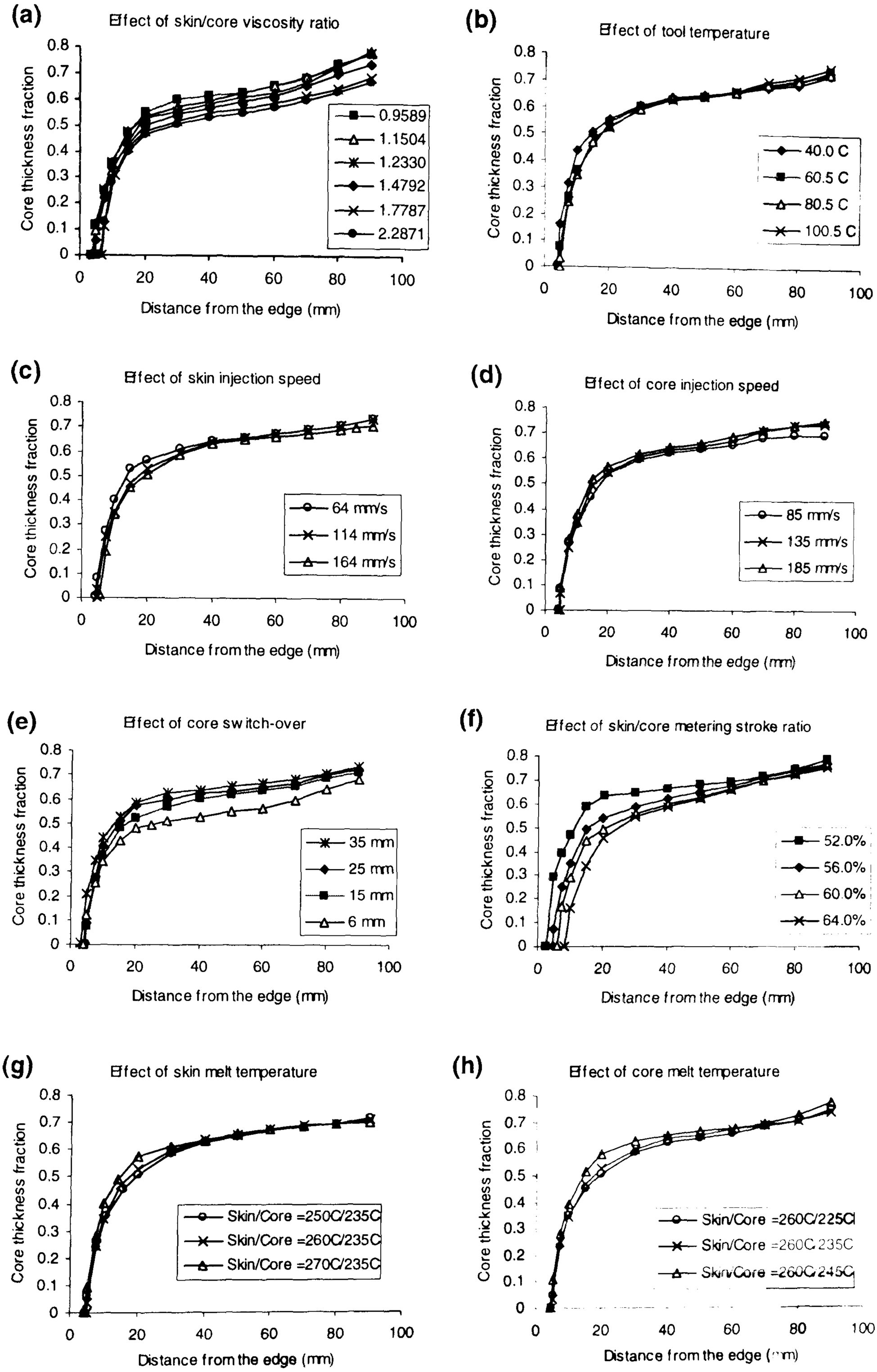

Figure 7.26 The sectional core thickness fractions of various moulding conditions of PA6/PP in the presence of compatibiliser system: effects of (a) skin/core viscosity ratios, (b) tool temperatures, (c)-(d) injection speeds, (e)-(f) the length of simultaneous phase, and (g)-(h) melt temperatures.

7.6 Relationship between Skin-Core Thickness and Their Mechanical Properties

7.6.1 Impact strength

Impact testing did not produce strong evidence to prove the skin-core adhesion level, but when adhesion between skin and core occurred, the impact strengths are increased in the PA6/PP system with compatibiliser. The results are summarised in Appendix VII (Table APVII.1).

In Figure 7.27 and Table 7.12, it was found that at a slightly different in CTF at the impact point, impact strength of the PA6/PP with compatibiliser moulding component was higher than one without compatibiliser significantly. It can be explained by the premise that the bonding between skin and core polymers are promoted by compatibiliser, whereas without compatibiliser the skin just laminated on the core polymer without any bonding and resulted in a lower impact strength.

Table 7.12 Impact strength of PA6/B31SK(skin)/PP/1100H(core) moulding systems.

Systems	Impact test			
	Without compatibiliser		With 10% compatibiliser	
	CTF	Strength (N)	CTF	Strength (N)
B31SK/1100H	0.6250±0.0289	1799.5±29.22	0.6099±0.0127	3701.0±16.35

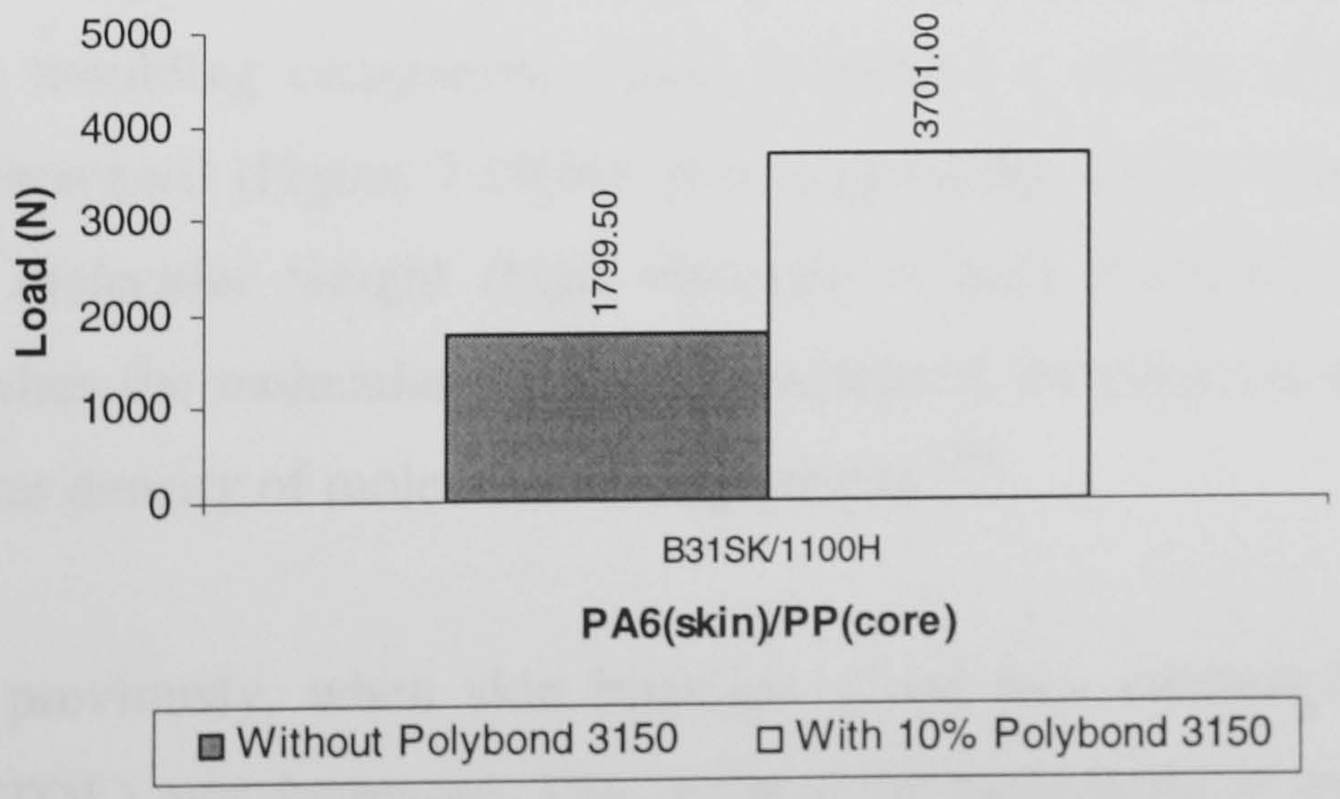

Figure 7.27 Comparison of impact strength of PA6/PP moulding component in the absence and presence of compatibiliser.

7.6.2 Peel strength

The peel strength curve was determined by plotting displacements between upper and lower jaws (as seen in Figure 6.9, Chapter VI) against load. The adhesion levels and the minimum skin thickness fractions of the moulding components were measured as seen in Figure 7.28(a)-(b) and summarised in Table 7.13.

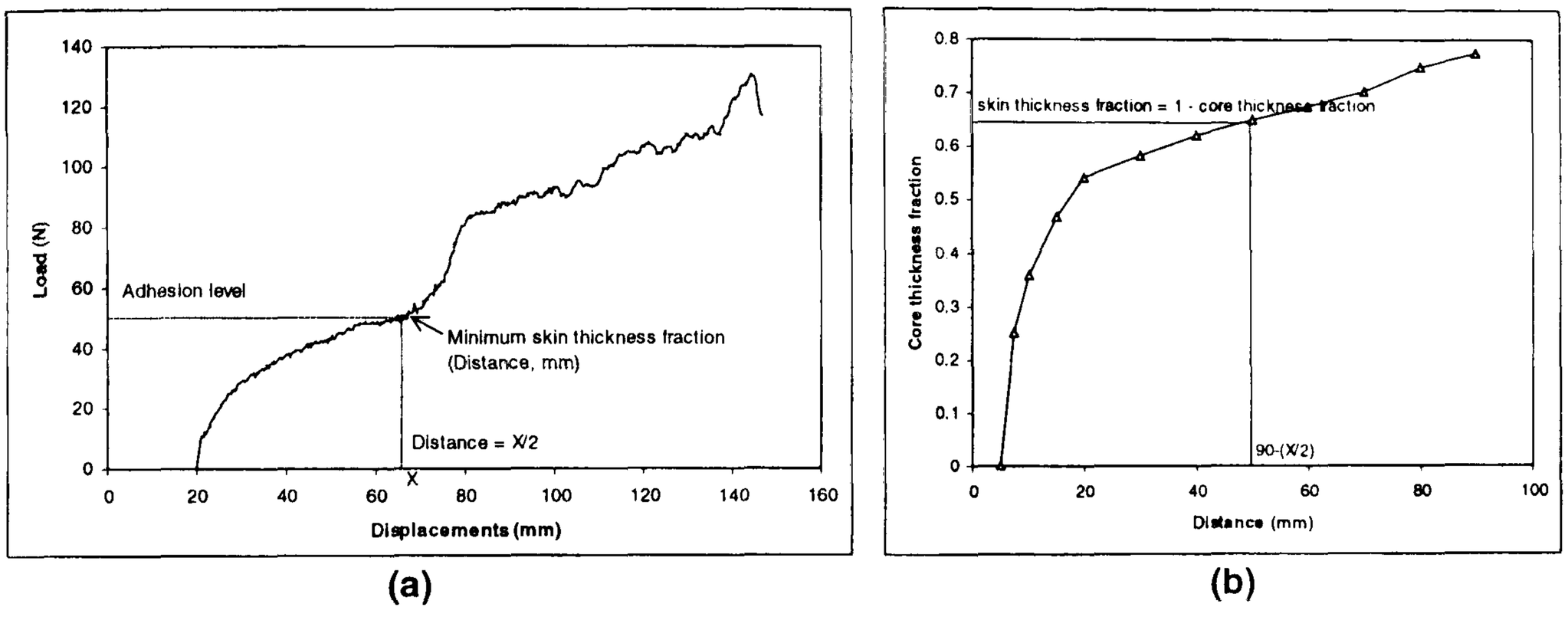

Figure 7.28 Measurement of the adhesion level and the minimum skin thickness fraction.

From the above relationship, peel strengths and skin thickness fractions are calculated and plotted as shown in Figure 7.29(a)-(i). In the presence of compatibiliser, it was found that different skin or core viscosities led to different adhesion levels of skin and core. As seen in Figure 7.29(a), the higher skin viscosity produced the high peel strength of the moulding component. Also, it showed a similar effect, when core viscosity was increased (Figure 7.29(b)). It was generally known that viscosity was related to the molecular weight (high viscosity is high molecular weight). It is proposed that when the molecular weight was increased, the cohesive strength rose as a result of greater density of molecular entanglements [15].

As mentioned previously, when skin injection speed was increased, simultaneous injection time (TOL) was decreased. This reduced the probability of reaction between active sites of skin and core polymer as it appears to be a time dependent reaction. Furthermore, the significant differences between skin and core injection speed (VA and VB) cause high shear resistance between skin and core polymer phases (Figure

7.29(c) and 7.29(d)). When the shear resistance between skin and core phases decreased, it led to skin-core turbulence mixing (Figure 7.33(b) and 7.33(c)) and this action resulted in the interlocking interfaces. On the other hand, the interlocking interfaces did not occur (Figure 7.33(a)) when shear resistance between skin and core polymer phases were high.

Figure 7.29(e) illustrates that peel strengths were increased dramatically when the switch over points for injecting core polymer (SWB) were increased (Table 7.13, effect of SWB). It was discussed that increasing of SWB led to a greater chance of reaction between skin and core active functional groups because this allowed more time together. The shear resistance between skin and core layer are also reduced and similarly result in the adhesion level of skin to core polymers being improved.

The skin/core metering stroke ratios were also a significant factor in affecting skin-core adhesion level (Figure 7.29(f) and Table 7.13, effect of SA/SB). It was explained that the higher peel strength was obtained by increasing skin thickness. A greater thickness of skin layer was necessary to allow more time for the skin and core active functional groups to react with each other.

Moreover, the skin-core adhesion level could be improved by an increase in the skin or core melt temperatures (not exceeding the upper limit of processing temperature, otherwise, the polymers would be degraded).

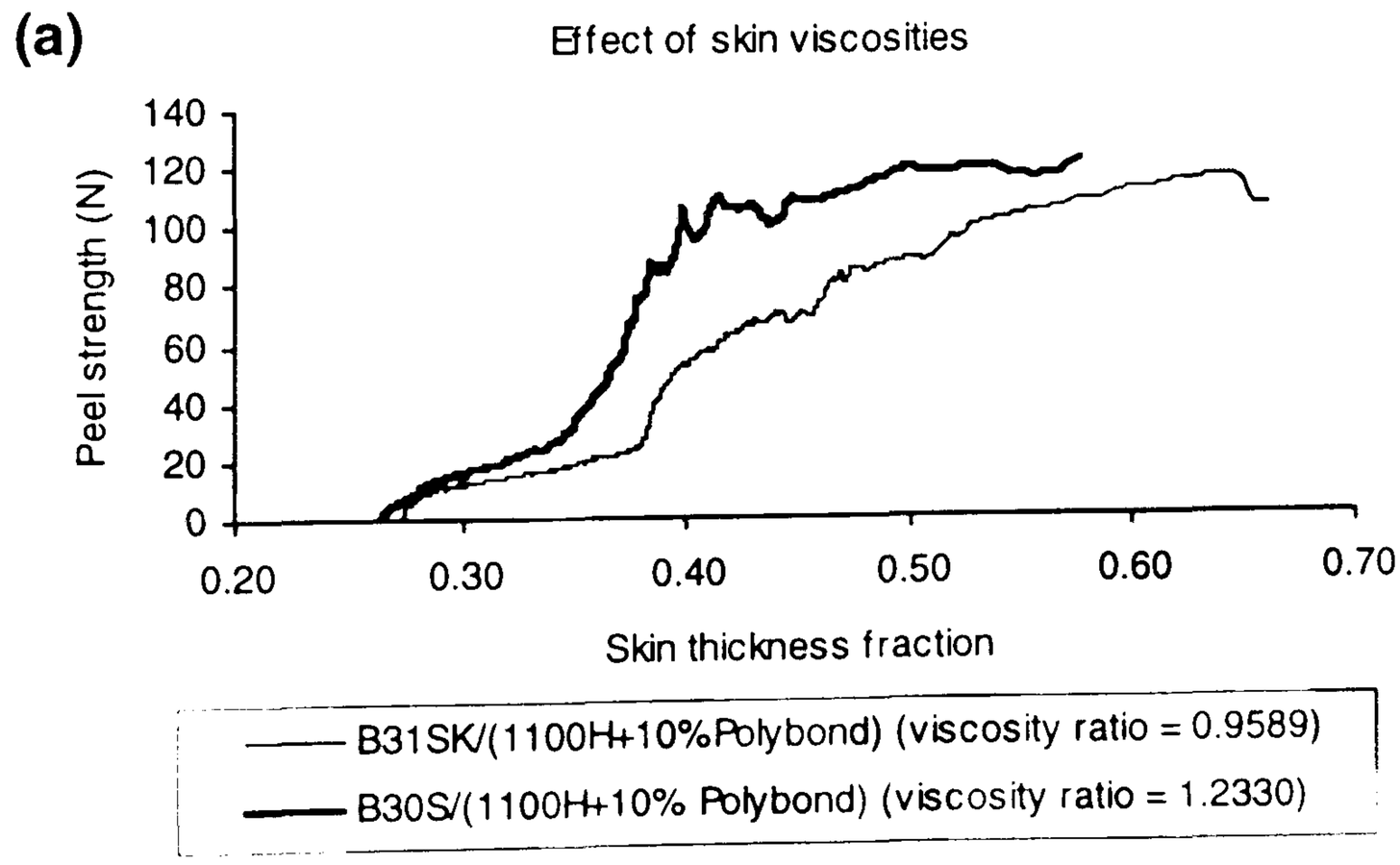

(b)

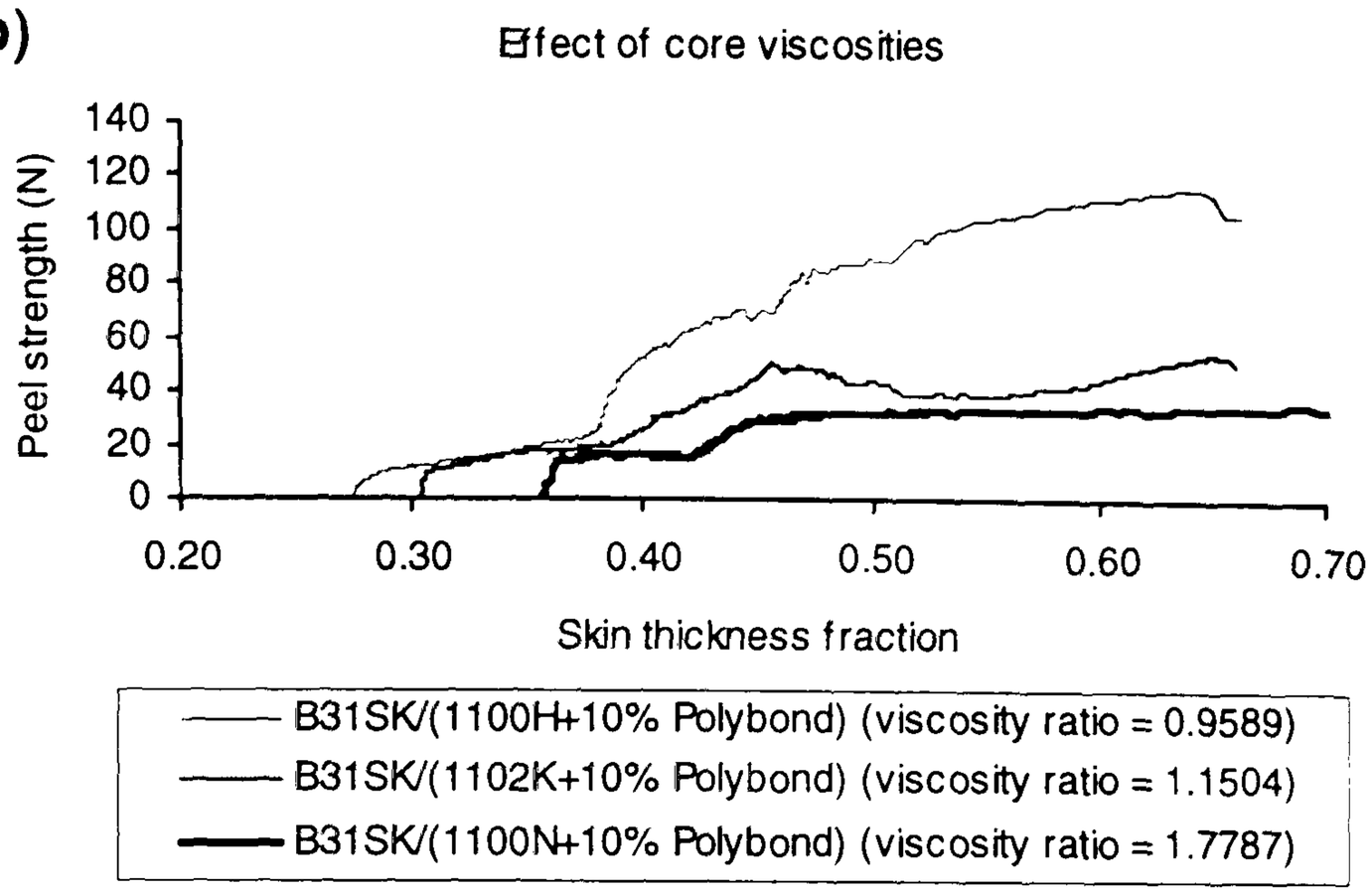
Effect of core viscosities
Peel strength (N)
140
120
100
80
60
40
20
0
0.20
0.30
0.40
0.50
0.60
0.70
Skin thickness fraction
B31SK/(1100H+10% Polybond) (viscosity ratio = 0.9589)
B31SK/(1102K+10% Polybond) (viscosity ratio = 1.1504)
B31SK/(1100N+10% Polybond) (viscosity ratio = 1.7787)

(c)

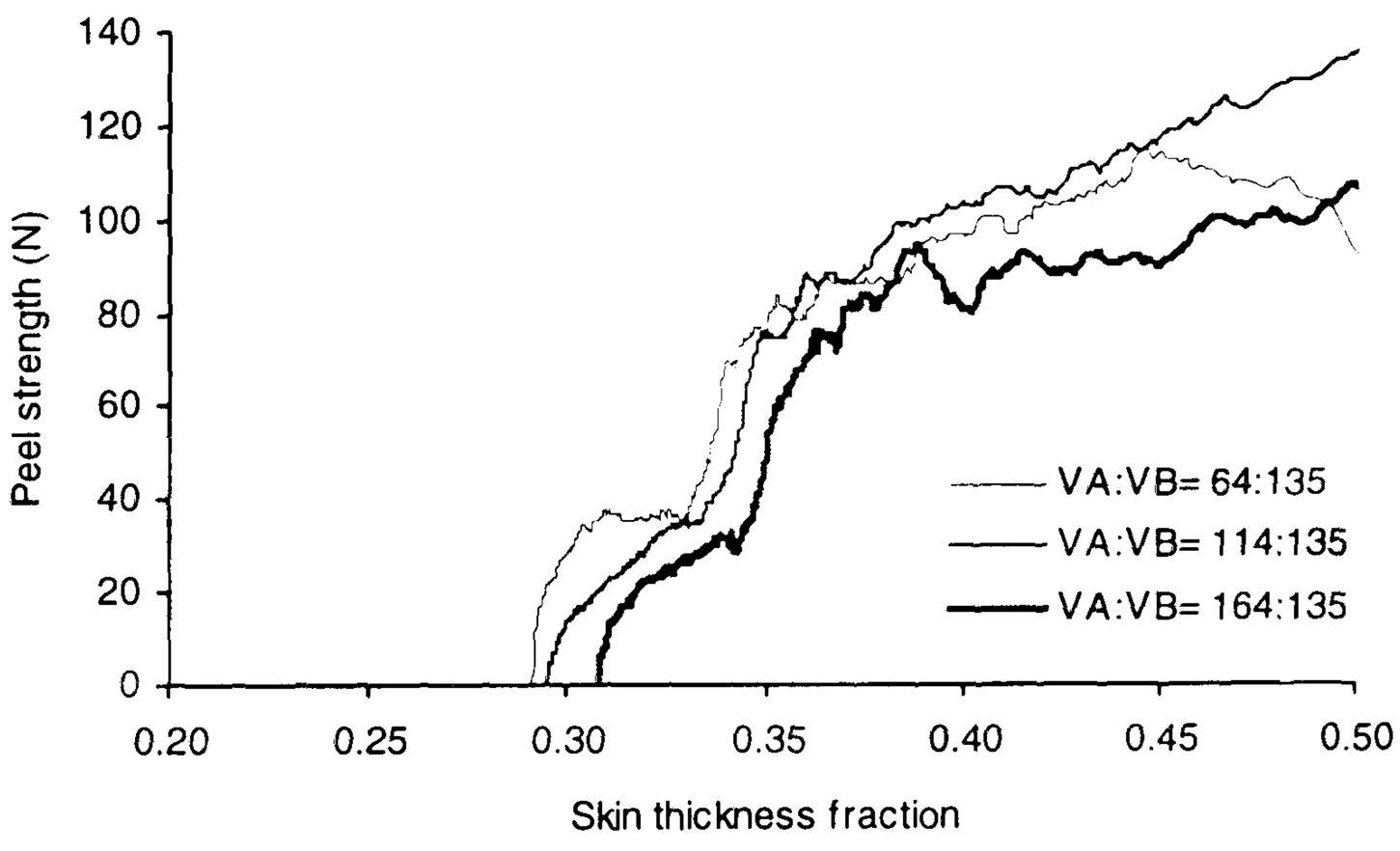
Effect of skin injection speed
Peel strength (N)
140
120
100
80
60
40
20
0
0.20
0.25
0.30
0.35
0.40
0.45
0.50
Skin thickness fraction
VA:VB= 64:135
VA:VB= 114:135
VA:VB= 164:135

(d)

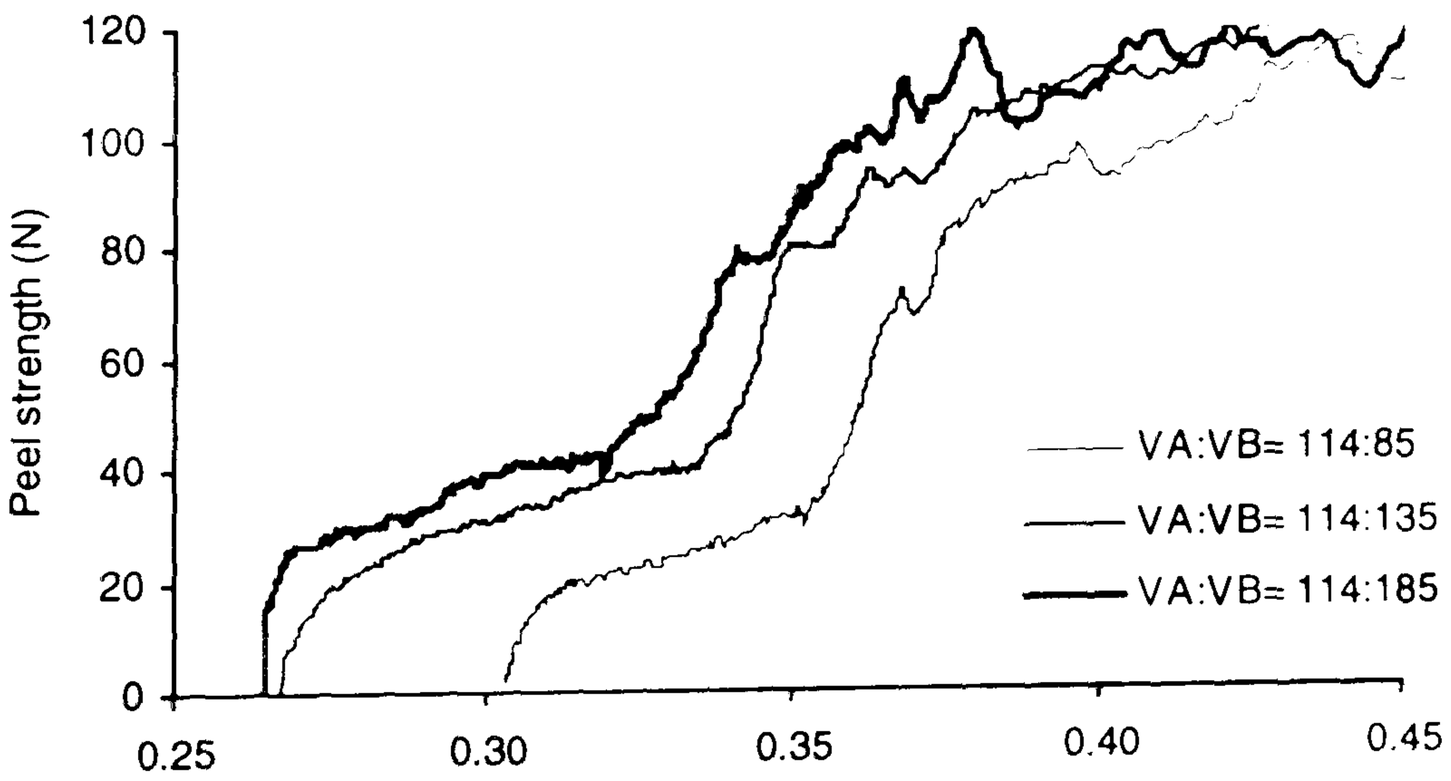
Effect of core injection speed
Peel strength (N)
120
100
80
60
40
20
0
0.25
0.30
0.35
0.40
0.45
Skin thickness fraction
VA:VB= 114:85
VA:VB= 114:135
VA:VB= 114:185

(e)

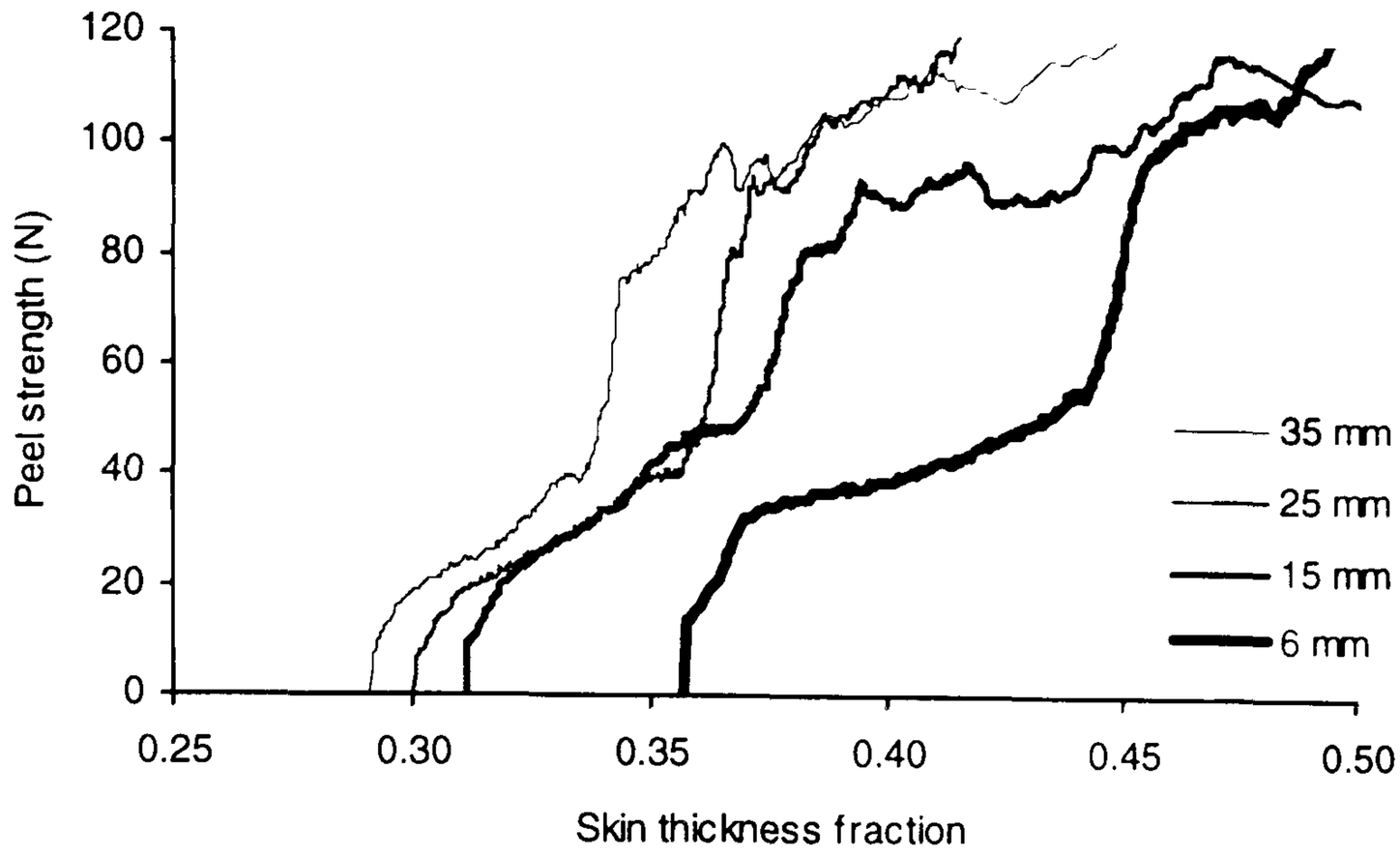
Effect of core switch-over
Peel strength (N)
120
100
80
60
40
20
0
0.25
0.30
0.35
0.40
0.45
0.50
Skin thickness fraction
35 mm
25 mm
15 mm
6 mm

(f)

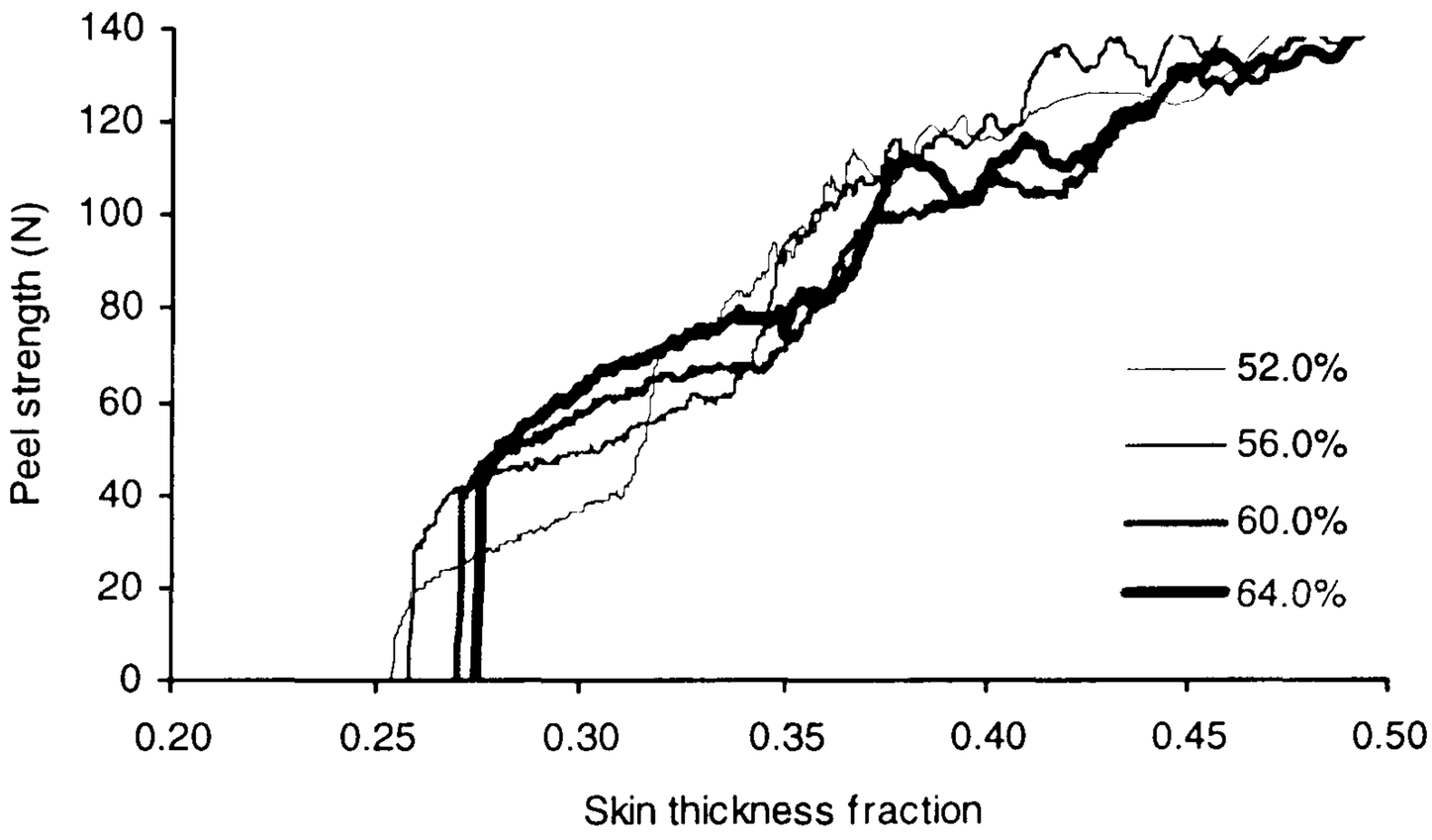
Effect of skin/core metering stoke ratio
Peel strength (N)
140
120
100
80
60
40
20
0
0.20
0.25
0.30
0.35
0.40
0.45
0.50
Skin thickness fraction
52.0%
56.0%
60.0%
64.0%

(g)

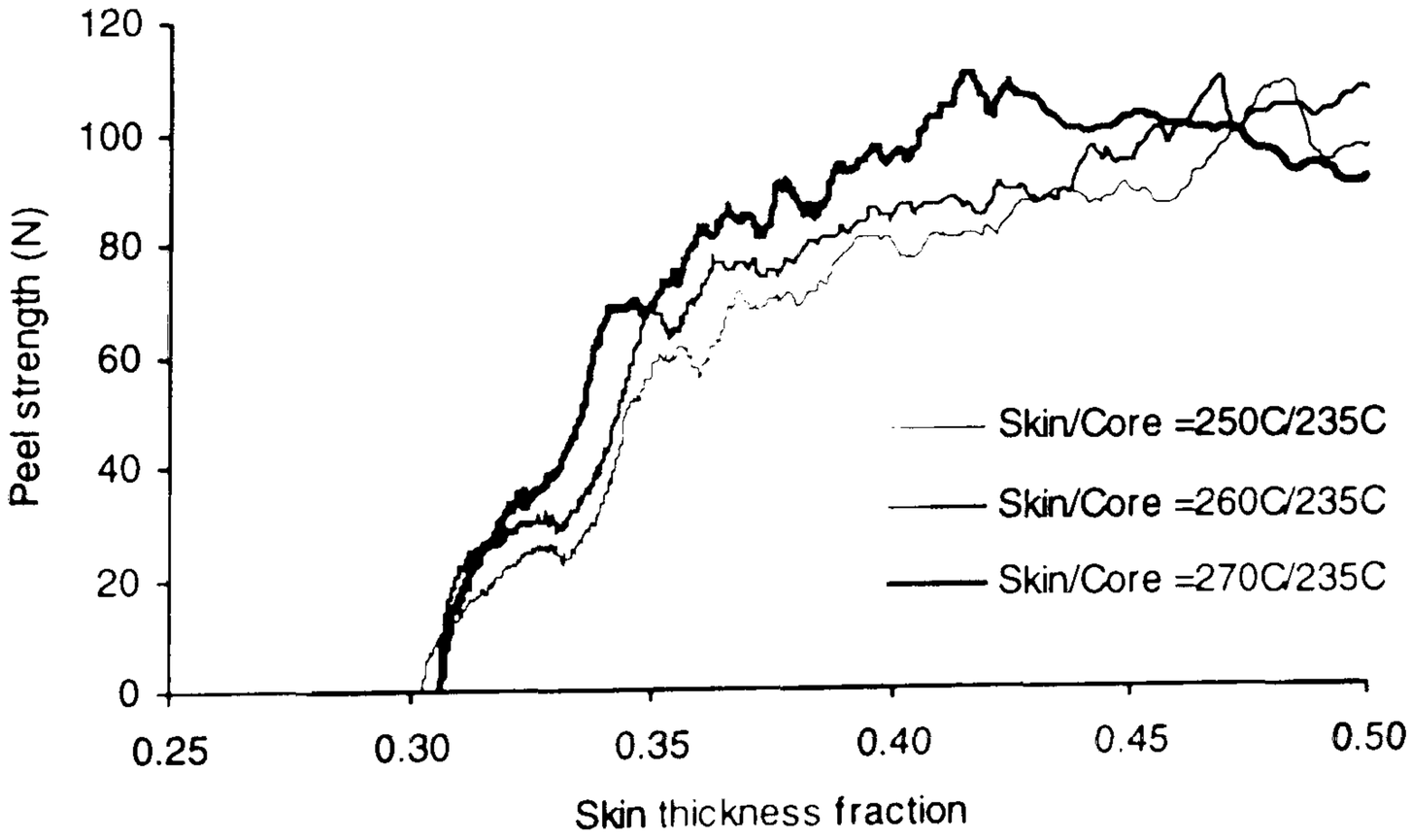
Effect of skin melt temperatures
Peel strength (N)
120
100
80
60
40
20
0
0.25
0.30
0.35
0.40
0.45
0.50
Skin thickness fraction
Skin/Core =250C/235C
Skin/Core =260C/235C
Skin/Core =270C/235C

(h)

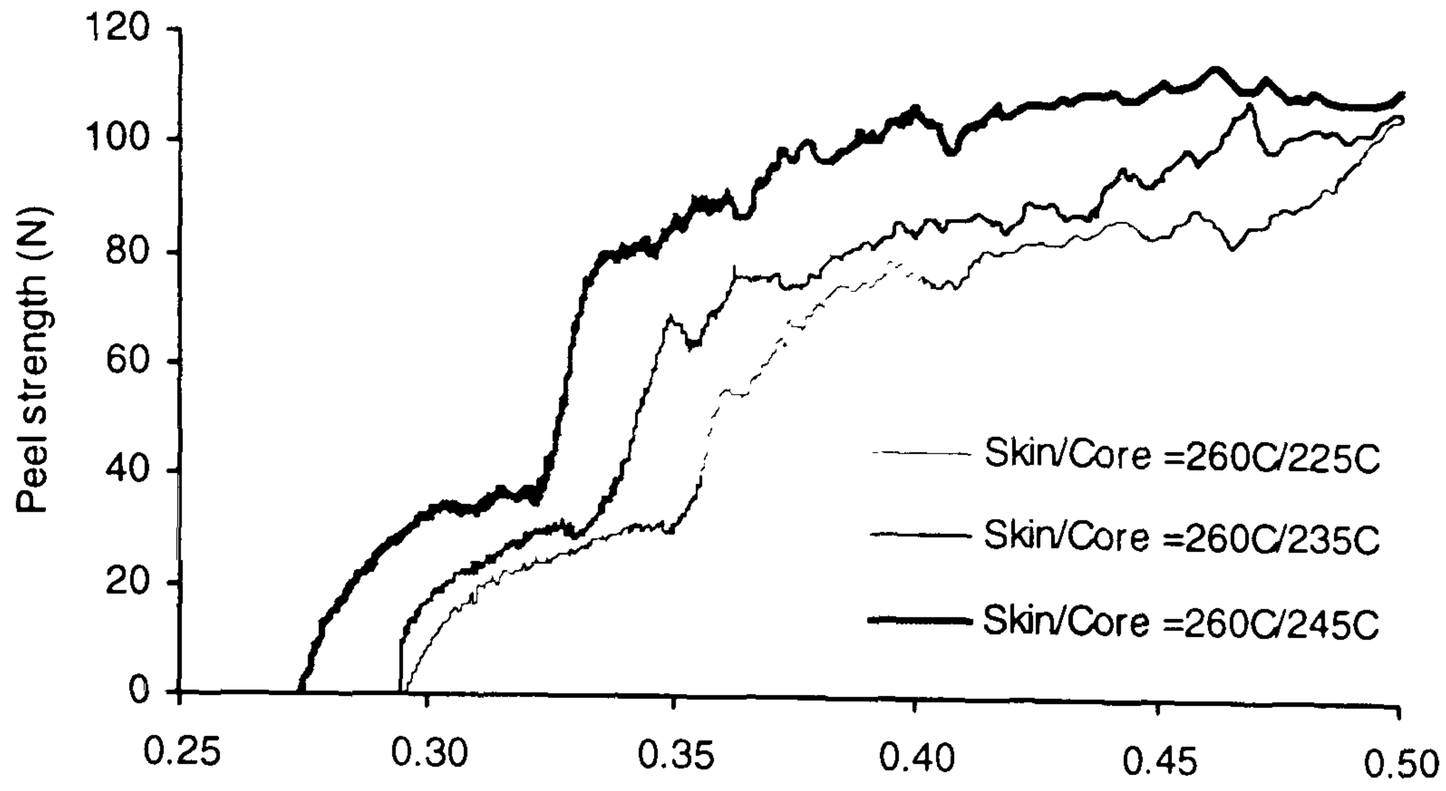

(i)

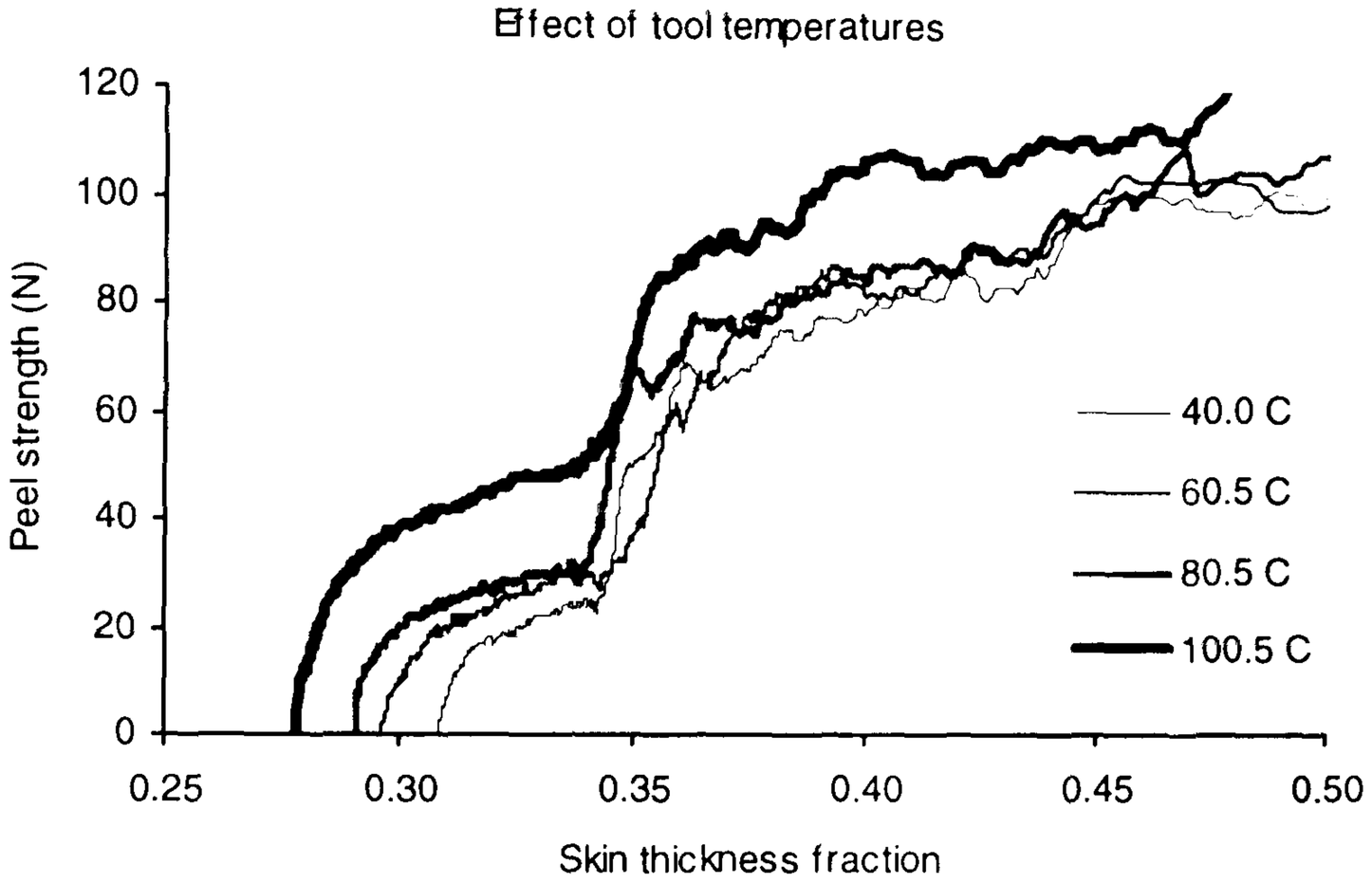

Figure 7.29 Relationships between peel strengths and skin thickness fractions at various moulding conditions of PA6/PP in the presence of compatibiliser system: effects of (a)-(b) skin-core viscosity, (c)-(d) injection speeds, (e)-(f) the length of simultaneous phase, (g)-(h) melt temperatures, and (i) tool temperatures.

In almost all of the cases, the peel strength depended on skin thickness fraction. But in the case of the high tool temperatures, even though the minimum skin thickness fractions were slightly different, peel strengths increased significantly.

It is considered that in the case of a higher tool temperature, the molten skin layers are allowed to stay longer in the molten condition than ones with lower tool temperatures. thus, skin and core have more probability to react and bond each other. This postulation assumes that the reaction is time dependent.

Table 7.13 The minimum skin thickness fractions and their peel strengths.

	Systems	Minimum skin thickness fraction	Adhesion level (peel strength, N)
	Effect of skin viscosities		
(1)	B31SK/(1100H+10%G3150) (viscosity ratio = 0.9589)	0.3803±0.0011	24.70±0.61
(2)	B30S/(1100H+10%G3150) (viscosity ratio = 1.2330)	0.3444±0.0010	26.90±0.67
	Effect of core viscosities		
(1)	B31SK/(1100H+10%G3150) (viscosity ratio = 0.9589)	0.3468±0.0010	16.60±0.41
(2)	B31SK/(1102K+10%G3150) (viscosity ratio = 1.1504)	0.3716±0.0011	17.80±0.44
(3)	B31SK/(1100N+10%G3150) (viscosity ratio = 1.7787)	0.4200±0.0013	15.70±0.39
	Effect of skin injection speeds (VA)		
(1)	64 mm/s	0.3296±0.0010	36.20±0.90
(2)	114 mm/s	0.3344±0.0010	35.50±0.88
(3)	164 mm/s	0.2965±0.0009	30.00±0.75
	Effect of core injection speeds (VB)		
(1)	85 mm/s	0.3529±0.0011	32.50±0.81
(2)	135 mm/s	0.3355±0.0010	41.00±1.02
(3)	185 mm/s	0.3214±0.0010	43.90±1.09
	Effect of core switch-over (SWB)		
(1)	35 mm	0.3358±0.0010	38.80±0.97
(2)	25 mm	0.3568±0.0011	41.80±1.04
(3)	15 mm	0.3602±0.0011	49.70±1.24
(4)	6 mm	0.4428±0.0013	56.80±1.42
	Effect of skin/core metering stroke ratios (SA/SB)		
(1)	52 %	0.3121±0.0009	43.20±1.08
(2)	56 %	0.3378±0.0010	62.90±1.57
(3)	60 %	0.3575±0.0011	68.30±1.70
(4)	64 %	0.3506±0.0011	77.10±1.92
	Effect of skin melt temperatures		
(1)	250 °C	0.3338±0.0010	24.10±0.60
(2)	260 °C	0.3322±0.0010	29.50±0.73
(3)	270 °C	0.3324±0.0010	34.90±0.87
	Effect of core melt temperatures		
(1)	225 °C	0.3499±0.0010	30.50±0.76
(2)	235 °C	0.3330±0.0010	31.40±0.78
(3)	245 °C	0.3225±0.0010	36.80±0.92
	Effect of tool temperatures		
(1)	40.0 °C	0.3427±0.0010	24.10±0.60
(2)	60.5 °C	0.3431±0.0010	28.50±0.71
(3)	80.5 °C	0.3334±0.0010	31.90±0.79
(4)	100.5 °C	0.3370±0.0010	49.60±1.24

7.6.3 Correlation between simultaneous injection times (TOL) and minimum skin thickness fractions (STF_{min})

The aim of this study was to investigate the relationship between simultaneous injection times (TOL) and minimum skin thickness fractions (STF_{min}). PA6 and PP with compatibiliser were used as skin and core materials. The simultaneous injection times could be varied by various core switch-over points (SWB) and by delaying the time of injection of core material (TDB) as shown in Table 7.14.

Table 7.14 Calculation of the simultaneous injection times by varying core switch-over points (SWB) and delaying the time of injection of core material (TDB)

Data no.	TDB (s)	SWB (mm)	Lsimul* (mm)	TOL** (s)
1	0.0	70.0	70.0	0.6140
2	0.0	60.0	60.0	0.5263
3	0.0	50.0	50.0	0.4386
4	0.0	40.0	40.0	0.3509
5	0.0	30.0	30.0	0.2632
6	0.0	20.0	20.0	0.1754
7	0.0	10.0	10.0	0.0877
8	0.1	30.0	18.6	0.1632
9	0.1	20.0	8.6	0.0754
10	0.1	10.0	-1.4	-0.0123
11	0.2	30.0	7.2	0.0632
12	0.2	20.0	-2.8	-0.0246
13	0.2	10.0	-12.8	-0.1123
14	0.3	40.0	5.8	0.0509
15	0.3	30.0	-4.2	-0.0368
16	0.3	20.0	-14.2	-0.1246
17	0.3	10.0	-24.2	-0.2123
18	0.4	50.0	4.4	0.0386
19	0.4	40.0	-5.6	-0.0491
20	0.4	30.0	-15.6	-0.1368
21	0.4	20.0	-25.6	-0.2246
22	0.4	10.0	-35.6	-0.3123
23	0.5	30.0	-27.0	-0.2368
24	0.5	20.0	-37.0	-0.3246
25	0.5	10.0	-47.0	-0.4123

Other constant parameters: skin metering stoke (SOA) = 70.0 mm, core metering stoke (SOB) = 55.0 mm, skin melt cushion (SCA) = 5.0 mm, core melt cushion (SCB) = 0.0 mm, skin injection speed (VA) = 114 mm/s, and core injection speed (VB) = 135 mm/s.

---

* Lsimul =TOL*VA (7.6)

** TOL= (SWB/VA) – TDB (7.5)

The minimum skin thickness fractions of each moulding component were measured using peel test and Image processing software as mentioned in section 7.6.2. The results are addressed in Table 7.15. It was found that the relationship between TOL and STF_{min} is a sigmoidal (growth) function and investigated as seen in Figure 7.30.

Table 7.15 STF_{min} and F_{peel} at various TOL

TOL (s)	STF_{min}	F_{peel} (N)
-0.4123	0.3453 ± 0.0007	19.86 ± 0.89
-0.3246	0.3281 ± 0.0043	21.49 ± 1.30
-0.2246	0.3516 ± 0.0019	23.77 ± 1.57
-0.2123	0.3484 ± 0.0025	17.01 ± 0.37
-0.1368	0.3470 ± 0.0040	22.20 ± 1.10
-0.1246	0.3617 ± 0.0070	21.28 ± 0.88
-0.1123	0.3641 ± 0.0019	18.97 ± 0.35
-0.0491	0.3447 ± 0.0060	20.45 ± 1.51
-0.0368	0.3580 ± 0.0101	22.37 ± 1.85
-0.0246	0.3461 ± 0.0074	22.03 ± 1.55
-0.0123	0.3478 ± 0.0000	16.12 ± 0.32
0.0386	0.3200 ± 0.0000	20.91 ± 1.55
0.0509	0.3346 ± 0.0069	19.71 ± 0.99
0.0754	0.3146 ± 0.0022	20.50 ± 1.13
0.0877	0.3468 ± 0.0026	16.74 ± 0.61
0.1754	0.3438 ± 0.0042	20.07 ± 1.12
0.2632	0.3308 ± 0.0015	23.61 ± 1.01
0.3509	0.3134 ± 0.0066	20.91 ± 2.45
0.4386	0.2941 ± 0.0000	21.60 ± 1.51
0.5263	0.2407 ± 0.0058	23.17 ± 2.61
0.6140	0.1948 ± 0.0026	22.85 ± 1.38

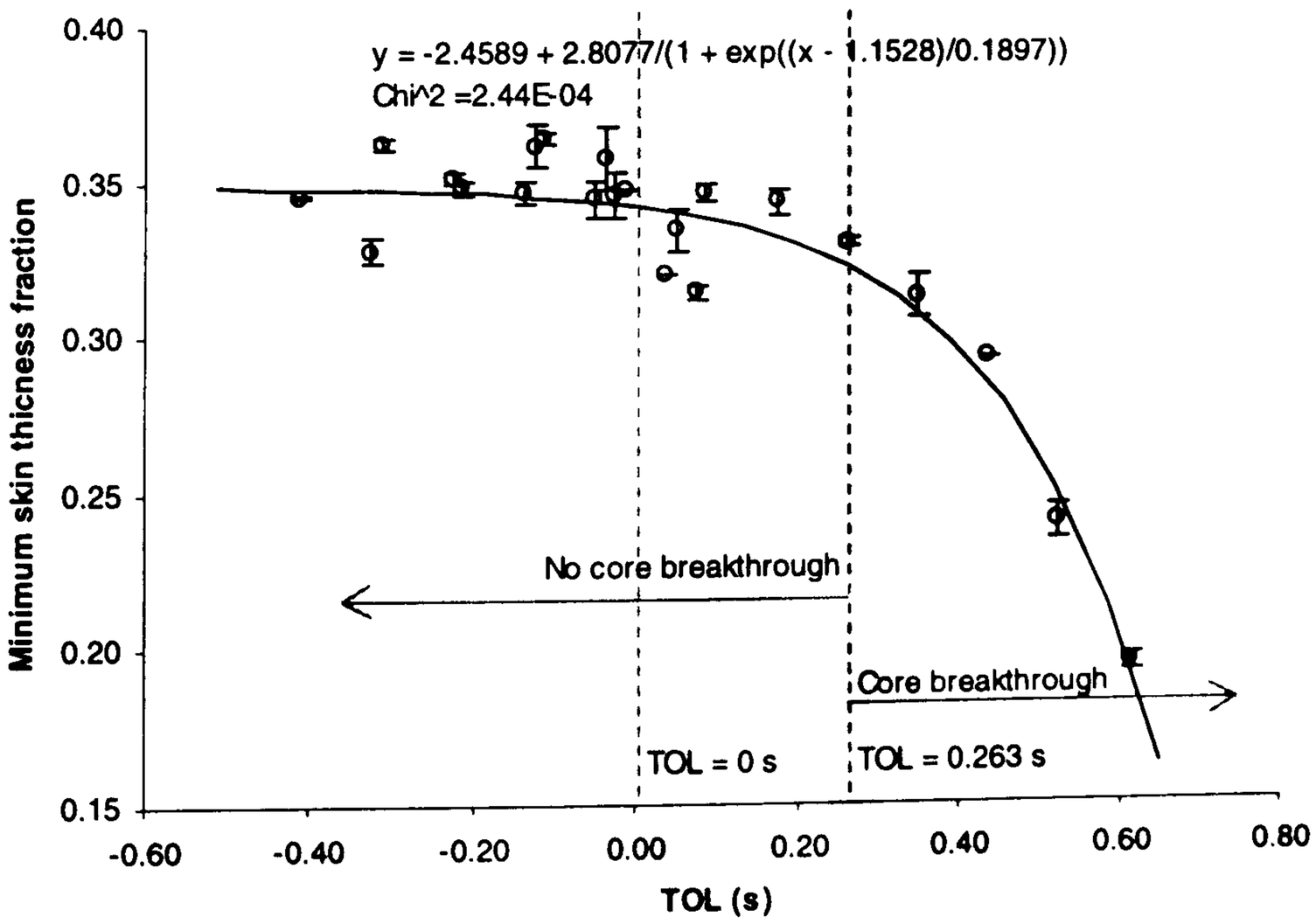

Figure 7.30 Relationship between STF_{min} and TOL

It was also observed that core breakthrough occurred, when TOL ≥ 0.263 second. Therefore, the optimum moulding components should be processed with TOL less than 0.263 second. (Photos of the moulding components, peel test curves, and plotting of thickness fractions against distances from the edge of the moulding components, are presented in Appendix VI.) It was concluded that the greater TOL produced a lower minimum skin thickness fraction but care has to be taken that too high TOL could result in core breakthrough.

7.6.4 Influence of simultaneous injection times (TOL) on normalised peel strength ($F_{peel, norm}$)

As mentioned previously, the adhesion strength of the minimum skin thicknesses were obtained from the peel test. Therefore, the normalised peel strength is determined from dividing peel strengths (at the minimum skin thickness fraction) by its minimum skin thickness fraction as shown in Table 7.16.

The relationship between simultaneous injection times (TOL) and normalised peel strength ($F_{peel, norm}$) was investigated by constructing a plot as in Figure 7.31.

As seen in Figure 7.27, it was explained that the level of adhesion could be improved by promoting the simultaneous process during co-injection moulding. In other words, a good adhesion between skin and core could be introduced by greater simultaneous injection times promoting greater residence of skin and core surface interlayer.

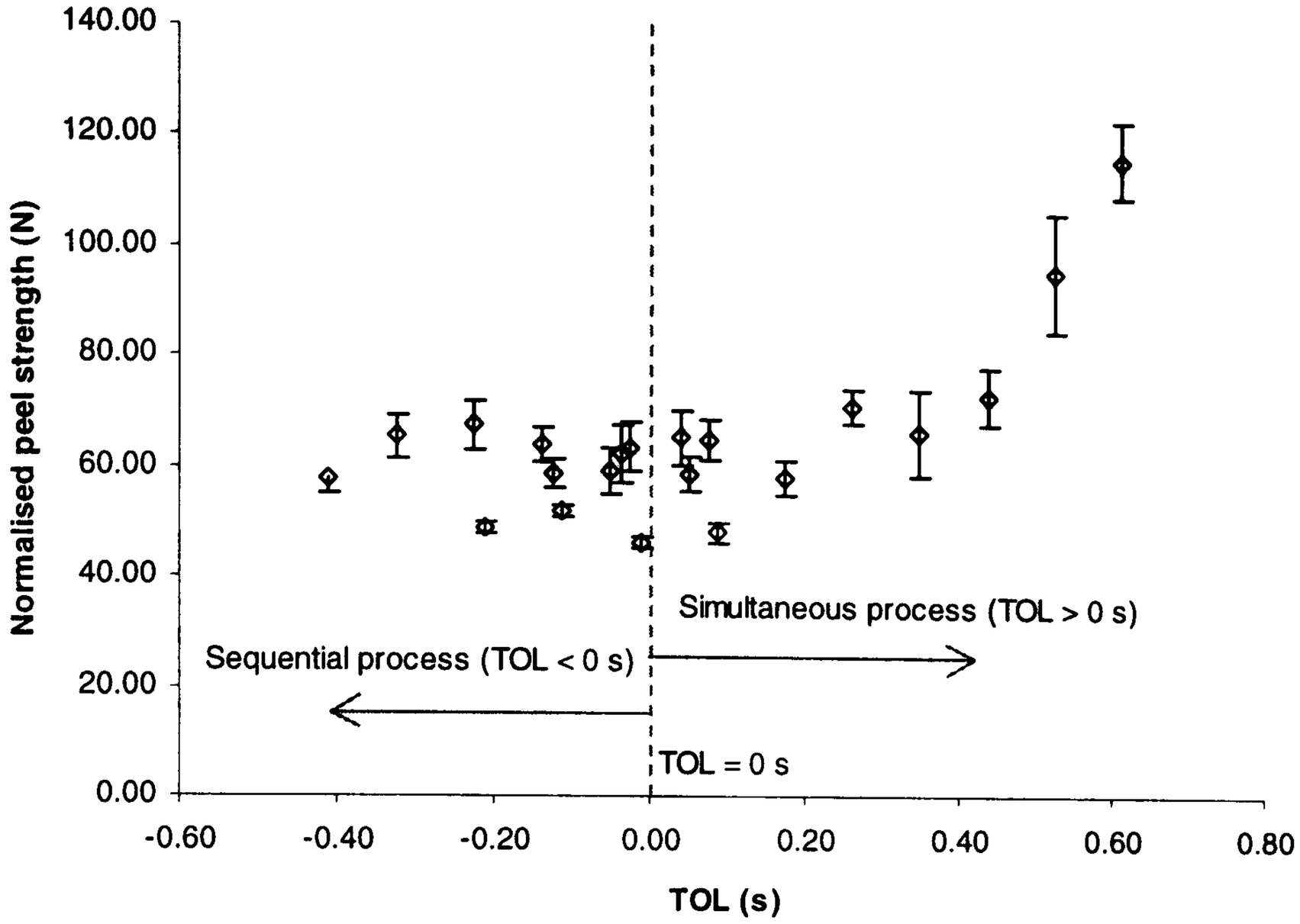

Figure 7.31 Relationship between $F_{peel,\ norm}$ and TOL

Table 7.16 The normalised peel strengths ($F_{peel,\ norm}$)

TOL (s)	STF_{min}	F_{peel} (N)	$F_{peel,\ norm}$ (N)
-0.4123	0.3453 ± 0.0007	19.86 ± 0.89	57.51± 2.57
-0.3246	0.3281 ± 0.0043	21.49 ± 1.30	65.49 ± 3.96
-0.2246	0.3516 ± 0.0019	23.77 ± 1.57	67.60 ± 4.46
-0.2123	0.3484 ± 0.0025	17.01 ± 0.37	48.82 ± 1.06
-0.1368	0.3470 ± 0.0040	22.20 ± 1.10	63.97 ± 3.17
-0.1246	0.3617 ± 0.0070	21.28 ± 0.88	58.83 ± 2.43
-0.1123	0.3641 ± 0.0019	18.97 ± 0.35	52.10 ± 0.96
-0.0491	0.3447 ± 0.0060	20.45 ± 1.51	59.32 ± 4.36
-0.0368	0.3580 ± 0.0101	22.37 ± 1.85	62.48 ± 5.15
-0.0246	0.3461 ± 0.0074	22.03 ± 1.55	63.65 ± 4.47
-0.0123	0.3478 ± 0.0000	16.12 ± 0.32	46.34 ± 0.92
0.0386	0.3200 ± 0.0000	20.91 ± 1.55	65.34 ± 4.82
0.0509	0.3346 ± 0.0069	19.71 ± 0.99	58.90 ± 2.97
0.0754	0.3146 ± 0.0022	20.50 ± 1.13	65.16 ± 3.57
0.0877	0.3468 ± 0.0026	16.74 ± 0.61	48.26 ± 1.74
0.1754	0.3438 ± 0.0042	20.07 ± 1.12	58.37 ± 3.24
0.2632	0.3308 ± 0.0015	23.61 ± 1.01	71.37 ± 3.05
0.3509	0.3134 ± 0.0066	20.91 ± 2.45	66.71 ± 7.81
0.4386	0.2941 ± 0.0000	21.60 ± 1.51	73.44 ± 5.11
0.5263	0.2407 ± 0.0058	23.17 ± 2.61	96.26 ± 10.84
0.6140	0.1948 ± 0.0026	22.85 ± 1.38	117.29 ± 7.08

Therefore, at optimum skin/core metering stroke ratio, it was found that:

- High skin thickness fraction led to high skin-core adhesion level.
- By allowing a longer simultaneous injection time, the minimum skin thickness fractions were reduced.
- At the same thickness of skin most skin-core adhesion levels were improved when simultaneous injection times were increased.
- Adhesion level and minimum skin thickness fraction could be improved by having an injection speed of core material faster than skin material.
- Different skin or core viscosities caused different adhesion levels of skin and core materials.

7.7 Optical and Scanning Electron Microscope Analysis

7.7.1 Optical microscope

In this analysis, the interfaces between polymer phases were studied. Specimens were prepared by sectioning along the centre line as seen in Figure 6.11. The specimens were polished using the soft material polishing technique. At the location of 20, 50 and 70 mm from the central gate, skin thickness fractions were 0.2749, 0.3805, and 0.4740, respectively. An optical microscope attached with a camera was used for determination of the interfaces between polymer phases (skin and core). After performing the peel test, the peel fractures of the specimens were also determined by the microscope at the same locations. The results are summarised as shown in Figure 7.32.

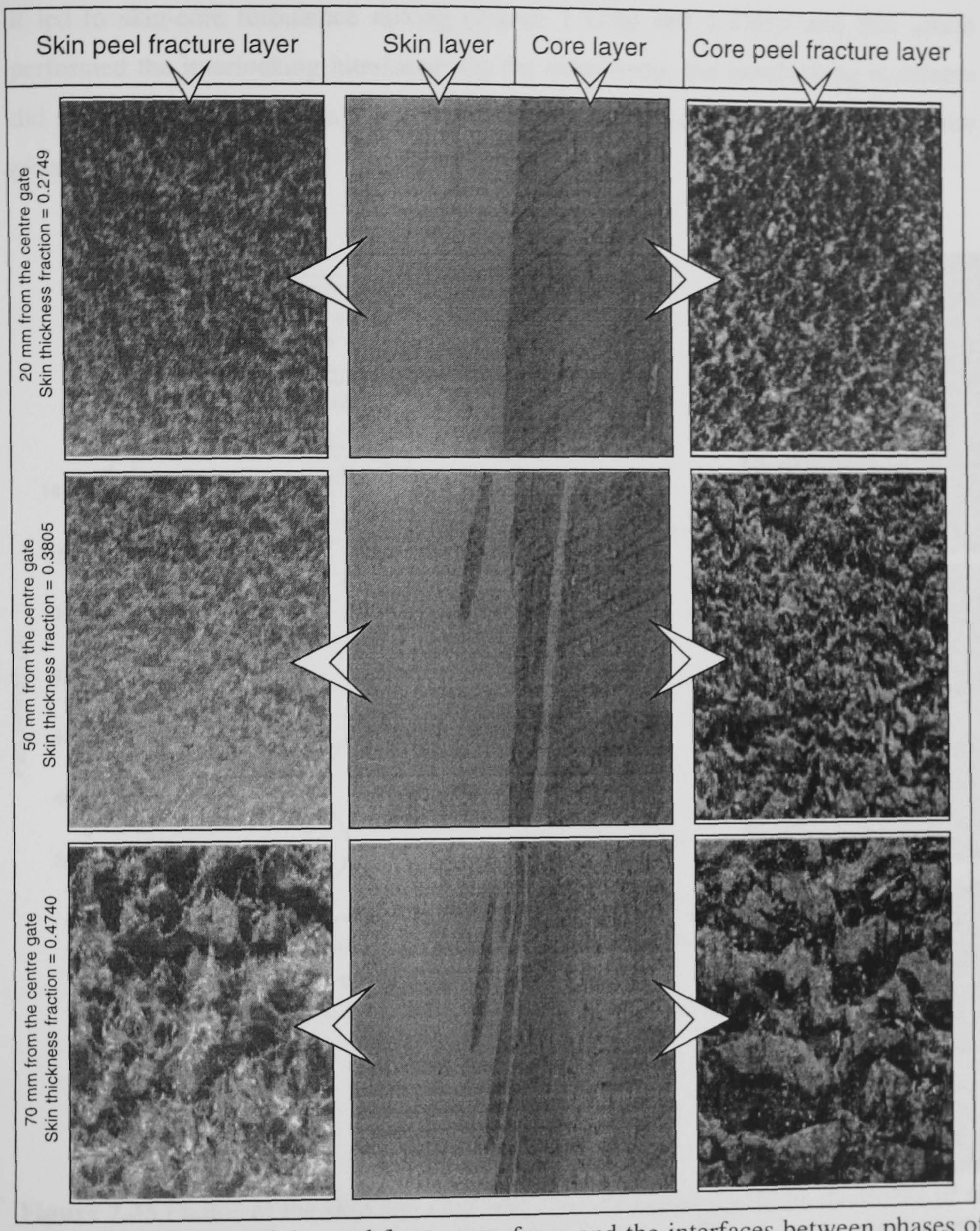

Figure 7.32 Photos of the peel fracture surfaces and the interfaces between phases of skin and core at the different skin thickness fraction area at: 20 mm, 50 mm, and 70 mm from central gate, respectively (magnification 6.3X).

As seen in Figure 7.33, it was found that, in the presence of compatibiliser, the levels of skin-core adhesion were improved when skin thickness fractions increased. It was also found that when the skin thickness fractions were increased, greater tie layers of skin and core peel fracture surfaces were observed. It was discovered that the shear resistance between skin and core at 70 mm from the gate could build up to less than one near the gate. When the shear resistance between skin and core phases decreased,

it led to skin-core turbulence mixing (Figure 7.33(b) and 7.33(c)) and this action performed the interlocking interfaces. On the other hand, the interlocking interfaces did not occur (Figure 7.33(a)) when shear resistance between skin and core polymer phases were high.

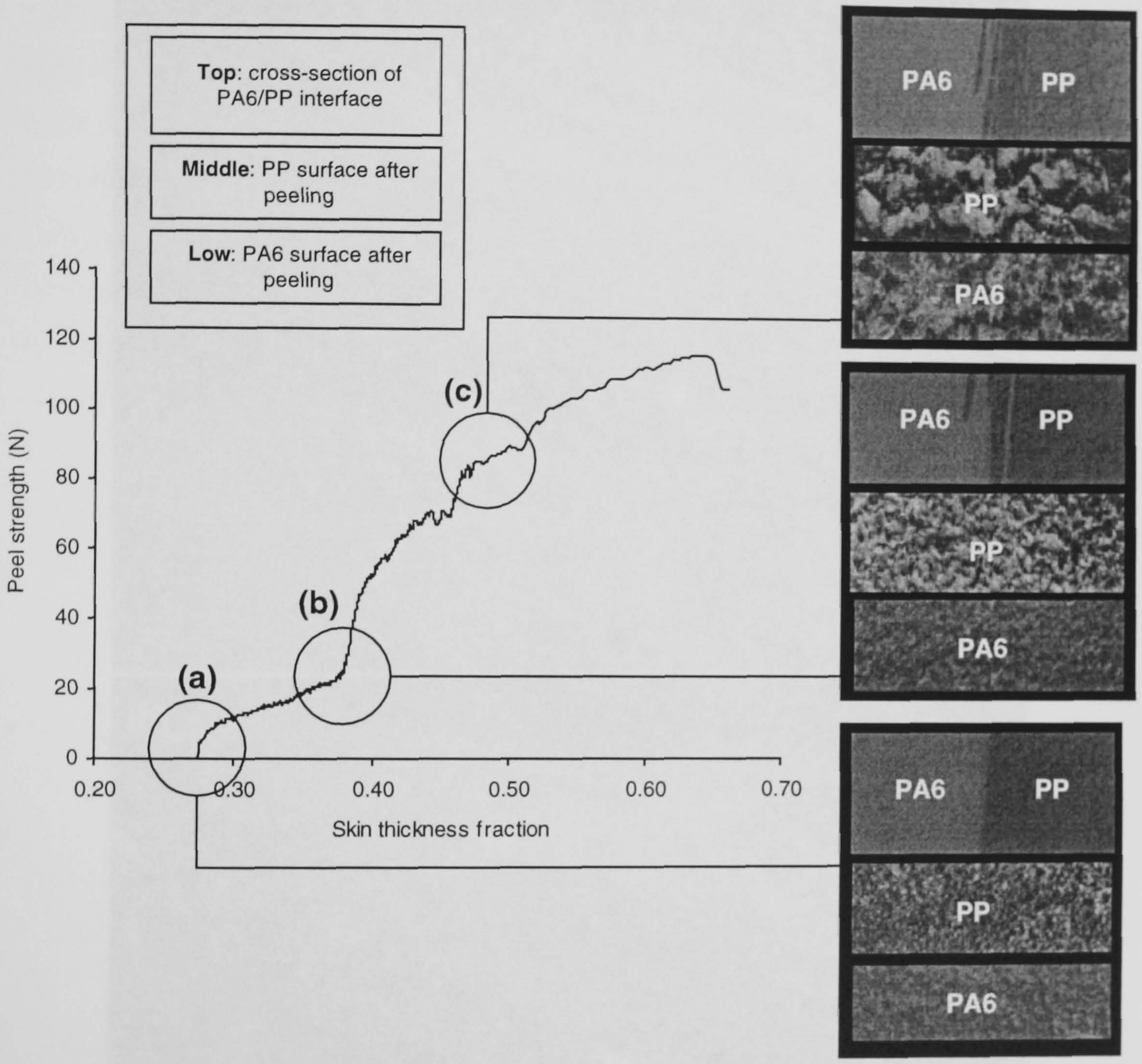

Figure 7.33 Photos of the skin and core peel fracture surfaces and the interlocks of skin and core at the different skin thickness fraction area overlayed on the peel strength curve: (a) near the gate, (b) at the minimum skin thickness fraction, and (c) 70 mm from central gate, respectively (magnification 6.3X).

7.7.2 Scanning electron microscope (SEM)

The crack tip was prepared by inserting a fresh razor blade tip into the mid-plane of the interface between skin and core as seen in Figure 6.10. Using SEM, it was possible to observed that the tie layers occurred and acted as linkage between polymer

phases (skin and core layer). It allowed the skin polymer phases to adhere to the core polymer phases (Figure 7.34(a)-(b)). The chemical mechanism of skin-core adhesion was investigated and is described in section 7.8, page 143.

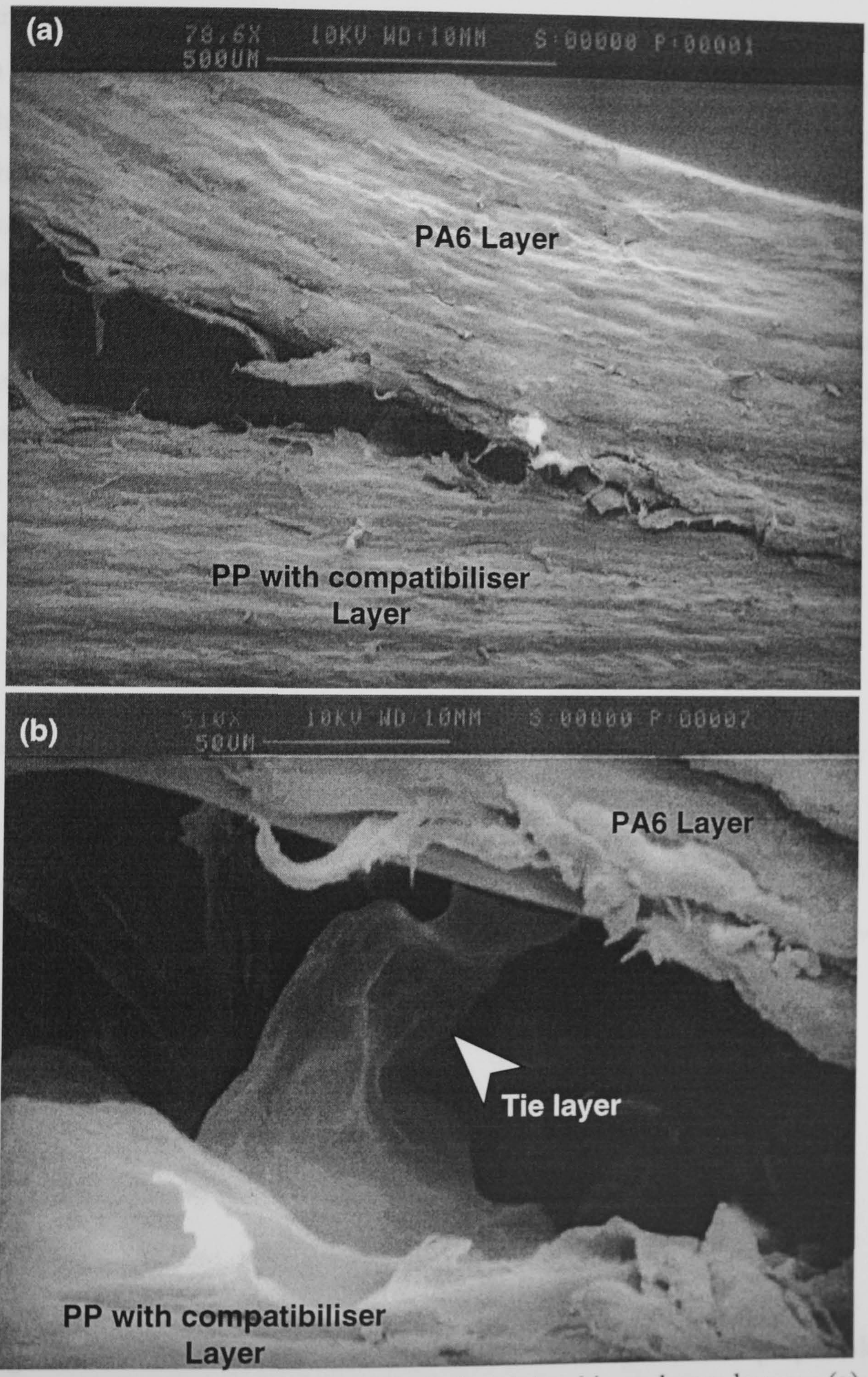

Figure 7.34 SEM of the peel crack tip of the skin and core layers : (a) low magnification (b) higher magnification.

7.8 Chemical Characterisation of PA6(skin) and PP(core) with Compatibiliser System

Chemical analyses were performed on the moulded plaques. These were selective dissolution experiments, where it was attempted to selectively dissolve the PA6 phase from a specimen of the moulded plaque using formic acid in which PP is insoluble. This should leave the PP untouched so that an examination of the PP surface could be made by IR spectroscopy [12, 24, 48]. The core surface was exposed and when analysed was showed to contain significant amounts of PA6 which suggests that the PP-g-MA (compatibiliser) formed a block copolymer with a PA6 chain during moulding. However, in other cases the whole sample completely dissolved. This could be explained if the PP-g-MA/PA6 block copolymer acted as a surfactant in the solvent allowing PP micelle formation. The main reaction leading to adhesion was thought to be that of the terminal amine group of a polyamide chain with the anhydride group of a compatibiliser molecule as shown in Figure 7.35.

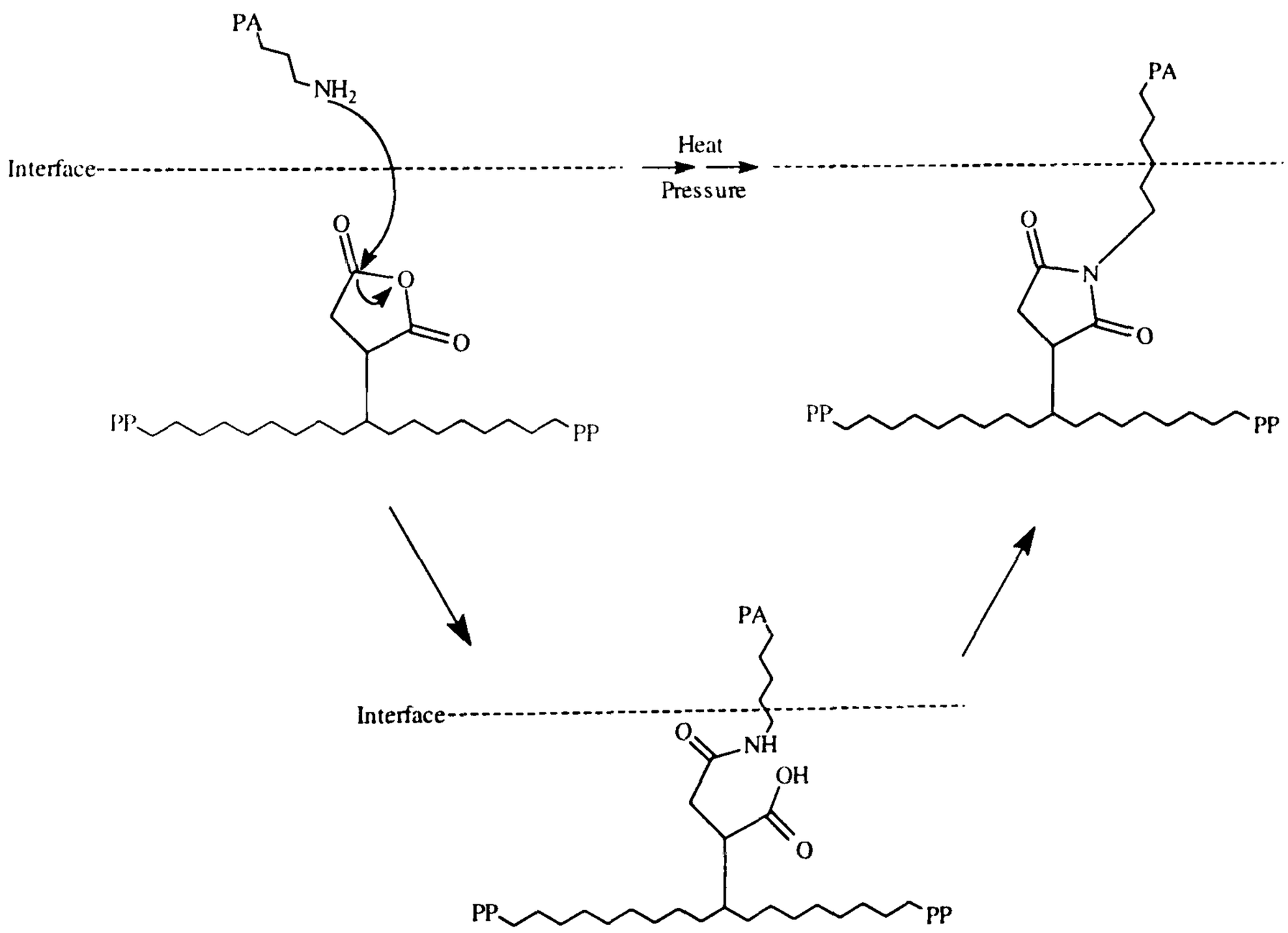

Figure 7.35 Reaction between the terminal amine group of a polyamide chain with the anhydride group of a compatibiliser molecule.

However, other interactions (both bonding and non-bonding) were theoretically possible such as the reaction of the amide N-H group of the polyamide with the anhydride group of the compatibiliser [12, 24] to give an amide or hydrogen bonding of the amide group with carbonyl group of the compatibiliser [23].

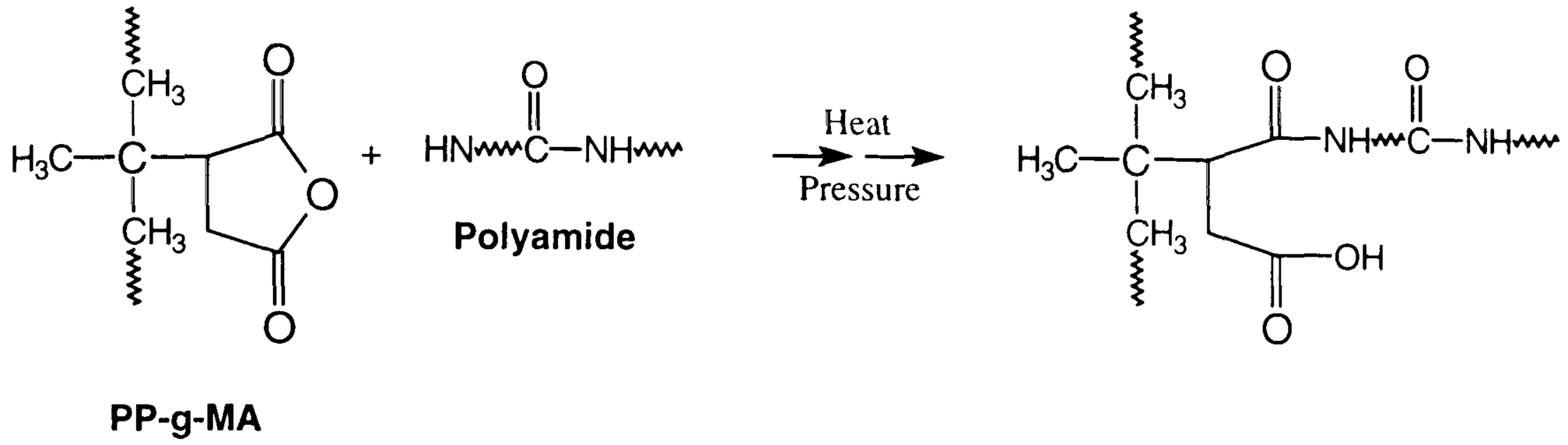

(a) reaction of the amide N-H group of the polyamide with the anhydride group of the compatibiliser

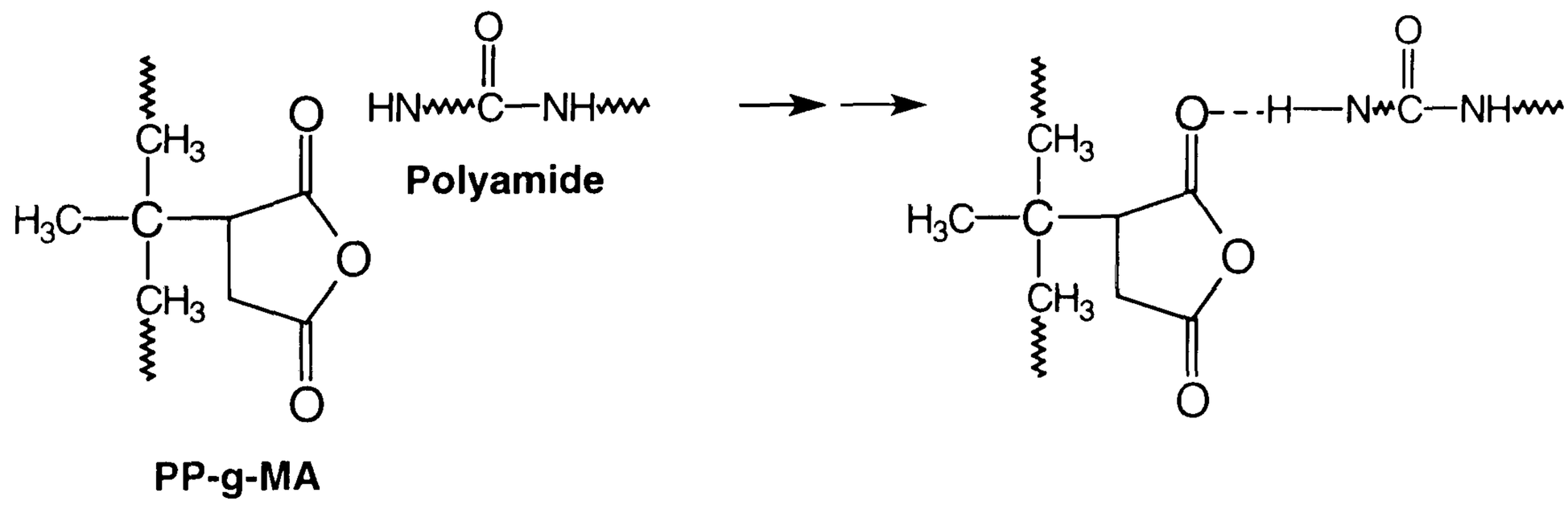

(b) hydrogen bonding of the amide group with carbonyl group of the compatibiliser

Figure 7.36 Reaction between the terminal amine group of a polyamide chain with the anhydride group.

7.9 Flow Behaviour of The Polymer Melts During Co-injection

Basically, most viscous fluid flow behaviour on a non-slip wall cavity is described by the Fountain flow [38, 46-47].

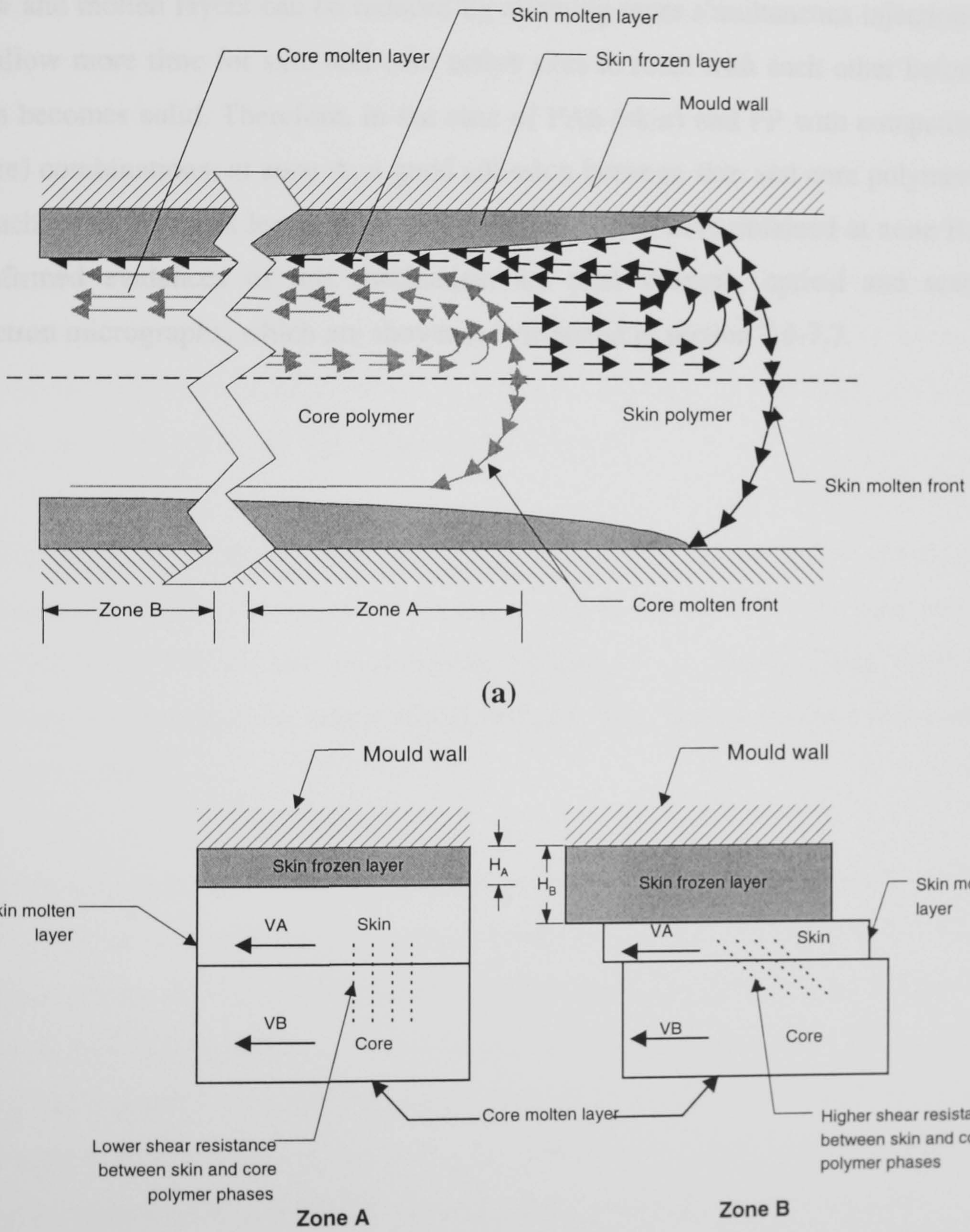

Figure 7.37 Fountain flow and interfacial interaction between skin and core polymer phases.

The above figure shows the skin-core interfacial interaction. It can be explained that at the advancing skin melt front, most skin melts are in the molten stage, whereas most frozen skin layers occur near the inlet gate. Hence the shear resistance between no-flow layer and molten core polymers build up higher at the inlet gate area than one at an advancing core melt front. On the other hand, the shear resistance between no-flow and molten layers can be reduced by allowing more simultaneous injection time to allow more time for skin and core active sites to react with each other before the skin becomes solid. Therefore, in the case of PA6 (skin) and PP with compatibiliser (core) combinations; at zone A, a good adhesion between skin and core polymers can be achieved. Whereas lower skin-core adhesion levels were obtained at zone B. The confirmed evidences of this mechanism are peel strength, optical and scanning electron micrographs, which are shown as mentioned in section 7.6-7.7.

Chapter VIII

Conclusions

The co-injection moulding process was studied. The experimental work from several tools, such as a square plaque plate moulding has led to an understanding of the mechanism of dual injection mould filling. Emphasis has been focussed on the relationships between the rheological property of the polymers and the relevant moulding parameters. The skin-core formations, which correlate to these relationships, were also studied. Many factors were introduced for understanding the effect on the skin-core adhesion where the two polymers are incompatible. In this case a compatibiliser was found to be one of the most important factors. From the obtained results, the conclusions can be summarised as follows:

- This study has provided a new way for finding the moulding parameters of co-injection moulding process based on the viscosity ratios of skin to core and their injection speed ratios. The simultaneous phase and the mould filling times were obtained from co-injection mould filling analysis. This has resulted in a refinement of previous work [8].

- Previously, Somnuk [8], the skin thickness fraction was simulated using the filling analysis of the conventional injection moulding process (1k) from Moldflow because at that time the filling analysis for co-injection moulding process (2k) did not exist. Thus, it was only possible to simulate this thickness fraction by a filling analysis using a 1k process. Somnuk had been obliged to use the skin frozen layer as the appropriate skin thickness as defined by the Moldflow 1k route. This work shows how it can be refined using C-Mold filling analysis for co-injection moulding (2k).

- The simultaneous injection times were discovered to have a non-linear correlation to the skin/core viscosity ratios.

• The techniques of co-injection moulding, such as sequential and simultaneous, could be determined by the simultaneous injection times and altered accordingly.

• It was found that the thickness of the skin layers were not of uniform thickness. The shape of the inner surface was always parabolic curve-like. At the beginning of the gate area it was thinnest and increased with length of the flow path.

• Compatibiliser, thickness of skin layer, and simultaneous injection times were the major factors to affect skin-core adhesion of incompatible thermoplastic systems. In the presence of compatibiliser, the chemical reaction between active functional groups of skin and compatibiliser in the core occurred. Suitable conditions were necessary to produce good bonding between skin and core. The greater thickness of skin layer and greater simultaneous injection times led to more probability for the skin and core active functional groups to react with each other before the skin became no-flow layer. Methods available to achieve these thicknesses and simultaneous injection times were possible by controlling the moulding parameters, such as melt temperature, tool temperature, injection speeds, and lengths of simultaneous phase; these parameters could affect the skin-core thickness formations and their adhesion to different degrees. These parameters are documented in this thesis.

• It was found that compatibilisers were acting as adhesive and plasticising agents. They influenced each core polymer viscosity depending on the initial viscosity of the polymer and the amount of compatibiliser. The percentage change in viscosity by the addition of compatibiliser was not the same for different polymers.

• The minimum skin thickness fractions for a good skin-core adhesion were obtained from the relationship between peel strengths and skin-core thickness fractions.

• Adhesion levels and minimum skin thickness fractions could be improved when simultaneous injection times were increased.

• The interfaces between the polymer phases were determined using scanning electron micrographs and showed material transfer from one phase to another, therefore confirming the adhesion model.

• The main reaction leading to adhesion was the terminal amine group of a polyamide chain with the anhydride group of the compatibiliser molecules; this was determined by IR spectroscopy.

• The mechanism of skin-core adhesion consisted of two types: chemical and physical interaction at the surface. The chemical mechanism was caused by the active functional groups on the compatibiliser molecules reacting with the terminal amine groups of the polyamide. The Fountain flow behaviour also provided a physical mechanism (interlocking between skin and core phases).

Recommendations for The Future Work

This work has provided a realistic process technology for skin-core formation during thin walled co-injection moulding of incompatible thermoplastic polymer melts. The recommendations for the further work can be suggested as follows:

• It should be possible to use the mechanism of this process to enable adhesion during co-injection moulding of other polymers to be considered. However, compatibilisers and moulding parameters are likely to produce other mechanisms of chemical and physical interaction. For instance, preliminary work on co-injection moulding and compatibilisation of a Polyester/Polypropylene system has been investigated and is presented in Appendix VIII.

• As reviewed in Chapter II (section 2.7), the mathematical modelling and computer simulation of the co-injection moulding process were almost sequential processes. So, the numerical implementation of the simultaneous co-injection moulding process is necessary to develop this process technology.

• The three-channel technique of co-injection moulding process* is an alternative process technology such that adhesion of the incompatible polymers could be promoted by inserting a compatibiliser blend between skin and core layers as shown in Figure 8.1. In this case, the compatibiliser must be bifunctional in order to have a good adhesion to skin and core polymer.

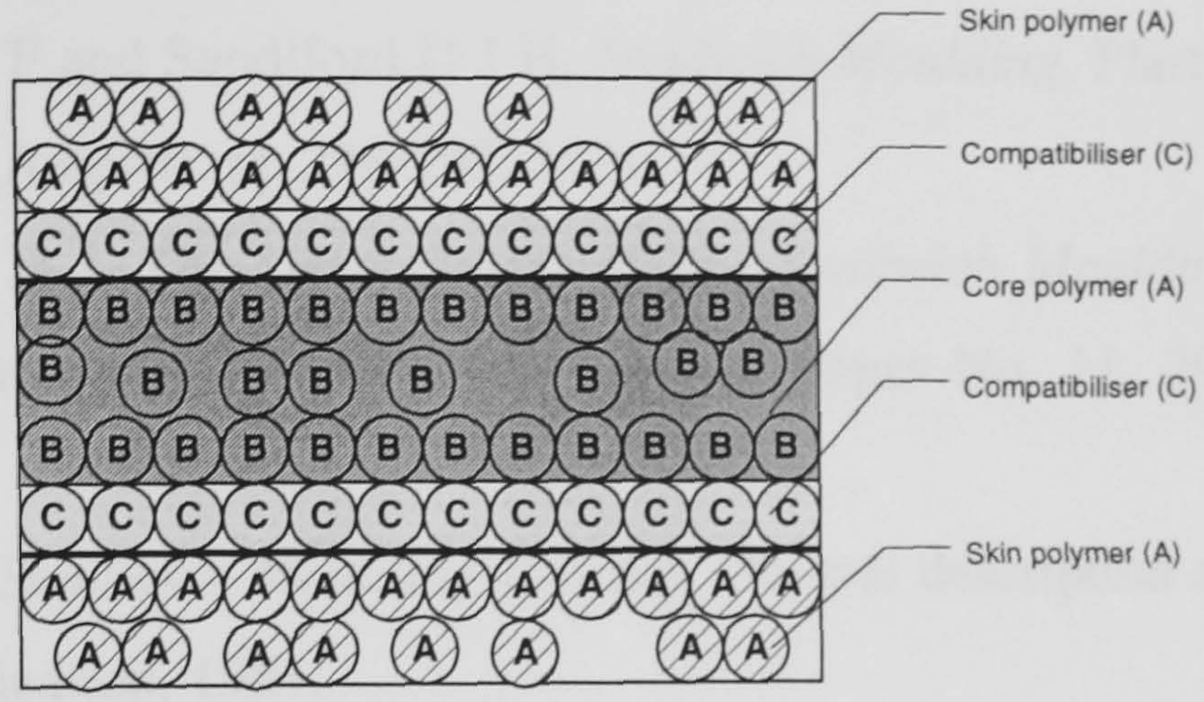

Figure 8.1 Multilayered structure which produced by three-channel technique.

* See Figure 2.8, page 8.

References

1 Smith G F and Easterlow R A, Plastic, Rubber and Composites, 25(3), pp.115-119, 1996.

2 Oxley D F and Sandiford D J H, *Sandwich Moulding*, Plastics & Polymers, Vol. 39 (August), pp.288-292, 1971.

3 Stafford D J, *The Development of The Sandwich Moulding Process*, The Plastic Institute, PENTEC 72, London, Paper No. 11, 29-30 November, 1972.

4 *The ICI Sandwich Moulding Process*, General description and applications, ICI publication, 1981.

5 Sandiford D J H and Oxley D F, *Serving Up a New Plastic Sandwich*, SPE Journal, Vol. 27, September 1971.

6 Donovan R C, Rabe K S, Mammel W K, and Lord H A, *Recycling Plastics by Two-shot Moulding*, Polymer Engineering and Science, 15(11), pp.774-780, 1975.

7 Eckardt H, *How to develop a successful coinjection application*, Fourteenth annual structural foam conference and parts competition, The society of the plastics industry, Inc., Boston, Massachusetts, April 21-23, 1986.

8 Somnuk P, *Ph.D. Thesis*, Department of Engineering, Faculty of Science, University of Warwick, 1995.

9 Seldén R, *Sandwich Injection Moulding of Thermoplastics: A Literature Survey*, Journal of Injection Moulding Technology, Vol.1, No.4, 1997, pp.189-203.

10 Datta S and Lohse D J, *Polymeric Compatibilisers : Uses and Benefits in Polymer Blends*, Hanser Publishers, 1996.

11 Hu G H, Sun Y J and Lambla M, *Melt Free-radical Grafting of Glycidyl methacrylate onto Polypropylene*, Die Angewandte Makromolekulare Chemie, 229, pp.1-13, 1995.

12 Ide F and Hasegawa A, *Studies on Polymer Blend of Nylon 6 and Polypropylene or Nylon 6 and Polystyrene Using the Reaction of Polymer*, J.Appl.Polym.Sci., 18, pp.963-974, 1974.

13 Okamoto K T, Eastenson K D and Guyaniyogi S C, *Engineering Resin-propylene Polymer Graft Composition*, US Patent no. 5,290,856, 1994.

14 Jacqueline I K, *High Performance Polymers and Composites*, John Wiley & Sons, Inc., 1991.

15 Jacqueline I K, *Encyclopaedia of Polymer Science and Engineering*, Vol.1, 4, 12-13, John Wiley & Sons, Inc., 1991.

16 *Innovative Injection Moulding*, Ferromatik Milakron Company Pub., 1996.

17 Addmix® Monosandwich Injection Moulding Technology, Addmix Inc., Internet website http://www.netlink.co.uk/users/addmix/main.html, 1997.

18 *Battenfeld's Operating Instructions for BMT-1100/2x300 Co-Injection Moulding Machine*, Battenfeld GmbH.

19 Kortec's Multigate Co-Injection Systems, Kortec Inc., Internet website http://www.kortec.com, 1997.

20 Wood R, *Automotive Engineering Plastics*, Pentech Press, 1991.

21 *Battenfeld's Operating Instructions for BM-2700/3x630 Co-Injection Moulding Machine*, Battenfeld GmbH.

22 Magalheas A, *Adhesion of PP on PA6 with PP-MA Compatibiliser for Rover Fenders*, DSM Research, 1997.

23 Trivedi B C, *Maleic anhydride*, Plenum Press, 1982.

24 Sathe S N, Devi S, Rao G S S, and Rao K V, *Relationship Between Morphology and Mechanical Properties of Binary and Compatibilised Ternary Blends of Polypropylrene and Nylon 6*, J.Appl.Polym.Sci., 61, pp.97-107, 1996.

25 Menges G and Mohren P, *How to Make Injection Moulds*, Hanser Publishers, 1993.

26 Buckleitner E V, *DuBois and Pribble's plastics mould engineering handbook*, 5th Edition, Chapman & Hall, 1995.

27 Pye R G W, *Injection Mould Design*, 4th Edition, Longman-Scientific & Technical, 1989.

28 Whelan A, *Injection Moulding Machines*, Elsevier Applied Science Publishers, 1984.

29 Fried J R, *Polymer Science and Technology*, Prentice-Hall, Inc., 1995.

30 Johannaber F, *Injection Moulding Machines: A User's Guide*, Hanser Publishers, 1983.

31 Betters J E and Duffy J, *The Benefits of a Sequential Fill Valve Gate Hot Runner System for Moulding Automotive Bumper Fascias*, SPE, Detroit Section and Automotive Division RETEC, 8-9 November, 1995.

32 White J L and Dee H B, Polym. Eng. Sci., Vol. 14, 1974, pp.212.

33 Young S S, White J L, Clark E S, and Oyanagi Y, *A Basic Experimental Study of Sandwich Injection Moulding With Sequential Injection*, SPE ANTEC, 1980, pp.163-165.

34 Schlatter G, Davidoff A, Agassant J F, and Vincent M, *Numerical Simulation of The Sandwich Injection Moulding Process*, SPE ANTEC, 1995, pp.456-459.

35 Lord H A and Williams G, SPE ANTEC, Tech. Papers Vol.21, 1975.

36 Somnuk P, and Smith G F, *Experimental Study of Simultaneous Co-injection Moulding Process*, SPE ANTEC, Boston, Massachusetts, pp.760-764, 1995.

37 Lanvers A and Michaeli W, *CAE for Co-injection and Gas-Assisted Injection Moulding*, SPE ANTEC, pp.1796-1799, 1992.

38 *C-MOLD Reference Manual*, Advanced CAE Technology Inc., 1996.

39 *C-MOLD User's Guide*, Advanced CAE Technology Inc., 1996.

40 Chen S C, Hsu K F, Hsu K S, and Jeng M C, Numerical Simulation and Experimental Studies of The Co-injection Moulding Process, SPE ANTEC, pp.82-86, 1993.

41 Lee D J, Isayev A I, and White J L, *Simultaneous Sandwich Injection Moulding: Simulation and Experiment*, SPE ANTEC, Atlanta, Georgia, 1998.

42 Champagne M F, *Interfaces in Polyolefin/Polyethylene Terephthalate Blends Reactively Compatibilized by Glycidyl Methacrylate Copolymers*, PPS-RM1999, December 19999, Bangkok.

43 Elf Atomchem, *Product data sheet - Orevac Graft PP, PE*, Internet website http://www.elf-atochem.fr/, May, 2000.

44 Ebeling T, Norek S, Hasan A, Hiltner A, and Baer E. *Effect of a tie layer on the delamination toughness of polypropylene and polyamide-66 microlayers*, Journal of Applied Polymer Science (USA). vol. 71, no. 9, pp. 1461-1467, 28 Feb. 1999.

45 Rungseesantivanon W, and Smith G F, *Factors Affecting Adhesion of Polymers during Coinjection*, PPS-RM1999, December 1999, Bangkok.

46 Coyle D J, Blake J W, and Macosko C W, *The Kinematics of Fountain Flow in Mould-Filling*, AIChE Journal, Vol.33, No.7, pp.1168-1177, 1987.

47 Mavridis H, Hrymak A N, and Vlachopoulos J, *Finite Element Simulation of Fountain Flow in Injection Moulding*, Polymer Engineering and Science, Vol.26, No.7, pp.449-454, 1986.

48 Coates R J, *SALVO1: The Primer Report*, Warwick Manufacturing Groups (WMG), Advanced Technology Centre (ATC), University of Warwick, 1999.

49 Charrier J, *Polymer Materials and Processing: Plastics, Elastromer, and Composites*, Hanser Publishers, 1991.

50 Kinloch A J, *Adhesion and Adhesives : Science and Technology*, Chapman & Hall Publishing, 1990.

51 Griskey R G, *Polymer Process Engineering*, Chapman & Hall, pp.105-114, 311-334, 1995.

52 Tanner R I, *Engineering Rheology*, Clarendon Press, pp.379-383, 1985.

53 Kaelble D H, *Computer-Aid Design of Polymers and Composites*, Marcel Dekker Inc., pp.145-148, 1985.

54 Kennedy P, *Flow Analysis of Injection Moulds*, Hanser Publishers, 1995.

55 Kennedy P, *Flow Analysis Reference Manual*, MoldFlow Pty. Ltd., 1993.

56 Agassant J F, Avenas P, Sergent J Ph. and Carreau P J, *Polymer Processing: Principles and Modelling*, Hanser Publishers, pp.31-39, 1991.

57 Turng L S and Wang V W, *Simulation of Co-injection and Gas-Assisted Injection Moulding*, SPE ANTEC, pp.297-300, 1991.

58 Turng L S, Wang V W and Wang K K, *Numerical Simulation of The Co-injection Moulding Process*, ASME, Heat and Mass Transfer in Solidification Processing, HTD-Vol. 175, pp.113-119, 1991.

59 *Standard Test Method for Determination of Properties of Polymeric Materials By Means of a Capillary Rheometer*, ASTM D3835 Vol.8.02, Annual Book of ASTM Standards, pp.466-475, 1996.

60 Eigl F A, *The sandwich Injection Moulding Technology-Effects and Limiting Quantities for the Spatial Distribution of the Components*, Journal of Reinforced Plastics and Composites, 17, pp.1404-1413, 1998.

61 Brydson J A, *Plastics Materials*, 6th Edition, Elsevier Science Publisher, 1995.

62 Himasekhar K, Turng L S, Wang V W, Chiang H H and Wang K K, *Current Trends in CAE Simulation of Latest Innovations in Injection Moulding*, Advance in Polymer Technology, Vol. 12, No. 3, pp.233-241, 1993.

63 Kuhmann K and Ehrenstein G W, *Monosandwich Injection Moulding: Skin-Core Structure and Properties of Sandwich-Moulded Antielectrostatic Components*, SPE ANTEC, pp.372-376, 1998.

64 Mascia L, *Thermoplastics: Materials Engineering*, Applied Science Publishers Ltd., 1982.

65 CAMPUS 4.0 (Computer Aided Material Preselection by Uniform Standards Version 4.0), A Joint Development of Companies in the Plastics Industry, ©Copyright 1996 CFW GmbH, Frankfurt/Main.

Appendix I

Calculation of Shear Viscosity (η) Using Cross-WLF Model

From Equation (4.11) and Equation (4.13), in Chapter IV, the shear viscosity of the polymer melts are obtained by using the following formulas,

$$\eta(T,\dot{\gamma},p) = \frac{\eta_0(T,p)}{1+\left(\frac{\eta_0\dot{\gamma}}{\tau^*}\right)^{1-n}} \qquad (4.11)$$

and

$$\eta_0(T,p) = D_1 \exp\left[-\frac{A_1(T-T_a)}{A_2+(T-T_a)}\right] \qquad (4.13)$$

Where $T_a = D_2 + D_3.p$,and $A_2 = \tilde{A} + D_3.p$

The 7-constants (n, τ^*, D_1, D_2, D_3, A_1, $\tilde{A}$) of each polypropylene (Novolen, grade: 1100N, 1102K, and 1100H) and polyamide 6 (Durethan, grade: B31SK and B30S) shown in Table API.1.

Table API.1 The resin-dependent constant for Cross-WLF viscosity model.

Constants	Polypropylene (Novolen)			Polyamide 6 (Durethan)		PBT (Arnite)
	1100N	1102K	1100H	B31SK	B30S	TM4 250
n	0.32799	0.28576	0.24309	0.43442	0.21924	0.29007
τ^*	13768	23258	28250	163910	247270	412390
D_1	1.64E+14	1.56E+16	7.25E+15	8.20E+20	1.69E+13	1.06E+18
D_2	263.15	263.15	263.15	323.15	323.15	323.15
D_3	0	0	0	0	0	0
A_1	30.801	35.42	33.434	53.247	30.953	44.803
$\tilde{A}$	51.6	51.6	51.6	51.6	51.6	51.6

Data source from C-MOLD Materials Database

So that, the zero-shear viscosity of each polymer grade are obtained from Equation (4.13) and parameters in Table API.1, then their shear viscosity are calculated using Equation (4.11) and show in Table API.2 as follows.

Table API.2 Shear viscosity data of polypropylene, polyamide 6, and PBT at the various temperatures.

Temp. (°C)	Shear viscosity (η) at shear rate (γ) of 10^3 s^{-1}, (Pa.s)					
	Polypropylene (Novolen)			Polyamide 6 (Durethan)		PBT (Arnite)
	1100N	1102K	1100H	B31SK	B30S	TM4 250
190	85.1601	126.8097	139.6493			
195	81.6334	121.6051	135.0899			
200	78.3674	116.7842	130.8360			
205	75.3360	112.3082	126.8590			
210	72.5160	108.1433	123.1338			
215	69.8874	104.2594	119.6378			
220	67.4324	100.6304	116.3513	332.4289	231.3575	
225	65.1351	97.2329	113.2564	284.5636	215.4223	
230	62.9816	94.0462	110.3373	244.2015	200.5876	307.4739
235	60.9594	91.0521	107.5797	210.0534	186.7895	272.3026
240	59.0575	88.2342	104.9709	181.0799	173.9678	241.1311
245	57.2660	85.5778	102.4994	156.4361	162.0652	213.5555
250	55.5758	83.0699	100.1548	135.4293	151.0263	189.2031
255				117.4876	140.7975	167.7298
260				102.1362	131.3269	148.8188
265				88.9787	122.5643	132.1801
270				77.6829	114.4611	117.5499
275				67.9696	106.9710	104.6895
280				59.6032	100.0496	93.3848

Appendix II

The Optimum Level Compatibiliser for Incompatible Skin (PA6) and Core (PP)

The confidential report for the FINIMOL project at DSM, which discussed methods of achieving good adhesion of PP on PA6, was documented by DSM Research [22]. The aim of this project was to develop the granular injection paint technology (GIPT) [1]. It was also one of SALVO projects at Advanced Technology Centre (ATC), University of Warwick, which were sponsored by ROVER Group Ltd. The skin material was polyamide 6, and the core material was polypropylene. The square plaque plate tool, dimension of 200 x 200 x 3 mm., was moulded. The core materials were modified by dry-blending PP with various amount of compatibiliser (Polybond 3150). After moulding, parts were removed, and compatibility of the component samples was tested using a peel test on the tensile testing machine. The results showed the optimum amount of compatibiliser at ca. 10% by weight and depicted in Figure APII.1.

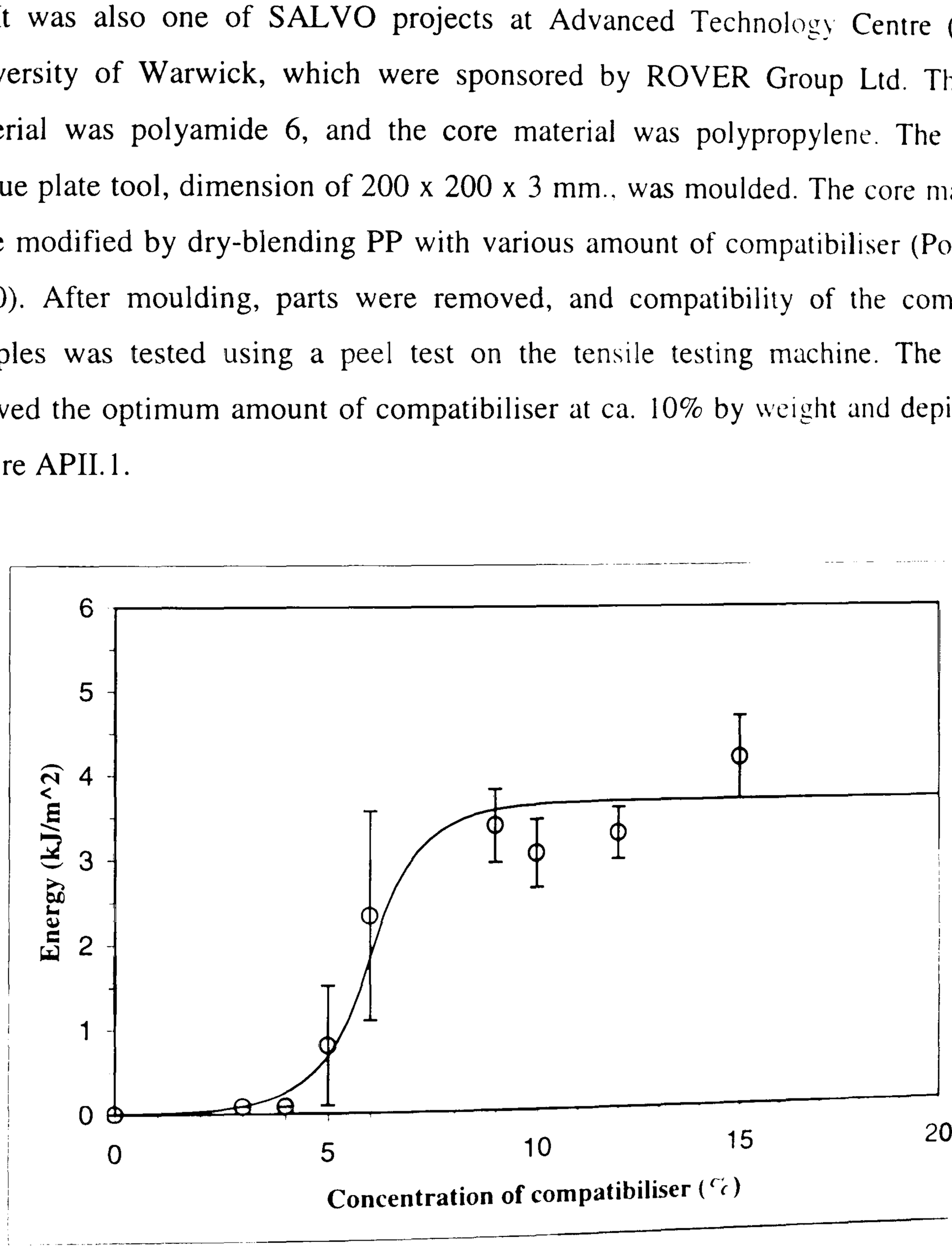

Figure APII.1 Relationship between peel test energy ($kJ.m^{-2}$) and concentration of compatibiliser (%), skin: PP Stamylan P43T1030, core: PA6 Akulon K222D, and compatibiliser: PP-g-MA Polybond 3150.

Appendix III
Simulation of Co-injection Moulding Process Using C-MOLD Software

C-MOLD, co-injection moulding process solution, simulated the mould filling and post-filling stages of the co-injection process. The co-injection process entailed the injection of two distinctly different plastic materials into the same mould to reduce part cost, reduce part weight, achieve a certain look or feel, or improve properties of the final product.

C-MOLD allowed the specification of properties of the "skin" and "core" materials and accurately simulated how these materials flow into the part cavity under sequential injection. This solution allowed you to determine the proper shot size for both materials and process conditions in order to achieve the desired skin/core ratio and extent of penetration of the core material. This solution is ideal for addressing part design, moulding, and appearance issues as well as quantifying the impact on part cost of the co-injection process.

Simulation overview

Basically, when we started simulation of any geometric shape with C-MOLD (version 99.1), it needed three component modules such that model and mesh, process conditions and simulation, and visualisation.

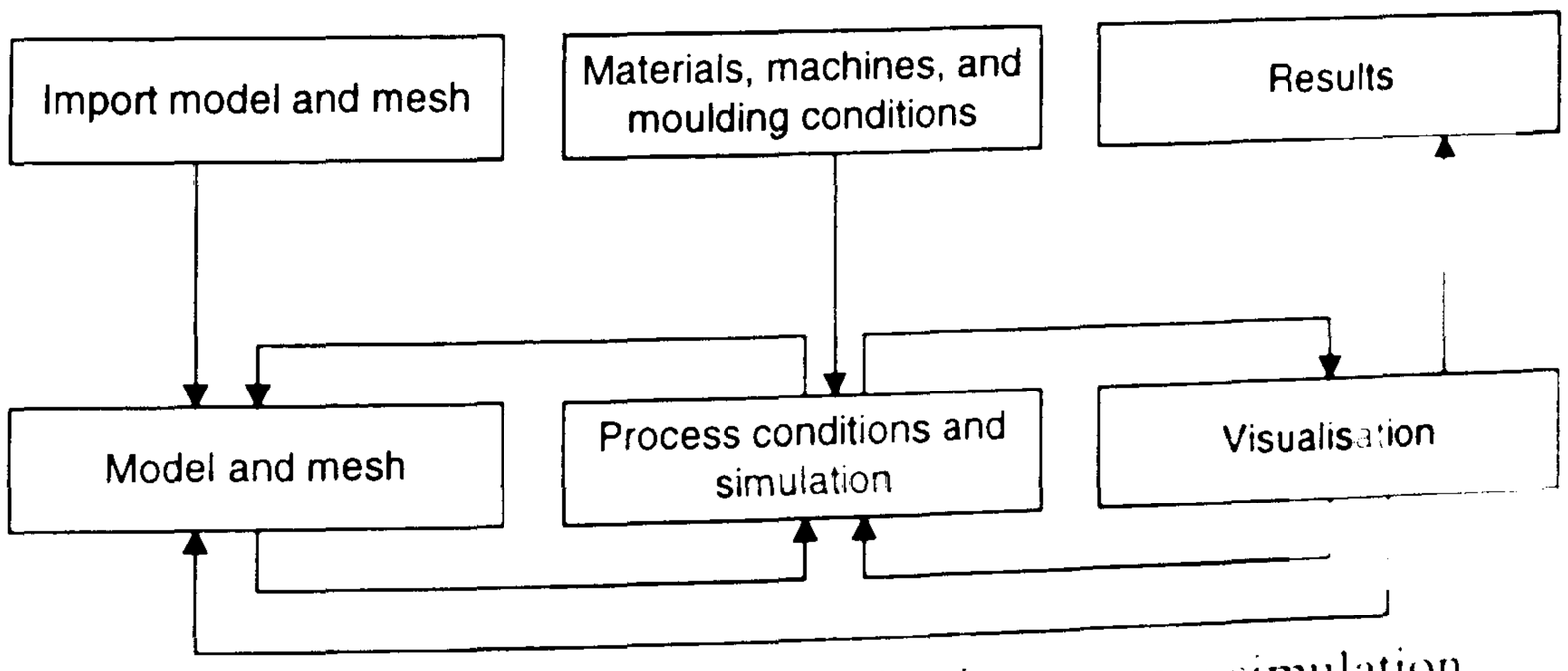

Figure APIII.1 C-MOLD co-injection process simulation

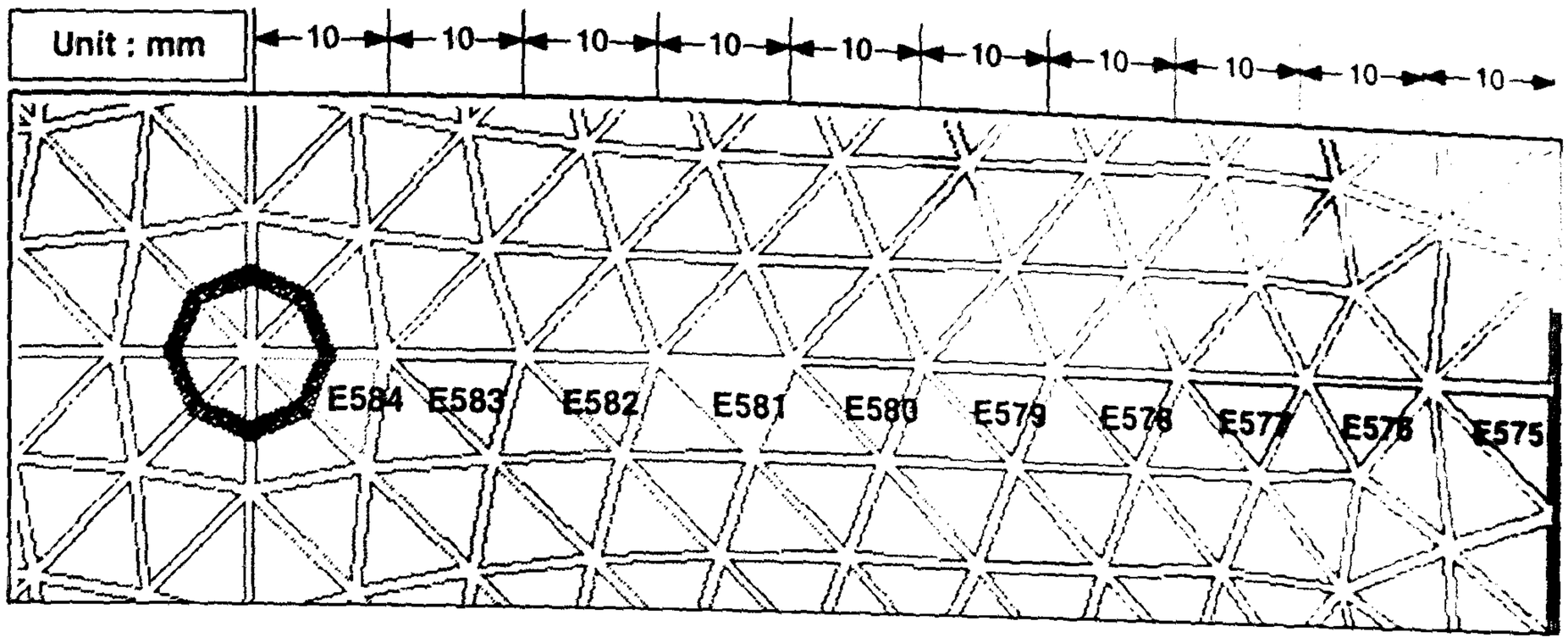

Figure APIII.2 The location of selected element from C-MOLD filling analysis for square plaque moulding.

Example of co-injection simulation files:

Materials

```
---- Beginning of title
TITL       sw23.mtl   : Co-injection Molding
FILE       08/24/98       09:22:45       C-MOLD v4.0
---- Beginning of << C-MOLD Material Properties - Version 4.0 >>
MTRL     1     12   Description of TCODE ....
      1000      1   Constant polymer density
                        970
      1101      2   Tabulated polymer specific heat
                      543.65        2390
      1201      2   Tabulated polymer therm conduct
                      543.15        0.11
      1313      7   Cross-WLF polymer viscosity
                       0.21924       247270    1.69E+013       323.15
                             0      30.953        51.6
      1500      1   Transition temperature
                      458.15
      1999      0   BAYER/PA 6 DURETHAN B30S DAM
      2000      1   Constant polymer density      -2
                        770
      2101      2   Tabulated polymer specific heat -2
                      527.65        2930
      2201      2   Tabulated polymer therm conduct -2
                      488.65        0.118
      2313      7   Cross-WLF polymer viscosity    -2
                       0.24309       28250    7.25E+015       263.15
                             0      33.434        51.6
      2500      1   Transition temperature        -2
                      408.15
```

2999 0 PP/BASF/PP NOVOLEN 1100 H
---- End of file
ENDF

Process conditions

---- Beginning of title
TITL sw23.prc : Co-injection Molding
FILE 08/24/98 09:23:18 C-MOLD v4.0
---- Beginning of << C-MOLD Process Conditions - Version 4.0 >>
PROC 1 10 Description of TCODE ....
---- Machine description: Battenfeld/BK 1000/315
10000 1 Max machine clamp force
1.07843E+006
10001 1 Max machine injection volume
0.000125
10002 1 Max machine injection pressure
1.75E+008
10005 1 Max machine injection rate
0.0003
10100 1 Fill time
0.903
10200 1 Timer for core or gas injection
0.50568
10300 1 F/P switch over by % volume
99
10602 22 Ram speed profile (rel)
0 44 10 44
20 44 30 44
40 44 56 44
60 44 70 44
80 44 90 44
100 44
11002 1 Inlet melt temperature
533.15
11003 1 Second melt temperature
508.15
---- End of file
ENDF

FEM

All simulation will be saved in text file format with extension "file_name.ojf"

Results

Table APIII.1 Core polymer thickness fraction vs. filling time

Filling time (s)	Core polymer thickness fraction									
	E584	E583	E582	E581	E580	E579	E578	E577	E576	E575
0.55	0.6206	0.4521	0.0000	0.0000	0.0000	0.0000	0.0000	0.0000	0.0000	0.0000
0.63	0.7831	0.7661	0.6629	0.5886	0.3768	0.0000	0.0000	0.0000	0.0000	0.0000
0.71	0.7686	0.7858	0.7640	0.6611	0.6239	0.4901	0.2654	0.0000	0.0000	0.0000
0.79	0.7687	0.7724	0.7871	0.6987	0.6509	0.6185	0.4883	0.2859	0.0000	0.0000
0.86	0.7836	0.7632	0.7861	0.7665	0.6495	0.6440	0.5882	0.4434	0.0217	0.0000
0.90	0.7908	0.7642	0.7830	0.7763	0.6490	0.6470	0.6116	0.4760	0.2226	0.0000

Table APIII.2 Frozen layer fraction vs. filling time

Filling time (s)	Frozen layer fraction									
	E584	E583	E582	E581	E580	E579	E578	E577	E576	E575
0.08	0.0674	0.0490	0.0000	0.0000	0.0000	0.0000	0.0000	0.0000	0.0000	0.0000
0.17	0.0813	0.0853	0.0869	0.0827	0.0000	0.0000	0.0000	0.0000	0.0000	0.0000
0.23	0.0819	0.0882	0.0923	0.0909	0.0856	0.0000	0.0000	0.0000	0.0000	0.0000
0.30	0.0823	0.0916	0.0990	0.0988	0.0948	0.0886	0.0000	0.0000	0.0000	0.0000
0.38	0.0824	0.0942	0.1049	0.1058	0.1022	0.0965	0.0886	0.0000	0.0000	0.0000
0.45	0.0823	0.0967	0.1110	0.1131	0.1100	0.1045	0.0971	0.0871	0.0000	0.0000
0.53	0.0819	0.0988	0.1168	0.1202	0.1175	0.1124	0.1053	0.0962	0.0754	0.0000
0.60	0.0814	0.1005	0.1249	0.1339	0.1305	0.1199	0.1132	0.1044	0.0939	0.0000
0.68	0.0808	0.1019	0.1346	0.1443	0.1435	0.1373	0.1229	0.1125	0.1023	0.0827
0.75	0.0802	0.1030	0.1419	0.1520	0.1532	0.1501	0.1405	0.1211	0.1104	0.0952
0.83	0.0796	0.1038	0.1477	0.1583	0.1612	0.1603	0.1541	0.1403	0.1185	0.1035
0.90	0.0791	0.1044	0.1518	0.1630	0.1672	0.1682	0.1641	0.1538	0.1352	0.1110

Appendix IV

Determination of Skin-Core Thickness Fraction Using Image Processing Software

Generally, the skin-core thickness fractions were obtained using optical microscope. The disadvantage of this method was taking long time. And sometime if the specimen was not cut and polished well, error will occurred. Therefore, the image processing software which programmed using Microsoft Visual Basic 4.0 (32 bit) was developed. Basically, the scanned photo of the cross-section of moulding component is loaded and then user moved cursor on the location of skin and core layers. With this software the skin-core thickness fractions are obtained more precisely. The main windows programme and plot result windows are shown in Figure APIV.1.

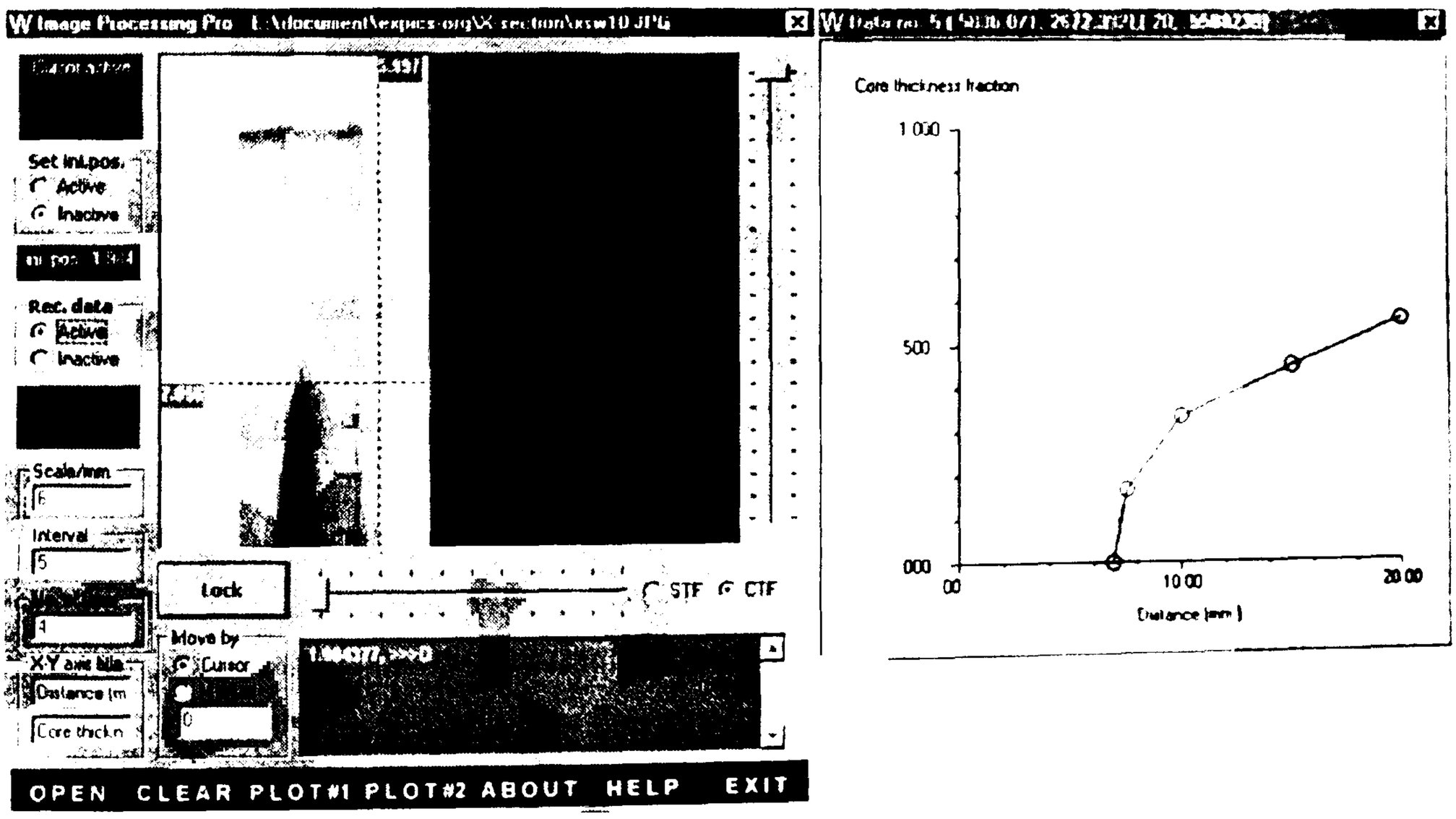

Figure APIV.1 Main window programme and resulted windows.

Appendix V

The Experimental and Simulated Results of Skin Frozen Layer Thickness Fractions and Core Thickness Fraction

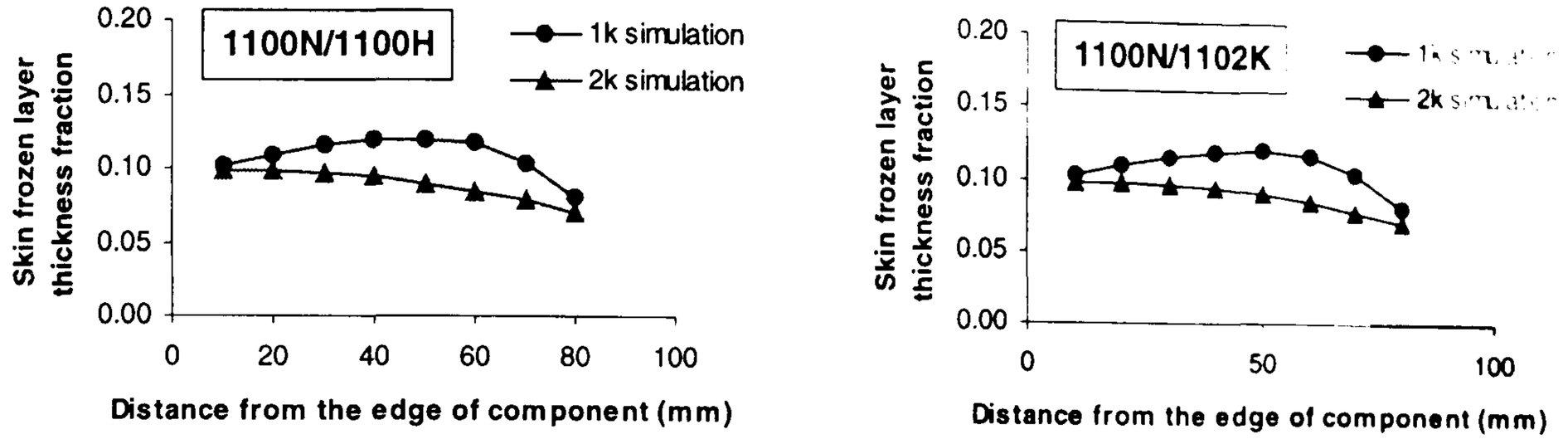

Figure APV.1 Skin frozen layer thickness fractions of PP(skin)/PP(core) moulding component.

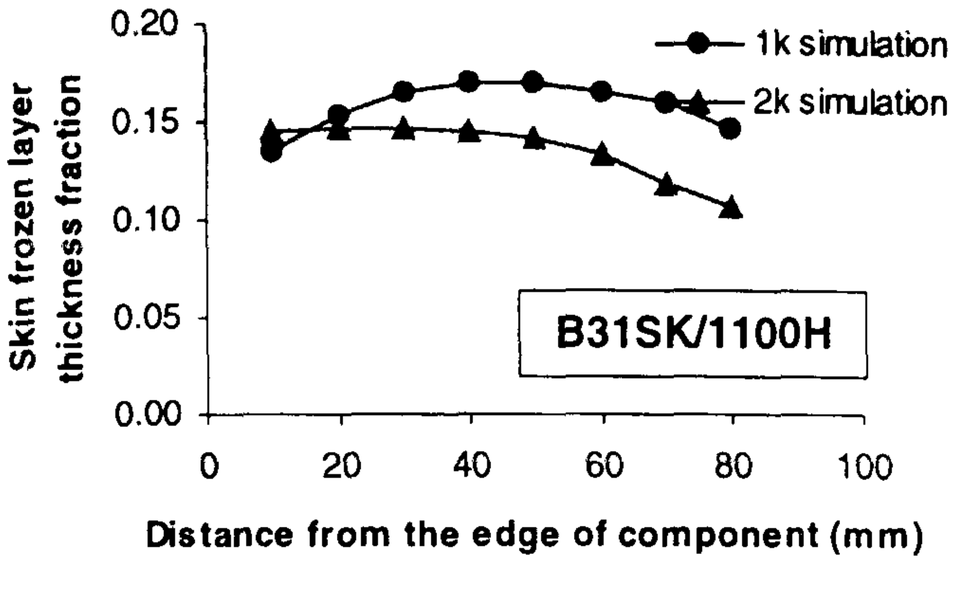

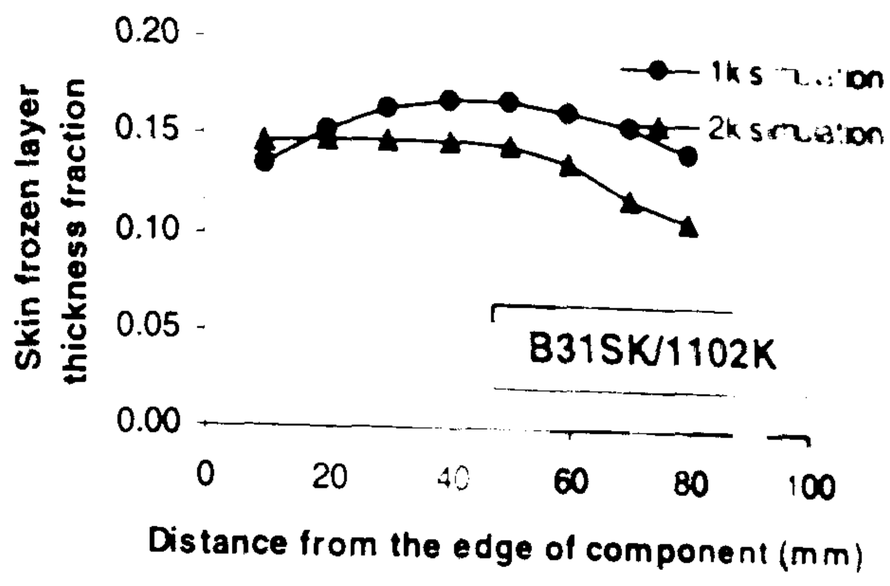

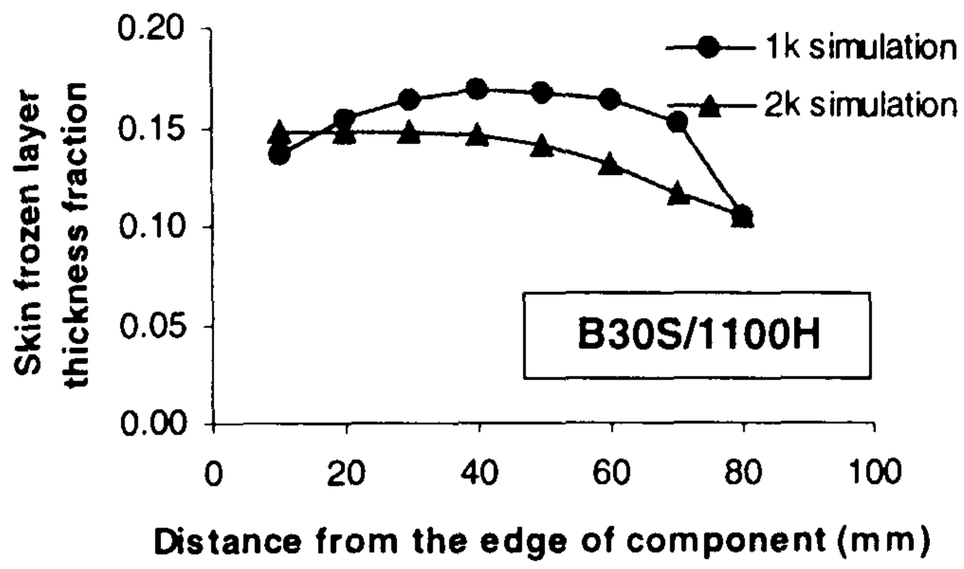

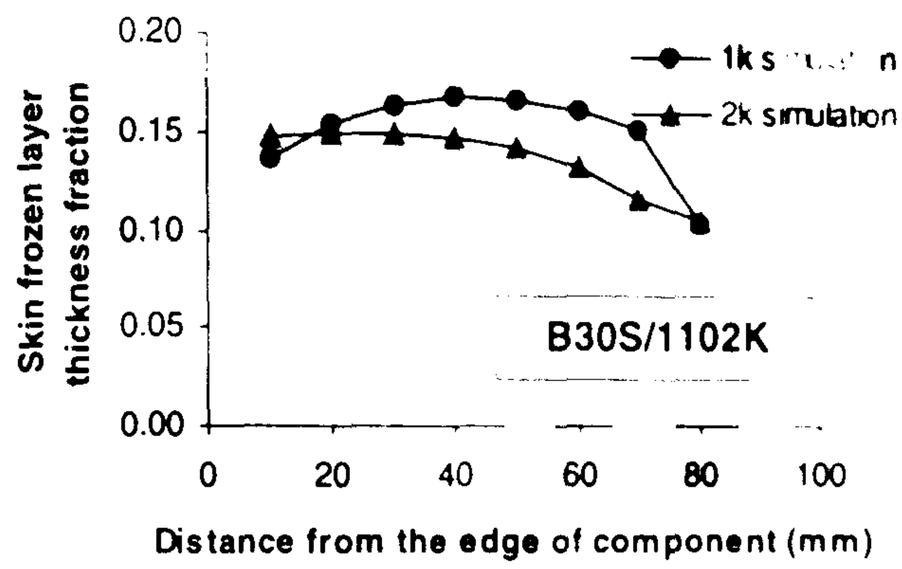

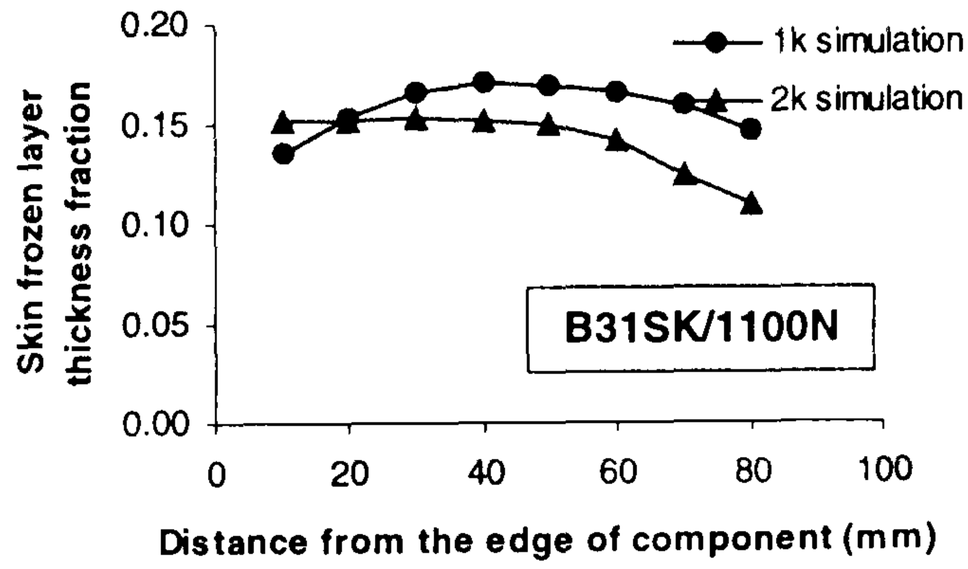

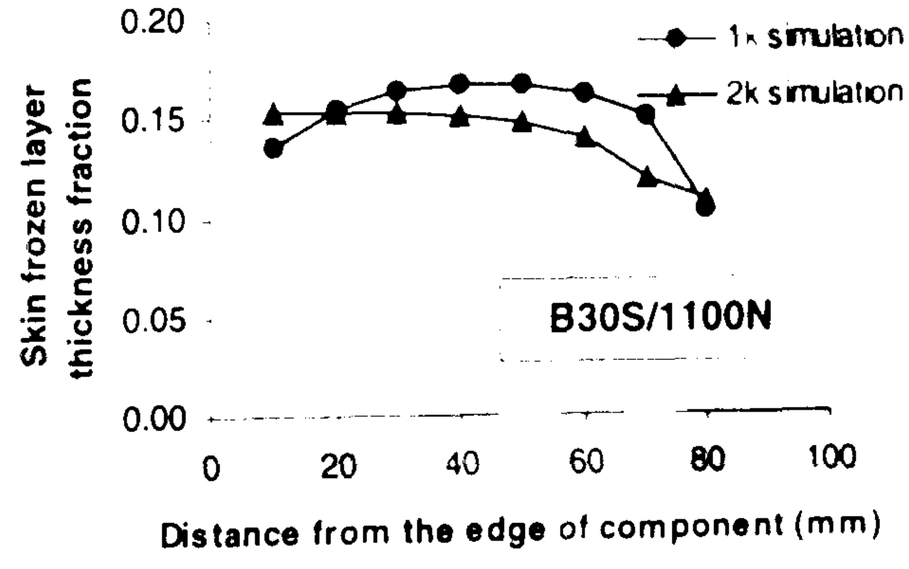

Figure APV.2 Skin frozen layer thickness fractions of PA6(skin)/PP(core) moulding component.

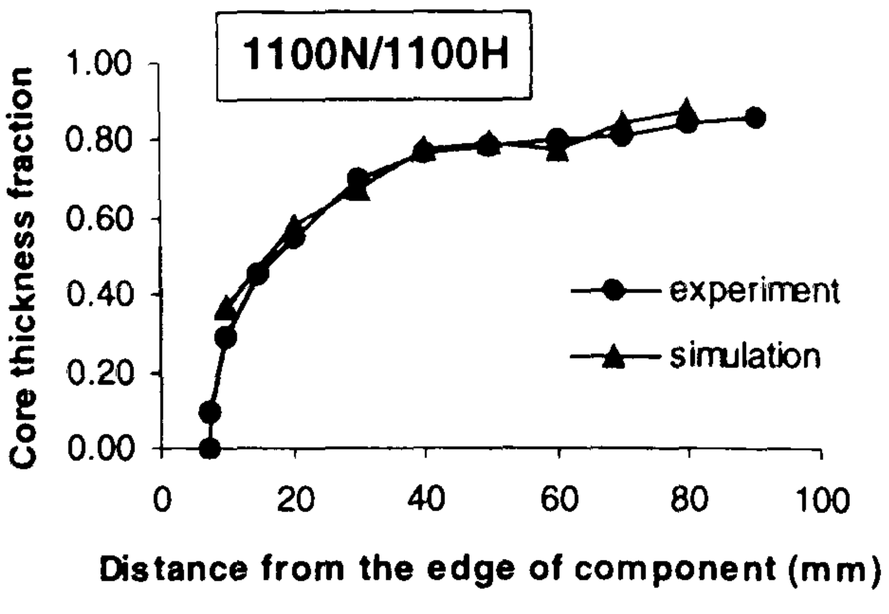

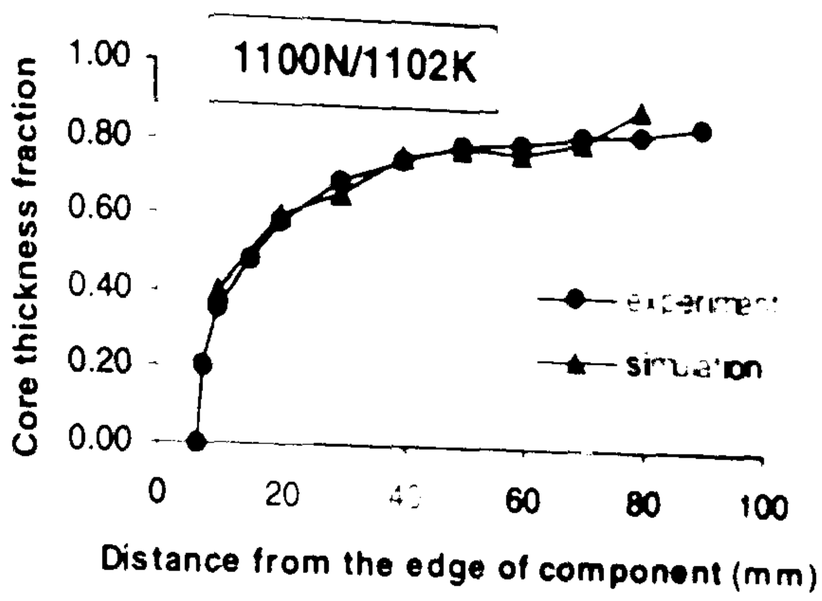

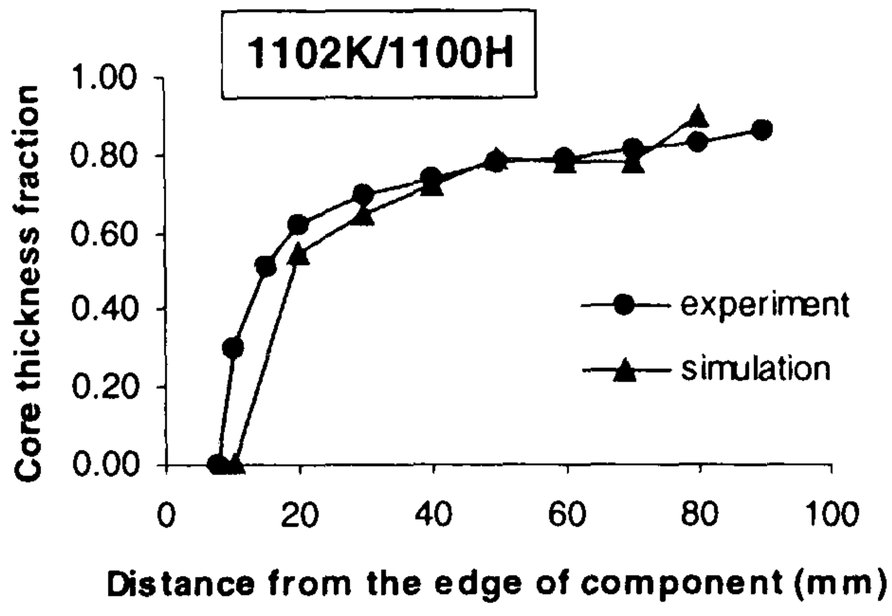

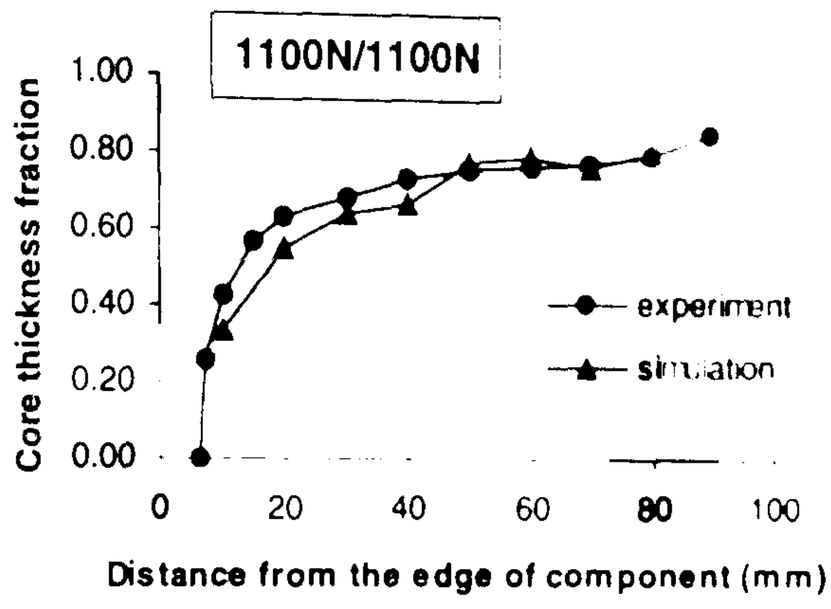

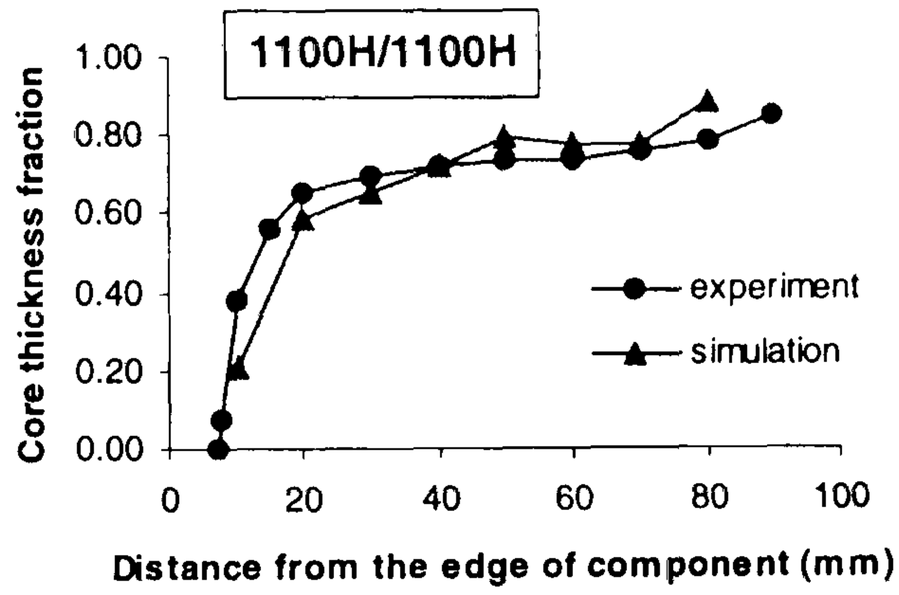

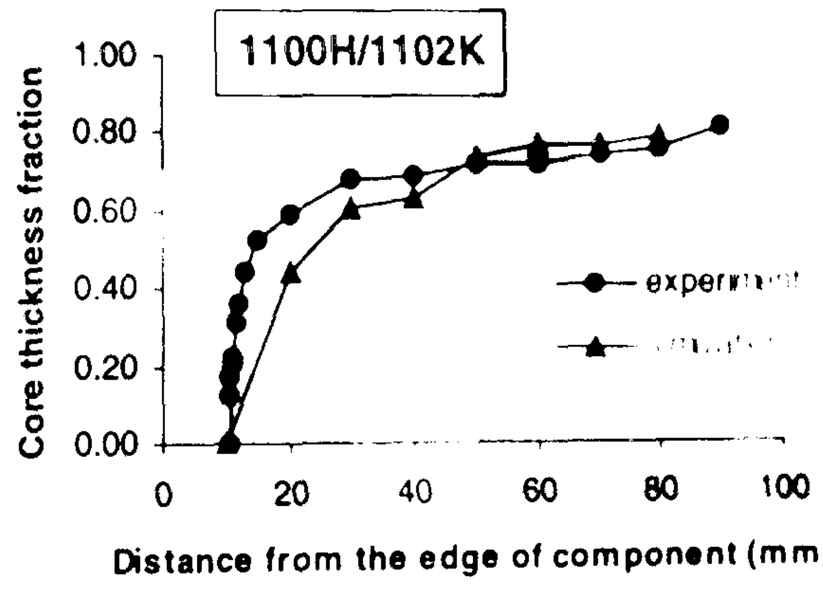

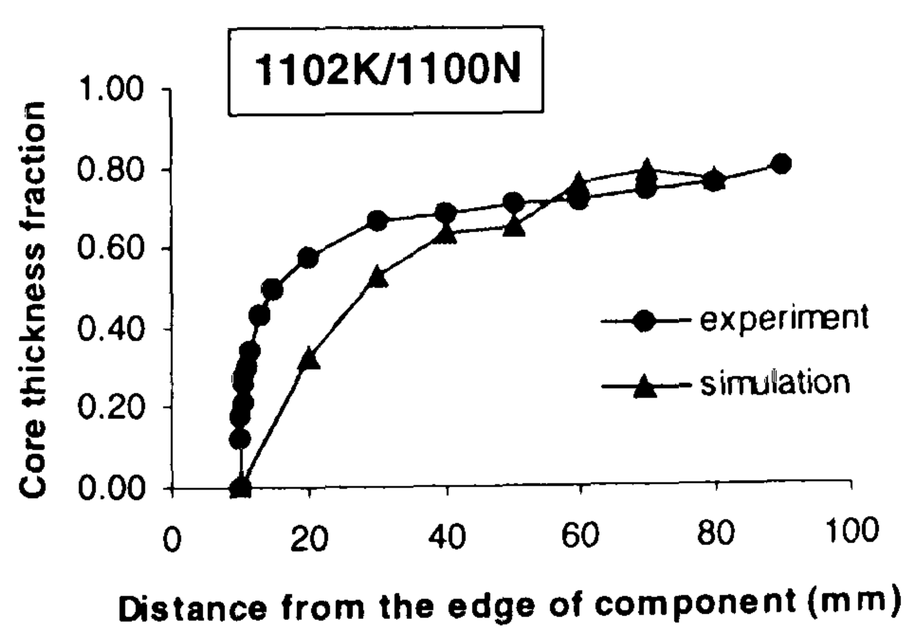

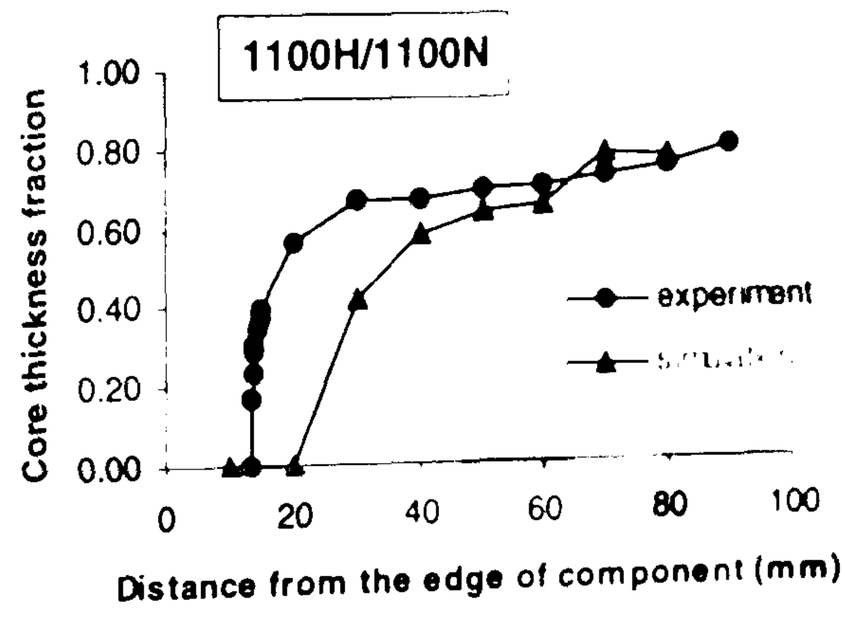

Appendix V.3 Core thickness fractions of PP(skin)/PP(core) moulding component.

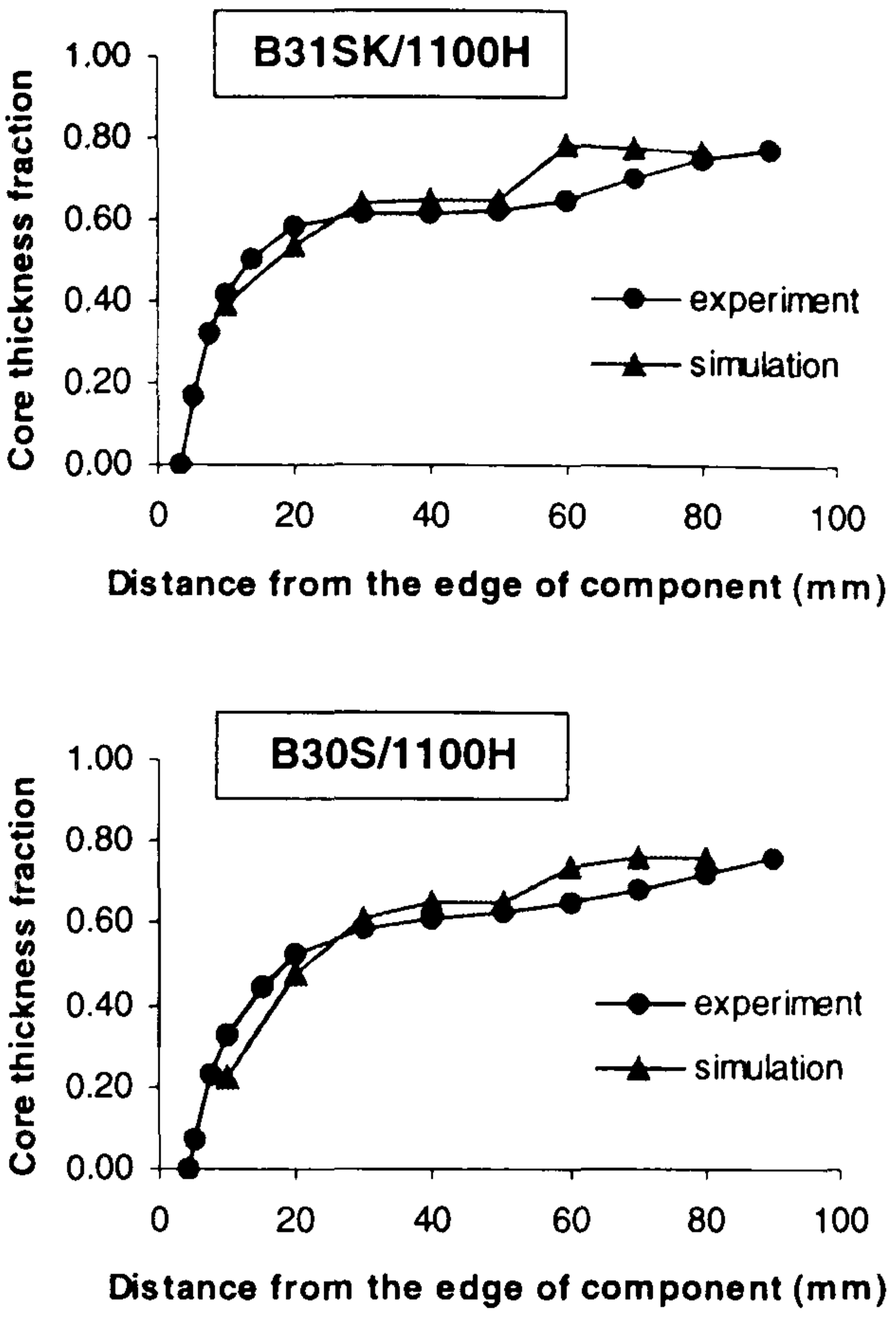

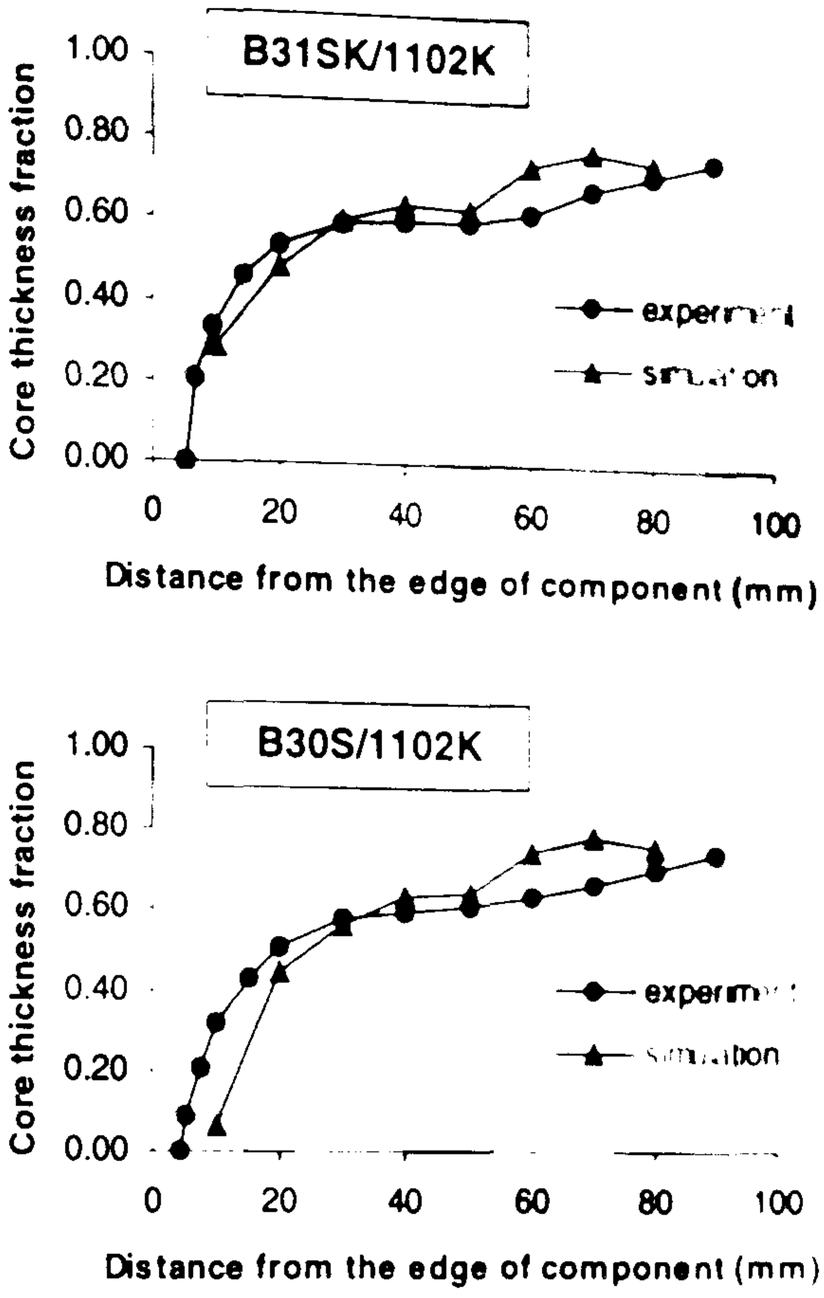

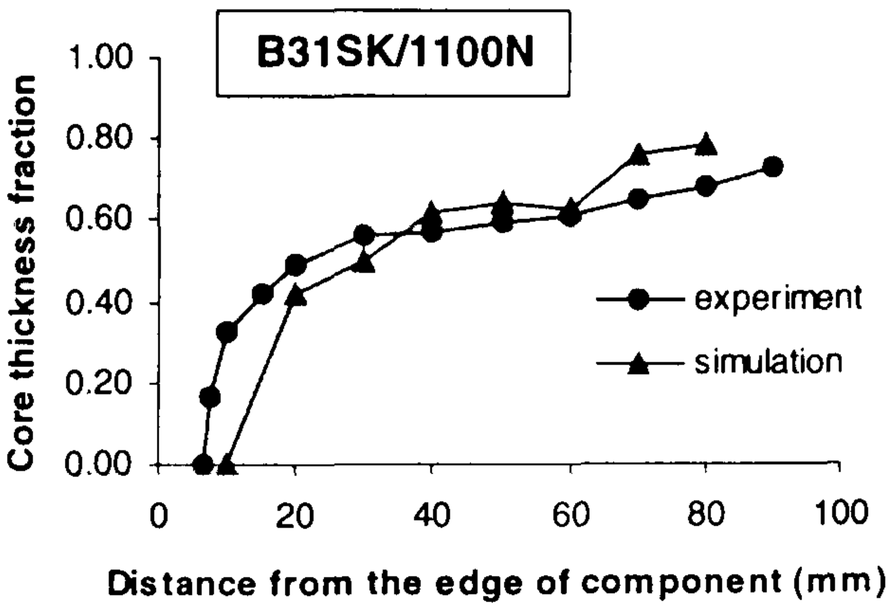

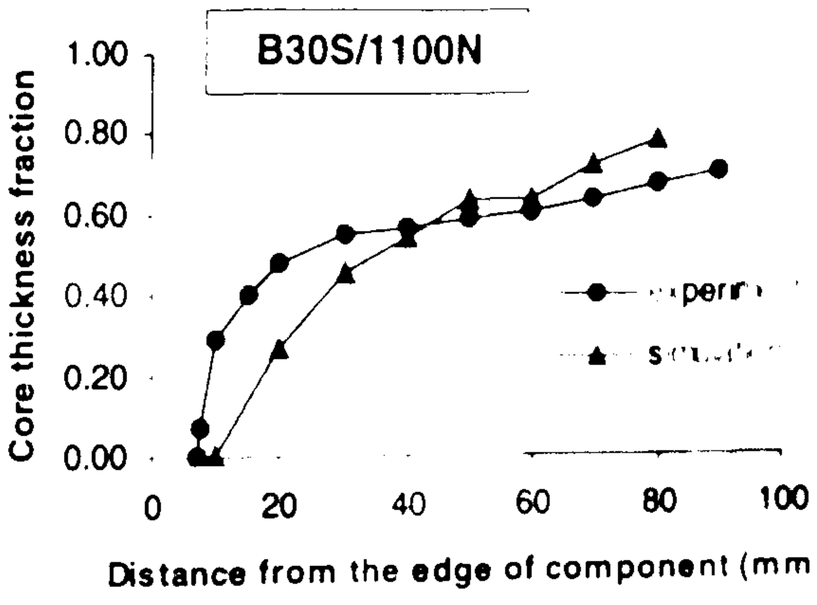

Appendix V.4 Core thickness fractions of PA6(skin)/PP(core) moulding component.

Appendix VI

Thickness Fractions and Peel Tests of The Moulding Components of PA6 (Durethan/B31SK) and PP (Novolen/1102K) with Compatibiliser at Various Simultaneous Injection Times (TOL)

In the case of PA6 (Durethan/B31SK) as skin and PP (Novolen/1102K) with compatibiliser as core material, core thickness fractions and peel strengths of the moulding components are measured by using Image processing software and peel test as mentioned in Chapter VI. The results are shown as seen in Figure APVI.1-APVI.6.

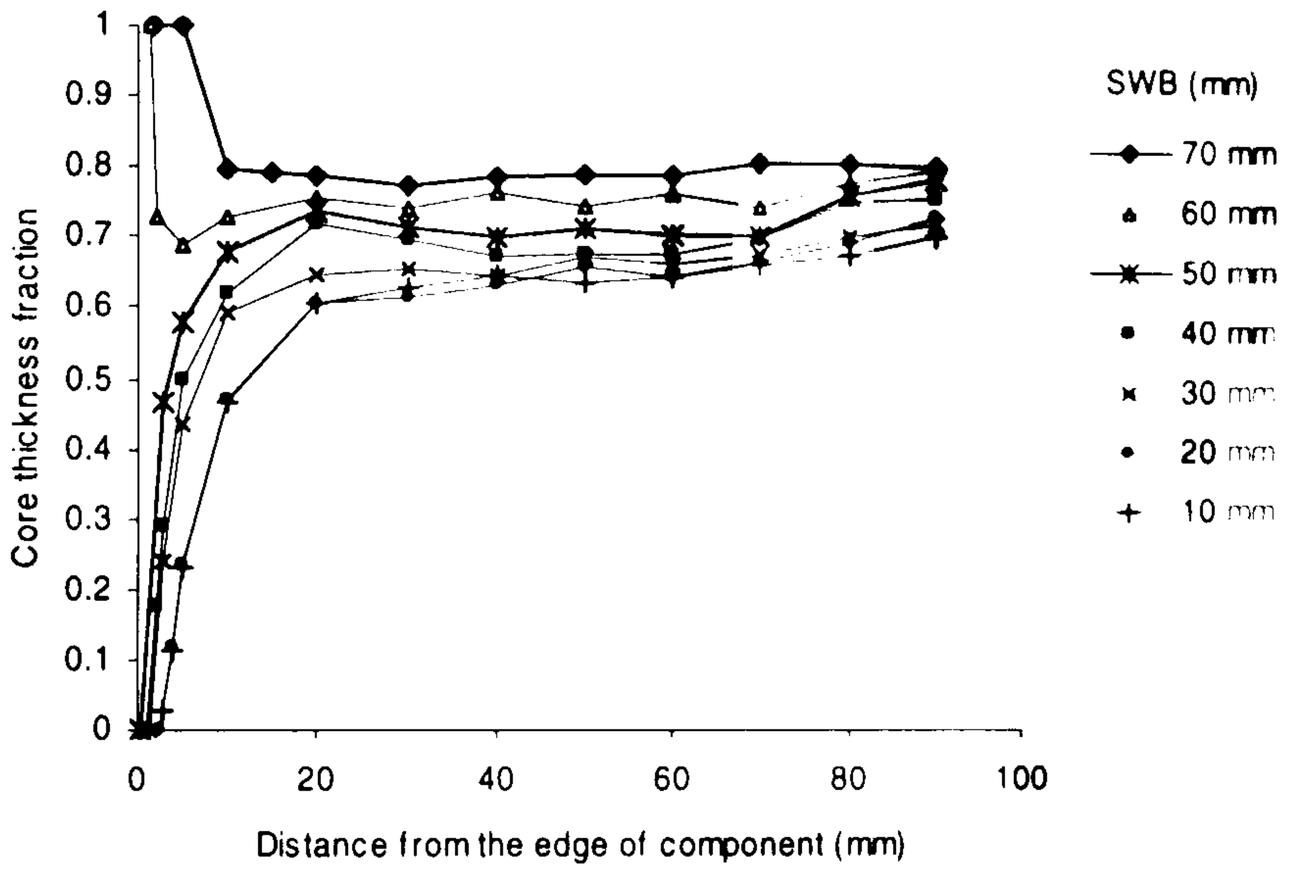

(a)

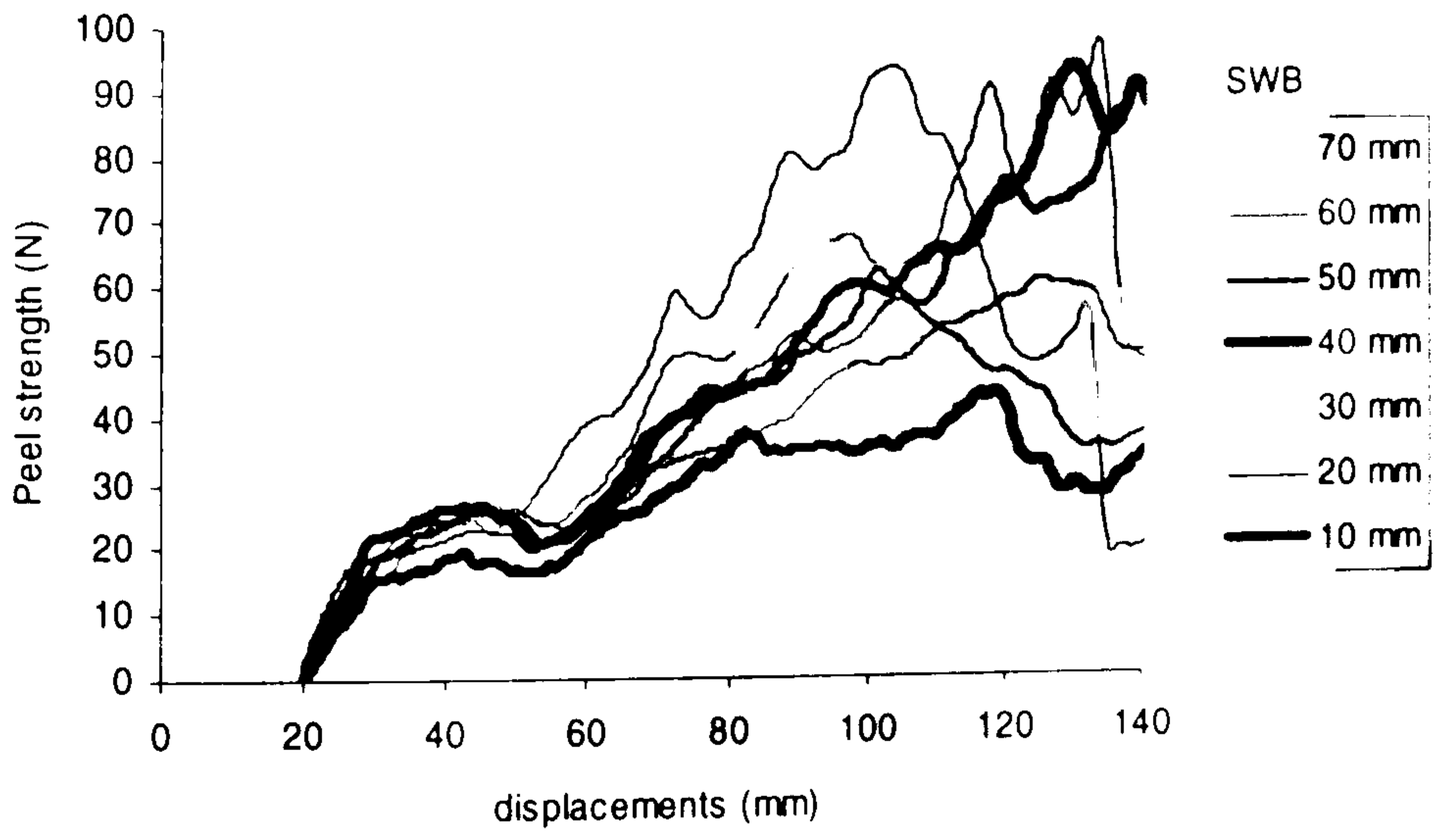

(b)

Figure APVI.1 (a) core thickness fraction and (b) peel strength curves at various simultaneous injection times (TOL): TDB = 0.0 second

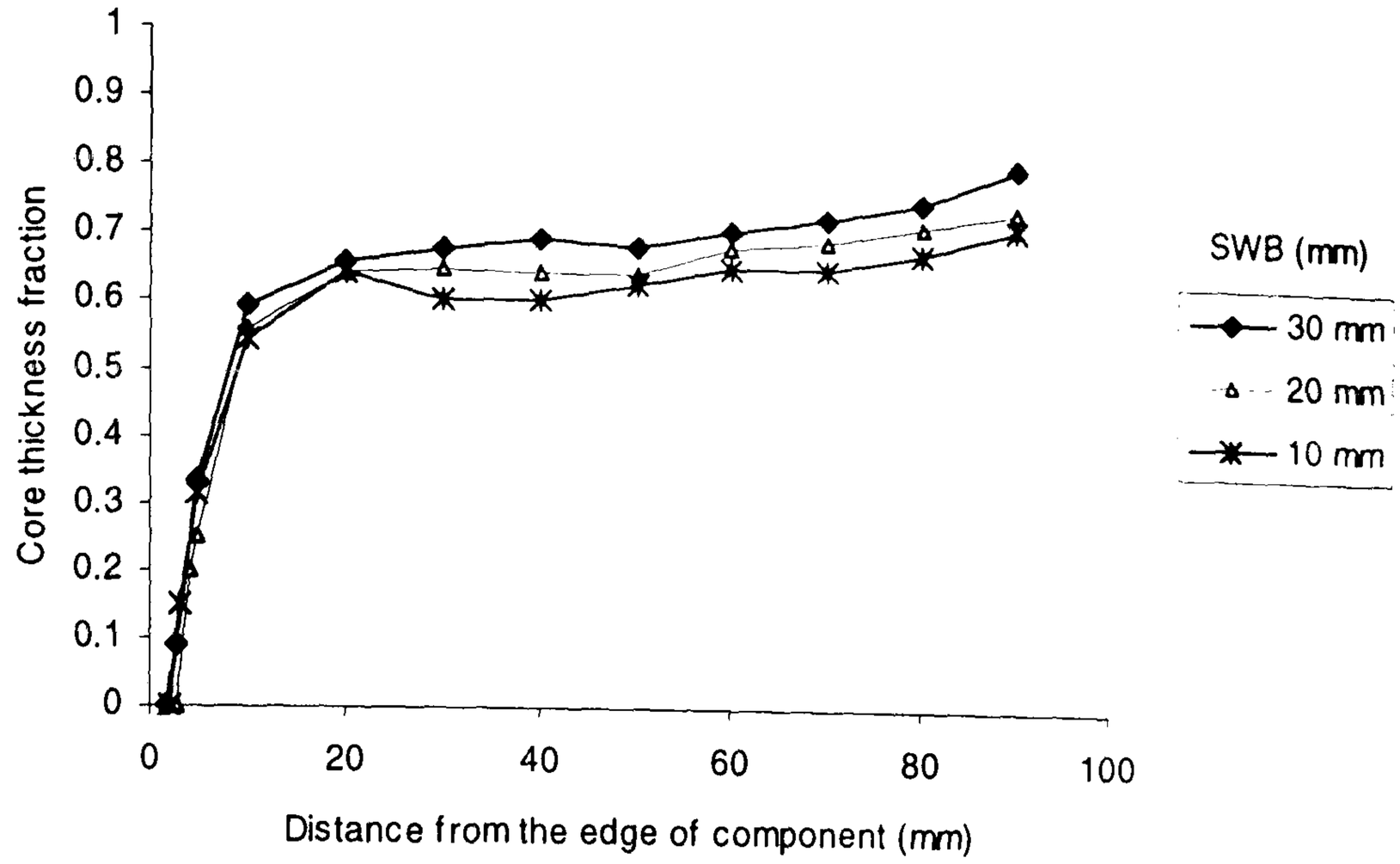

(a)

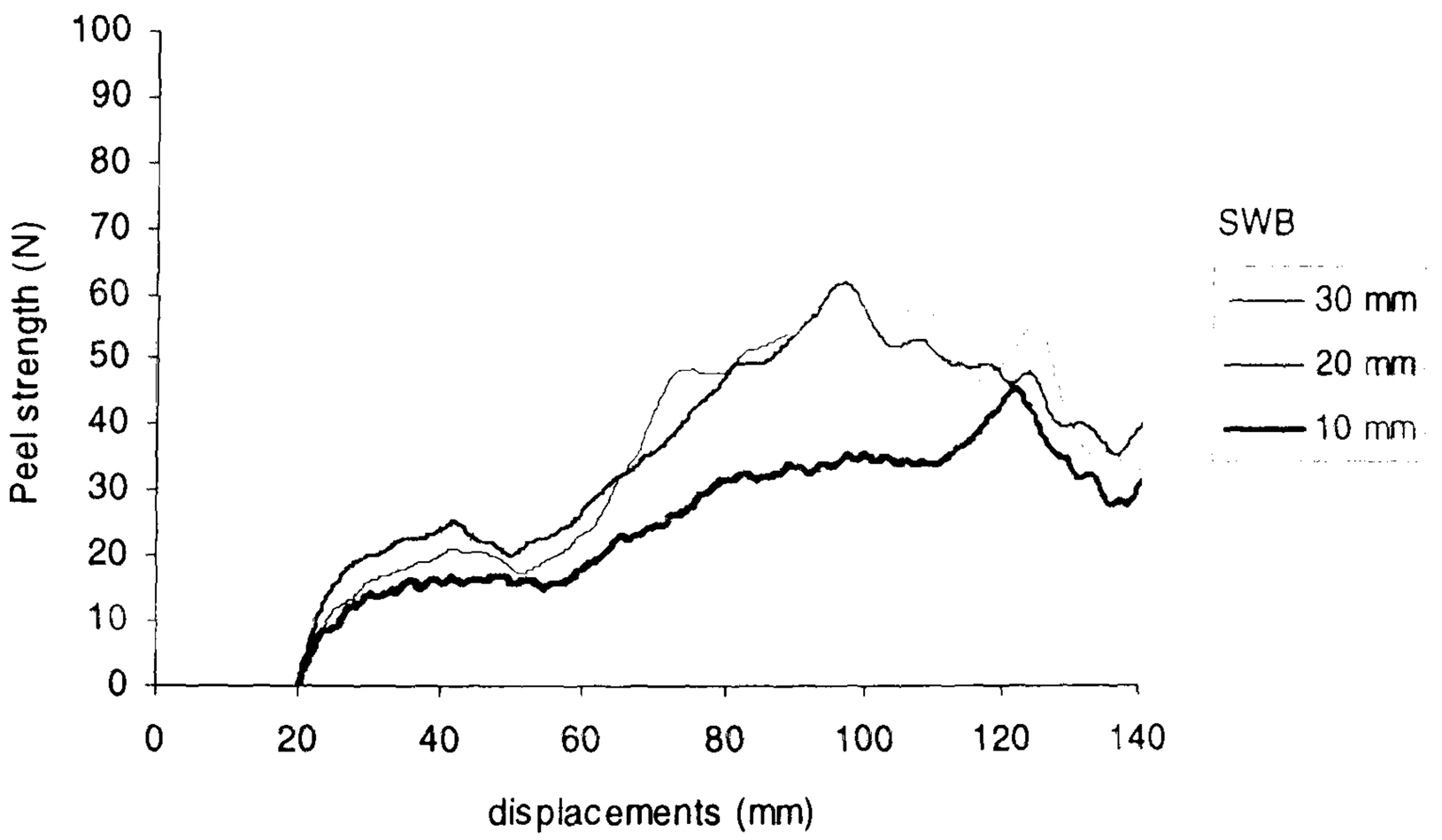

(b)

Figure APVI.2 (a) core thickness fraction and (b) peel strength curves at various simultaneous injection times (TOL): TDB = 0.1 second

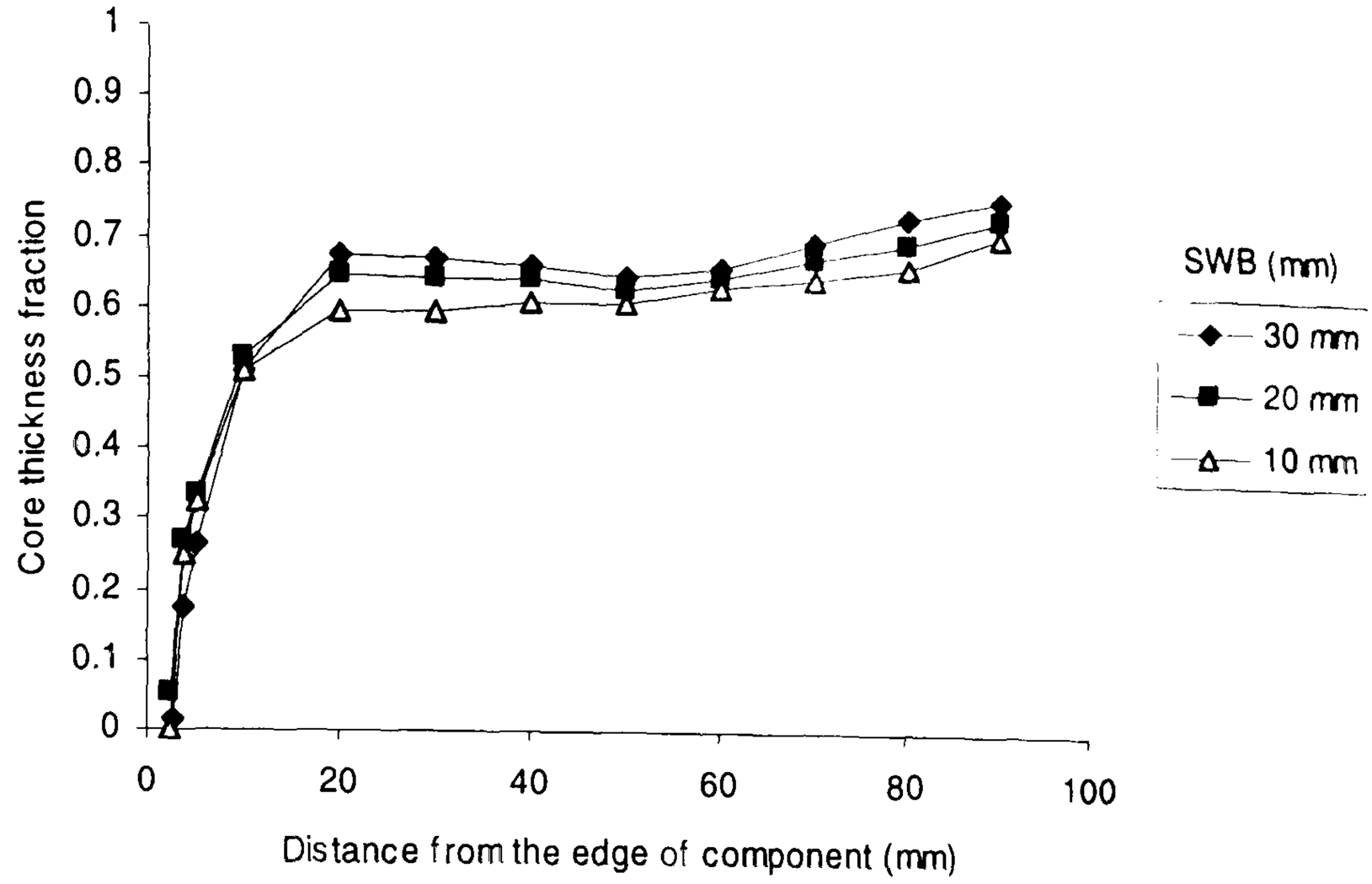

(a)

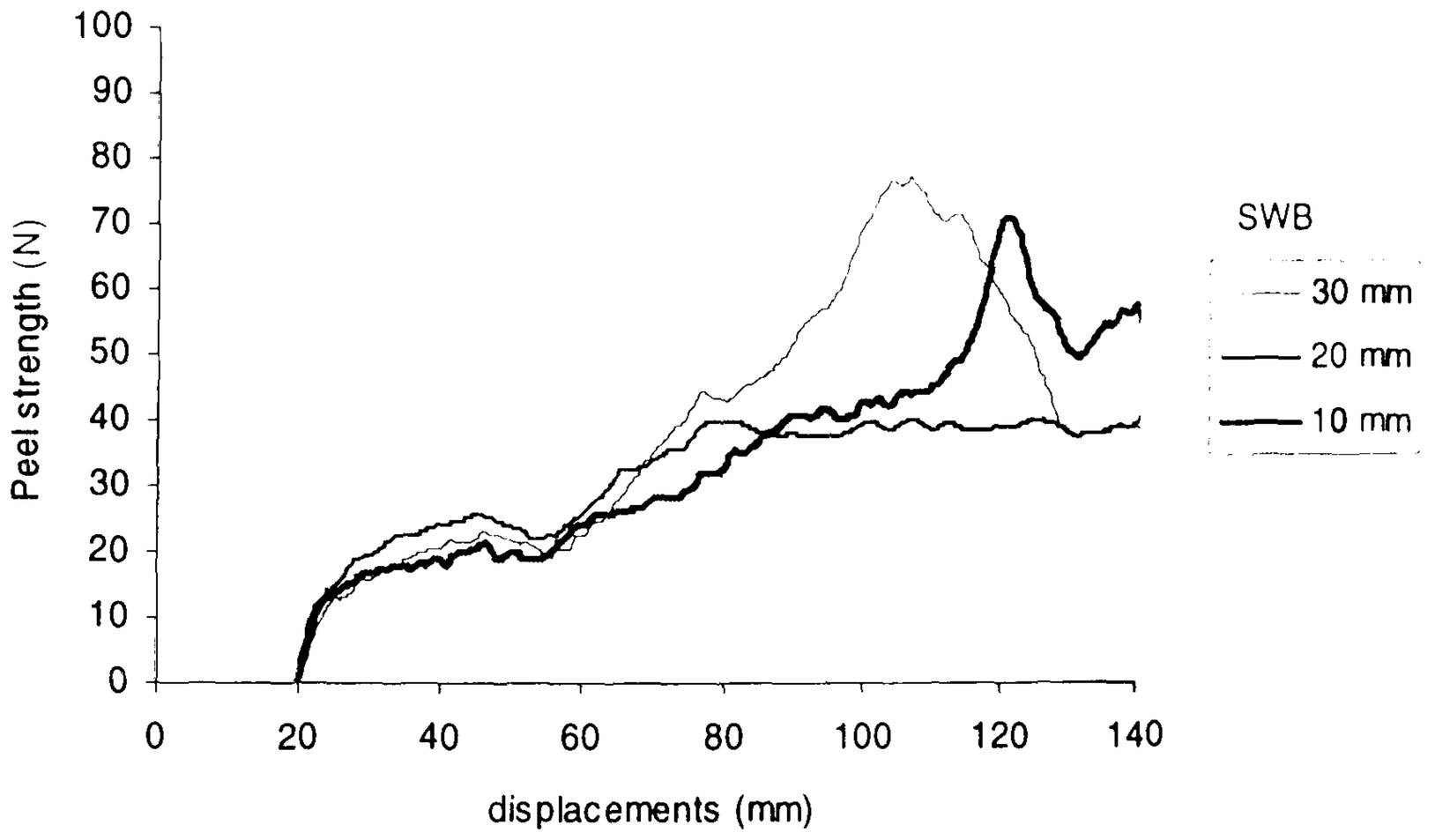

(b)

Figure APVI.3 (a) core thickness fraction and (b) peel strength curves at various simultaneous injection times (TOL): TDB = 0.2 second

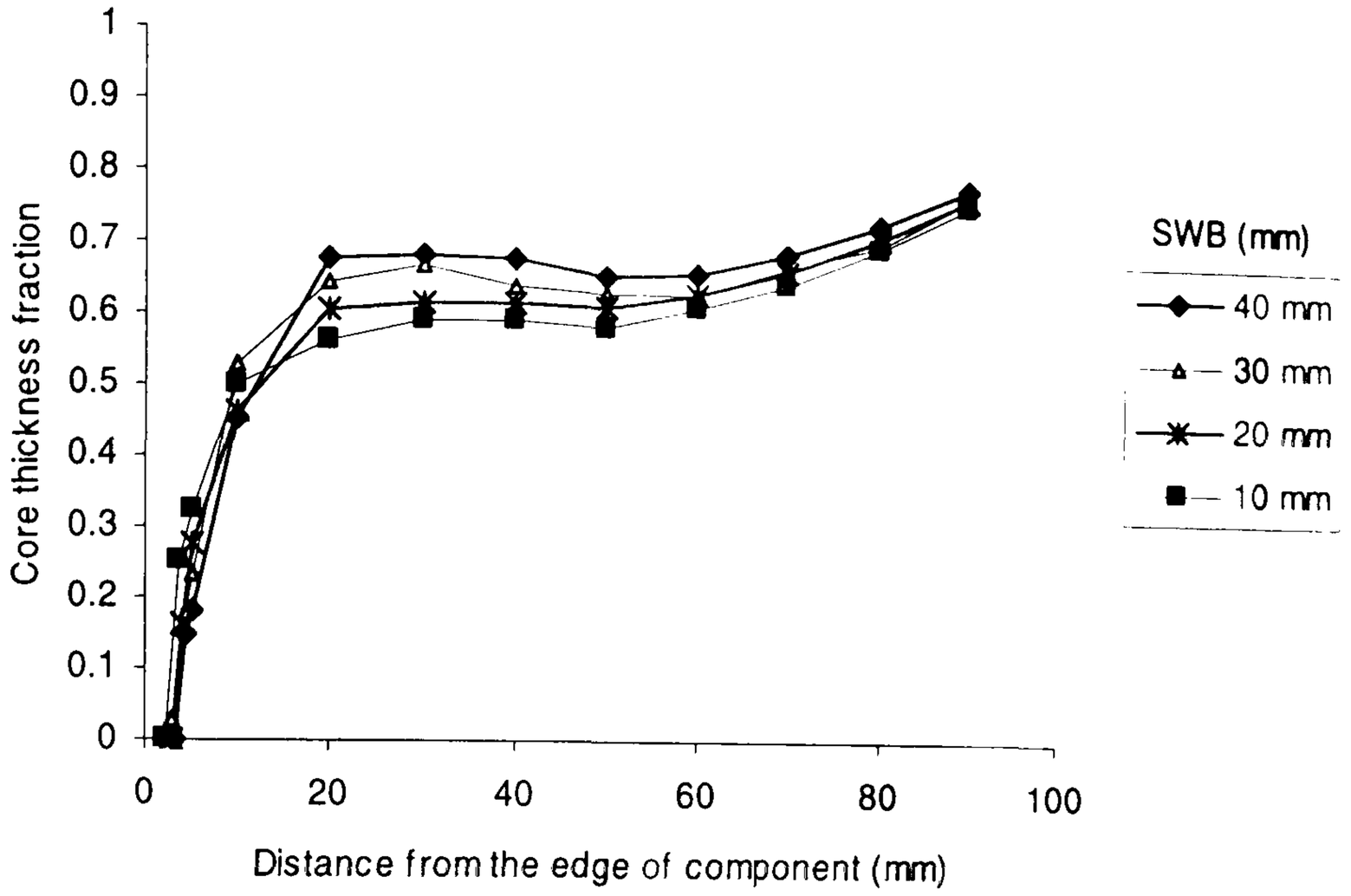

(a)

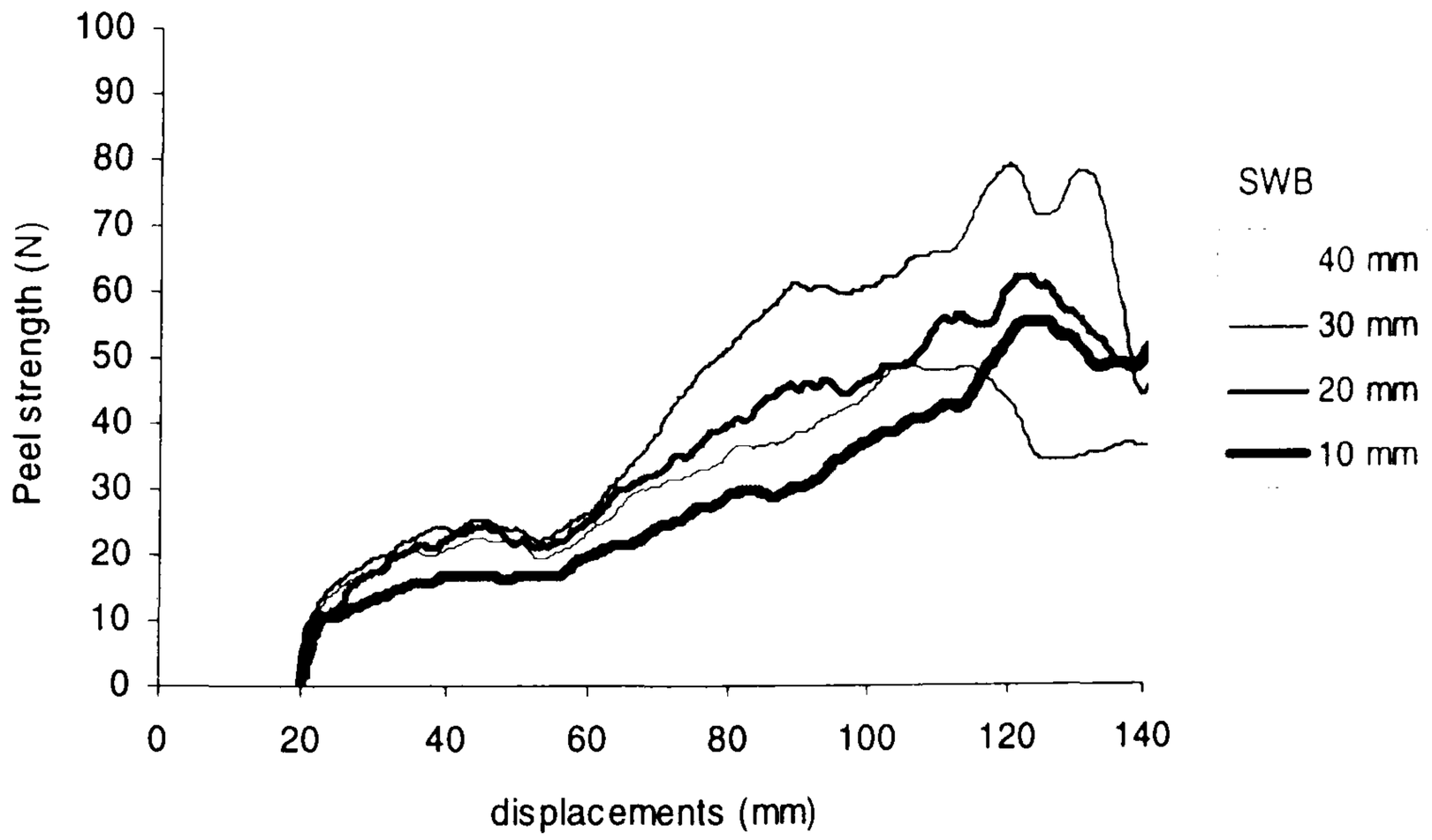

(b)

Figure APVI.4 (a) core thickness fraction and (b) peel strength curves at various simultaneous injection times (TOL): TDB = 0.3 second

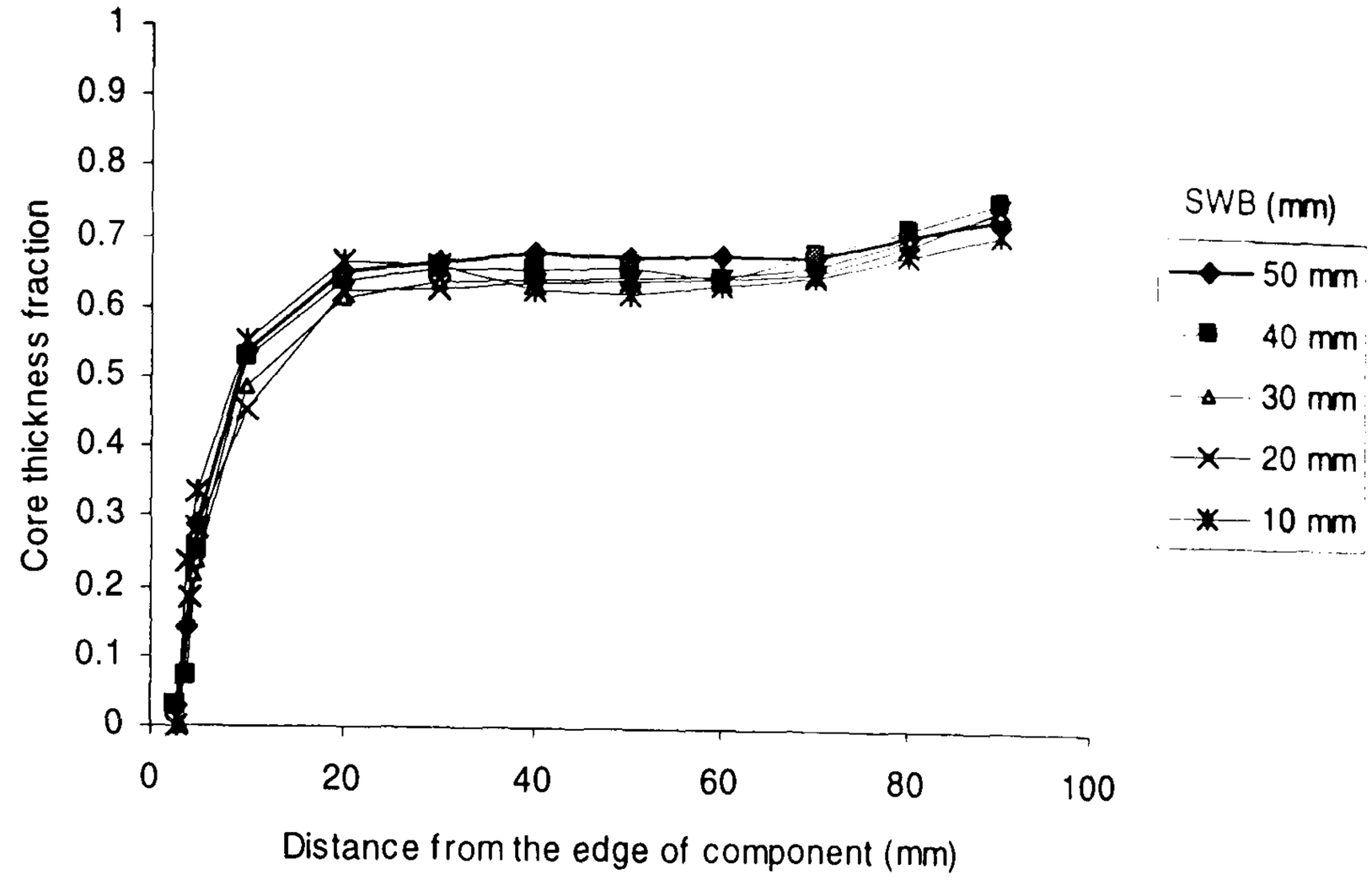

(a)

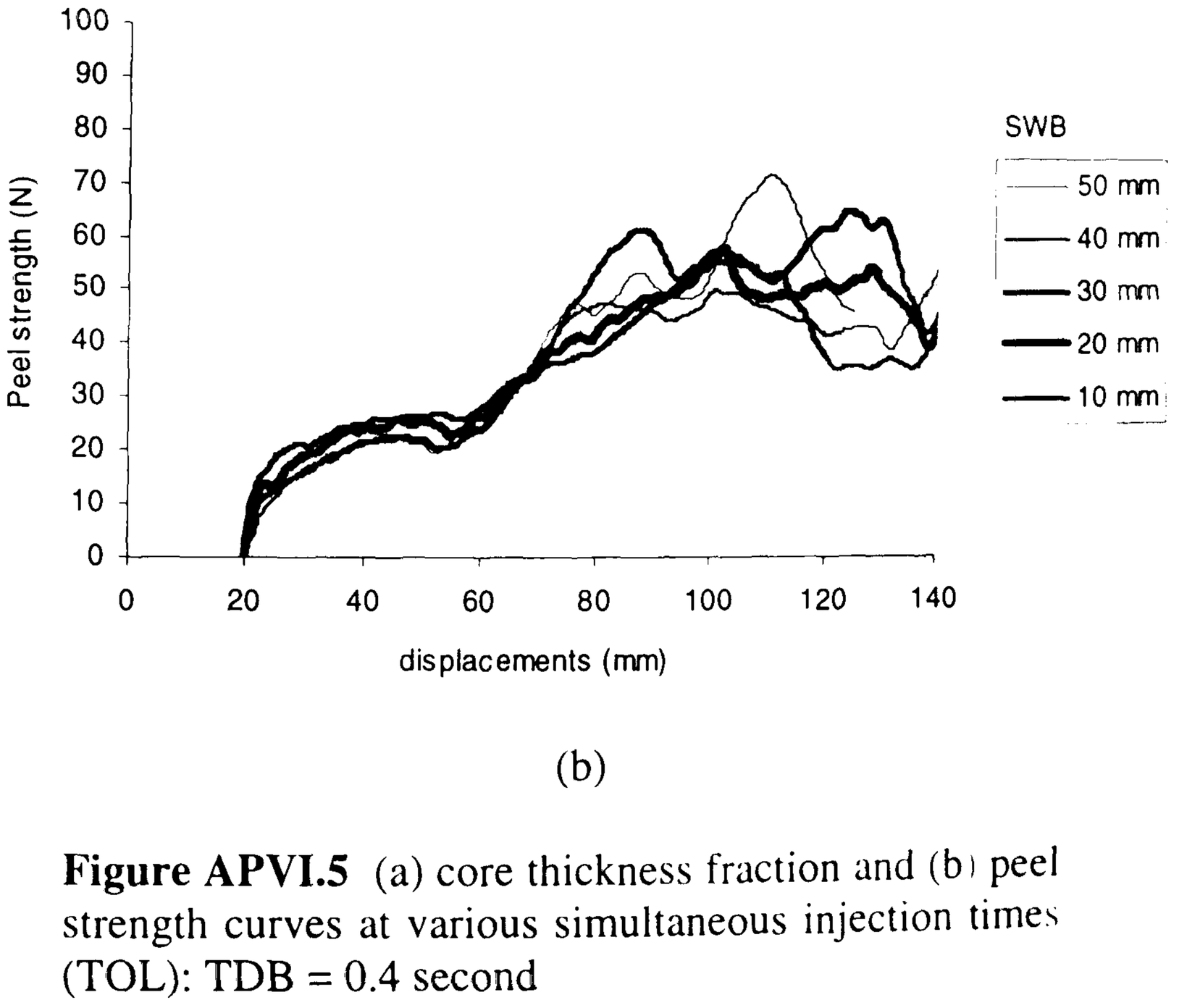

(b)

Figure APVI.5 (a) core thickness fraction and (b) peel strength curves at various simultaneous injection times (TOL): TDB = 0.4 second

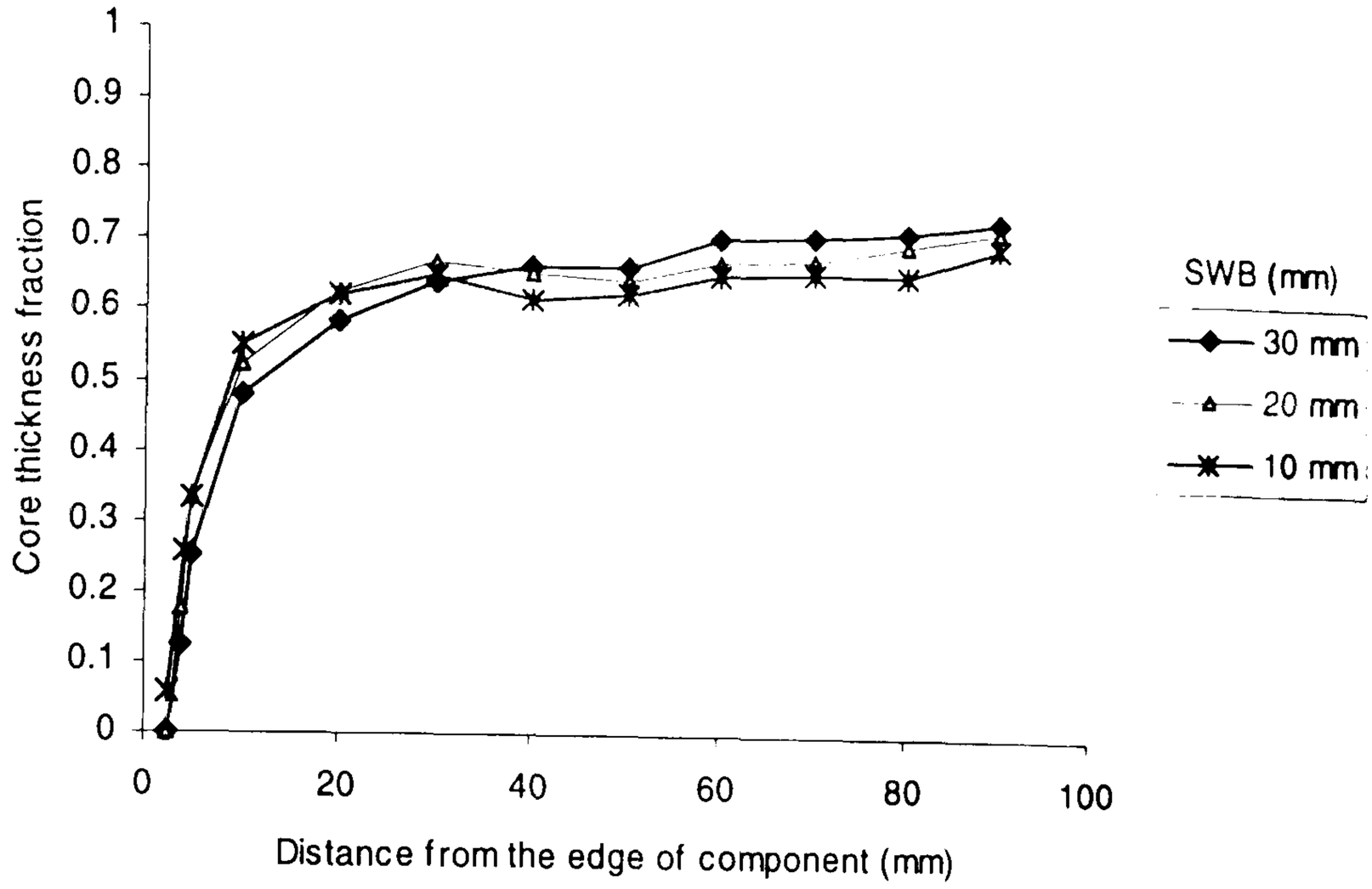

(a)

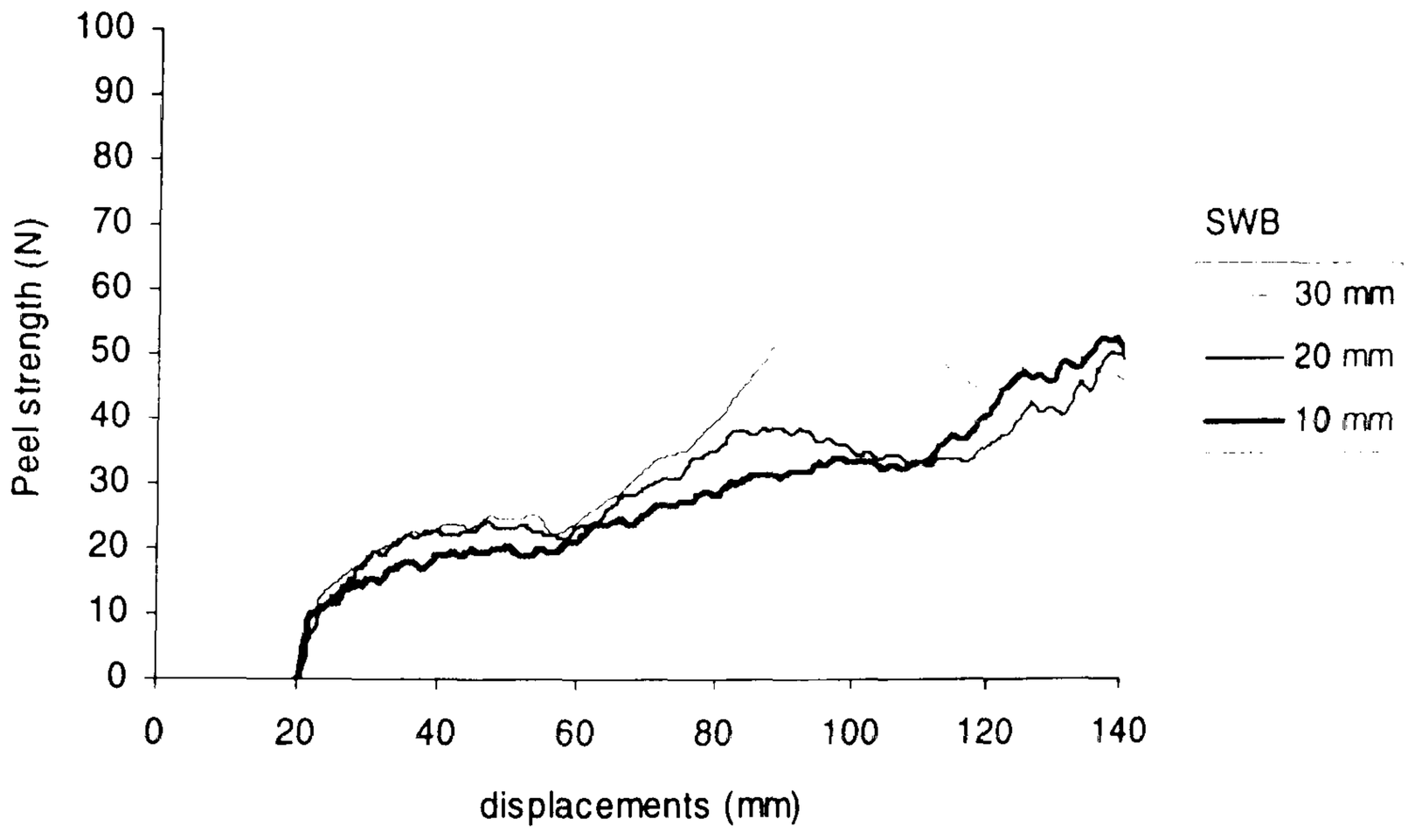

(b)

Figure APVI.6 (a) core thickness fraction and (b) peel strength curves at various simultaneous injection times (TOL): TDB = 0.5 second

Table APVI.1 Photos of the moulding components from experimental no.6

Data no.	TDB (s)	SWB (mm)	TOL (s)	Filling results
1	0.0	70.0	0.6140	
2	0.0	60.0	0.5263	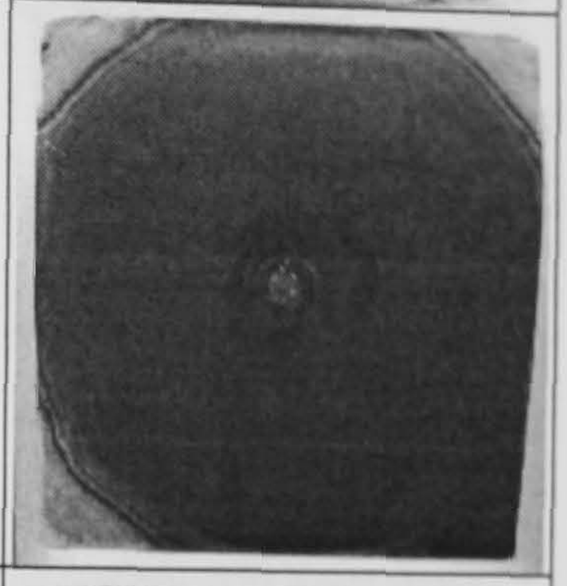
3	0.0	50.0	0.4386	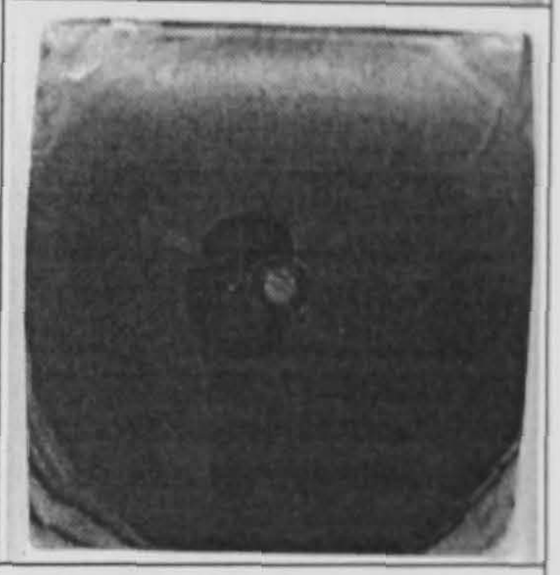
4	0.0	40.0	0.3509	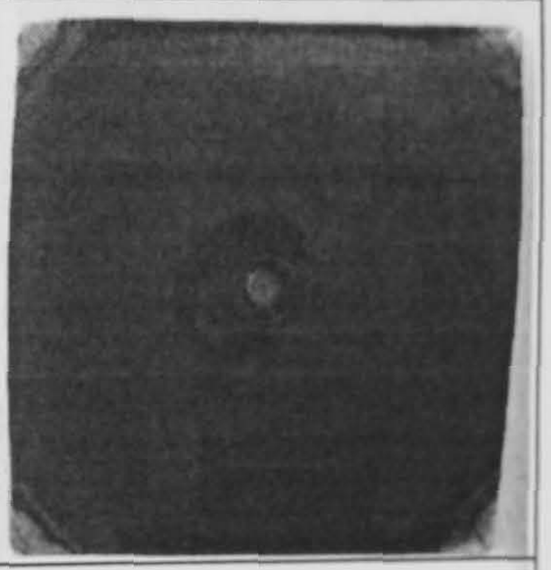
5	0.0	30.0	0.2632	

(Table APVI.1 continue)

Data no.	TDB (s)	SWB (mm)	TOL (s)	Filling results
6	0.0	20.0	0.1754	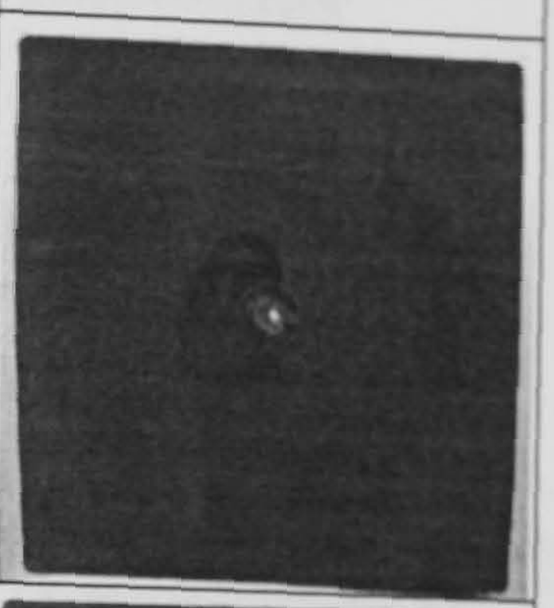
7	0.0	10.0	0.0877	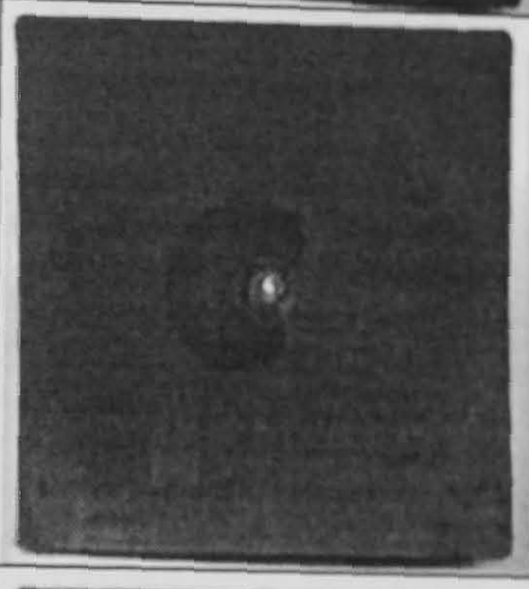
8	0.1	30.0	0.1632	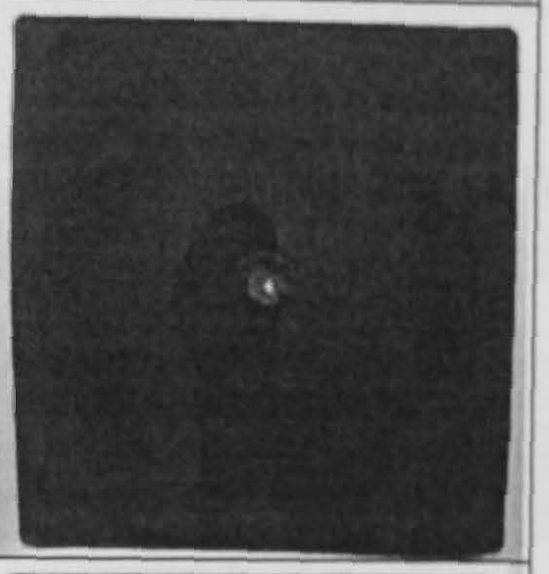
9	0.1	20.0	0.0754	
10	0.1	10.0	-0.0123	
11	0.2	30.0	0.0632	
12	0.2	20.0	-0.0246	
13	0.2	10.0	-0.1123	
14	0.3	40.0	0.0509	
15	0.3	30.0	-0.0368	
16	0.3	20.0	-0.1246	
17	0.3	10.0	-0.2123	No core breakthrough (results were similar as seen in photo of data no.9)
18	0.4	50.0	0.0386	
19	0.4	40.0	-0.0491	
20	0.4	30.0	-0.1368	
21	0.4	20.0	-0.2246	
22	0.4	10.0	-0.3123	
23	0.5	30.0	-0.2368	
24	0.5	20.0	-0.3246	
25	0.5	10.0	-0.4123	

Appendix VII

Impact Test of PA6 and PP Moulding Components

Table APVII.1 Impact strength of PA6 (skin)/ PP (core) moulding systems.

Systems		Impact test			
		Without compatibiliser		With 10% compatibiliser	
		Core thickness fraction	Strength (N)	Core thickness fraction	Strength (N)
Effect of skin/core viscosity ratios					
(1)	B31SK/1100H	0.6250±0.0289	1799.5±29.22	0.6099±0.0127	3701.0±16.35
(2)	B31SK/1102K	0.6050±0.0060	2082.0±14.40	0.5931±0.0173	2632.0±46.58
(3)	B30S/1100H	0.6294±0.0015	1797.5±37.83	0.6268±0.0153	3615.5±5.97
(4)	B30S/1102K	0.6090±0.0112	1871.5±3.41	0.6268±0.0114	3272.5±137.21
(5)	B31SK/1100N	0.5963±0.0228	2263.5±94.57	0.5650±0.0230	1065.0±8.47
(6)	B30S/1100N	0.589±0.0197	2236.0±82.76	0.5490±0.0186	855.5±8.70
Effect of skin injection speeds					
(1)	64 mm/s	0.6510±0.0323	2126.0±64.30	0.6569±0.0160	3693.5±166.21
(2)	114 mm/s	0.6350±0.0167	2010.0±43.99	0.6522±0.0017	2914.0±64.46
(3)	164 mm/s	0.6050±0.0035	2049.0±102.33	0.6715±0.0215	3915.5±1.84
Effect of core injection speeds					
(1)	85 mm/s	0.5540±0.0064	2866.0±97.87	0.6383±0.0221	4246.0±77.67
(2)	135 mm/s	0.5970±0.0013	2069.5±102.32	0.6520±0.0043	3219.0±122.52
(3)	185 mm/s	0.6130±0.0122	2191.0±34.83	0.6600±0.0144	3015.5±136.89
Effect of core switch-over					
(1)	35 mm	0.5880±0.0235	2129.5±86.37	0.6570±0.0187	3359.0±84.90
(2)	25 mm	0.6014±0.0088	2107.5±2.05	0.6340±0.0220	3738.0±73.06
(3)	15 mm	0.6204±0.0190	2324.0±2.57	0.6197±0.0066	3819.5±0.59
(4)	6 mm	0.5141±0.0252	2835.5±140.76	0.5493±0.0199	4788.0±215.70
Effect of skin/core metering stroke ratios					
(1)	52 %	0.6640±0.0186	2136.0±70.64	0.6815±0.0025	2862.0±91.57
(2)	56 %	0.6000±0.0055	2167.5±24.22	0.6500±0.0154	3129.5±93.20
(3)	60 %	0.5890±0.0049	2454.0±107.23	0.6304±0.0271	2986.0±122.90
(4)	64 %	0.5530±0.0201	2482.0±80.51	0.6241±0.0213	3763.5±51.71
Effect of skin melt temperatures					
(1)	250 °C	0.6230±0.0257	2021.0±39.37	0.6571±0.0166	3152.5±154.99
(2)	260 °C	0.6480±0.0060	2107.5±104.73	0.6522±0.0109	3219.0±145.66
(3)	270 °C	0.6154±0.0088	2226.0±10.15	0.6490±0.0148	3431.5±145.40
Effect of core melt temperatures					
(1)	225 °C	0.6250±0.0310	2336.0±100.27	0.6400±0.0063	3501.5±161.70
(2)	235 °C	0.6480±0.0263	2207.5±18.09	0.6522±0.0260	3219.0±7.81
(3)	245 °C	0.6338±0.0227	2223.5±109.06	0.6670±0.0033	2811.0±116.42
Effect of tool temperatures					
(1)	40.0 °C	0.6310±0.0162	2177.0±15.88	0.6519±0.0305	4017.0±167.63
(2)	60.5 °C	0.6220±0.0211	1908.5±7.58	0.6418±0.0122	3838.5±183.67
(3)	80.5 °C	0.6480±0.0285	2247.0±27.50	0.6522±0.0208	3875.0±110.24
(4)	100.5 °C	0.6340±0.0214	2162.0±90.10	0.6470±0.0270	3999.5±93.51

Appendix VIII

POLYMER ADHESIONS DURING COINJECTION

PART 1:- PBT(SKIN) AND PP(CORE)

Rungseesantivanon W. and Smith G. F.

Advanced Technology Centre (ATC)
School of Engineering, Faculty of Science,
University of Warwick, Coventry CV4 7AL, UK

Introduction

This works was based on the development of granular injection paint technology (GIPT) [1] using simultaneous co-injection moulding process [2-8]. Selection of raw materials for use as skin or core of the sandwich moulding depended on the properties required of the final part. Care had to be taken in order to ensure that the selected two materials would adhere to each other during the moulding phase. There were several studies on the combination of incompatible polymers incorporating compatibilisers, such as those utilising maleic anhydride grafted polypropylene (PP-g-MA) to interface polyamide (PA) with polypropylene (PP) [9-17]. However, the purpose of this study was to investigate and understand the suitable condition for the combination of polybutylene terephthalate (PBT) and PP. The main problem which had to be overcome was interfacial adhesion when moulding incompatible material, compatibilisers were used to promote this bond. The main objective was to investigate the mechanism, which produces good adhesion of incompatible skin and core materials (PBT and PP).

Methodology

A Battenfeld co-injection moulding machine series BMT-1100/2x300 controlled with the UNILOG 9000 system was used in this study. A rectangular plaque mould with cavity dimension 150 x 150 x 3 mm fed via fan gate which was readily available was used in these and other studies. PP (Novolen 1102K) and PBT (TPE Arnitel PL380) were used as core and skin materials, respectively. Their viscosity data was obtained from materials supplier database (C-MOLD). Elf-Atochem Lotader Ax8900 and Uniroyal Polybond G3200 were used as compatibilisers. The combinations of PBT and PP with or without compatibilisers are shown in Table 1. After remove the moulding components, they were cut with the dimension of 150x20 mm along the centre line. The specimens thickness were 3.0±0.1 mm, precisely. Before performing the peel test, the specimens had to initiate the peel skin layer of 10 mm for clamping with grip (Figure 1), then applied load to measure the peel strength.

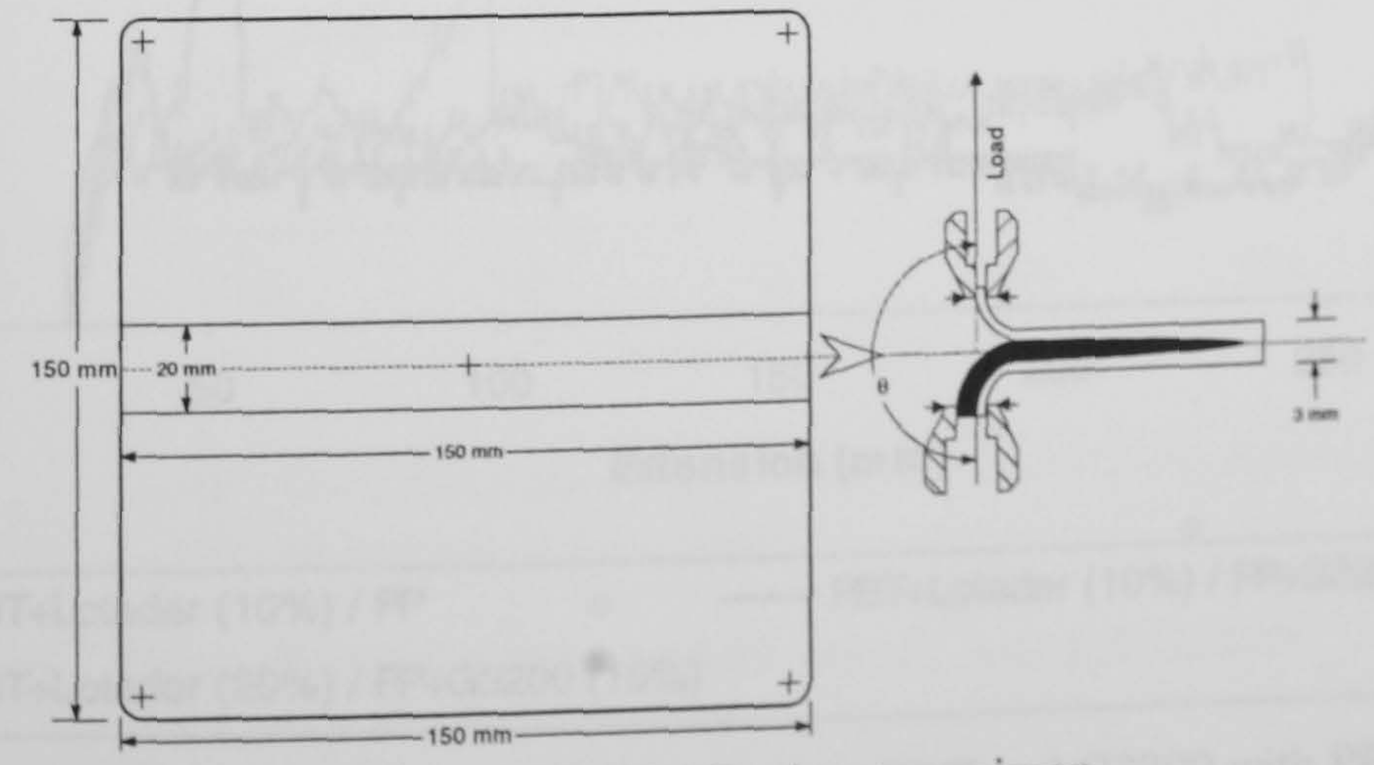

Figure APVIII.1 Peel test specimen

Table APVIII.1 Combinations of PBT and PP

Combinations	Skin	Core
1	PBT + Lotader (10%)	PP + G3200 (10%)
2	PBT + Lotader (20%)	PP + G3200 (10%)
3	PBT	PP + PBT (5%)
4	PBT	PP + PBT (10%)
5	PBT	PP + PBT (20%)
6	PBT	PP + PBT (30%)
7	PBT	PP + PBT (5%) + Lotader (5%)
8	PBT	PP + PBT (10%) + Lotader (5%)
9	PBT	PP + PBT (20%) + Lotader (5%)
10	PBT	PP + PBT (5%) + Lotader (10%)
11	PBT	PP + PBT (10%) + Lotader (10%)
12	PBT	PP + PBT (20%) + Lotader (10%)
13	PBT	PP + PBT (30%) + Lotader (10%)
14	PBT	PP + PBT (30%)
15	PBT	PP + PBT (30%) + Lotader (2.5%)
16	PBT	PP + PBT (30%) + Lotader (5%)
17	PBT	PP + PBT (30%) + Lotader (10%)
18	PBT	PP
19	PBT + Lotader (10%)	PP

Results and Discussions

It was found that when the mix was 10% Lotader into PBT (skin) together with a mix of 10% Polybond into PP (core), skin/core adhesion was achieved but at a low level and increasing Lotader up to 20% still did not improve adhesion level. It also found that Polybond G3200 had a small number of affect on skin/core adhesion of PBT/PP moulding components.

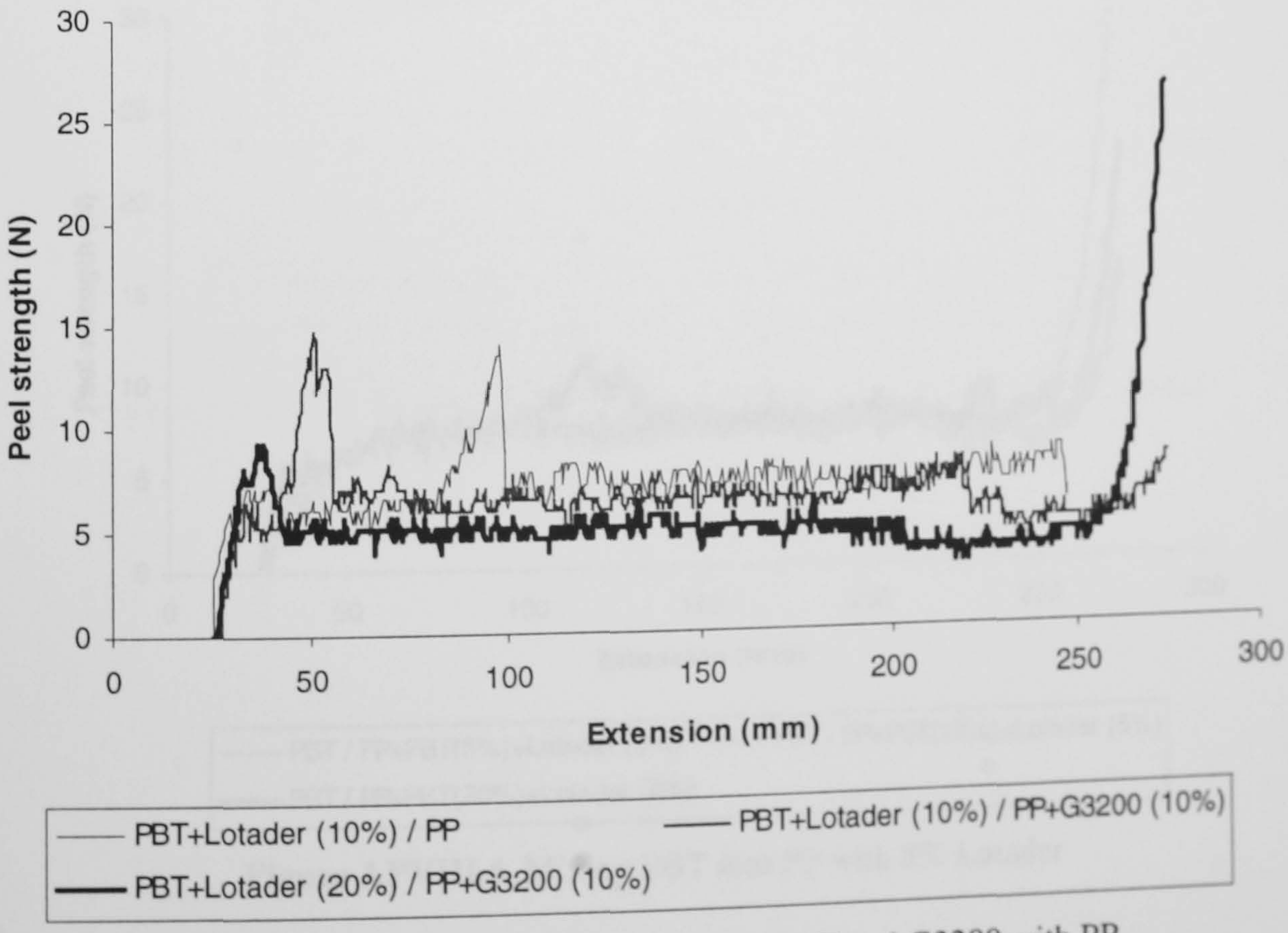

Figure APVIII.2 Mixing Lotader with PBT and G3200 with PP

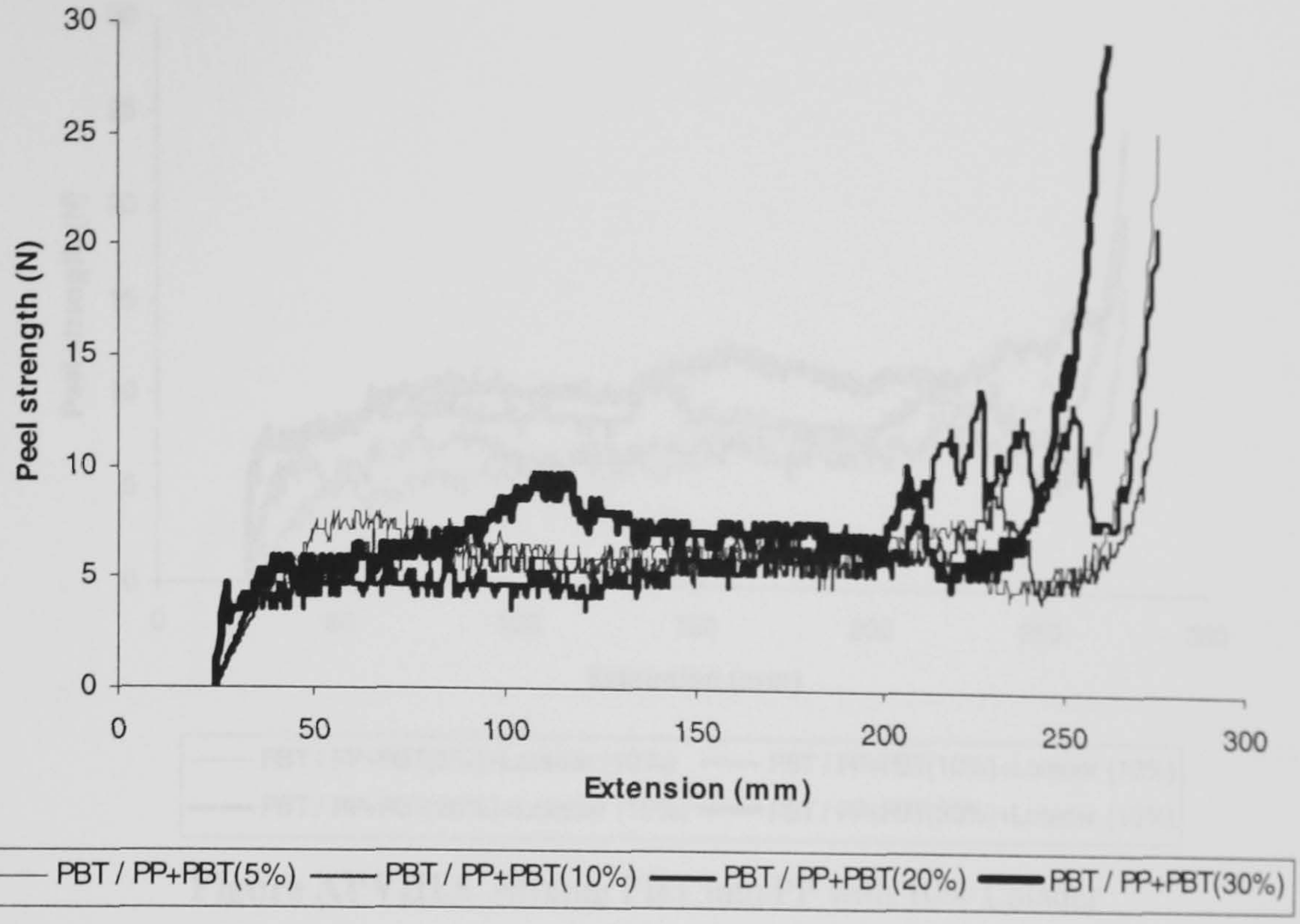

Figure APVIII.3 Mixing PBT into PP

The following experiments investigated the effect of an addition of PBT in to PP, effectively trying use PBT as compatibiliser. The adhesion affect was minimal. In the next experiments, it was found that the domain size of PBT blend with PP could be decreased when adding amounts of compatibiliser such as Lotader. It also found that the PBT/PP/Lotader mixture was a semi-miscible blend. Comparison effect of amout of Lotader and PBT in the core material are shown in Figures 3 to Figures 7.

It also found that the addition of 30% PBT and 10% Lotader into PP and its use as core polymer resulted in a significant increase in the peel strength which relates to skin/core adhesion, this can be shown if it is compared to the one without Lotader (figure 7). However, at 2.5% and 5% of Lotader (figure 6), peel strengths are not significant change.

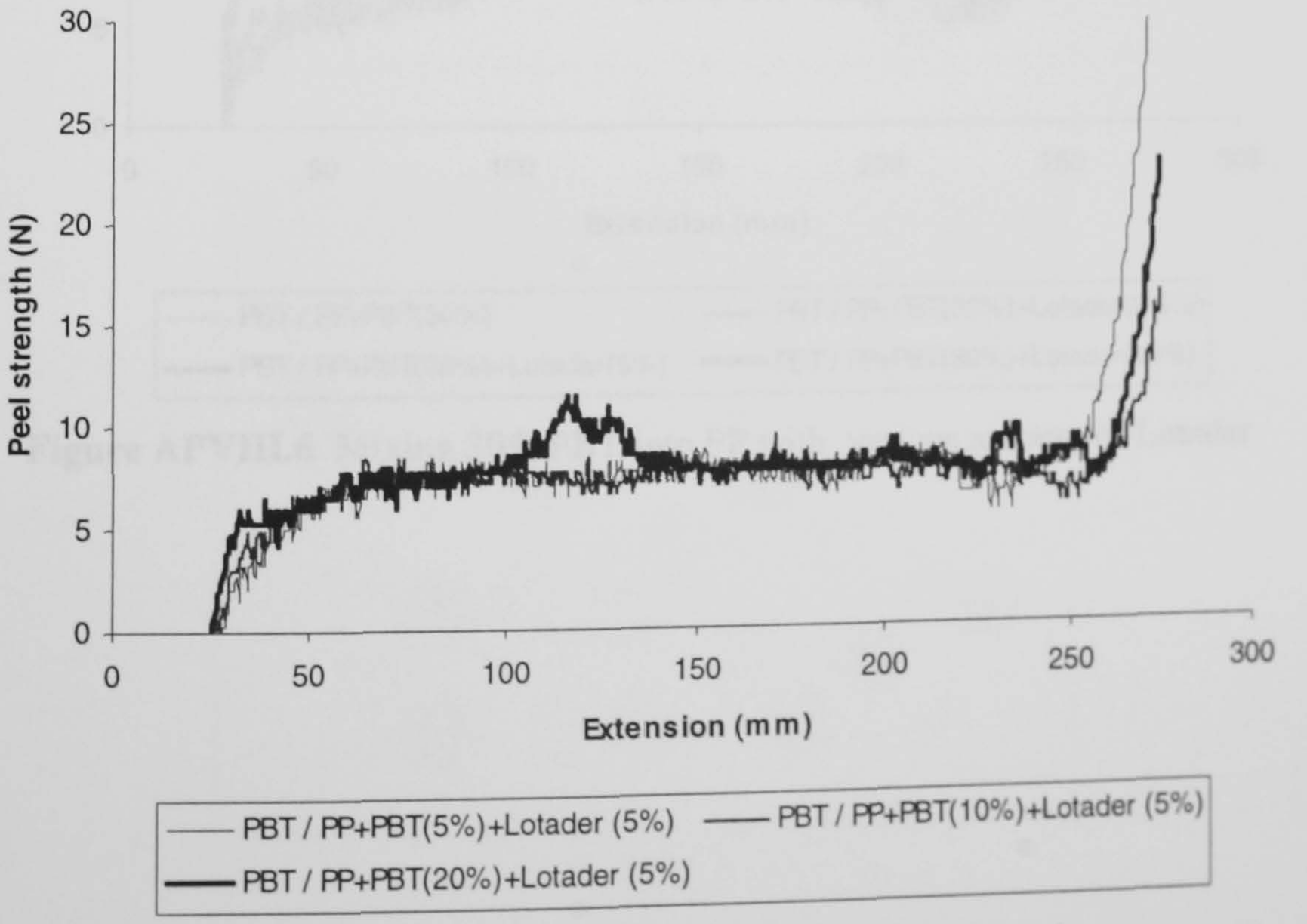

Figure APVIII.4 Mixing PBT into PP with 5% Lotader

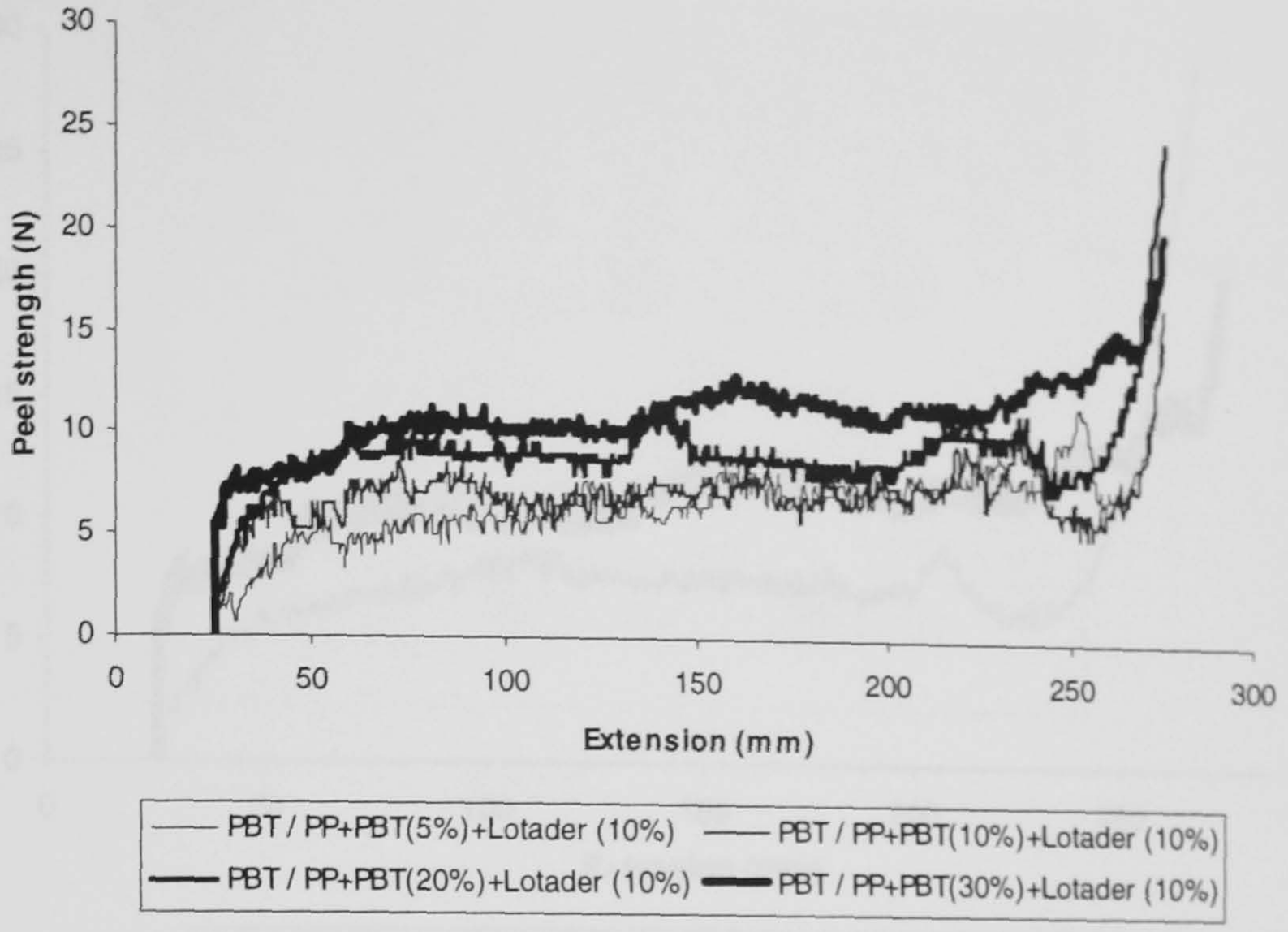

Figure APVIII.5 Mixing PBT into PP with 10% Lotader

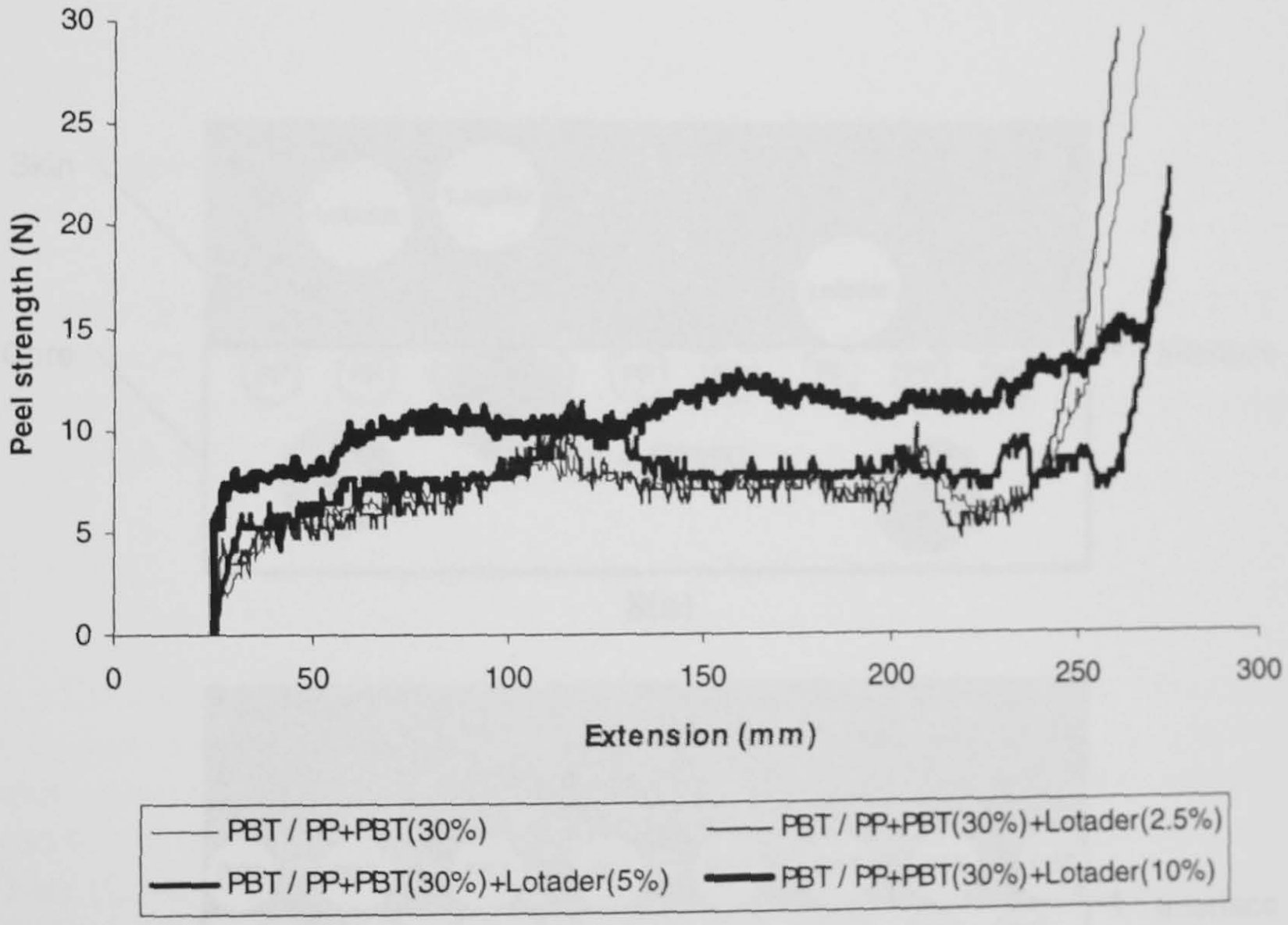

Figure APVIII.6 Mixing 30% PBT into PP with various amount of Lotader

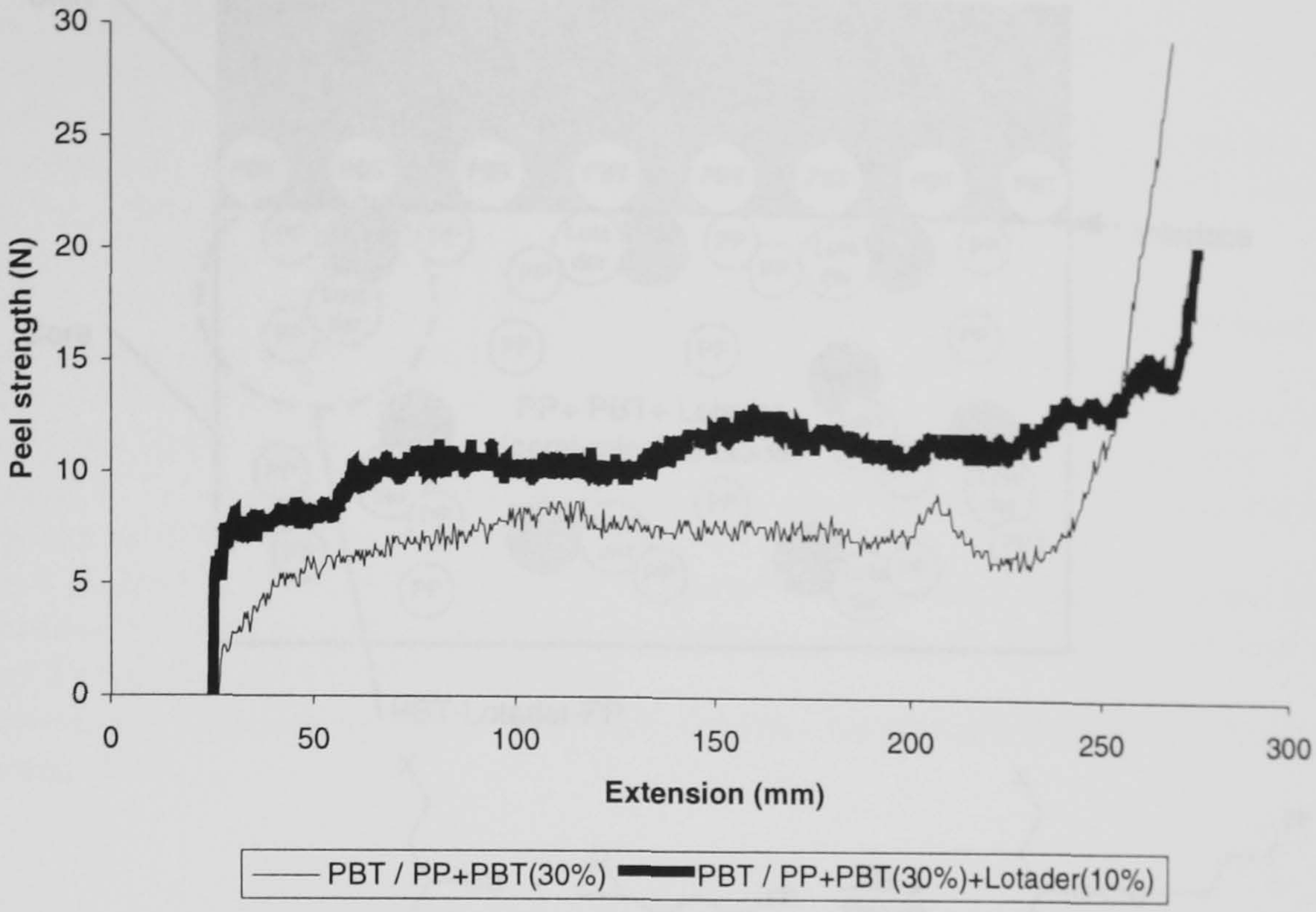

Figure APVIII.7 Effect of amount of Lotader

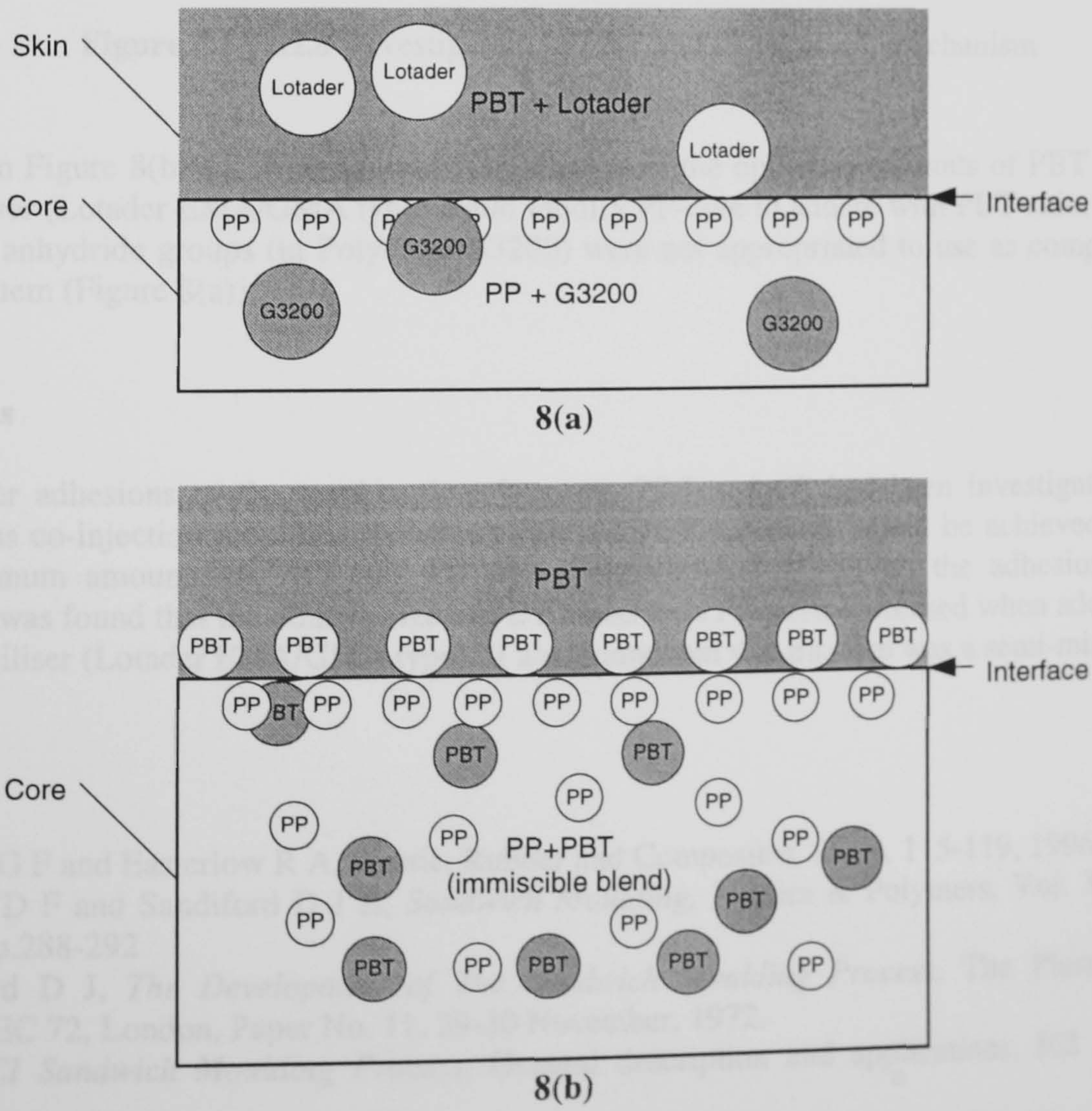

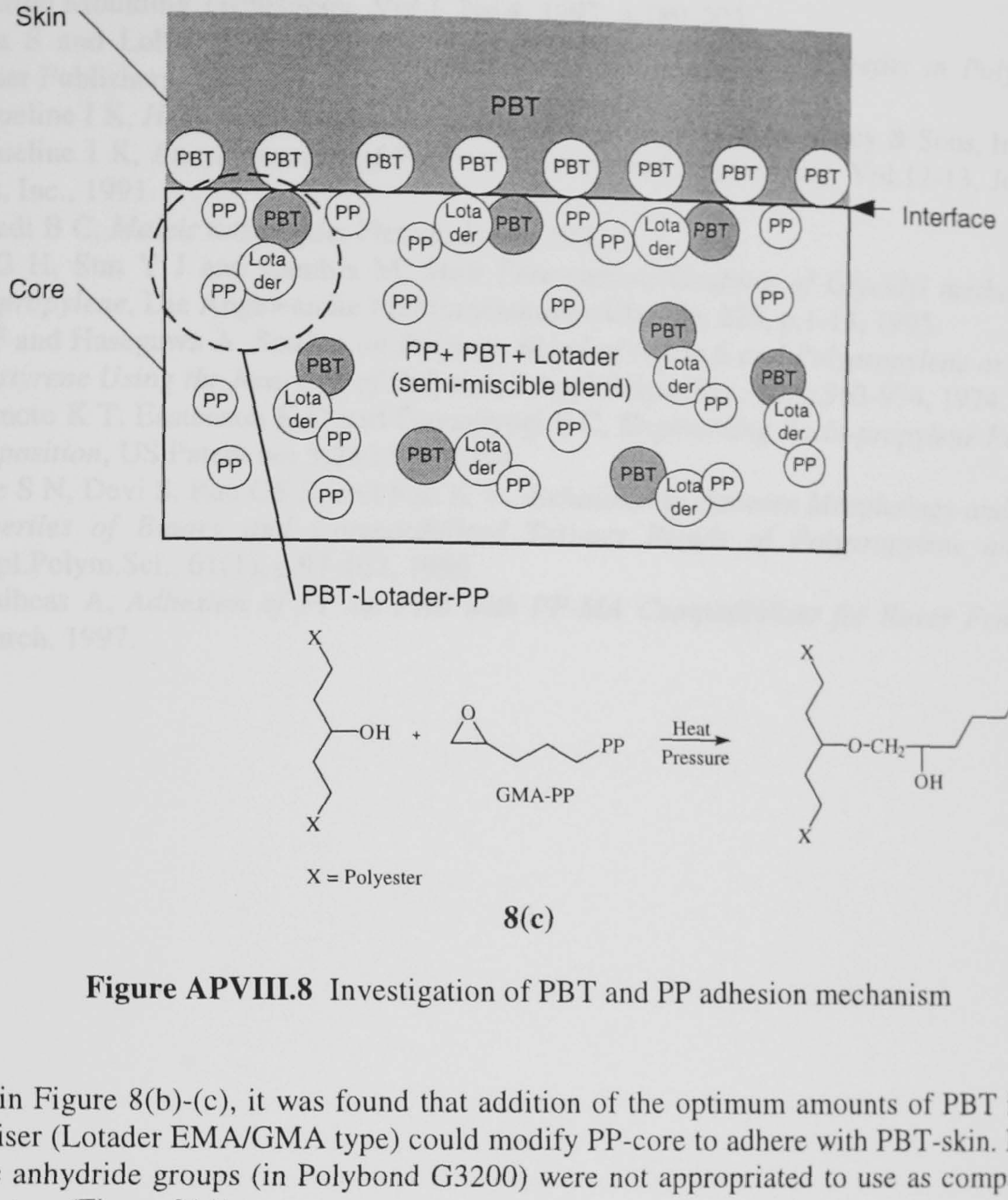

Figure APVIII.8 Investigation of PBT and PP adhesion mechanism

As shown in Figure 8(b)-(c), it was found that addition of the optimum amounts of PBT into PP with compatibiliser (Lotader EMA/GMA type) could modify PP-core to adhere with PBT-skin. It also found that maleic anhydride groups (in Polybond G3200) were not appropriated to use as compatibiliser for PBT/PP system (Figure 8(a)).

Conclusions

The polymer adhesions of the combinations between PBT and PP had been investigated using the simultaneous co-injection moulding technique. The PBT/PP adhesions could be achieved by addition of the optimum amounts of PBT into PP with compatibiliser. However, the adhesion affect was minimal. It was found that the domain size of PBT blend with PP were decreased when adding amounts of compatibiliser (Lotader EMA/GMA type). It also found that this mixture was a semi-miscible blend.

References

1 Smith G F and Easterlow R A, Plastic, Rubber and Composites, **25**(3), 115-119, 1996
2 Oxley D F and Sandiford D J H, *Sandwich Moulding*, Plastics & Polymers, Vol. 39 (August), 1971, p.288-292
3 Stafford D J, *The Development of The Sandwich Moulding Process*, The Plastic Institute, PENTEC 72, London, Paper No. 11, 29-30 November, 1972.
4 *The ICI Sandwich Moulding Process*, General description and applications, ICI publication, 1981.
5 Sandiford D J H and Oxley D F, *Serving Up a New Plastic Sandwich*, SPE Journal, Vol. 27, September 1971.
6 Eckardt H, *How to develop a successful coinjection application*, Fourteenth annual structural foam conference and parts competition, The society of the plastics industry, Inc., 1986.
7 Somnuk P, *Ph.D. Thesis*, Department of Engineering, Faculty of Science, University of Warwick, 1995.
8 Seldén R, *Sandwich Injection Moulding of Thermoplastics: A Literature Survey*, Journal of

Injection Moulding Technology, Vol.1, No.4, 1997, p.189-203
9 Datta S and Lohse D J, *Polymeric Compatibilisers : Uses and Benefits in Polymer Blends*, Hanser Publishers, 1996.
10 Jacqueline I K, *High Performance Polymers and Composites*, John Wiley & Sons. Inc., 1991.
11 Jacqueline I K, *Encyclopaedia of Polymer Science and Engineering*, Vol.12-13, John Wiley & Sons, Inc., 1991.
12 Trivedi B C, *Maleic anhydride*, Plenum Press, 1982.
13 Hu G H, Sun Y J and Lambla M, *Melt Free-radical Grafting of Glycidyl methacrylate onto Polypropylene*, Die Angewandte Makromolekulare Chemie, 229, p.1-13, 1995.
14 Ide F and Hasegawa A, *Studies on Polymer Blend of Nylon 6 and Polypropylene or Nylon 6 and Polystyrene Using the Reaction of Polymer*, J.Appl.Polym.Sci., 18, p.963-974, 1974.
15 Okamoto K T, Eastenson K D and Guyaniyogi S C, *Engineering Resin-propylene Polymer Graft Composition*, US Patent no. 5,290,856, 1994.
16 Sathe S N, Devi S, Rao GS S, and Rao K V., *Relationship Between Morphology and Mechanical Properties of Binary and Compatibilised Ternary Blends of Polypropylene and Nylon 6*, J.Appl.Polym.Sci., 61(1), p.97-107, 1996.
17 Magalheas A, *Adhesion of PP on PA6 with PP-MA Compatibiliser for Rover Fenders*, DSM Research, 1997.